UNIVERSIDADE FEDERAL DO TOCANTINS
PROGRAMA DE PÓS-GRADUAÇÃO EM
BIODIVERSIDADEE BIOTECNOLOGIA -
REDE BIONORTE

ANÁLISE DA EFICIÊNCIA DO USO DE BIOPOLÍMEROS A BASE DE CARBOIDRATOS COMO INIBIDORES DE CORROSÃO DO AÇO DO CONCRETO ARMADO

MARIA CAROLINA DE PAULA ESTEVAM D'OLIVERA

Palmas - TO

2024

MARIA CAROLINA DE PAULA ESTEVAM D'OLIVEIRA

ANÁLISE DA EFICIÊNCIA DO USO DE BIOPOLÍMEROS A BASE DE CARBOIDRATOS COMO INIBIDORES DE CORROSÃO DO AÇO DO CONCRETO ARMADO

Defesa de Tese de Doutorado apresentada ao Curso de Doutorado do Programa de Pós-Graduação em Biodiversidade e Biotecnologia da Rede BIONORTE, na Universidade Federal do Tocantins, como requisito parcial para a obtenção do Título de Doutor em Biodiversidade e Biotecnologia.

Orientador: Prof. Dr. Emerson Adriano Guarda
Coorientadora: Prof. Drª. Patrícia Martins Guarda

Palmas - TO
MAIO/2024

Dados Internacionais de Catalogação na Publicação (CIP)
Sistema de Bibliotecas da Universidade Federal do Tocantins

D999a D'Oliveira, Maria Carolina de Paula Estevam.

Análise da eficiência do uso de biopolímeros a base de carboidratos como inibidores de corrosão do aço do concreto armado. / Maria Carolina de Paula Estevam D'Oliveira. – Palmas, TO, 2024.

134 f.

Tese (Doutorado) - Universidade Federal do Tocantins – Câmpus Universitário de Palmas - Curso de Pós-Graduação (Doutorado) em Biodiversidade e Biotecnologia, 2024.

Orientador: Emerson Adriano Guarda

Coorientadora : Patrícia Martins Guarda

1. hidroxipropilmetilcelulose. 2. inibidor de corrosão. 3. solução de pors de concreto sinulado. 4. técnicas eletroquímicas e espectroscopia. I. Título

CDD 660.6

Elaborado pelo sistema de geração automática de ficha catalográfica da UFT com os dados fornecidos pelo(a) autor(a).

MARIA CAROLINA DE PAULA ESTEVAM D'OLIVEIRA

ANÁLISE DA EFICIÊNCIA DO USO DE BIOPOLÍMEROS A BASE DE CARBOIDRATOS COMO INIBIDORES DE CORROSÃO DO AÇO DO CONCRETO ARMADO

Tese de Doutorado apresentada ao Curso de Doutorado do Programa de Pós-Graduação em Biodiversidade e Biotecnologia - RedeBIONORTE, na Universidade Federal do Tocantins, como requisito parcial para a obtenção do Título de Doutor em Biodiversidade e Biotecnologia.

Aprovada em 24/05/2024

Banca examinadora

Prof. Dr. Emerson Adriano Guarda (Orientador)
Universidade Federal do Tocantins

Documento assinado digitalmente
gov.br ELTON CARVALHO DE LIMA
Data: 17/06/2024 15:37:47-0300
Verifique em https://validar.iti.gov.br

Prof. Dr. Elton Carvalho de Lima
Universidade Federal do Tocantins

Documento assinado digitalmente
gov.br DANIEL ARAUJO GONCALVES
Data: 18/06/2024 09:05:01-0300
Verifique em https://validar.iti.gov.br

Prof. Dr. Daniel Araújo Gonçalves
Universidade Federal da Grande Dourados

Documento assinado digitalmente
gov.br CICERO RAFAEL CENA DA SILVA
Data: 19/06/2024 11:27:45-0300
Verifique em https://validar.iti.gov.br

Prof. Dr. Cícero Rafael Cena da Silva
Universidade Federal de Mato Grosso do Sul

Documento assinado digitalmente
gov.br ANSELMO FORTUNATO RUIZ RODRIGUEZ
Data: 20/06/2024 12:39:36-0300
Verifique em https://validar.iti.gov.br

Prof. Dr. Anselmo Fortunato Ruiz Rodriguez
Universidade Federal do Acre

AGRADECIMENTOS

Não há outra maneira de iniciar esses agradecimentos, a não ser agradecendo meu esposo Salmo Moreira Sidel, que se dedicou demais para que esse doutorado tivesse êxito, portanto agradeço a ele por todo o tempo dedicado e pela paciência, carinho e apoio indispensável nas horas mais difícies da nossa vida e deste trabalho. Agradeço também aos meus filhos José Marcos e João Lucca que se comportaram muito bem nesses anos de estudo.

Aos meus amigos e orientadores, Prof. Dr. Emerson Adriano Guarda e Patrícia Martins Guarda, pela paciência, dedicação e gentileza de fazer parte da construção deste trabalho, proporcionando um conhecimento inigualável em eletroquímica.

A todos que fazem parte do LAPEQ – Laboratório de Pesquisas em Química Ambiental e Biocombustíveis da UFT, pela ajuda e apoio na realização deste trabalho e pelo uso do espaço e equipamentos.

A todos aqueles que de alguma forma colaboraram com este trabalho e que, mesmo não citados os nomes, tem meu reconhecimento, gratidão e respeito.

A Universidade Federal do Tocantins e a coordenação de aperfeiçoamento de pessoal de nível superior (CAPES) pelo auxilio concedido.

RESUMO

Devido ao aumento da consciência ambiental e da legislação rígida, nos últimos anos tem havido uma tendência crescente de usar abordagens verdes caracterizadas por uma carga ambiental mínima. Os inibidores de corrosão verdes têm atraído mais atenção nos últimos anos como uma técnica eficaz e ecológica. Os biopolímeros a base de carboidratos estão disponíveis na natureza, são renováveis e uma alternativa ecológica aos inibidores orgânicos com potencial tóxico. Os principais polissacarídeos de interesse comercial são a celulose e o amido, em especial aos carboidratos mais complexos, pois tais polímeros são formados por unidades básicas de glicose, ligadas como anéis de grupos acetais e, portanto, com alta hidrofilicidade. Dentro desse contexto, o presente trabalho realizou ensaios exploratórios para seleção dos candidatos potenciais entre os compostos testados, com base na dissolução, para avaliação em solução de poros de concreto simulado (SPC), composta de cimento e água filtrada á vácuo, além da simulação de ambiente corrosivo com o uso de cloreto de sódio (NaCl). O aditivo que apresentou melhor potencialidade para uso como inibidor de corrosão foi a hidroxipropilmetilcelulose (HPMC). Para otimização do experimento foi utilizado um delineamento experimental para determinar as melhores concentrações de HPMC como inibidor de corrosão em ambiente contaminado por cloretos. Para tal análise foram executados os seguintes experimentos em células eletroquímicas: circuito de potencial aberto (OCP), espectroscopia de impedância eletroquímica (EIS) e voltametria linear de varredura (LSV), além da aferição do pH e da condutividade. O planejamento experimental adotado foi do tipo delineamento composto central rotacional (DCCR), tendo como variáveis a quantidade de HPMC e NaCl, e como respostas o potencial de corrosão (Ecor), a resistência a polarização (Rp), e a condutividade. A avaliação estatística do planejamento mostrou que para Ecor, Rp e condutividade, as variáveis HPMC e NaCl foram significativas ($p<0,10$), sendo que o modelo estatístico mostrou correlação superior a 90% com os dados experimentais. As análises do OCP e das curvas de polarização indicam a formação de um filme passivo no aço imerso em solução contendo HPMC. A polarização Tafel demonstra desempenho anticorrosivo promissor de HPMC. A análise estatística, por meio do DCCR, confirmou que o meio contendo HPMC apresenta melhores propriedades passivantes, mostrando que esse biopolímero pode ser utilizado como inibidor de corrosão para concreto armado na construção civil. Já os resultados de EIS revelaram um aumento na resistência a transferência de carga das amostras na presença de HPMC, em comparação com o sistema referência. O HPMC teve uma maior eficiência como inibidor de corrosão nas amostras contaminadas com 17,5 g/L de NaCl, de 75% a 98%. Já nas soluções que continham 35,1 g/L de NaCl somente a dosagem máxima de HPMC (1,2 g/L) obteve êxito como inibidor de corrosão, com eficiência de 58%.

Palavras chave: Biopolímero; HPMC; Inibidor de corrosão; Solução de poro de concreto simulado; Célula eletroquímica; Potenciostato.

ABSTRACT

Due to increasing environmental awareness and strict legislation, in recent years there has been an increasing tendency to use green approaches characterized by a minimal environmental load. Green corrosion inhibitors have attracted more attention in recent years as an effective and environmentally friendly technique. Carbohydrate-based biopolymers are available in nature, renewable and an ecological alternative to organic inhibitors with toxic potential. The main polysaccharides of commercial interest are cellulose and starch, especially more complex carbohydrates, as these polymers are formed by basic glucose units, linked as rings of acetal groups and, therefore, have high hydrophilicity. Within this context, the present work carried out exploratory tests to select potential candidates among the tested compounds, based on dissolution, for evaluation in simulated concrete pore solution (SPC), composed of cement and vacuum filtered water, in addition to simulation corrosive environment with the use of sodium chloride (NaCl). The additive that showed the best potential for use as a corrosion inhibitor was hydroxypropylmethylcellulose (HPMC). To optimize the experiment, an experimental design was used to determine the best concentrations of HPMC as a corrosion inhibitor in an environment contaminated by chlorides. For this analysis, the following experiments were carried out in an electrochemical cell: open potential circuit (OCP), electrochemical impedance spectroscopy (EIS) and linear scanning voltammetry (LSV), in addition to measuring pH and conductivity. The experimental design adopted was a central composite rotational design (DCCR), with variables being the amount of HPMC and NaCl, and the responses being corrosion potential (Ecor), polarization resistance (Rp), and conductivity. The statistical evaluation of the planning showed that for Ecor, Rp and conductivity, the HPMC and NaCl variables were significant ($p<0.10$), and the statistical model showed a correlation greater than 90% with the experimental data. OCP and polarization curve analyzes indicate the formation of a passive film on steel immersed in a solution containing HPMC. Tafel polarization demonstrates promising anticorrosive performance of HPMC. Statistical analysis, through DCCR, confirmed that the medium containing HPMC has better passivating properties, showing that this biopolymer can be used as a corrosion inhibitor for reinforced concrete in civil construction. The EIS results revealed an increase in the charge transfer resistance of the samples in the presence of HPMC, compared to the reference system. HPMC had greater efficiency as a corrosion inhibitor in samples contaminated with 17.5 g/L of NaCl, from 75% to 98%. In solutions containing 35.1 g/L of NaCl, only the maximum dosage of HPMC (1.2 g/L) was successful as a corrosion inhibitor, with an efficiency of 58%.

Keywords: Biopolymer; HPMC; Corrosion inhibitor; Simulated concrete pore solution; Electrochemical cell; Potentiostat

LISTA DE FIGURAS

Capítulo I

Capítulo II

Capítulo III

Capítulo IV

LISTA DE TABELAS

Capítulo I

Capítulo II

Capítulo III

Capítulo IV

SUMÁRIO

1. INTRODUÇÃO

A construção civil é uma das indústrias econômicas de qualquer país, que consome inúmeros recursos, sendo o concreto mais importante o material, devido às suas fortes propriedades mecânicas, durabilidade e custo-benefício (YAO, Nan *et al.*, 2022). A perspectiva é a demanda global por cimento e aço aumentar 12% a 23% e 14% a 40%, respectivamente, até 2050 em comparação a 2014. O uso excessivo de materiais de construção esgota os recursos naturais e prejudica o meio ambiente, sendo necessária a busca por alternativas de materiais sustentáveis (AHER et al., 2023).

Apesar de serem considerados um material altamente durável, as estruturas de concreto armado ainda enfrentam certos problemas de durabilidade que podem levar à redução da sua capacidade de serviço e vida útil. De modo geral, as estruturas de concreto armado facilita a formação espontânea de um filme passivo de óxido estável (Fe^{2+}/Fe^{3+}-óxidos/hidróxidos) na superfície do aço (ALHOZAIMY; HUSSAIN; AL-NEGHEIMISH, 2016; SINGH; SINGH, 2012), o que dificulta o ataque de íons agressivos de forma eficaz.

No entanto, em ambientes marinhos, costeiros, salinos e outros ambientes salgados, a durabilidade das estruturas de concreto é severamente comprometida pela difusão de íons agressivos (WU; SHI, 2021). Os filmes passivos podem ser desdruídos, por exemplo, pelo ataque por cloretos (BOUBITSAS; TANG, 2015; NAHALI; DHOUIBI; IDRISSI, 2015; SHI; SUN, 2014) resultando assim na degradação prematura de estruturas de concreto armado (LIN; ZUO, 2019).

O colapso repentino de um condomínio de concreto armado à beira-mar de 40 anos na Flórida, EUA (24 de junho de 2021), em parte devido à severa deterioração por corrosão e à falta de manutenção, atraiu novamente grande atenção para a durabilidade estrutural. Os óxidos de ferro, que resultam da corrosão das armaduras, tendem a ocupar um volume até dez vezes maior comparado ao aço original da armadura, resultando em tensões internas maiores e levando a estrutura à fissuração e, por consequência, a entrada de dióxido de carbono no interior da estrutura (PINA, 2009).

Para evitar esses desastres e mitigar a corrosão dos vergalhões, os inibidores de corrosão são amplamente utilizados devido ao seu baixo custo, alta eficiência e facilidade de processo (LIU *et al.*, 2024). Isso envolve o isolamento de um metal de agentes corrosivos via adsorção de compostos contendo moléculas inibidoras na superfície do metal que forma uma barreira protetora (ARUKALAM *et al.*, 2014; OGUZIE *et al.*, 2011).

O filme adsorvido resultante atua como uma barreira que separa o metal do corrosivo e a eficiência da inibição depende das características mecânicas, estruturais e químicas das camadas de adsorção formadas sob condições particulares (OKAFOR; EBENSO; EKPE, 2010).

O inibidor de corrosão à base de nitrito, como o nitrito de cálcio , foi o primeiro inibidor de corrosão comercial para concreto armado e ainda é usado hoje (LIU; SRIDHAR, 2021).

Durante as últimas décadas, utilizou-se inibidores como fosfato (NAHALI; DHOUIBI; IDRISSI, 2015), monofluorofosfato (ELSENER; ANGST, 2017), aminas e alcanol amina. Contudo, tais inibidores tradicionais são sempre tóxicos e prejudiciais ao meio ambiente.

A química verde, a sustentabilidade e a engenharia ecológica estão a ser consideradas para o desenvolvimento de novos produtos, materiais e processos ecológicos para abordar questões ambientais globais (AHER et al., 2023).

Os inibidores verdes ecológicos e econômicos obtidos da natureza estão ganhando popularidade (ALVAREZ et al., 2023). Pesquisadores têm tentado extrair inibidores de corrosão verdes de produtos naturais ricos em O, C, N e S, que são os centros ativos com alta densidade eletrônica para a adsorção na superfície do metal (RANI; BASU, 2012).

Os grupos funcionais dos polímeros interagem com os íons metálicos e formam complexos que atuam como uma barreira que separa a solução agressiva da superfície do metal. Portanto, a inibição da corrosão é alcançada por meio de adsorção (KUMPAWAT; GARG; TAK, 2009; UMOREN, 2008).

O biopolímero é um desses desenvolvimentos de produtos ecologicamente corretos. O biopolímero e seu uso no concreto podem ser um material mais promissor que o petróleo (AHER et al., 2023).

A celulose é um biopolímero de carboidrato existente em maior quantidade em comparação com outros biopolímeros. A celulose encontra-se nos tecidos da planta e constitui cerca de um terço dela. Tem aplicações farmacêuticas, cosméticas e alimentícias (NWANONENYI *et al.*, 2016; SOLOMON *et al.*, 2010), e vários derivados dela têm sido usados como inibidores de corrosão (NWANONENYI *et al.*, 2016; UMOREN *et al.*, 2018)

O estudo dos biopolímeros a base de carboidratos objetiva fornecer informações importantes para o desenvolvimento da ciência na área da Biotecnologia, pois com a investigação desta pesquisa pretende-se estabelecer e comprovar a capacidade de ação contra o desenvolvimento da corrosão do aço nas estruturas de concreto armado, utilizando soluções de poros de concreto simulado (SPC). Espera-se que o efeito anticorrosivo oriundo do biopolímero analisado seja eficiente em comparação aos inibidores de corrosão de base orgânica já disponíveis no mercado.

1.1. Objetivo geral

Analisar a eficiência do uso de biopolímeros a base de celulose como inibidores de corrosão do aço do concreto armado por meio de uma solução de poros de concreto simulado (SPC), utilizando um Potenciostato/Galvanostato.

1.2. Objetivos específicos

1. Verificar a diferença entre as soluções de poros de concreto com e sem incorporação de biopolímero.
2. Verificar se a incorporação de biopolímero modifica a resistência à corrosão do aço em soluções de poros de concreto simulado.
3. Definir um delineamento experimental que permita otimizar a dosagem do biopolímero como inibidor de corrosão.
4. Otimizar a dosagem de biopolímero a ser utilizado como inibidor de corrosão por meio de análise estatística.
5. Avaliar o mecanismo de corrosão por meio da voltametria linear de varredura (LSV).
6. Avaliar a eficiência do HPMC como inibidor de corrosão por meio da espectroscopia de impedância eletroquímica (EIS).

2. ESTRUTURA DA TESE

Esta tese é composta por 6 Capítulos, dentre os quais:

A revisão bibliográfica é composta por 2 capítulos, sendo que ambos foram escritos em formato de artigos de revisão sistemática utilizando a metodologia PRISMA.

O Capítulo I é intitulado "**Estudos recentes sobre compósitos de carboidratos para inibição da corrosão: uma revisão sistemática**", sendo que este artigo foi publicado na revista **Research, Society and Development** em 14/07/2022, DOI: 10.33448/rsd-v11i9.32021.

O capítulo II é intitulado "**Recent studies on the use of simulated concrete pore solution for corrosion evaluation: a systematic review using prisma**", sendo que este artigo foi publicado na revista **Observatorio de La Economia Latino Americana** em 04/10/2023, DOI: 10.55905/oelv21n10-040.

O capítulo III refere-se ao artigo "**Evaluation of Cellulose-Derived Biopolymers on Steel Corrosion Susceptibility in Environments Simulating Concrete Pore Solutions - A Statistical Analysis Using CCRD**", submetido na revista **Construction and Building Materials**, aguardando publicação.

O capítulo IV refere-se ao artigo "**Evaluation of the use of hydroxypropylmethylcellulose (HPMC) as a steel corrosion inhibitor, in media that simulate concrete pore solutions: an electrochemical investigation**", que está em fase de revisão para posterior publicação.

O Capítulo V refere-se a Discussão iNTEGRADORA.

O capítulo VI refere-se a Conclusão.

Os Capítulos I, II, III e IV foram apresentados no formato requerido pelos editoriais onde foram ou serão publicados.

Capítulo I: Estudos recentes sobre compósitos de carboidratos para inibição da corrosão: uma revisão sistemática

Research, Society and Development, v. 11, n. 9, e41811932021, 2022
(CC BY 4.0) | ISSN 2525-3409 | DOI: http://dx.doi.org/10.33448/rsd-v11i9.32021

Estudos recentes sobre compósitos de carboidratos para inibição da corrosão: uma revisão sistemática

Recent studies on carbohydrate compounds for corrosion inhibition: a systematic review

Estudios recientes sobre compuestos de carbohidratos para la inhibición de la corrosión: una revisión sistemática

Recebido: 21/06/2022 | Revisado: 01/07/2022 | Aceito: 05/07/2022 | Publicado: 14/07/2022

Maria Carolina de Paula Estevam D'Oliveira
ORCID: https://orcid.org/0000-0001-5240-6879
Universidade Federal do Tocantins, Brasil
E-mail: carolina.doliveira@uft.edu.br
Emerson Adriano Guarda
ORCID: https://orcid.org/0000-0003-0227-3881
Universidade Federal do Tocantins, Brasil
E-mail: emersonprof@uft.edu.br
Patrícia Martins Guarda
ORCID: https://orcid.org/0000-0003-0937-6779
Universidade Federal do Tocantins, Brasil
E-mail: patriciaguarda@uft.edu.br
Salmo Moreira Sidel
ORCID: https://orcid.org/0000-0002-8939-1794
Universidade Federal do Tocantins, Brasil
E-mail: sidel@uft.edu.br

Resumo
Os biopolímeros de carboidratos constituem uma das alternativas ecológicas em relação a outros inibidores de corrosão orgânicos com potencial tóxico. Na inibição de corrosão eles representam um conjunto de compostos quimicamente estáveis, biodegradáveis e ecologicamente corretos, com forças de inibição confiáveis para proteção de superfícies metálicas, tornando-os revestimentos de proteção de metais eficazes. Portanto, este artigo apresenta uma revisão sistemática de biopolímeros de carboidratos utilizados como inibidores de corrosão desde 2018. A investigação seguiu o protocolo PRISMA, que fornece um resumo meticuloso de todas as pesquisas primárias disponíveis em resposta a uma pergunta de pesquisa. Depois de incluir/excluir etapas, quarenta e cinco estudos foram incluídos na revisão. Os resultados são apresentados enfocando os tipos de biopolímeros avaliados, como Quitosana, Dextrano, Celulose, e Goma Arábica, além disso os metais analisados, os meios utilizados para aceleração do processo de corrosão, o tipo de inibidor e a eficiência atingida em cada estudo também foram apresentados. Em suma, essa metodologia ajudou a identificar as principais lacunas de conhecimento nessa área.
Palavras-chave: Revisão sistemática; Biopolímeros; Carboidratos; Inibição da corrosão.

Abstract
Carbohydrate biopolymers are one of the ecological alternatives to other organic corrosion inhibitors with toxic potential. In corrosion inhibition, they represent a set of chemically stable and environmentally friendly coatings for protecting metal surfaces, making them effective coatings for metal protection. Thus, this article presents a systematic review of carbohydrate biopolymers used as corrosion inhibitors since 2018. The investigation followed the PRISMA statement, which provides a meticulous summary of all available primary research in response to a research question. After including/excluding steps, forty-five studies were included in the review. The results are presented with a focus on the types of biopolymers evaluated, such as chitosan, cellulose, and gum arabic. In addition, the analyzed metals, the means used to accelerate the corrosion process, the type of inhibitor and the efficiency achieved in each study were also presented. In summary, this methodology helped to identify the main knowledge gaps in this area.
Keywords: Systematic review; Biopolymers; Carbohydrates; Corrosion inhibition.

Resumen
Los biopolímeros de carbohidratos son una de las alternativas ecológicas a otros inhibidores de corrosión orgánicos con potencial tóxico. En la inhibición de la corrosión representan un conjunto de compuestos químicamente estables, biodegradables y amigables con el medio ambiente con fuerzas de inhibición confiables para proteger superficies metálicas, convirtiéndolos en recubrimientos efectivos para la protección de metales. Por lo tanto, este artículo presenta una revisión sistemática de los biopolímeros de carbohidratos utilizados como inhibidores de la corrosión

desde 2018. La investigación siguió el protocolo PRISMA, que brinda un resumen meticuloso de toda la investigación primaria disponible en respuesta a una pregunta de investigación. Después de incluir/excluir los pasos, se incluyeron cuarenta y cinco estudios en la revisión. Los resultados se presentan enfocándose en los tipos de biopolímeros evaluados, como Chitosan, Dextrano, Celulosa y Goma Arábiga, además de los metales analizados, los medios utilizados para acelerar el proceso de corrosión, el tipo de inhibidor y la eficiencia alcanzada en cada uno. estudio. fueron presentados. En definitiva, esta metodología ayudó a identificar los principales vacíos de conocimiento en esta área.
Palabras clave: Revisión sistemática; Biopolímeros; Carbohidratos; Inhibición de la corrosión.

1. Introdução e Cenário Global

Estima-se que cerca de 15% a 35% do custo global provocados por corrosão podem ser economizados utilizando estratégias de proteção (Koch, 2017). Essas estatísticas revelam o importante papel dos métodos de proteção contra corrosão, a fim de melhorar a vida útil das estruturas metálicas e reduzir os custos de manutenção e reparo nas indústrias.

A corrosão ocorre devido a efetividade de alguns agentes por meio de mecanismos degradantes, sendo eles: carbonatação - transformação do hidróxido de cálcio em carbonato de cálcio, que é mais neutro, induzindo a redução do pH no concreto; despassivação da armadura - acontece quando o íon cloreto rompe a camada passivadora, camada insolúvel que protege o aço (Vitório, 2003).

O custo da intervenção para recuperação estrutural vai muito além dos serviços de reparo, pois envolve também a interdição do local, quando necessário, transferência de atividades para outro local, além do risco que uma estrutura danificada oferece às pessoas, materiais e equipamentos (Ribeiro & Helene, 2013).

Existem várias técnicas para proteger o aço do ataque de corrosão, como a modificação de material, alteração no ambiente circundante, revestimento superficial, proteção catódica e uso de inibidores de corrosão. Alguns métodos dependem da remoção da umidade/oxigênio, enquanto os outros fazem uso de revestimento permanente na superfície metálica. No entanto, algumas abordagens são baseadas na conversão do material anódico em um cátodo. No entanto, as aplicações das técnicas existentes são limitadas por várias restrições. Por exemplo, a modificação do material é muitas vezes impossível ou cara (Wolynec, 2003).

A substituição do ambiente de processo não é uma solução opcional em muitas aplicações industriais, pois o metal tem que experimentar um determinado meio reativo. A implementação de alguns métodos, por exemplo, o revestimento, pode elevar as emissões de CO2 além dos níveis aceitáveis. Além disso, alguns métodos, como a proteção catódica requerem equipamentos caros, aumentando assim o custo global. Os inibidores de corrosão, no entanto, oferecem uma solução alternativa econômica e viável. (Rani & Basu, 2012).

O inibidor é a substância adicionada em pequena quantidade no ambiente corrosivo com o propósito de retardar a reação de corrosão formando uma película protetora. Os inibidores possuem inúmeras aplicações, e na construção civil servem como agentes eficazes para proteger estruturas de aço em caldeiras, trocadores de calor (óleo e gás) e recipientes de corrosão. Metais e aços, em particular, são comumente expostos a meios ácidos antes de realizar um processo, por exemplo, soldagem ou revestimento (Umoren et al., 2020).

A acidificação de estruturas corroídas (por exemplo, poços de petróleo, petroleiros, trocadores de calor, dutos) é realizada para remover produtos de corrosão. O uso de inibidores durante esses tratamentos demonstrou resultados promissores na inibição das reações de corrosão e do dano metálico associado (Darmokoesoemo et al., 2018; Farhadian et al., 2020; Umoren et al., 2020). Várias considerações essenciais determinam a seleção de inibidores, um dos fatores chave é a toxicidade do inibidor. Em geral, a alta volatilidade de inibidores tradicionais tóxicos, como cromatos, fosfatos e nitratos resulta na liberação de gases tóxicos, afetando assim o meio ambiente (Pakseresht et al., 2018; Raja & Sethuraman, 2008).

Tendo em vista os diversos problemas de corrosão identificados a partir da década de 60, muitas pesquisas foram

desenvolvidas com a tentativa de solucionar este desafio e prolongar a vida útil das estruturas das edificações (Ribeiro & Helene, 2013). Foi observado que alguns produtos, quando aplicados, preservavam a integridade do aço frente aos agentes agressivos, sendo estes os inibidores que atuam dificultando a efetividade da pilha de corrosão formada pelo aço e o eletrodo. Os inibidores são dos tipos catódicos, anódicos ou mistos possibilitando obter a inibição de corrosão do aço (Figueiredo & Meira, 2013).

Para serem efetivos os inibidores devem portar um forte receptor e/ou doador de elétrons, tem que apresentar também um certo grau de insolubilidade de forma que não seja facilmente lixiviado, deve atender ao sistema de proteção sem produzir efeitos colaterais imprevistos e também suportar e agir na presença de pH e temperatura do ambiente onde é aplicado (Ribeiro & Helene, 2013).

Os revestimentos orgânicos constituem a abordagem mais comum para a proteção da corrosão de estruturas metálicas, atuando como barreira física para separar a superfície metálica do ambiente corrosivo (Hernández-Padrón et al., 2006; Liu et al., 2018; Tran et al., 2020). No entanto, os revestimentos orgânicos não podem fornecer proteção contra corrosão a longo prazo devido à estrutura frágil e à degradação hidrolítica durante a exposição ao ambiente corrosivo. Além disso, poros são criados dentro da matriz de polímeros durante o processo de cura devido à evaporação de solventes orgânicos e tensões ambientais externas. Estes micro poros são um caminho para difusão de agentes corrosivos por meio dos revestimentos para o substrato metálico (Pourhashem et al., 2017; Ramezanzadeh et al., 2015; Skale et al., 2007; Tang et al., 2020)

Devido ao aumento da consciência ambiental e da legislação rígida, nos últimos anos tem havido uma tendência crescente de usar abordagens verdes caracterizadas por uma carga ambiental mínima. Eles trabalham com os princípios da química verde, que incluem a prevenção de resíduos; economia atômica; síntese química perigosa reduzida; projetar produtos químicos mais seguros; solventes e auxiliares mais seguros; design para eficiência energética; uso de matérias-primas renováveis; reduzir derivados; uso de catalisadores em vez de reagentes estequiométricos; design para degradação; prevenção da poluição em tempo real; química mais segura para a prevenção de acidentes (Wei et al., 2020).

Os inibidores de corrosão verdes têm atraído mais atenção nos últimos anos como uma técnica eficaz e ecológica. São fontes comuns de inibidores ecológicos de corrosão os extratos de plantas, as drogas farmacêuticas, os líquidos iônicos e os inibidores sintéticos. As plantas (ou seja, extrato e óleos) são fonte essencial da extensa gama de inibidores de corrosão verde em diferentes meios ácidos devido às propriedades físicas, químicas e biológicas. Outras vantagens das plantas como fontes de inibidores de corrosão incluem baixo custo, disponibilidade abundante e sua biodegradabilidade. As plantas são conhecidas como uma fonte rica em compostos químicos naturais que podem ser facilmente extraídos com baixo custo e mínima poluição ambienta (Marzorati et al., 2019; Sharma et al., 2015).

Os biopolímeros são polímeros produzidos por seres vivos, como a celulose, o amido, a quitina, a quitosana e os alginatos. Devido sua decomposição rápida, em condições favoráveis, os biopolímeros são uma das principais alternativas aos materiais plásticos derivados do petróleo. Muitos estudos estão ocorrendo na área a fim de viabilizar seu uso como produto final em diversas aplicações, pois essa classe de polímeros apresenta um grande potencial de substituição para os polímeros obtidos a partir de fontes fosseis (Avérous & Pollet, 2012).

Biopolímeros de carboidratos são macro compostos que possuem unidades monoméricas ligadas covalentemente para formar longas cadeias de açúcar macromoleculares, com massas moleculares relativamente altas. Eles estão prontamente disponíveis na natureza, são benignos, renováveis e uma alternativa ecológica a outros inibidores orgânicos com potencial tóxico. Na inibição de corrosão, eles representam um conjunto de compostos quimicamente estáveis, biodegradáveis e ecologicamente corretos, com forças de inibição confiáveis para proteção de superfícies metálicas, tornando-os revestimentos de proteção e de metal eficazes (Umoren & Eduok, 2016).

Os principais polissacarídeos de interesse comercial são celulose e amido, havendo uma atenção especial aos

carboidratos mais complexos: quitosanas, quitinas e xantanas. Comparando-se as estruturas de alguns destes polímeros, verifica-se que são formados por unidades básicas de glicose, ligadas como anéis de grupos acetais (aldeído e álcool) e, portanto, com grande quantidade de grupos hidroxilas (alta hidrofilicidade) (Franchetti & Marconato, 2006).

Os biopolímeros possuem algumas limitações técnicas que tornam difícil sua processabilidade e seu uso como produto final. Assim, muitos grupos de pesquisa vêm se dedicando ao estudo da modificação dos biopolímeros para viabilizar o processamento e uso deles em diversas aplicações. Para isso, blendas, compósitos, nanocompósitos, têm sido estudados no intuito de melhorar propriedades como processabilidade, resistência térmica, propriedades mecânicas, propriedades reológicas, permeabilidade a gases e taxa de degradação (Brito et al., 2011).

O objetivo deste artigo é discutir trabalhos após uma revisão sistemática, utilizando o protocolo PRISMA, para acompanhar o progresso recente no uso de biopolímeros de carboidratos para inibição da corrosão de metais. Os biopolímeros avaliados, os metais analisados, os meios utilizados para aceleração do processo de corrosão, o tipo de inibidor, o método de monitoramento da corrosão e a eficiência atingida em cada estudo analisados são detalhados nas seções a seguir.

2. Revisão Sistemática e Metodologia

Uma Revisão Sistemática de Literatura procura estabelecer um levantamento formal do estado da arte de forma consistente e planejada, visando implementar critérios para seleção de pesquisas que possam ser úteis e trazer informações relevantes sobre o assunto em estudo, sendo uma estratégia para reduzir predisposições e erros aleatórios que podem ocorrer em uma revisão tradicional (Urra Medina & Barría Pailaquilén, 2010). Além disso, consiste na identificação e descrição de pesquisas anteriores, avaliação sistemática de pesquisas seguindo protocolos rigorosos, e coleta sintética e coerente de evidências no universo de pesquisas selecionado (O'Connor et al., 2017). Ferramentas facilitadoras para a realização da revisão sistemática de literatura são empregadas, como o protocolo PRISMA (Preferred Reporting Items for Systematic Reviews and Meta Analyses), que possui 17 diretrizes compondo um fluxograma de informações (Moher et al., 2015).

Diferente de uma revisão de literatura, que é baseada em um resumo ou visão geral de um determinado tópico, uma revisão sistemática de literatura é focada na resposta de uma questão, eliminando os vieses e preconceitos. Além disso, é importante salientar que o planejamento que ocorre antes da revisão permite que outros comparem, reproduzam e julguem a validade do protocolo e da revisão, prevenindo assim decisões arbitrárias com relação à inclusão e exclusão de dados (Moher et al., 2015; O'Connor et al., 2017).

Na área de biopolímeros de carboidratos, não há uma revisão sistemática de literatura que siga ou adapte a metodologia PRISMA, principalmente no que tange ao uso como inibidores de corrosão, sendo que a única revisão sistemática encontrada está relacionada a compósitos epóxi de celulose com foco em fibras vegetais (Neves et al., 2021).

Artigos de revisão de literatura vem sendo publicados sobre o uso da quitosana como inibidor de corrosão (Ashassi-Sorkhabi & Kazempour, 2020; Azmana et al., 2021) e na indústria do petróleo e gás (Chauhan et al., 2021; Negi et al., 2021); e da goma arábica como material anticorrosivo (Verma & Quraishi, 2021). Tais artigos discutem profundamente estes tópicos. Porém, a vantagem deste trabalho é permitir, com facilidade, a verificação e rastreamento do que foi publicado desde 2018 até a presente data em compósitos de carboidratos com foco no uso como inibidores de corrosão.

Nesse contexto, o objetivo desta revisão sistemática é compilar dados entre 2018 e 2021, sobre compósitos de carboidratos utilizados como inibidores de corrosão, sendo que, este trabalho, foi realizado seguindo as diretrizes metodológicas definidas pelo protocolo PRISMA (Moher et al., 2015), e o software Mendeley© foi utilizado para organizar os resultados de acordo com cada uma das bases de dados e também auxiliou na organização dos dados facilitando o processo laborioso e repetitivo de uma revisão sistemática de literatura.

Os artigos foram selecionados por meio das bases de dados on line: PubChem (https://pubchem.ncbi.nlm.nih.gov/),

PubMed (https://pubmed.ncbi.nlm.nih.gov/), Science Direct (https://www.sciencedirect.com/), Scopus (https://www.scopus.com/home.uri), Web of science (https://www.sciencedirect.com/) e Periódicos da CAPES (www.periodicos.capes.gov.br). Os termos de pesquisa foram: (Biopolymer AND Carbohydrate AND Corrosion inhibitor). Os resultados foram limitados a artigos em inglês publicados entre 2018-2021. Os artigos identificados tiveram seus títulos e resumos avaliados de forma independente por dois revisores (D'Oliveira, MCPE e Guarda, EA).

Foram excluídos os artigos de revisão, livros e capítulos de livros, resumos de congressos e estudos de caso.

Para a etapa seguinte foi utilizado o conceito Qualis CAPES que é um sistema de classificação de produção científica brasileira, baseada nos artigos publicados em periódicos de todos os programas de pós-graduações do país onde o principal objetivo é avaliar a qualidade da produção científica e auxiliar os professores e alunos no processo de submissão de artigos, sendo que essa qualidade é classificada em artigos A1, A2, A3, A4, B1, B2, B3, B4 e C.

Em seguida foram aplicados os seguintes critérios de exclusão: artigos com Qualis inferior a A2, trabalhos que não mencionavam biopolímeros de carboidratos e inibidores de corrosão, trabalhos sem texto completo. Os artigos foram incluídos, comparados e os registros duplicados foram removidos, alcançando um número final de 45 artigos de interesse.

É importante salientar que esta pesquisa irá relacionar os tipos de biopolímeros avaliados, os metais analisados, os meios utilizados para aceleração do processo de corrosão, o tipo de inibidor, o método de monitoramento da corrosão e a eficiência atingida em cada estudo; não está incluída a discussão dos ensaios de caracterização dos materiais.

3. Resultados e Coleta de Dados

A seleção dos estudos é apresentada em um fluxograma de acordo com os requisitos do PRISMA (Figura 1), ilustrando o número de artigos identificados, incluídos e excluídos, evidenciando o motivo. A busca nas bases de dados on line PubMed, Science Direct, Periódicos da CAPES, Scopus e Web of Science identificou um total de 2092 artigos. Destes, foram excluídos artigos cujo ano da publicação é inferior a 2018 (1053), artigos de revisão (284), livros, capítulos de livro e enciclopédias (134), resumos de congressos e estudos de caso (54), aqueles cujo Qualis é inferior a A2 (276), os que não possuem texto completo disponível (30), excluídos por duplicação (21) e os excluídos após a revisão do título, palavras-chave e resumo (151), chegando a 89 artigos.

Figura 1. Fluxograma de revisão sistemática, de acordo com o protocolo PRISMA.

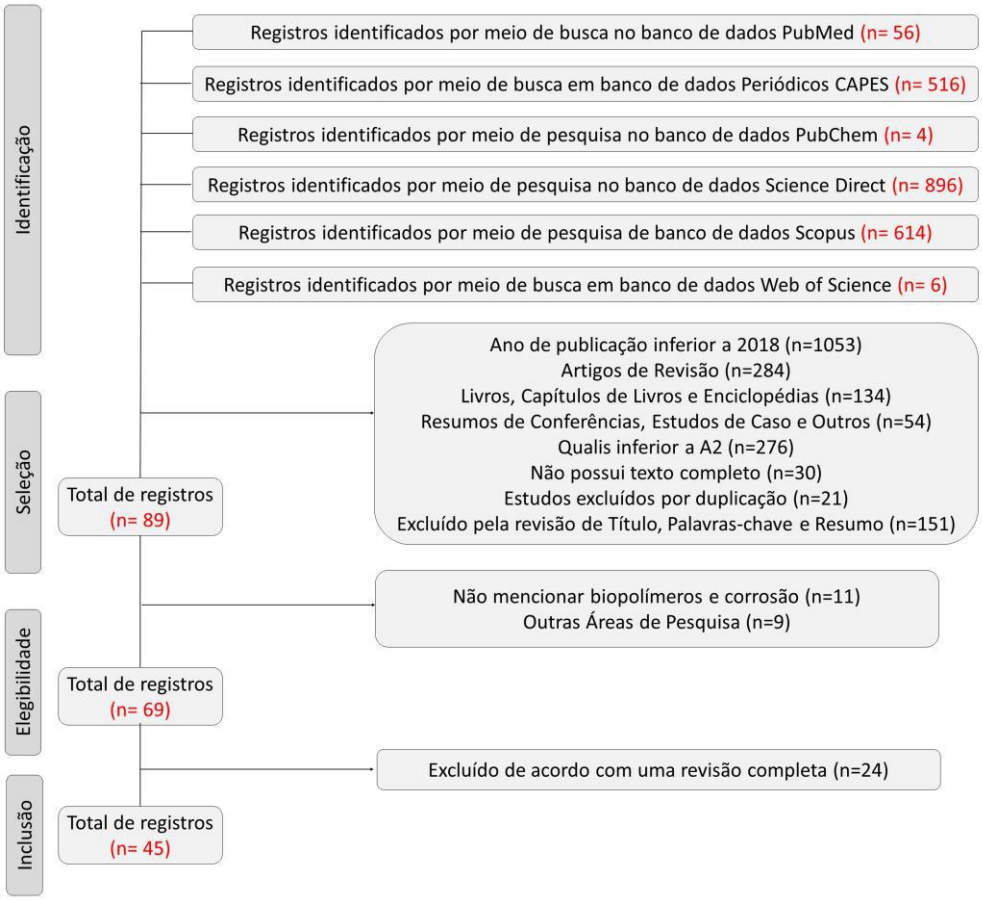

Fonte: Autores.

Também foram excluídos aqueles artigos que não mencionam biopolímeros e corrosão (11) e os de outras áreas de pesquisa (9). Após esta etapa, permaneceram 69 artigos dos quais 24 foram excluídos após uma revisão integral do texto. Desta maneira, 45 artigos foram submetidos à análise de texto completo e incluídos nesta pesquisa.

4. Discussão de Resultados

Com base na Figura 2, pode-se observar que o número de artigos foi maior em 2018. No ano de 2021, até julho, quando os dados foram compilados, já existiam 8 trabalhos nessa área, e mais estudos são esperados, o que indica que no ano de 2021 haverá mais publicações que nos anos anteriores sobre o assunto pesquisado. A revisão sistemática permitiu rastrear quais os tipos de compósitos de carboidratos foram estudados, os tipos de metais avaliados, o meio aquoso utilizado no processo de aceleração da corrosão, o tipo de inibidor, o método de monitoramento da corrosão e a eficiência de cada compósito de carboidrato como inibidor de corrosão.

Figura 2. Estudos publicados encontrados nesta revisão sistemática sobre biopolímeros de carboidratos, por ano, desde 2018.

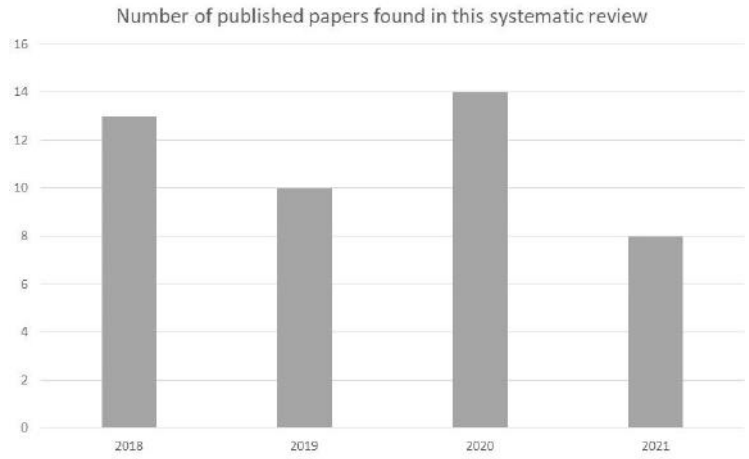

Fonte: Autores.

Os artigos foram classificados com base no biopolímero foco da pesquisa, metais utilizados para avaliação da corrosão e meio utilizado para aceleração da corrosão nos estudos analisados, e isso está ilustrado na Figura 3. Em relação ao biopolímero estudado, a maioria dos artigos utilizaram a quitosana, seguido da dextrana. Outros biopolímeros estudados desde 2018 foram a celulose, a goma arábica e alguns compostos por polissacarídeos e extratos.

Figura 3. Tipo de biopolímeros, metais, meio de imersão e eficiência alcançada relatado nos estudos desde 2018. (a) tipos de biopolímeros estudados; (b)metais utilizados; (c) meios de imersão do metal para aceleração da corrosão.

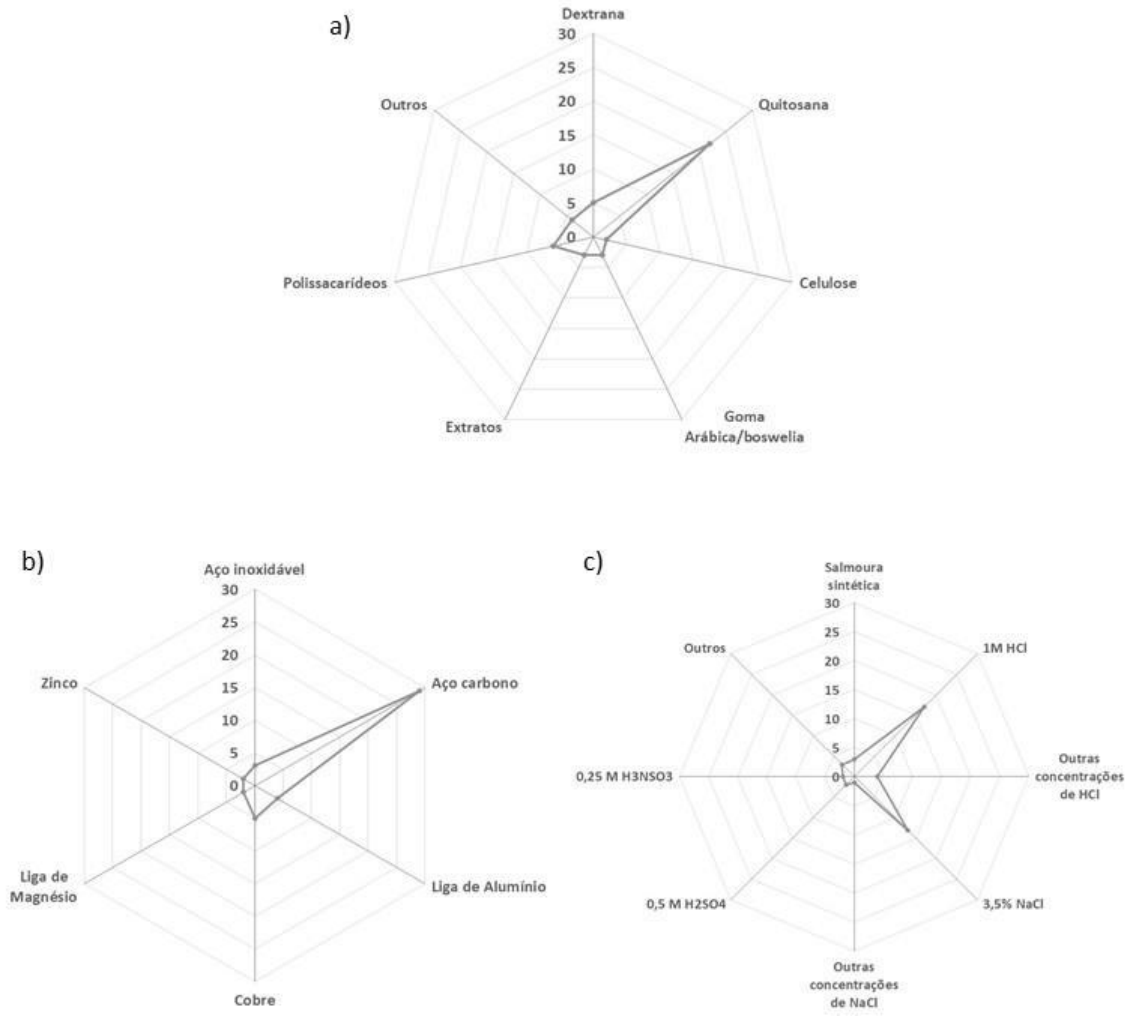

Fonte: Autores.

Em relação aos tipos de biopolímeros analisados nos artigos, 49% deles utilizaram a quitosana pura ou modificada, 11% eram compósitos de dextrana. Gomas, celulose, extratos e polissacarídeos foram menos utilizados (Figura 3a). O metal mais utilizado nas pesquisas foi o aço carbono, 64%, seguido do cobre, 11%. As ligas de alumínio e magnésio, o zinco e o aço inoxidável também foram abordados em uma quantidade menor de artigos (Figura 3b). Os meios de imersão do metal para aceleração da corrosão mais utilizados foram 1M HCl e 3,5% de NaCl, com 38% e 29%, respectivamente, em menor quantidade apareceram meios aquosos com H2SO4, H3NSO3 além da salmoura sintética (Figura 3c).

A eficiência como inibidores de corrosão alcançadas nos estudos e os biopolímeros mais eficientes estão ilustrados na Figura 4.

Figura 4. Eficiência alcançada e biopolímeros mais eficientes relatados nos estudos desde 2018.

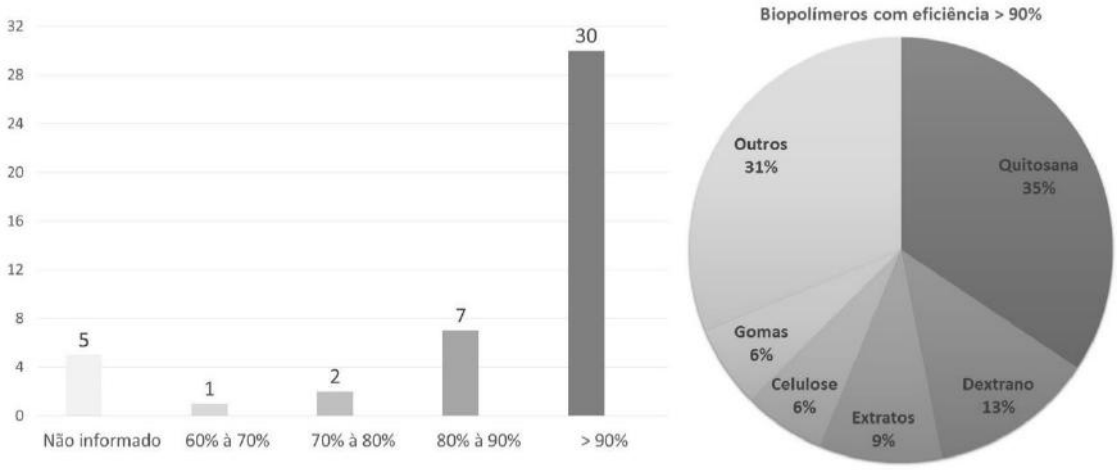

Fonte: Autores.

Em relação a análise da eficiência dos biopolímeros como inibidores de corrosão, a grande maioria dos artigos, 30, apresentaram uma eficiência de inibição de corrosão superior a 90%, sendo que destes, o biopolímero mais estudado foi a quitosana, 11 estudos, seguido da dextrana com 4 estudos, celulose, 2 estudos, e gomas, 2 estudos (Figura 4).

Os referidos 45 artigos incluídos na síntese qualitativa, o tipo de biopolímero e a eficiência destes como inibidores de corrosão são apresentados no Quadro 1 . As informações completas, incluindo tipo de metal, o meio utilizado para aceleração da corrosão, o tipo de inibidor, o método de monitoramento da corrosão e os resultados relatados pelos 45 artigos, podem ser encontrados no Material Suplementar (Tabela S1) e indicam os recentes desenvolvimentos na área de pesquisa em questão.

Quadro 1. Tipo de biopolímero e eficiência como inibidores de corrosão.

ID	REFERÊNCIA	BIOPOLÍMERO ESTUDADO	EFICIÊNCIA
1	(Rbaa et al., 2020)	CH-HQ 5-clorometil-8-hidroxiquinolina (5-CMHQ) quitosana (CH)	CH, 78% CH-HQ, 93%
2	(Chugh, Singh, Chaouiki, et al., 2020)	BPCH MBPCH CBPCH Sintetizados benzaldeído, 2-metoxibenzaldeído 2-clorobenzaldeído	MBPCH, 94,1% BPCH, 91,3% CBPCH, 78,5%
3	(K. Zhang, Yang, Yin, et al., 2018)	KGMA - Pó de konjac comercial KGMH - Polímeros de carboidratos modificados com aminoácidos	KGMA, 90% KGMH, 92%
4	(Chauhan et al., 2020)	aminotriazoletiol-quitosana	97,80%
5	(Yang et al., 2019)	beta-ciclodextrina carboximetilada (CM-b-CD)	99,20%
6	(W. Zhang, Wu, et al., 2021)	polissacarídeo de Apostichopus japonicus (AJPS)	96,03%
7	(Fardioui et al., 2021)	8-hidroxiquinolina- g- Alginato	92,60%
8	(Biswas et al., 2019)	dextrin- enxerto -polyvinyl de etilo (ViciadosMu-g-PVAC)	98,39%
9	(Mobin et al., 2018)	goma Boswellia serrata (BSG)	91,80%
10	(Oliveira et al., 2020)	quitosana-tungstênio (Chit-W)	não houve melhora significativa na resistência à corrosão
11	(Srivastava et al., 2019)	quitosana-cobalto quitosana-SnS 2	quitosana-cobalto, 95%
12	(Lai et al., 2021)	CP foi preparado pela reação de Schiff Base com quitosana e 4-piridinocarboxaldeído. TiO 2foi disperso em CP para preparar nanocompósito de CPT.	94,50%
13	(Zhao et al., 2020)	CHC CAHC	CHC, 87,97% CAHC, 93,95%
14	(Bahari et al., 2020)	matriz de quitosana com 2-MBT e nanopartículas de sílica	85%

ID	REFERÊNCIA	BIOPOLÍMERO ESTUDADO	EFICIÊNCIA
15	(Cui et al., 2019)	sal de amônio quaternário de oligossacarídeo N-propil quitosana (PHC) sal de amônio quaternário de N-benzil quitosana (BHC)	PHC, 85,70% BHC, 88,59%
16	(El Mouaden et al., 2018)	Quitosana	89%
17	(Ansari et al., 2020)	Salicylaldeyde-Chitosan Schiff Base (SCSB), foi sintetizada pela reação de quitosana e salicilaldeído	95,40%
18	(Gupta et al., 2018)	quitosana como inibidor de corrosão sozinho e em combinação com iodeto de potássio)	Quitosana,73,8% Quitosana com KI, 90%
19	(EL. Mouaden et al., 2020)	quitosana modificada por cinamaldeído (Cinn-CS).	89%
20	(Q. H. Zhang et al., 2021)	L-cisteína e S-benzil-L-cisteína foram usados como reagentes de esterificação para modificar a molécula de dextrano para obter dois inibidores ecológicos (LDT e S-LDT)	S-LDT, 99,7%
21	(Eduok et al., 2018)	Composto de carboximetilquitosana grafitizado com PVI (CMCh-g-PVI)	não informado
22	(Sambyal et al., 2018)	compósito de poli (anilina-anisidina), quitosana e SiO_2	não informado
23	(Hasanin & Al Kiey, 2020)	compósito de etilcelulose-niacina (NEC) compósito de celulose-niacina microcristalina (NMCC) composto de carboximetilcelulose-niacina (NCMC)	NEC, 94,7% NMCC, 33,2% NCMC, 83,4%
24	(Nikpour et al., 2019)	Extrato da folha de Eriobotrya japonica Lindl (EJL)	de 85 à 95%
25	(Solomon, Umoren, et al., 2018)	Dextrano, incorporação de nanopartículas de prata (AgNPs) em matrizes de dextrano e combinação com KI 1 mM	Dextrano, 86,82% combinação com KI , 94,21%
26	(Umoren et al., 2020)	alginato de sódio (ALG), hidroxiletilcelulose (HEC)	HEC, 80,56% ALG, 77,43%
27	(W. Zhang et al., 2020)	Extrato de Polygonatum cyrtonema Hua (PF)	94,73%
28	(Chai et al., 2018)	ácido poliaspártico ecológico (PASP) PASP / N - (3-aminopropil) imidazol (PD-1) PASP / N - (3-aminopropil) -imidazol- co-n- dodecilamina (PD-2)	PD-2, 94%
29	(Pais et al., 2021)	Nanopartículas de glicogênio	92%
30	(Jena et al., 2020)	composto Óxido de grafeno - quitosana - prata	99%
31	(Rbaa et al., 2021)	macromolécula de oligossacarídeo de quitosana carregando uma porção de glicose (COS-g-Glu)	97%
32	(Shen et al., 2019)	goma arábica	83,5 à 90%
33	(Solomon, Gerengi, et al., 2018)	goma arábica, nanopartículas de prata e mel natural (GA-AgNPs)	em soluções de HCl, 88,60% em soluções de H2SO4, 84,54%
34	(W. Zhang, Nie, et al., 2021)	polissacarídeo natural composto de sulfato de condroitina derivado de cartilagem de porco (CS-PC) e alginato de sódio (SA)	95,18%
35	(K. Zhang, Yang, Xu, et al., 2018)	konjac glucomanan	94%
36	(Hassan et al., 2018)	polissacarídeo aniônico polieletrólito condroitina-4-sulfato (CS)	64,12%
37	(Pais & Rao, 2020)	maltodextrina	72%
38	(Farhadian et al., 2021)	Hidroxietilcelulose modificada	93%
39	(Charitha & Rao, 2018)	Pullulan (polissacarídeo fúngico)	89%
40	(Chugh, Singh, Poddar, et al., 2020)	cinco diferentes bases de Schiff de cinamaldeído de quitosana (Chi-Cn1-5) usando quitosana e cinamaldeído como unidades monoméricas	não informado
41	(Nadi et al., 2019)	extrato de algas marinhas invasivas Sargassum muticum (ESM)	97%
42	(Pozzo et al., 2019)	revestimentos de quitosana pura e de quitosana	não informado
43	(Chauhan et al., 2018)	Quitosana funcionalizada com tiosemicarbazida e tiocarbo-hidrazida	92%
44	(Chauhan et al., 2019)	modificação química da quitosana usando 4-amino-5-metil-1,2,4-triazol-3-tiol.	95%
45	(Macedo et al., 2019)	Carboximetilquitosana (CMC)	67% à 80%

Fonte: Autores.

4.1 Quitosana

A quitosana é um biopolímero de ocorrência natural, podendo ser obtido como produto da reação de desacetilação alcalina da quitina, que é um polissacarídeo encontrado nas cascas de crustáceos, paredes celulares de fungos e cutículas de insetos (Giuliani et al., 2018; Heise et al., 2017). Devido suas propriedades como biocompatibilidade, atividade antibacteriana, não toxicidade, biodegradabilidade e capacidade de formar bons filmes, a quitosana tem despertado o interesse da comunidade científica nos últimos anos (Clifford et al., 2018; Gebhardt et al., 2012). Assim, os revestimentos à base de quitosana podem ser aplicados em diversos setores, como na produção de materiais biomédicos, biossensores, indústria alimentícia, indústria têxtil e cosmética, entre outras aplicações (Carneiro et al., 2015; Clavijo et al., 2016).

Em geral, os polímeros da família dos polissacarídeos são considerados como potenciais inibidores naturais devido seus sítios ativos que interagem com os íons metálicos na solução (Luo et al., 2019; Umoren et al., 2018a). Entre eles, a quitosana é um polissacarídeo adequado como inibidor verde de aço macio e liga de alumínio no meio corrosivo (Ashassi-Sorkhabi & Kazempour, 2020), devido ao seu maior número de locais de adsorção e compatibilidade ecológica (An et al., 2015; Sangeetha et al., 2015). O mecanismo de inibição de corrosão da quitosana e seus derivados está ilustrado na Figura 5.

Apesar de suas vantagens, a baixa solubilidade em água da quitosana limita seu uso como um inibidor de corrosão (Figura 5a). A carboximetilquitosana, como um derivado da quitosana, resolve o problema de solubilidade em água, ao mesmo tempo que retém o número de locais de adsorção na quitosana, que podem obter um melhor efeito protetor (Figura 5b) (El Mouaden et al., 2018).

A carboximetilquitosana foi modificada e dois derivados da carboximetilquitosana foram preparados pela adição de amônio quaternário e grupos de base de Schiff. Experimentos eletroquímicos e de perda de peso foram usados para testar o efeito dos inibidores de corrosão, enquanto SEM-EDS, AFM foram usados para estudar o mecanismo de proteção dos inibidores de corrosão Os resultados teóricos e práticos mostram que os derivados sintéticos podem adsorver melhor na superfície do metal e formar uma película protetora mais forte (Figura 5c). Foi feita a análise da corrosão por dióxido de carbono do aço P110 em 3,6% em peso de solução de NaCl a 80 ℃. Na concentração de 100 mg.L-1, CHC e CAHC atingiram eficiências de inibição máximas de 87,97% e 93,95%, respectivamente. Além disso, comparando o potencial de corrosão antes e depois da adição de inibidores, o desvio máximo do CHC é 48 mV, enquanto o do CAHC é 36 mV. Seja na direção do cátodo ou na direção do ânodo, o deslocamento do potencial de corrosão é inferior a 85 mV, o que pode ser uma forte evidência de CHC e CAHC pertencentes a inibidores de corrosão de tipo misto. (Zhao et al., 2020).

Figura 5. Mecanismo de inibição da corrosão da quitosana e seus derivados.

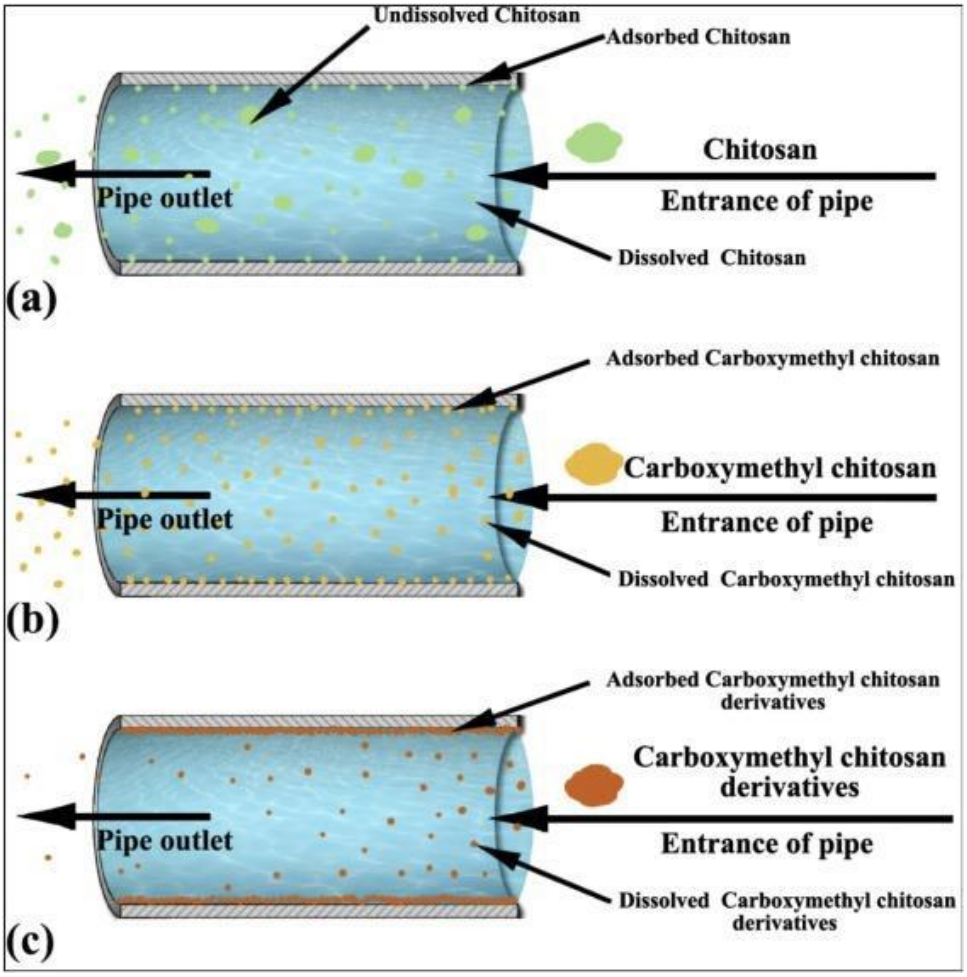

Fonte: El Mouaden et al. (2018)

A copolimerização, em particular, é uma ferramenta de modificação química que permite a introdução de cadeias de polímero solúvel em água na quitosana, e os novos produtos compostos de polímero híbrido resultantes possuem propriedades físicas e químicas inteiramente novas para uma ampla gama de aplicações potenciais (El-Sherbiny et al., 2005; Joshi & Sinha, 2007).

O enxerto de poli (vinil imidazol) na cadeia molecular de carboximetilquitosana (CMCh), foi avaliado como um inibidor de corrosão para o aço API X70 em 1 M HCl. O compósito CMCh-g-PVI reduziu significativamente a corrosão do aço X70 quando comparado com a concentração equimolar de quitosana e carboximetilquitosana no mesmo meio devido à formação de filmes poliméricos de proteção estáveis na superfície do metal (Eduok et al., 2018).

Avaliaram o comportamento de uma carboximetilquitosana (CMC) hidrossolúvel como inibidor preventivo dos processos de corrosão em dutos de aço carbono 1020, utilizados nas instalações de poços de petróleo, considerando a alta salinidade no meio de 3,5% NaCl, sem qualquer adição de ácido ou base. CMC mostrou boas propriedades como inibidor de corrosão em meios onde continha cloreto, e se comportou como um inibidor anódico. A CMC exibiu eficiência inibitória em torno de 80% e 67%, de acordo com a curva de Tafel e impedância eletroquímica, respectivamente, a qual foi atribuída ao mecanismo de quimissorção. (Macedo et al., 2019).

Sambyal et al. (2018) desenvolveram um revestimento composto para proteção contra corrosão do aço carbono em ambiente marinho, utilizando o processo de polimerização química oxidativa in situ para sintetizar poli (anilina-anisidina) /quitosSiO2 em meio aquoso NaCl 3,5%. As medições eletroquímicas demonstraram claramente uma excelente melhoria nas

propriedades de resistência à corrosão do substrato após a aplicação de revestimentos.

O teste de pulverização de sal revelou que os revestimentos compostos podem resistir sob condições de corrosão acelerada de alto teor de sal e umidade por períodos prolongados. A melhora na resistência à corrosão dos revestimentos compostos é atribuída à combinação eficaz de enchimentos (SiO2 nanopartículas), biopolímero (quitosana) em matriz condutora (poli (anilina-anisidina)) (Sambyal et al., 2018).

Os revestimentos de quitosana atuam como uma barreira física e fornecem proteção contra a corrosão, retardando a difusão de espécies corrosivas através do revestimento e inibindo a transferência de carga entre locais anódicos e catódicos (Carneiro et al., 2013). Portanto, a modificação da quitosana para aumentar sua rigidez e obter propriedade de barreira superior melhoraria suas propriedades anticorrosão.

A quitosana pode ser auto reticulada ligando uma molécula a outra com reticuladores como tripolifosfato (TPP) para ligação iônica ou glutaraldeído (GA) para ligações covalentes (Umoren et al., 2020). Os inibidores de corrosão, sejam inorgânicos ou orgânicos, são comumente usados em revestimentos de proteção para minimizar a degradação da corrosão de substratos metálicos (Izadi et al., 2018). Eles podem retardar a taxa de corrosão afetando o processo de corrosão das reações anódicas, onde os íons metálicos se difundem para a solução a partir do ânodo, reduzindo as reações catódicas, onde os elétrons fluem do metal para um aceptor. Portanto, exceto o aglutinante e o enchimento que têm impacto nas propriedades de barreira dos revestimentos, os inibidores de corrosão também podem ajudar a reduzir a possibilidade de ocorrência de reações redox na interface metal/solução.

Foi desenvolvido por Bahari et al. (2020) um revestimento nanocompósitos à base de quitosana para proteção anticorrosiva de cobre. A superfície de cobre foi primeiro preparada com ácido mercaptocarboxílico para facilitar a formação de revestimentos de quitosana no cobre por meio da interação de ácido carboxílico e grupos amina através da automontagem. Para testar os efeitos do enchimento inorgânico, inibidor de corrosão, bem como a reticulação da matriz polimérica na proteção corrosiva do cobre, diferentes revestimentos empregando aglutinante de quitosana à base de água com uma variedade de composições contendo inibidor de corrosão bem conhecido, 2-mercaptobenzotiazol (MBT), e NPs de sílica em matrizes de quitosana não reticulada e reticulada com GA foram desenvolvidas e aplicadas a placas de cobre.

Os efeitos sinérgicos de diferentes composições e suas porcentagens em peso no revestimento foram estudados para estabelecer sua influência na eficiência de inibição de corrosão, além da aplicação na prevenção de corrosão. Verificou-se que após a reticulação dos revestimentos de quitosana, uma maior resistência à corrosão poderia ser alcançada e a maior eficiência de inibição para revestimentos de nanocompósitos de quitosana é calculada como 85%, mostra a eficiência aprimorada do nanocompósito e o potencial dos revestimentos de quitosana na prevenção da corrosão do cobre (Bahari et al., 2020).

Quitosana (CS) foi reticulada utilizando cinamaldeído (Cinn) em um procedimento de etapa única após irradiação de microondas para produzir quitosana modificada por cinamaldeído (Cinn-CS). O Cinn-CS sintetizado foi usado como um novo inibidor de corrosão para cobre em ácido clorídrico 1 M.L-1. O inibidor Cinn-CS funcionou por adsorção na superfície do cobre e mostrou uma eficiência de inibição de> 89% na dose de 1000 mg.L-1, além de exibir um tipo misto de desempenho de inibição com natureza catódica. (EL. Mouaden et al., 2020).

Foi investigada a influência do grau de reticulação de revestimentos de quitosana, reticulada com genipina, na proteção contra corrosão da liga de magnésio AZ31 em um fluido corporal simulado (SBF). Os revestimentos de quitosana pura e de quitosana reticulada com 1 mmol de genipina são eficientes na proteção da https://www-sciencedirect.ez6.periodicos.capes.gov.br/topics/materials-science/magnesium-alloysAZ31 da corrosão em SBF, porém os resultados obtidos usando uma solução de NaCl a 3,5% em peso, mostram que um aumento no grau de reticulação não é benéfico para o nível de proteção dos revestimentos em SBF, sendo que revestimentos de quitosana com grau de reticulação de até 42% são eficientes na proteção da liga em SBF, com desempenho superior a revestimentos semelhantes relatados na

literatura. Com graus de reticulação mais elevados, o revestimento torna-se frágil e suscetível a rachaduras, diminuindo suas propriedades protetoras (Pozzo et al., 2019).

A quitosana pode ser degradada em oligossacarídeos de quitosana solúveis em água de baixo peso molecular por peróxido de hidrogênio (Chang et al., 2001), quitinas e (Sørbotten et al., 2005) e peroxotungstato (Ma et al., 2014).

Cui et al., 2019, avaliaram oligossacarídeos de quitosana com boa solubilidade em água como material de partida e sintetizaram dois derivados de oligossacarídeos de quitosana, sal de amônio quaternário de oligossacarídeo N-propil quitosana (PHC) e sal de amônio quaternário de N-benzil quitosana (BHC) para proteger o aço P110 em uma solução saturada de CO2 com 3,5% em peso de NaCl à 80 ℃. A eficiência da inibição aumentou conforme a concentração do inibidor aumentou. Nas concentrações de PHC e BHC de 100 mg.L-1, as eficiências de inibição foram 85,70% e 88,59%, respectivamente. Medições de energia dispersiva de raios-X (EDX), ângulo de contato e espectroscopia de impedância eletroquímica (EIS) mostraram que os inibidores foram adsorvidos com sucesso à superfície do aço P110. Os resultados da polarização potenciodinâmica indicaram que ambos os compostos eram inibidores do tipo misto.

Uma alternativa é realizar a funcionalização química da quitosana e usá-lo como um inibidor de corrosão. A base de Schiff sintetizada é um composto químico seguro e ambientalmente benigno de acordo com as diretrizes do PARCOM, a presença de ligação imina (−HC = N) pode aumentar sua adsorção e efeito de inibição de corrosão (Antony et al., 2019; Singh et al., 2019) e é muito mais solúvel em comparação com a quitosana não modificada (Anush et al., 2018; Baran & Menteş, 2015).

Uma base de Schiff de quitosana foi sintetizada pela reação do quitosana com salicilaldeído (SCSB) como um inibidor da corrosão para o aço J55 em CO2 saturado 3,5% de NaCl, a 65 °C. O efeito de inibição da corrosão foi analisado usando métodos de perda de peso, espectroscopia de impedância eletroquímica (EIS) e polarização potenciodinâmica (PDP). Os resultados do PDP revelaram que o SCSB atua como um inibidor de tipo misto e reduz o processo de corrosão efetivamente a 150 mg.L-1 de concentração com uma eficiência de inibição de 95,2% e taxa de corrosão de 0,444 mm/ano. (Ansari et al., 2020).

Foram sintetizadas cinco diferentes bases de Schiff de cinamaldeído de quitosana (Chi-Cn1-5) usando quitosana e cinamaldeído como unidades monoméricas, variando o grau de substituição (0,73 mL para Chi-Cn1; 1,46 mL para Chi-Cn2; 2,19 mL para Chi-Cn3; 2,92 mL para Chi-Cn4; 3,65 mL para Chi-Cn5), em 0,5M H2SO4. A propriedade anticorrosiva dos biopolímeros foi analisada por Microscopia eletrônica de varredura com espectroscopia dispersiva de energia (SEM-EDS), microscopia de força atômica (AFM), microscopia eletroquímica de varredura (SECM) e espectroscopia de fotoelétrons de raios-X (XPS). Os resultados mostraram que o Chi-Cn5 tem um desempenho melhor contra a corrosão do aço-carbono em meio ácido entre todos os outros biopolímeros devido ao seu grau máximo de substituição (Chugh, Singh, Poddar, et al., 2020).

4.2 Dextrano e dextrina

O Dextrano (DT), como um recurso renovável no ecossistema, está amplamente presente em vários fungos e plantas, como cogumelos, leveduras e aveia. Devido sua biocompatibilidade e estabilidade química, o dextrano e seus derivados são amplamente aplicados nas indústrias alimentícia e farmacêutica. Recentemente, alguns pesquisadores tentaram usar o dextrano como inibidores ecológicos, considerando sua forte afinidade, boa solubilidade e capacidade de adsorção em superfícies metálicas (Charitha et al., 2017; Solomon, Umoren, et al., 2018; Umoren et al., 2020; Umoren & Eduok, 2016).

Dextrano é um polissacarídeo que consiste em cadeias de comprimentos variados de α-D-pirano. A cadeia linear contém ligações α-1,6 glicosídicas entre as moléculas de glicose e os ramos começam nas ligações α-1,3, conforme ilustrado na Figura 6a. Esta ramificação única o distingue de uma dextrina, um polímero de glicose de cadeia linear ligado por ligações α-1,4 ou α-1,6. O dextrano contém vários heteroátomos de oxigênio, conforme ilustrado na Figura 6b, cumprindo assim um

dos requisitos essenciais para um inibidor de corrosão de metal.

Figura 6. (a) A estrutura química do dextrano e **(b)** Modelo de bola e bastão da molécula de dextrano (o heteroátomo que poderia servir como possível local de adsorção é pintado de vermelho).

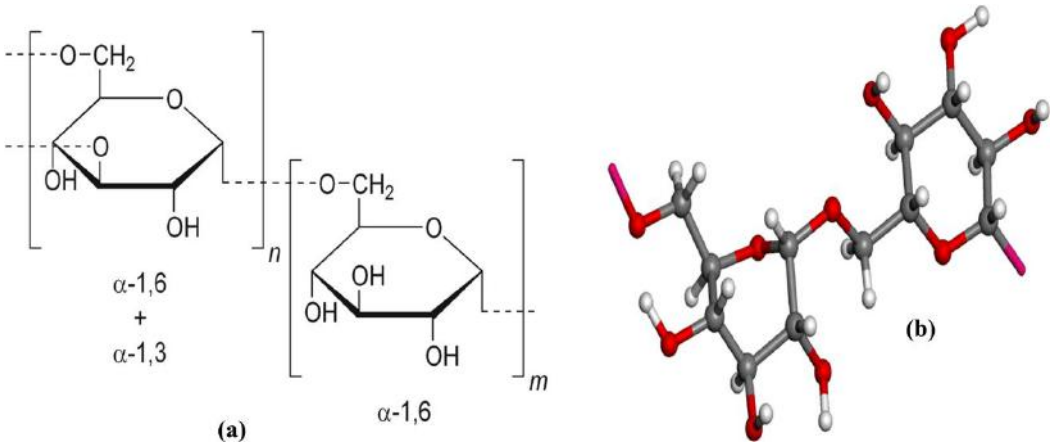

Fonte: Adaptado de Q. H. Zhang et al. (2021)

Foi avaliado o uso de dois derivados de dextrana modificados por aminoácidos (LDT e S-LDT), como inibidores de corrosão para aço carbono em uma simulação de água produzida em poços petrolíferos saturada por CO2. Os aminoácidos conquistaram um interesse renovado na inibição da corrosão devido ao pedido de desenvolvimento sustentável do ambiente ecológico (Kokalj et al., 2020; Olivares et al., 2006). Os grupos carboxila de aminoácidos podem reagir com os grupos hidroxila na estrutura de dextrana, realizando assim a modificação verde dos inibidores de corrosão à base de dextrana. As medições eletroquímicas mostram que o S-LDT exibe um desempenho de inibição com alta eficiência de inibição e estabilidade, com 99,7% após 72 imersão (Q. H. Zhang et al., 2021)

O efeito do peso molecular do dextrano como inibidor de corrosão para aço carbono em meio ácido forte (15% de H2SO4) foi avaliado utilizando as técnicas de perda de peso, eletroquímica (EIS, EFM e PDP) e de triagem de superfície (SEM, EDAX, AFM e XPS). O dextrano com peso molecular de 100.000–200.000 g.mol-1 exibiu a maior eficiência de inibição de 51,38% a 25 °C. Com base nos resultados da polarização potenciodinâmica (PDP), o dextrano se comportou como um inibidor de corrosão do tipo misto. A eficiência de inibição do dextrano varia inversamente com o peso molecular, mas diretamente com a temperatura (Solomon, Umoren, et al., 2018). Também foi avaliada a incorporação de nanopartículas de prata (AgNPs) em matrizes de dextrano e combinação com KI 1 mM com o intuito de aumentar a eficiência de inibição do dextrano. A capacidade protetora do dextrano aumentou de 51,38% para 86,82% por infusão de AgNPs e para 94,21% por combinação com KI a 25 ° C. Os resultados da análise de superfície confirmam a presença de moléculas de aditivos na superfície metálica estudada. Os resultados de XPS revelam que os AgNPs estão na forma de óxido, enquanto os íons iodeto estão na forma de triiodeto e íons pentaiodeto na superfície do metal (Solomon, Umoren, et al., 2018).

A síntese do copolímero de dextrina grafitizado com acetato de polivinila foi aplicada como inibidor de corrosão para o aço carbono em solução de 15% de HCl. Foram feitas medições eletroquímicas para comparar as propriedades anticorrosivas da dextrina e seu copolímero. Os resultados do estudo de polarização confirmaram que ambos os polímeros eram do tipo misto. O copolímero de enxerto sintetizado apresentou excelente eficiência anticorrosiva, 98,39%, em comparação com a dextrina nativa ,84,56%, conforme confirmado por estudos eletroquímicos (Biswas et al., 2019).

4.3 Celulose

A celulose é um biopolímero de carboidrato existente em maior quantidade em comparação com outros biopolímeros, e encontra-se nos tecidos da planta, constituindo cerca de um terço destas, tendo aplicações farmacêuticas, cosméticas e alimentícias (Nwanonenyi et al., 2016; Solomon et al., 2010). Os derivados da celulose apresentam uma reatividade química na qual podem ser usados como inibidores de corrosão (Cheng et al., 2007; Nwanonenyi et al., 2016; Umoren et al., 2018b).

A carboximetilcelulose (CMC) e a hidroxiletilcelulose (HEC) foram avaliadas como inibidores de corrosão da liga AZ31 Mg em solução de NaCl 3,5% em peso. A eficiência como inibidores de corrosão foi avaliada por Perda de massa, gasometria, espectroscopia de impedância eletroquímica, e técnicas de polarização potenciodinâmica. A CMC acelerou o processo de corrosão da liga de Mg, enquanto que a HEC inibiu moderadamente a corrosão, com eficiência de 64,13% (Umoren et al., 2020).

Outro estudo avaliou aumentar a atividade de inibição da hidroxietilcelulose (HEC) com base na química do poliuretano. Foi analisado o uso da hidroxietilcelulose quimicamente modificada (CHEC), em solução de 15% de HCl em elevadas temperaturas. A capacidade da CHEC em suprimir a corrosão do aço macio (MS) foi avaliada usando técnicas de perda de peso, espectroscopia de impedância eletroquímica (EIS), potencial de circuito aberto (OCP) e polarização potenciodinâmica (PDP), e posteriormente confirmada por campo microscópio eletrônico de varredura por emissão (FESEM), espectroscopia de fotoelétrons de raios-X (XPS), e microscopia de força atômica (AFM). As medições eletroquímicas revelaram que a incorporação de apenas 1% do pré-polímero de poliuretano à estrutura do CHEC aumentou muito sua eficiência de inibição na solução ácida, mesmo em altas temperaturas. O CHEC adsorveu na superfície do MS e funcionou como um inibidor do tipo misto, com uma eficiência de inibição máxima de 93% a 80°C (Farhadian et al., 2021).

O desempenho anticorrosivo de compósitos de celulose-niacina para cobre em soluções de NaCl a 3,5% foi avaliado por meio de técnicas de polarização e espectroscopia de impedância eletroquímica (EIS). As medições de polarização potenciodinâmica confirmaram que os inibidores à base de celulose atuam como um inibidor do tipo misto. A eficiência de inibição do compósito de etilcelulose-niacina (NEC) foi 94,7% superior aos do compósito de celulose-niacina microcristalina (NMCC) e do composto de carboximetilcelulose-niacina (NCMC) que foram 33,2 e 83,4%, respectivamente (Hasanin & Al Kiey, 2020)

4.4 Goma Arábica

A goma arábica (GA) é uma goma natural, feita a partir da exsudação de goma seca que pode ser extraída de algumas espécies de acácias, e é amplamente utilizada em alimentos, litografia, produtos farmacêuticos e cosméticos; sendo altamente solúvel em água e amplamente utilizada como emulsificante e estabilizante na indústria alimentícia e como aglutinante em tintas e composições pirotécnicas. Quimicamente, GA é uma mistura de cálcio, magnésio, sódio e potássio, sais de ácido arábico além de polissacarídeos de alto peso molecular (Manawi et al., 2017).

Métodos eletroquímicos e de simulação molecular foram usados para investigar a aplicação de GA como um polímero natural inibidor de corrosão para aço carbono. Os resultados da análise Tafel mostraram que a GA funciona como um inibidor de corrosão do tipo misto em aço carbono com o potencial de circuito aberto aumentado. Em salmoura sintética, o estudo de isoterma de adsorção mostrou que os filmes inibidores de GA foram formados principalmente por quimissorção. A eficiência de corrosão do GA medida pela curva de polarização, resistência de polarização e medidas de impedância, foram 94,0, 83,5 e 90%, respectivamente (Shen et al., 2019).

Um composto de GA com nanopartículas de prata (AgNPs) foi formulado como inibidor de corrosão para aço carbono em meio 15%HCl e 15% H2SO4, e avaliado por meio de técnicas gravimétricas, eletroquímicas (EIS, EFM, DEIS, & TP) e de avaliação de superfície (SEM, EDAX, AFM e XPS) no estudo anticorrosão. Os resultados mostram que GA-AgNPs atua como

inibidor do tipo misto em solução de H2SO4 a 15% , mas como tipo anódico em solução de HCl a 15%, já a eficiência como inibidor de corrosão se dá em soluções de HCl com 88,60% (Solomon, Gerengi, et al., 2018).

5. Considerações Finais

O uso de biopolímeros está ganhando terreno na fabricação de formulações de inibidores para várias aplicações práticas, e sua química é simples, uma vez que o mecanismo de adsorção que os acompanha envolve adsorção física em superfícies metálicas ou por quimissorção. Algumas misturas de polímeros de carboidratos também são conhecidas por conterem constituintes químicos capazes de formar camadas de passivação que impedem a passagem de íons corrosivos e moléculas através da interface metal/solução.

Biopolímeros de carboidratos, como usados nesta revisão, são macro compostos que possuem unidades monoméricas ligadas covalentemente para formar longas cadeias de açúcar macromoleculares com massas moleculares relativamente altas. Na inibição de corrosão, eles representam um conjunto de macromoléculas quimicamente estáveis, biodegradáveis e ecologicamente corretas com forças de inibição que podem garantir a proteção de superfícies metálicas; tornando-os revestimentos de proteção e revestimentos de metal eficazes.

Este artigo de revisão sistemática descreveu os avanços recentes no que diz respeito à utilização eficiente de biopolímeros a base de carboidratos como inibidores de corrosão. Todos os artigos listados nesta revisão sistemática relataram que a modificação química dos biopolímeros a base de carboidratos melhorou a eficiência dos compósitos no que tange a inibição da corrosão. É nítido que a maioria dos artigos abordam o problema da corrosão em dutos e poços de petróleo, onde o meio é altamente corrosivo.

A quitosana é o biopolímero mais amplamente estudado, seguida do dextrano das gomas e da celulose, seja in natura ou em compósitos. Extratos e outros polissacarídeos também foram avaliados quando a eficiência como inibidores de corrosão.

O metal mais estudado para a análise de corrosão foi o aço carbono, visto que é o metal mais utilizado no mundo, desde dutos e poços de petróleo a infraestrutura e construção civil. Metais como cobre, ligas de alumínio e magnésio e aço inoxidável também foram abordados, porém em quantidade muito inferior.

Para aceleração da corrosão os artigos mostram que o uso de soluções de HCl e NaCl são as mais utilizadas para se aproximar da realidade do processo corrosivo.

No monitoramento da corrosão os métodos mais empregados foram a Espectroscopia de impedância eletroquímica (EIS), Polarização potenciodinâmica (PDP), perda de peso, Microscopia eletrônica de varredura (SEM), Potencial de circuito aberto (OCP) e Espectroscopia de infravermelho com transformada de Fourier (FT-IR). Também foi abordada o uso de ferramentas computacionais/teóricas, como as simulações de Dinâmica Molecular (MD), que além de promoverem uma maior compreensão dos processos de corrosão ajudam no estudo da reatividade dos inibidores para o entendimento da adsorção nas superfícies.

A maioria dos artigos analisados apresentaram estudos onde a eficiência contra a corrosão é superior a 90%, porém muitos destes artigos evidenciam que tal proteção contra corrosão ocorre por um curto tempo, concluindo que a solubilidade do biopolímeros pode interferir na proteção no longo prazo. A quitosana possui um ótimo desempenho, segundo os autores estudados, porém a eficiência do polímero é diminuída com o passar do tempo, já seus compósitos carboximetilcelulose (CMC) e a hidroxiletilcelulose (HEC), por exemplo, apresentam melhores desempenho no longo prazo, mostrando que uma menor solubilidade melhora a eficiência de inibição no longo prazo. Os compósitos de etilcelulose modificados e/ou micro cristalizados e hidroxietilcelulose apresentaram eficiência superior a 90% mesmo em períodos maiores de análise.

Para trabalhos futuros sugere-se que seja estudado a eficiência das técnicas utilizadas para avaliação da inibição da corrosão bem como o meio aquoso que simula o ambiente corrosivo, visto que este impacta diretamente nos resultados

apresentados.

Agradecimentos

Os autores agradeceram a Rede de Biodiversidade e Biotecnologia da Amazônia Legal (BIONORTE) e a Coordenação de Aperfeiçoamento de Pessoal de Nível Superior (CAPES) por apoiar o trabalho.

Referências

An, Y., Jiang, G., Ren, Y., Zhang, L., Qi, Y., & Ge, Q. (2015). An environmental friendly and biodegradable shale inhibitor based on chitosan quaternary ammonium salt. *Journal of Petroleum Science and Engineering*, 135, 253–260. https://doi.org/10.1016/j.petrol.2015.09.005

Ansari, K. R., Chauhan, D. S., Quraishi, M. A., Mazumder, M. A. J., & Singh, A. (2020). Chitosan Schiff base: an environmentally benign biological macromolecule as a new corrosion inhibitor for oil & gas industries. *International Journal of Biological Macromolecules*, 144, 305–315. https://doi.org/10.1016/j.ijbiomac.2019.12.106

Antony, R., Arun, T., & Manickam, S. T. D. (2019). A review on applications of chitosan-based Schiff bases. *International Journal of Biological Macromolecules*, 129, 615–633. https://doi.org/10.1016/j.ijbiomac.2019.02.047

Anush, S. M., Vishalakshi, B., Kalluraya, B., & Manju, N. (2018). Synthesis of pyrazole-based Schiff bases of Chitosan: Evaluation of antimicrobial activity. *International Journal of Biological Macromolecules*, 119, 446–452. https://doi.org/10.1016/j.ijbiomac.2018.07.129

Ashassi-Sorkhabi, H., & Kazempour, A. (2020). Chitosan, its derivatives and composites with superior potentials for the corrosion protection of steel alloys: A comprehensive review. *Carbohydrate Polymers*, 237(March), 116110. https://doi.org/10.1016/j.carbpol.2020.116110

Avérous, L., & Pollet, E. (2012). Environmental Silicate Nano-Biocomposites. *Green Energy and Technology*, 50. https://doi.org/10.1007/978-1-4471-4108-2

Azmana, M., Mahmood, S., Hilles, A. R., Rahman, A., Arifin, M. A. Bin, & Ahmed, S. (2021). A review on chitosan and chitosan-based bionanocomposites: Promising material for combatting global issues and its applications. In *International Journal of Biological Macromolecules* (Vol. 185, pp. 832–848). https://doi.org/10.1016/j.ijbiomac.2021.07.023

Bahari, H. S., Ye, F., Carrillo, E. A. T., Leliopoulos, C., Savaloni, H., & Dutta, J. (2020). Chitosan nanocomposite coatings with enhanced corrosion inhibition effects for copper. *International Journal of Biological Macromolecules*, 162, 1566–1577. https://doi.org/10.1016/j.ijbiomac.2020.08.035

Baran, T., & Menteş, A. (2015). Cu(II) and Pd(II) complexes of water soluble O-carboxymethyl chitosan Schiff bases: Synthesis, characterization. *International Journal of Biological Macromolecules*, 79, 542–554. https://doi.org/10.1016/j.ijbiomac.2015.05.021

Biswas, A., Das, D., Lgaz, H., Pal, S., & Nair, U. G. (2019). Biopolymer dextrin and poly (vinyl acetate) based graft copolymer as an efficient corrosion inhibitor for mild steel in hydrochloric acid: Electrochemical, surface morphological and theoretical studies. Journal of Molecular Liquids, 275, 867–878. https://doi.org/10.1016/j.molliq.2018.11.095

Brito, G. F., Agrawal, P., Araújo, E. M., & Mélo, T. J. A. (2011). Biopolímeros, Polímeros Biodegradáveis e Polímeros Verdes. *Revista Eletrônica de Materiais e Processos*, 6(2), 127–139. http://www.ncbi.nlm.nih.gov/pubmed/19998664

Carneiro, J., Tedim, J., Fernandes, S. C. M., Freire, C. S. R., Gandini, A., Ferreira, M. G. S., & Zheludkevich, M. L. (2013). Functionalized chitosan-based coatings for active corrosion protection. *Surface and Coatings Technology*, 226, 51–59. https://doi.org/10.1016/j.surfcoat.2013.03.035

Carneiro, J., Tedim, J., & Ferreira, M. G. S. (2015). Chitosan as a smart coating for corrosion protection of aluminum alloy 2024: A review. *Progress in Organic Coatings*, 89, 348–356. https://doi.org/10.1016/j.porgcoat.2015.03.008

Chai, C., Xu, Y., Shi, S., Zhao, X., Wu, Y., Xu, Y., & Zhang, L. (2018). Functional polyaspartic acid derivatives as eco-friendly corrosion inhibitors for mild steel in 0.5 M H2SO4 solution. *RSC Advances*, 8(44), 24970–24981. https://doi.org/10.1039/c8ra03534b

Chang, K. L. B., Tai, M. C., & Cheng, F. H. (2001). Kinetics and products of the degradation of chitosan by hydrogen peroxide. In Journal of Agricultural and *Food Chemistry* (Vol. 49, Issue 10, pp. 4845–4851). https://doi.org/10.1021/jf001469g

Charitha, B. P., Chenan, A., & Rao, P. (2017). Enhancement of Surface Coating Characteristics of Epoxy Resin by Dextran: An Electrochemical Approach. In *Industrial and Engineering Chemistry Research* (Vol. 56, Issue 5, pp. 1137–1147). https://doi.org/10.1021/acs.iecr.6b03274

Charitha, B. P., & Rao, P. (2018). Pullulan as a potent green inhibitor for corrosion mitigation of aluminum composite: Electrochemical and surface studies. *International Journal of Biological Macromolecules*, 112, 461–472. https://doi.org/10.1016/j.ijbiomac.2018.01.218

Chauhan, D. S., Ansari, K. R., Sorour, A. A., Quraishi, M. A., Lgaz, H., & Salghi, R. (2018). Thiosemicarbazide and thiocarbohydrazide functionalized chitosan as ecofriendly corrosion inhibitors for carbon steel in hydrochloric acid solution. *International Journal of Biological Macromolecules*, 107, 1747–1757. https://doi.org/10.1016/j.ijbiomac.2017.10.050

Chauhan, D. S., Mouaden, K. EL, Quraishi, M. A., & Bazzi, L. (2020). Aminotriazolethiol-functionalized chitosan as a macromolecule-based bioinspired corrosion inhibitor for surface protection of stainless steel in 3.5% NaCl. *International Journal of Biological Macromolecules*, 152, 234–241. https://doi.org/10.1016/j.ijbiomac.2020.02.283

Chauhan, D. S., Quraishi, M. A., & Qurashi, A. (2021). Recent trends in environmentally sustainable Sweet corrosion inhibitors. *Journal of Molecular Liquids*, 326, 115117. https://doi.org/10.1016/j.molliq.2020.115117

Chauhan, D. S., Quraishi, M. A., Sorour, A. A., Saha, S. K., & Banerjee, P. (2019). Triazole-modified chitosan: A biomacromolecule as a new environmentally benign corrosion inhibitor for carbon steel in a hydrochloric acid solution. *RSC Advances*, 9(26), 14990–15003. https://doi.org/10.1039/c9ra00986h

Cheng, S., Chen, S., Liu, T., Chang, X., & Yin, Y. (2007). Carboxymenthylchitosan as an ecofriendly inhibitor for mild steel in 1 M HCl. *Materials Letters*, 61(14–15), 3276–3280. https://doi.org/10.1016/j.matlet.2006.11.102

Chugh, B., Singh, A. K., Chaouiki, A., Salghi, R., Thakur, S., & Pani, B. (2020). A comprehensive study about anti-corrosion behaviour of pyrazine carbohydrazide: Gravimetric, electrochemical, surface and theoretical study. *Journal of Molecular Liquids*, 299, 112160. https://doi.org/10.1016/j.molliq.2019.112160

Chugh, B., Singh, A. K., Poddar, D., Thakur, S., Pani, B., & Jain, P. (2020). Relation of degree of substitution and metal protecting ability of cinnamaldehyde modified chitosan. *Carbohydrate Polymers*, 234, 115945. https://doi.org/10.1016/j.carbpol.2020.115945

Clavijo, S., Membrives, F., Quiroga, G., Boccaccini, A. R., & Santillán, M. J. (2016). Electrophoretic deposition of chitosan/Bioglass® and chitosan/Bioglass®/TiO2 composite coatings for bioimplants. *Ceramics International*, 42(12), 14206–14213. https://doi.org/10.1016/j.ceramint.2016.05.178

Clifford, A., Pang, X., & Zhitomirsky, I. (2018). Biomimetically modified chitosan for electrophoretic deposition of composites. Colloids and Surfaces A: *Physicochemical and Engineering Aspects*, 544(December 2017), 28–34. https://doi.org/10.1016/j.colsurfa.2018.02.028

Cui, G., Guo, J., Zhang, Y., Zhao, Q., Fu, S., Han, T., Zhang, S., & Wu, Y. (2019). Chitosan oligosaccharide derivatives as green corrosion inhibitors for P110 steel in a carbon-dioxide-saturated chloride solution. *Carbohydrate Polymers*, 203, 386–395. https://doi.org/10.1016/j.carbpol.2018.09.038

Darmokoesoemo, H., Suyanto, S., Anggara, L. S., Amenaghawon, A. N., & Kusuma, H. S. (2018). Application of carboxymethyl chitosan-benzaldehyde as anticorrosion agent on steel. *International Journal of Chemical Engineering*, 2018. https://doi.org/10.1155/2018/4397867

Eduok, U., Ohaeri, E., & Szpunar, J. (2018). Electrochemical and surface analyses of X70 steel corrosion in simulated acid pickling medium: Effect of poly (N-vinyl imidazole) grafted carboxymethyl chitosan additive. Electrochimica Acta, 278, 302–312. https://doi.org/10.1016/j.electacta.2018.05.060

El-Sherbiny, I. M., Lins, R. J., Abdel-Bary, E. M., & Harding, D. R. K. (2005). Preparation, characterization, swelling and in vitro drug release behaviour of poly[N-acryloylglycine-chitosan] interpolymeric pH and thermally-responsive hydrogels. *European Polymer Journal*, 41(11), 2584–2591. https://doi.org/10.1016/j.eurpolymj.2005.05.035

EL. Mouaden, K., Chauhan, D. S., Quraishi, M. A., Bazzi, L., & Hilali, M. (2020). Cinnamaldehyde-modified chitosan as a bio-derived corrosion inhibitor for acid pickling of copper: Microwave synthesis, experimental and computational study. *International Journal of Biological Macromolecules*, 164, 3709–3717. https://doi.org/10.1016/j.ijbiomac.2020.08.137

El Mouaden, K., El Ibrahimi, B., Oukhrib, R., Bazzi, L., Hammouti, B., Jbara, O., Tara, A., Chauhan, D. S., & Quraishi, M. A. (2018). Chitosan polymer as a green corrosion inhibitor for copper in sulfide-containing synthetic seawater. *International Journal of Biological Macromolecules*, 119, 1311–1323. https://doi.org/10.1016/j.ijbiomac.2018.07.182

Fardioui, M., Rbaa, M., Benhiba, F., Galai, M., Guedira, T., Lakhrissi, B., Warad, I., & Zarrouk, A. (2021). Bio-active corrosion inhibitor based on 8-hydroxyquinoline-grafted-Alginate: Experimental and computational approaches. *Journal of Molecular Liquids*, 323, 114615. https://doi.org/10.1016/j.molliq.2020.114615

Farhadian, A., Assar Kashani, S., Rahimi, A., Oguzie, E. E., Javidparvar, A. A., Nwanonenyi, S. C., Yousefzadeh, S., & Nabid, M. R. (2021). Modified hydroxyethyl cellulose as a highly efficient eco-friendly inhibitor for suppression of mild steel corrosion in a 15% HCl solution at elevated temperatures. *Journal of Molecular Liquids*, 338, 116607. https://doi.org/10.1016/j.molliq.2021.116607

Farhadian, A., Varfolomeev, M. A., Shaabani, A., Nasiri, S., Vakhitov, I., Zaripova, Y. F., Yarkovoi, V. V., & Sukhov, A. V. (2020). Sulfonated chitosan as green and high cloud point kinetic methane hydrate and corrosion inhibitor: Experimental and theoretical studies. *Carbohydrate Polymers*, 236, 116035. https://doi.org/10.1016/j.carbpol.2020.116035

Figueiredo, E. P., & Meira, G. (2013). Corrosión de armadura de estructuras de hormigón. ALCONPAT Internacional - Associación Latinoamericana de Control de Calidad, *Patología y Recuperación de La Construcción*, 30.

Franchetti, S. M. M., & Marconato, J. C. (2006). Polímeros biodegradáveis - uma solução parcial para diminuir a quantidade dos resíduos plásticos. *Química Nova*, 29(4), 811–816. https://doi.org/10.1590/s0100-40422006000400031

Gebhardt, F., Seuss, S., Turhan, M. C., Hornberger, H., Virtanen, S., & Boccaccini, A. R. (2012). Characterization of electrophoretic chitosan coatings on stainless steel. *Materials Letters*, 66(1), 302–304. https://doi.org/10.1016/j.matlet.2011.08.088

Giuliani, C., Pascucci, M., Riccucci, C., Messina, E., Salzano de Luna, M., Lavorgna, M., Ingo, G. M., & Di Carlo, G. (2018). Chitosan-based coatings for corrosion protection of copper-based alloys: A promising more sustainable approach for cultural heritage applications. *Progress in Organic Coatings*, 122(April), 138–146. https://doi.org/10.1016/j.porgcoat.2018.05.002

Gupta, N. K., Joshi, P. G., Srivastava, V., & Quraishi, M. A. (2018). Chitosan: A macromolecule as green corrosion inhibitor for mild steel in sulfamic acid useful for sugar industry. *International Journal of Biological Macromolecules*, 106, 704–711. https://doi.org/10.1016/j.ijbiomac.2017.08.064

Hasanin, M. S., & Al Kiey, S. A. (2020). Environmentally benign corrosion inhibitors based on cellulose niacin nano-composite for corrosion of copper in sodium chloride solutions. *International Journal of Biological Macromolecules*, 161, 345–354. https://doi.org/10.1016/j.ijbiomac.2020.06.040

Hassan, R. M., Ibrahim, S. M., Takagi, H. D., & Sayed, S. A. (2018). Kinetics of corrosion inhibition of aluminum in acidic media by water-soluble natural polymeric chondroitin-4-sulfate as anionic polyelectrolyte inhibitor. *Carbohydrate Polymers*, 192, 356–363. https://doi.org/10.1016/j.carbpol.2018.03.066

Heise, S., Höhlinger, M., Hernández, Y. T., Palacio, J. J. P., Rodriquez Ortiz, J. A., Wagener, V., Virtanen, S., & Boccaccini, A. R. (2017). Electrophoretic deposition and characterization of chitosan/bioactive glass composite coatings on Mg alloy substrates. *Electrochimica Acta*, 232, 456–464. https://doi.org/10.1016/j.electacta.2017.02.081

Hernández-Padrón, G., Rojas, F., & Castaño, V. (2006). Development and testing of anticorrosive SiO2/phenolic-formaldehydic resin coatings. *Surface and Coatings Technology*, 201(3–4), 1207–1214. https://doi.org/10.1016/j.surfcoat.2006.01.070

Izadi, M., Shahrabi, T., & Ramezanzadeh, B. (2018). Active corrosion protection performance of an epoxy coating applied on the mild steel modified with an eco-friendly sol-gel film impregnated with green corrosion inhibitor loaded nanocontainers.pdf. *Applied Surface Science*, 491–505. https://doi.org/https://doi.org/10.1016/j.apsusc.2018.01.185

Jena, G., Anandkumar, B., Vanithakumari, S. C., George, R. P., Philip, J., & Amarendra, G. (2020). Graphene oxide-chitosan-silver composite coating on Cu-Ni alloy with enhanced anticorrosive and antibacterial properties suitable for marine applications. *Progress in Organic Coatings*, 139, 105444. https://doi.org/10.1016/j.porgcoat.2019.105444

Joshi, J. M., & Sinha, V. K. (2007). Ceric ammonium nitrate induced grafting of polyacrylamide onto carboxymethyl chitosan. In Carbohydrate Polymers (Vol. 67, Issue 3, pp. 427–435). https://doi.org/10.1016/j.carbpol.2006.06.021

Koch, G. (2017). Cost of corrosion. In Trends in Oil and Gas Corrosion Research and Technologies: Production and Transmission. Elsevier Ltd. https://doi.org/10.1016/B978-0-08-101105-8.00001-2

Kokalj, A., Behzadi, H., & Farahati, R. (2020). DFT study of aqueous-phase adsorption of cysteine and penicillamine on Fe(110): Role of bond-breaking upon adsorption. *Applied Surface Science*, 514(February), 145896. https://doi.org/10.1016/j.apsusc.2020.145896

Lai, X., Hu, J., Ruan, T., Zhou, J., & Qu, J. (2021). Chitosan derivative corrosion inhibitor for aluminum alloy in sodium chloride solution: A green organic/inorganic hybrid. *Carbohydrate Polymers*, 265, 118074. https://doi.org/10.1016/j.carbpol.2021.118074

Liu, J., Yu, Q., Yu, M., Li, S., Zhao, K., Xue, B., & Zu, H. (2018). Silane modification of titanium dioxide-decorated graphene oxide nanocomposite for enhancing anticorrosion performance of epoxy coatings on AA-2024. *Journal of Alloys and Compounds*, 744, 728–739. https://doi.org/10.1016/j.jallcom.2018.01.267

Luo, X., Ci, C., Li, J., Lin, K., Du, S., Zhang, H., Li, X., Cheng, Y. F., Zang, J., & Liu, Y. (2019). 4-aminoazobenzene modified natural glucomannan as a green eco-friendly inhibitor for the mild steel in 0.5 M HCl solution. *Corrosion Science*, 151(November 2017), 132–142. https://doi.org/10.1016/j.corsci.2019.02.027

Ma, Z., Wang, W., Wu, Y., He, Y., & Wu, T. (2014). Oxidative degradation of chitosan to the low molecular water-soluble chitosan over peroxotungstate as chemical scissors. In PLoS ONE (Vol. 9, Issue 6). https://doi.org/10.1371/journal.pone.0100743

Macedo, R. G. M. de A., Marques, N. do N., Tonholo, J., & Balaban, R. de C. (2019). Water-soluble carboxymethylchitosan used as corrosion inhibitor for carbon steel in saline medium. Carbohydrate Polymers, 205, 371–376. https://doi.org/10.1016/j.carbpol.2018.10.081

Manawi, Y., Kochkodan, V., Mohammad, A. W., & Ali Atieh, M. (2017). Arabic gum as a novel pore-forming and hydrophilic agent in polysulfone membranes. In Journal of Membrane Science (Vol. 529, pp. 95–104). https://doi.org/10.1016/j.memsci.2017.02.002

Marzorati, S., Verotta, L., & Trasatti, S. P. (2019). Green corrosion inhibitors from natural sources and biomass wastes. Molecules, 24(1). https://doi.org/10.3390/molecules24010048

Mobin, M., Basik, M., & Aslam, J. (2018). Boswellia serrata gum as highly efficient and sustainable corrosion inhibitor for low carbon steel in 1 M HCl solution: Experimental and DFT studies. *Journal of Molecular Liquids*, 263, 174–186. https://doi.org/10.1016/j.molliq.2018.04.150

Moher, D., Shamseer, L., Clarke, M., Ghersi, D., Liberati, A., Petticrew, M., Shekelle, P., Stewart, L. A., & Group, P. (2015). Preferred reporting items for systematic review and meta-analysis protocols (PRISMA-P) 2015 statement. 4(1), 1–9. https://doi.org/10.1186/2046-4053-4-1

Nadi, I., Belattmania, Z., Sabour, B., Reani, A., Sahibed-dine, A., Jama, C., & Bentiss, F. (2019). Sargassum muticum extract based on alginate biopolymer as a new efficient biological corrosion inhibitor for carbon steel in hydrochloric acid pickling environment: Gravimetric, electrochemical and surface studies. International Journal of Biological Macromolecules, 141, 137–149. https://doi.org/10.1016/j.ijbiomac.2019.08.253

Negi, H., Verma, P., & Singh, R. K. (2021). A comprehensive review on the applications of functionalized chitosan in petroleum industry. Carbohydrate Polymers, 266. https://doi.org/10.1016/j.carbpol.2021.118125

Neves, R. M., Jr, H. L. O., Zattera, A. J., & Amico, S. C. (2021). Recent studies on modified cellulose/nanocellulose epoxy composites: A systematic review. Carbohydrate Polymers, 255, 1–17.

Nikpour, S., Ramezanzadeh, M., Bahlakeh, G., Ramezanzadeh, B., & Mahdavian, M. (2019). Eriobotrya japonica Lindl leaves extract application for effective corrosion mitigation of mild steel in HCl solution: Experimental and computational studies. *Construction and Building Materials*, 220, 161–176. https://doi.org/10.1016/j.conbuildmat.2019.06.005

Nwanonenyi, S., Ogbobe, O., Madufor, I., & Oguzie, E. (2016). Inhibitive Performance of Hydroxypropyl Cellulose and Potassium Iodide on the Corrosion of Mild Steel in Sulphuric Acid Environment. *American Chemical Science Journal*, 16(2), 1–12. https://doi.org/10.9734/acsj/2016/28250

O'Connor, A., Sargeant, J., & Wood, H. (2017). Systematic reviews. Veterinary Epidemiology: Fourth Edition, 397–420. https://doi.org/10.1002/9781118280249.ch19

Olivares, O., Likhanova, N. V., Gómez, B., Navarrete, J., Llanos-Serrano, M. E., Arce, E., & Hallen, J. M. (2006). Electrochemical and XPS studies of decylamides of α-amino acids adsorption on carbon steel in acidic environment. In *Applied Surface Science* (Vol. 252, Issue 8, pp. 2894–2909). https://doi.org/10.1016/j.apsusc.2005.04.040

Oliveira, J. A. M., de Santana, R. A. C., & Wanderley Neto, A. de O. (2020). Characterization of the chitosan-tungsten composite coating obtained by electrophoretic deposition. Progress in Organic Coatings, 143, 105631. https://doi.org/10.1016/j.porgcoat.2020.105631

Pais, M., George, S. D., & Rao, P. (2021). Glycogen nanoparticles as a potential corrosion inhibitor. International Journal of Biological Macromolecules, 182, 2117–2129. https://doi.org/10.1016/j.ijbiomac.2021.05.185

Pais, M., & Rao, P. (2020). Maltodextrin for corrosion mitigation of zinc in sulfamic acid: Electrochemical, surface and spectroscopic studies. International Journal of Biological Macromolecules, 145, 575–585. https://doi.org/10.1016/j.ijbiomac.2019.12.197

Pakseresht, A., Alizadeh, H., Hanaei, A., Heidarshenas, B., Shahbazkhan, A., & Ahmadi, N. P. (2018). The Effect of accelerator types on the phosphate Zn-%12Ni electrodeposite coating. Material Science & Engineering International Journal, 2(6). https://doi.org/10.15406/mseij.2018.02.00062

Pourhashem, S., Vaezi, M. R., Rashidi, A., & Bagherzadeh, M. R. (2017). Exploring corrosion protection properties of solvent based epoxy-graphene oxide nanocomposite coatings on mild steel. Corrosion Science, 115, 78–92. https://doi.org/10.1016/j.corsci.2016.11.008

Pozzo, L. de Y., Conceição, T. F. da, Spinelli, A., Scharnagl, N., & Nunes Pires, A. T. (2019). The influence of the crosslinking degree on the corrosion protection properties of chitosan coatings in simulated body fluid. Progress in Organic Coatings, 137, 105328. https://doi.org/10.1016/j.porgcoat.2019.105328

Raja, P. B., & Sethuraman, M. G. (2008). Natural products as corrosion inhibitor for metals in corrosive media - A review. Materials Letters, 62(1), 113–116. https://doi.org/10.1016/j.matlet.2007.04.079

Ramezanzadeh, B., Ghasemi, E., Mahdavian, M., Changizi, E., & Mohamadzadeh Moghadam, M. H. (2015). Covalently-grafted graphene oxide nanosheets to improve barrier and corrosion protection properties of polyurethane coatings. Carbon, 93, 555–573. https://doi.org/10.1016/j.carbon.2015.05.094

Rani, B. E. A., & Basu, B. B. J. (2012). Green inhibitors for corrosion protection of metals and alloys: An overview. International Journal of Corrosion, 2012(6), 16–25. https://doi.org/10.1155/2012/380217

Rbaa, M., Benhiba, F., Hssisou, R., Lakhrissi, Y., Lakhrissi, B., Touhami, M. E., Warad, I., & Zarrouk, A. (2021). Green synthesis of novel carbohydrate polymer chitosan oligosaccharide grafted on D-glucose derivative as bio-based corrosion inhibitor. Journal of Molecular Liquids, 322, 114549. https://doi.org/10.1016/j.molliq.2020.114549

Rbaa, M., Fardioui, M., Verma, C., Abousalem, A. S., Galai, M., Ebenso, E. E., Guedira, T., Lakhrissi, B., Warad, I., & Zarrouk, A. (2020). 8-Hydroxyquinoline based chitosan derived carbohydrate polymer as biodegradable and sustainable acid corrosion inhibitor for mild steel: Experimental and computational analyses. International Journal of Biological Macromolecules, 155, 645–655. https://doi.org/10.1016/j.ijbiomac.2020.03.200

Ribeiro, D. V., & Helene, P. (2013). Corrosão em Estruturas de Concreto: Teoria, Controle e Métodos de Análise. Elsevier, 1, 240 p. https://barnard.edu/sites/default/files/inline/student_user_guide_for_spss.pdf%0Ahttp://www.ibm.com/support%0Ahttp://www.spss.com/sites/dm-book/legacy/ProgDataMgmt_SPSS17.pdf%0Ahttps://www.neps-data.de/Portals/0/Working Papers/WP_XLV.pdf%0Ahttp://www2.psy

Sambyal, P., Ruhi, G., Dhawan, S. K., Bisht, B. M. S., & Gairola, S. P. (2018). Enhanced anticorrosive properties of tailored poly(aniline-anisidine)/chitosan/SiO2 composite for protection of mild steel in aggressive marine conditions. Progress in Organic Coatings, 119, 203–213. https://doi.org/10.1016/j.porgcoat.2018.02.014

Sangeetha, Y., Meenakshi, S., & SairamSundaram, C. (2015). Corrosion mitigation of N-(2-hydroxy-3-trimethyl ammonium)propyl chitosan chloride as inhibitor on mild steel. International Journal of Biological Macromolecules, 72, 1244–1249. https://doi.org/10.1016/j.ijbiomac.2014.10.044

Sharma, S. K., Peter, A., & Obot, I. B. (2015). Potential of Azadirachta indica as a green corrosion inhibitor against mild steel, aluminum, and tin: a review. Journal of Analytical Science and Technology, 6(1). https://doi.org/10.1186/s40543-015-0067-0

Shen, C., Alvarez, V., Koenig, J. D. B., & Luo, J. L. (2019). Gum Arabic as corrosion inhibitor in the oil industry: experimental and theoretical studies. Corrosion Engineering Science and Technology, 54(5), 444–454. https://doi.org/10.1080/1478422X.2019.1613780

Singh, P., Chauhan, D. S., Chauhan, S. S., Singh, G., & Quraishi, M. A. (2019). Chemically modified expired Dapsone drug as environmentally benign corrosion inhibitor for mild steel in sulphuric acid useful for industrial pickling process. Journal of Molecular Liquids, 286, 110903. https://doi.org/10.1016/j.molliq.2019.110903

Skale, S., Doleček, V., & Slemnik, M. (2007). Substitution of the constant phase element by Warburg impedance for protective coatings. Corrosion Science, 49(3), 1045–1055. https://doi.org/10.1016/j.corsci.2006.06.027

Solomon, M. M., Gerengi, H., Umoren, S. A., Essien, N. B., Essien, U. B., & Kaya, E. (2018). Gum Arabic-silver nanoparticles composite as a green anticorrosive formulation for steel corrosion in strong acid media. Carbohydrate Polymers, 181, 43–55. https://doi.org/10.1016/j.carbpol.2017.10.051

Solomon, M. M., Umoren, S. A., Obot, I. B., Sorour, A. A., & Gerengi, H. (2018). Exploration of Dextran for Application as Corrosion Inhibitor for Steel in Strong Acid Environment: Effect of Molecular Weight, Modification, and Temperature on Efficiency. ACS Applied Materials and Interfaces, 10(33), 28112–28129. https://doi.org/10.1021/acsami.8b09487

Solomon, M. M., Umoren, S. A., Udosoro, I. I., & Udoh, A. P. (2010). Inhibitive and adsorption behaviour of carboxymethyl cellulose on mild steel corrosion in sulphuric acid solution. Corrosion Science, 52(4), 1317–1325. https://doi.org/10.1016/j.corsci.2009.11.041

Sørbotten, A., Horn, S. J., Eijsink, V. G. H., & Vårum, K. M. (2005). Degradation of chitosans with chitinase B from Serratia marcescens. In FEBS Journal (Vol. 272, Issue 2, pp. 538–549). https://doi.org/10.1111/j.1742-4658.2004.04495.x

Srivastava, M., Srivastava, S. K., Nikhil, Ji, G., & Prakash, R. (2019). Chitosan based new nanocomposites for corrosion protection of mild steel in aggressive chloride media. International Journal of Biological Macromolecules, 140, 177–187. https://doi.org/10.1016/j.ijbiomac.2019.08.073

Tang, G., Ren, T., Yan, Z., Ma, L., Hou, X., & Huang, X. (2020). Preparation and anticorrosion resistance of a self-curing epoxy nanocomposite coating based on mesoporous silica nanoparticles loaded with perfluorooctyl triethoxysilane. Journal of Applied Polymer Science, 137(36), 1–11. https://doi.org/10.1002/app.49072

Tran, V. T., Lee, D. K., Kim, J., Jeong, K. J., Kim, C. S., & Lee, J. (2020). Magnetic Layer-by-Layer Assembly: From Linear Plasmonic Polymers to Oligomers. ACS Applied Materials and Interfaces, 12(14), 16584–16591. https://doi.org/10.1021/acsami.9b22684

Umoren, S. A., AlAhmary, A. A., Gasem, Z. M., & Solomon, M. M. (2018a). Evaluation of chitosan and carboxymethyl cellulose as ecofriendly corrosion inhibitors for steel. International Journal of Biological Macromolecules, 117, 1017–1028. https://doi.org/10.1016/j.ijbiomac.2018.06.014

Umoren, S. A., AlAhmary, A. A., Gasem, Z. M., & Solomon, M. M. (2018b). Evaluation of chitosan and carboxymethyl cellulose as ecofriendly corrosion inhibitors for steel. International Journal of Biological Macromolecules, 117, 1017–1028. https://doi.org/10.1016/j.ijbiomac.2018.06.014

Umoren, S. A., & Eduok, U. M. (2016). Application of carbohydrate polymers as corrosion inhibitors for metal substrates in different media: A review. Carbohydrate Polymers, 140, 314–341. https://doi.org/10.1016/j.carbpol.2015.12.038

Umoren, S. A., Solomon, M. M., Madhankumar, A., & Obot, I. B. (2020). Exploration of natural polymers for use as green corrosion inhibitors for AZ31 magnesium alloy in saline environment. Carbohydrate Polymers, 230, 115466. https://doi.org/10.1016/j.carbpol.2019.115466

Urra Medina, E., & Barría Pailaquilén, R. M. (2010). Systematic Reviews and Meta-analysis: Understanding the Best Evidence in Primary Healthcare. Revista Latino-Americana de Enfermagem, 18(4), 824–831. http://www.scielo.br/scielo.php?script=sci_arttext&pid=S0104-11692010000400023&lng=en&nrm=iso&tlng=en%5Cnhttp://www.ncbi.nlm.nih.gov/pubmed/20922332

Verma, C., & Quraishi, M. A. (2021). Gum Arabic as an environmentally sustainable polymeric anticorrosive material: Recent progresses and future opportunities. International Journal of Biological Macromolecules, 184(April), 118–134. https://doi.org/10.1016/j.ijbiomac.2021.06.050

Vitório, J. A. P. (2003). Fundamentos da patologia das estruturas nas perícias de engenharia. Instituto Pernambucano de Avaliações e Perícias de Engenharia, 58. http://www.vitorioemelo.com.br/publicacoes/Fundamentos_Patologia_Estruturas_Pericias_Engenharia.pdf

Wei, H., Heidarshenas, B., Zhou, L., Hussain, G., Li, Q., & Ostrikov, K. (Ken). (2020). Green inhibitors for steel corrosion in acidic environment: state of art. Materials Today Sustainability, 10, 100044. https://doi.org/10.1016/j.mtsust.2020.100044

Wolynec, S. (2003). Técnicas Eletroquimicas de corrosão (EdUSP (ed.); 1a).

Yang, F., Liu, Y., Liu, T., Liu, S., & Zhao, H. (2019). Aniline trimer-including carboxymethylated β-cyclodextrin as an efficient corrosion inhibitor for Q235 carbon steel in 1 M HCl solution. RSC Advances, 9(52), 30249–30258. https://doi.org/10.1039/c9ra04047a

Zhang, K., Yang, W., Xu, B., Chen, Y., Yin, X., Liu, Y., & Zuo, H. (2018). Inhibitory effect of konjac glucomanan on pitting corrosion of AA5052 aluminium alloy in NaCl solution. Journal of Colloid and Interface Science, 517, 52–60. https://doi.org/10.1016/j.jcis.2018.01.092

Zhang, K., Yang, W., Yin, X., Chen, Y., Liu, Y., Le, J., & Xu, B. (2018). Amino acids modified konjac glucomannan as green corrosion inhibitors for mild steel in HCl solution. Carbohydrate Polymers, 181, 191–199. https://doi.org/10.1016/j.carbpol.2017.10.069

Zhang, Q. H., Hou, B. S., Li, Y. Y., Zhu, G. Y., Lei, Y., Wang, X., Liu, H. F., & Zhang, G. A. (2021). Dextran derivatives as highly efficient green corrosion inhibitors for carbon steel in CO2-saturated oilfield produced water: Experimental and theoretical approaches. Chemical Engineering Journal, 424, 130519. https://doi.org/10.1016/j.cej.2021.130519

Zhang, W., Li, H. J., Chen, L., Zhang, S., Ma, Y., Ye, C., Zhou, Y., Pang, B., & Wu, Y. C. (2020). Fructan from Polygonatum cyrtonema Hua as an eco-friendly corrosion inhibitor for mild steel in HCl media. Carbohydrate Polymers, 238, 116216. https://doi.org/10.1016/j.carbpol.2020.116216

Zhang, W., Nie, B., Li, H. J., Li, Q., Li, C., & Wu, Y. C. (2021). Inhibition of mild steel corrosion in 1 M HCl by chondroitin sulfate and its synergistic effect with sodium alginate. Carbohydrate Polymers, 260, 117842. https://doi.org/10.1016/j.carbpol.2021.117842

Zhang, W., Wu, Y. C., & Li, H. J. (2021). Apostichopus japonicus polysaccharide as efficient sustainable inhibitor for mild steel against hydrochloric acid corrosion. Journal of Molecular Liquids, 321, 114923. https://doi.org/10.1016/j.molliq.2020.114923

Zhao, Q., Guo, J., Cui, G., Han, T., & Wu, Y. (2020). Chitosan derivatives as green corrosion inhibitors for P110 steel in a carbon dioxide environment. Colloids and Surfaces B: Biointerfaces, 194, 111150. https://doi.org/10.1016/j.colsurfb.2020.111150

Capítulo II:Recent studies on the use of simulated concrete pore solution for corrosion evaluation: a systematic review using prisma

ISSN: 1696-8352

Recent studies on the use of simulated concrete pore solution for corrosion evaluation: a systematic review using prisma

Estudos recentes sobre o uso de solução de poros de concreto simulada para avaliação de corrosão: uma revisão sistemática utilizando prisma

DOI: 10.55905/oelv21n10-040

Recebimento dos originais: 01/09/2023
Aceitação para publicação: 04/10/2023

Maria Carolina de Paula Estevam D'Oliveira
PhD in Biotechnology by Programa de Pós-Graduação em Biodiversidade e Biotecnologia (PPG - BIONORTE)
Institution: Universidade Federal do Tocantins
Address: Avenida ns 15, Quadra 109, Alcno 14, Norte, s/n, bloco D, Plano Diretor Norte, Palmas - TO, CEP: 77001-090
E-mail: carolina.doliveira@uft.edu.br

Salmo Moreira Sidel
PhD in Materials Science
Institution: Universidade Federal do Tocantins
Address: Avenida ns 15, Quadra 109, Alcno 14, Norte, s/n, bloco D, Plano Diretor Norte, Palmas - TO, CEP: 77001-090
E-mail: sidel@uft.edu.br

Patrícia Martins Guarda
PhD in Biotechnology
Institution: Universidade Federal do Tocantins
Address: Avenida ns 15, Quadra 109, Alcno 14, Norte, s/n, bloco D, Plano Diretor Norte, Palmas - TO, CEP: 77001-090
E-mail: patriciaguarda@uft.edu.br

Emerson Adriano Guarda
Doctor in Organic Chemistry
Instituion: Universidade Federal do Tocantins
Adrres: Avenida NS-15, Quadra 109, Alcno 14, Norte, s/n, bloco D, Plano Diretor Norte, Palmas - TO, CEP: 77001-090
Email: emersonprof@uft.edu.br

ABSTRACT

The use of simulated concrete pore solutions (SCP) is a viable alternative for studying the behavior of the steel/concrete interface, mainly due to the possibility of reproducibility in

ISSN: 1696-8352

the laboratory. However, this solution needs to represent the reality of what happens in the concrete pores, regarding the ions present in the solution and a stable pH, close to 12.5. Therefore, this article presents a systematic review of the use of SCP in the assessment of adherence since 2018. The investigation followed the PRISMA protocol. After including/excluding steps, 58 studies were included in the review. After the evaluation of these studies, the results were presented focusing on the types of SCP, the experiments carried out and the resistance monitoring methods that used electrochemical experiments, spectroscopy and image analysis. In short, this methodology makes it possible to identify the main knowledge gaps in this area.

Keywords: simulated concrete pore solution, corrosion, monitoring, electrochemistry, systematic review, prisma.

RESUMO

O uso de soluções de poros de concreto simulado (SPC) é uma alternativa viável para estudo do comportamento da interface aço/concreto, principalmente pela possibilidade de reprodutibilidade dentro do laboratório. No entanto, essa solução precisa representar a realidade do que acontece nos poros do concreto, no que tange aos íons presentes na solução e pH estável, próximo dos 12,5. Portanto, este artigo apresenta uma revisão sistemática quanto ao uso de SPC na avaliação da corrosão desde 2018. A investigação seguiu o protocolo PRISMA. Depois de incluir/excluir etapas, 58 estudos foram incluídos na revisão. Após avalição desses estudos, os resultados foram apresentados focando os tipos de SPC, os experimentos realizados e os métodos de monitoramento da corrosão que utilizaram experimentos eletroquímicos, espectroscopias e análises de imagens. Em suma, essa metodologia possibilita a identificação das principais lacunas de conhecimento nessa área.

Palavras-chave: solução de poros de concreto simulado, corrosão, monitoramento, eletroquímica, revisão sistemática, prisma.

1 INTRODUCTION

Concrete is the most used building material in the world and the second most consumed by mankind, behind only water (HELENE; ANDRADE, 2007), being the most man-made (GU; BEAUDOIN; RAMACHANDRAN, 2001). Its production will reach 10,000 million tons/year, and in the next 30 years it will increase by around 100% (PACHECO-TORGAL et al., 2015).

Reinforced concrete structures are found in the most diverse environments subject to aggressive agents, such as sea salt spray, deicing salts, carbon dioxide present in industrialized areas and many others that can impair performance and decrease durability.

ISSN: 1696-8352

Even being constituted by elements composed of concrete and steel, so that they can act together in the load bearing process of a building, there are many problems that can affect this structure, characterized as simple or complex pathologies, compromising the integrity of the building (RIBEIRO et al., 2013).

In reinforced concrete, there is a phenomenon of steel degradation, which is one of the challenges of civil engineering, the corrosion process. Corrosion is a natural electrochemical phenomenon with progressive detrimental effects on the integrity of materials as well as huge economic losses for various industries (HOU; LI; CHEN, 2018; TRAN et al., 2020).

It is estimated that about 15% to 35% of the overall corrosion cost can be saved by using available corrosion protection strategies. These statistics reveal the important role of corrosion protection methods to improve the life of metal structures and reduce maintenance and repair costs in industries (KOCH, 2017).

Corrosion occurs due to the effectiveness of some agents through degrading mechanisms, as follows: carbonation - transformation of calcium hydroxide into calcium carbonate, which is more neutral, inducing a reduction in the pH of the concrete; depassivation of the reinforcement - happens when the chloride ion breaks the passivation layer, an insoluble layer that protects steel (VITÓRIO, 2003).

Of the cases identified in Brazil, a recent example of damage caused by steel corrosion in structures was the Maracanã stadium in Rio de Janeiro, which underwent a series of investigations and reports for renovation and adaptation to receive the 2014 World Cup. The steel corrosion was the most present and intense pathological manifestation, occurring loss of more than 60% of the steel section, and the consequences of this process as the appearance of cracks and concrete spalling were also observed, especially in the marquee of the stadium in which the report presented by engineers concluded by recommending the demolition of the same, because the structure was too compromised by the corrosive process representing a risk to the safety of users (SOUZA; TAVARES; TEIXEIRA, 2014).

The cost of an intervention for structural recovery goes far beyond the cost of repair services, as it also involves the interdiction of the site, when necessary, transfer of

ISSN: 1696-8352

activities to another location, in addition to the risk that a damaged structure offers to people, materials and equipment (BOLINA; TUTIKIAN; HELENE, 2019).

There are various techniques to protect steel from corrosion attack, such as material modification, alteration in the surrounding environment, surface coating, cathodic protection, and the use of corrosion inhibitors. Some methods rely on moisture/oxygen removal, while others make use of a permanent coating on the metal surface. However, some approaches are based on the conversion of anodic material into a cathode. However, the applications of existing techniques are limited by various constraints. For example, material modification is often impossible or expensive (GENTIL, 1996).

Process environment substitution is not an optional solution in many industrial applications, because the metal has to experience a certain reactive medium. The implementation of some methods, for example, coating, can raise CO2 emissions beyond acceptable levels. In addition, other methods such as cathodic protection require expensive equipment, thus increasing the overall cost. Corrosion inhibitors, however, offer an economical and viable alternative solution (RANI; BASU, 2012).

The purpose of this article is to discuss papers following a systematic review, using the PRISMA protocol, to follow recent progress in the use of simulated concrete pore solution (SCP) for corrosion assessment. The evaluation of the simulated concrete pore solutions, the experiments performed, and the corrosion monitoring methods used in each study are detailed in the following sections.

2 MATERIALS AND METHODS

A Systematic Literature Review seeks to establish a formal survey of the state of the art in a consistent and planned way, aiming to implement criteria for selection of research that may be useful and bring relevant information on the subject under study, being a strategy to reduce predispositions and random errors that can occur in a traditional review (URRA MEDINA; BARRÍA PAILAQUILÉN, 2010). In addition, it consists of the identification and description of previous research, systematic evaluation of research following rigorous protocols, and synthetic and coherent collection of evidence in the

ISSN: 1696-8352

selected research universe (O'CONNOR; SARGEANT; WOOD, 2017). Facilitating tools for carrying out a systematic literature review are used, such as the PRISMA protocol (Preferred Reporting Items for Systematic Reviews and Meta Analyses), which has 17 guidelines composing an information flowchart (MOHER et al., 2015).

Unlike a literature review, which is based on a summary or overview of a particular topic, a systematic literature review is focused on answering a question, eliminating the biases and prejudices. Furthermore, it is important to note that the planning that takes place prior to the review allows others to compare, replicate, and judge the validity of the protocol and review, thus preventing arbitrary decisions regarding the inclusion and exclusion of data (MOHER et al., 2015; O'CONNOR; SARGEANT; WOOD, 2017).

In the area of corrosion assessment using simulated concrete pores (SCP), there is no systematic literature review that follows or adapts the PRISMA methodology, the only systematic review found is related to the use of cement-based materials modified with double hydroxides in layers (LDHs) (ZHAI et al., 2022).

In this context, the objective of this systematic review is to compile data between 2018 and 2022, on the use of simulated concrete pore solutions in corrosion evaluation, using the methodological guidelines defined by the PRISMA protocol (MOHER et al., 2015), and the, Mendeley© software, used to organize the results according to each of the databases, and which also helped in the organization of the data, facilitating the laborious and repetitive process of a systematic literature review.

The articles were selected through the Capes Journals platform (www.periodicos.Capes.gov.br), using CAFE, where it was possible to search the PubMed, Science Direct, Springer and Web of Science databases. The search terms were: ("Concrete pore Solution" AND corrosion). The results were limited to articles in English published between 2018-2022. The identified articles had their titles and abstracts evaluated independently by two reviewers.

Review articles, books and book chapters, conference abstracts and case studies were excluded.

For the next step, the Qualis CAPES concept was used, which is a Brazilian scientific production classification system, based on articles published in journals of all postgraduate programs in the country, where the main objective is to evaluate the quality of scientific production and help teachers and students in the article submission process, and this quality is classified, in descending order, in articles ranging from A1, A2, A3, A4, B1, B2, B3, B4 to C.

The following exclusion criteria were applied: articles with Qualis lower than A2, articles that did not mention, in the title, pores of simulated concrete and corrosion or passivation, articles without full text. Articles were included, compared and duplicate records were removed, reaching a final number of 58 articles of interest.

It is important to point out that this research will relate the articles that evaluated the types of simulated concrete pore solutions, the experiments carried out and the corrosion monitoring methods used.

3 RESULTS AND DISCUSSIONS

The selection of studies is presented in a flowchart according to the requirements of PRISMA (see Figure1), illustrating the number of articles identified, included and excluded, evidencing the reason. The search in PubMed, Science Direct, Springer, and Web of Science databases identified a total of 805 articles. Of these, articles whose year of publication is less than 2018 (468), review articles (4), conference abstracts and case studies (2), those whose Qualis is less than A2 (58), those without full text available (4), excluded for duplication (99), and those that do not mention, in the title, concrete pores and corrosion or passivation (34) were excluded, reaching 136 articles.

Also excluded after reviewing the title, keywords, and abstract (59) were those from other research areas (14). After this step, 63 articles remained of which 5 were excluded after a full text review. Thus, 58 articles were submitted to full text analysis and included in this research (Table 1)

Figure 1. Systematic review flowchart according to PRISMA protocol.

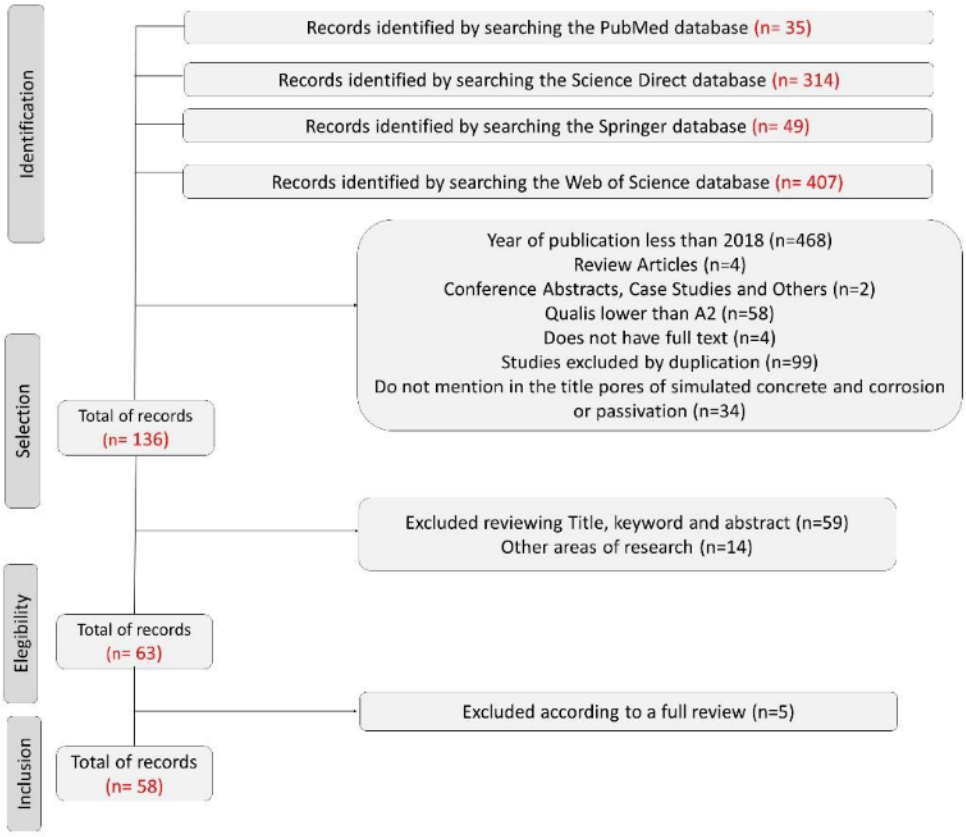

Source: Authors' private collection (May 2023)

Table 1. Summary of systematic literature review: main articles that presented studies on reinforcement corrosion in simulated concrete pore solution

ID	Reference	Simulated pore solutions	Measures
1	(CAO et al., 2019)	Ca(OH)2	XRD; FT-IR; SEM
2	(TEYMOURI et al., 2021)	Ca(OH)2, KOH, NaOH	EIS; MS; XPS.
3	(MANDAL et al., 2020)	CaO, NaOH, KOH	CPP; OCP; EIS; SEM; RAMAN
4	(WU & SHI, 2021)	Ca(OH)2	CV; EIS; CPP; SEM-EDS; AFM; MO; MS
5	(QU et al., 2021)	Ca(OH)2, KOH, NaOH	SEM-EDS; FT-IR; XRD; EIS; LSV
6	(CAI et al., 2021)	Ca(OH)2	OCP; EIS; LPR; XPS; MS
7	(SUBBIAH et al., 2021)	Ca(OH)2, KOH, NaOH	EIS; CPP; FT-IR; DRX; SEM-EDS; AFM; XPS
8	(SHEN & ZHANG, 2022)	Ca(OH)2	XPS; FT-IR; SEM; CPP; EIS
9	(P. XU et al., 2021)	Ca(OH)2	EIS; LSV; SEM; AFM; XPS
10	(ZHAO et al., 2019)	Ca(OH)2, KOH, NaOH	OCP; LPR; EIS; MS; XRD; XPS
11	(LEE et al., 2018)	CaO, NaOH, KOH	OCP; LSV; EIS
12	(W. LIU et al., 2021)	Not Informed	SEM; UV-VIS; XRD; FT-IR; OCP; EIS; CPP

ISSN: 1696-8352

ID	Reference	Simulated pore solutions	Measures
13	(J. XU, TAN, et al., 2020)	Ca(OH)2, KOH, NaOH	Ecorr; EIS; DRX; FT-IR
14	(Y LIU & SHI, 2022)	Ca(OH)2, KOH, NaOH	OCP; EIS; MS; CPP; XPS; AFM; SEM
15	(FENG et al., 2020)	NaOH	OCP; CPP; EIS; XPS; SIMS
16	(YONGQI LIU et al., 2019)	Ca(OH)2	LSV; LPR; EIS; FT-IR; XPS
17	(J. XU, WEI, et al., 2020)	Cement and water	OCP; EIS; SEM; XRD; FT-IR; OM; XPS
18	(ETIM et al., 2021)	Not Informed	SEM-EDS; LSV; XRD; XPS; OCP; EIS
19	(MANSOUR et al., 2018)	Ca(OH)2	LSV; OM; EIS; CV
20	(PENG et al., 2018)	Ca(OH)2, NaOH	OCP; LSV; EIS; MS; XPS; SEM
21	(C. CHEN et al., 2019)	Ca(OH)2	LPR; EIS; XPS
22	(D. WANG et al., 2020)	Cement and water	Ecorr; LPR; EIS; CPP; MS; XPS; SEM
23	(WU et al., 2020)	Ca(OH)2	EIS; LSV; XPS; OM; SEM-EDS; CV
24	(MA et al., 2022)	Ca(OH)2	EIS; OCP; CPP; PZC; SEM; FT-IR; DRX
25	(TIWARI et al., 2021)	Ca(OH)2, KOH, NaOH	CPP; SEM; EDX; XRD; FTIR; UV-Vis
26	(NADERI et al., 2022)	Ca(OH)2, KOH, NaOH	EIS; OCP; XPS; SEM-EDS; FT-IR
27	(GROMBONI et al., 2021)	Cement and water	OCP; EIS; SEM-EDS; XPS
28	(J SHI et al., 2020)	Ca(OH)2, KOH, NaOH	EIS; CV; CPP; AFM; XPS; EPMA; EDS
29	(ZHENG et al., 2021)	Ca(OH)2	FT-IR; OCP; LPR; EIS; CPP; SEM; EDS
30	(ZHENG, DAI, POON, et al., 2018)	Ca(OH)2	OCP; SEM-EDS; XRD; EIS; CV
31	(ZHENG, DAI, LI, et al., 2018)	Ca(OH)2	LPR; EIS; MS; XRD; SEM-EDS.
32	(P. XU et al., 2019)	Ca(OH)2	EIS; CV; MS
33	(ZHI et al., 2020)	Ca(OH)2	LPR; EIS; CPP; XPS
34	(YISHAN WANG et al., 2018)	Ca(OH)2	LSV; PZC; SEM-EDS; XPS; M-IR
35	(LIN & ZUO, 2019)	KOH, NaOH	CPP; EIS; XPS
36	(YAN QI WANG et al., 2018)	Ca(OH)2, KOH	SEM; XPS; XRD; LPR
37	(ZHU & ZHANG, 2021)	Ca(OH)2	OCP; FT-IR; CPP; EIS
38	(VERBRUGGEN et al., 2019)	Ca(OH)2, KOH, NaOH	GDEOS; XPS; RAMAN; SEM; LSV
39	(YUAN et al., 2020)	Ca(OH)2	EIS; XPS; LPR; MO; SEM-EDS
40	(M. CHEN et al., 2021)	Ca(OH)2	OCP; LPR; EIS; SEM
41	(JIN et al., 2022)	Ca(OH)2, KOH, NaOH	EIS; XPS; AFM
42	(J SHI et al., 2018)	Ca(OH)2, KOH, NaOH	EIS; OCP; CPP
43	(TEYMOURI et al., 2022)	Ca(OH)2, KOH	OCP; CPP; EIS; MS; SEM; EDS; XPS
44	(YANG et al., 2019)	Ca(OH)2, KOH, NaOH	OCP; EIS; SEM-EDS; FT-IR
45	(ZUO et al., 2019)	Ca(OH)2	FT-IR; SEM; TG-DSC; EIS; LPR

ID	Reference	Simulated pore solutions	Measures
46	(XIONG et al., 2018)	Ca(OH)2, KOH, NaOH	OCP; LPR; EIS; SEM-EDS;
47	(YE WANG et al., 2021)	Ca(OH)2	EIS; OCP; SEM; DRX; FIB; EDS
48	(SINGH et al., 2021)	CaO, NaOH, KOH	CPP; OCP; EIS; SEM; XPS; RAMAN
49	(JINJIE SHI et al., 2021)	Cement and water	OCP; EIS; MS; XPS; SEM-EDS; AFM
50	(ZHANG et al., 2019)	Ca(OH)2, KOH, NaOH	EIS
51	(YAO et al., 2022)	Cement and water.	EIS; CV; CPP
52	(JOHARI et al., 2021)	Ca(OH)2, KOH, NaOH	EIS; LSV; OCP; SEM; AFM; XPS
53	(FAZAYEL et al., 2018)	Ca(OH)2	FT-IR; LPR; EIS; SEM-EDS; AFM
54	(TIAN et al., 2020)	Ca(OH)2	EIS; OM; OCP; XPS; MS
55	(HU et al., 2021)	Ca(OH)2, NaOH	EIS; CPP; OCP; SEM; EDS; RAMAN
56	(NADERI et al., 2021)	Ca(OH)2, KOH, NaOH	XPS; SEM-EDS
57	(SONG, ZHANG, et al., 2021)	Ca(OH)2	OCP; EIS; XPS
58	(SONG, LIU, et al., 2021)	NaNO2-E51/UF encapsulated	LSV; EIS

Source: Authors organization

Studies on the corrosion of reinforced concrete using steel work electrodes of civil construction immersed in concrete pore solutions were initiated in the whose purpose was to solve the problem of the uncertainty of electrochemical measurements and the high resistivity of reinforced concrete. The idea was to extract pore solutions from concrete by means of a pressurizing device in order to characterize them. The technique, however, depended on sophisticated equipment and the amount of solution extracted from each sample was very small (LONGUET, 1973).

For this reason, in 1996 it was proposed the simulation of concrete pore solution by preparing pH solutions similar to those of concrete pores made of saturated Ca(OH)2 or simulated concrete solution made of NaOH, KOH and Ca(OH)2, since these compounds are the most abundant in the pore solution of concrete. Thus, steel samples were prepared and immersed in these alkaline solutions, facilitating the execution of electrochemical measures (L.T. MAMMOLITI; BROWN; HOPE, 1996). From this study, several researchers used the preparation of SCP to study the corrosion of steel, mainly from the decade of 2010.

As already informed in this paper, a temporal cut was made between 2018 and mid-2022. The number of articles was higher in 2021 (Figure 2). In the year 2022, until

August, when the data were compiled, there were already 7 works in this area, and more studies are expected. The systematic review allowed to track which types of pore solutions of simulated concrete were studied, the types of experiments used, the method of corrosion monitoring evaluated.

The liquid phase of the concrete, called pore solution, has an alkaline pH with typical values between 12.5 and 13.5, because of the main constituents of the solution that are alkaline. Its composition is basically composed of sodium hydroxide (NaOH), potassium hydroxide (KOH) and saturated calcium hydroxide (Ca(OH)2) (POURSAEE; ANGST, 2023). Although Ca (OH)2 is also alkaline, the pH above 13 is maintained, mostly, by hydroxyls from NaOH and KOH (POURSAEE, 2010). In this pH range, it is feasible to use steel reinforcement together with concrete, considering that at these hydrogenic potentials the reinforcement remains in a passivation state (METHA; MONTEIRO, 2014).

Figure 2. Published studies found in this systematic review on simulated concrete pores per year since 2018.

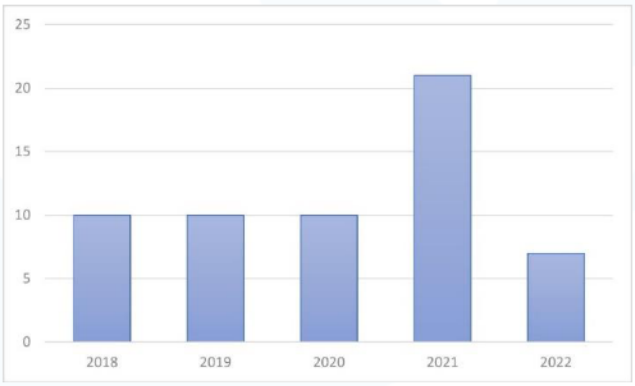

Source: Authors' private collection (May 2023)

Some studies, which took into account the liquid phase of concrete, demonstrate that these solutions are mostly composed of K+ and Na+ ions, representing up to 95% of the alkalis present in the liquid phase of concretes, the other 5% were Ca2+, Mg2+ and S4+ (KEMPL; ÇOPUROGLU, 2015). Regarding Ca2+ ions, its lower concentration is expected due to its low solubility in the usual pH range of concrete (SCOTT; ALEXANDRE, 2016). The composition of the liquid phase also changes with the

ISSN: 1696-8352

presence of external agents such as chlorides and CO2. It was also found that after carbonation there was a decrease in the concentration of Na+ and K+ from approximately 95% to 5.1%. On the other hand, there was an increase in concentrations of S4+ (53.6%), Ca2+ (28.2%) and Mg2+ (13.1%) (KEMPL; ÇOPUROGLU, 2015).

Some authors show that the characteristics of cement, the presence of additions and substitutions by supplementary cementitious materials, the water/cement ratio, the degree of hydration and the external environment influence the composition of the pore liquid phase (KULAKOWSKI, 2002; SCOTT; ALEXANDRE, 2016). In this sense, studies were performed by extracting the solution from the pores to determine the influence of the solution on the durability of the concrete (ORTOLAN, 2015; PLUSQUELLEC et al., 2017; SCOTT; ALEXANDRE, 2016).

Corrosion occurs due to the effectiveness of some agents through degrading mechanisms such as carbonation and depassivation of the steel reinforcement. Figure 3 shows the carbonation front and the change in concrete pH over time. Carbonation starts from the concrete surface and a carbonation front is formed. Then two different pH zones are formed, one with pH still in the natural state of the concrete, around 12 to 13, and another with pH close to 8 (BAKKER, 1988; METHA; MONTEIRO, 2014).

With the ingress of CO2 through concrete in time and the reactions of this gas with calcium hydroxide (Ca(OH)2) available in the cementing matrix occurs the formation of calcium carbonate (CaCO3), and the consequent reduction of the pH of the concrete. When this process reaches the vicinity of the steel reinforcement, it is said that it is depassivated, being susceptible to corrosion. With this, the carbonation front imposes itself inside the concrete and can reach the reinforcement, causing depassivation of the steel, which happens when the chloride ion breaks the passivation layer, which is the layer that protects the steel.

ISSN: 1696-8352

Figure 3. Representation based on the advance of carbonation and pH change in concrete over time

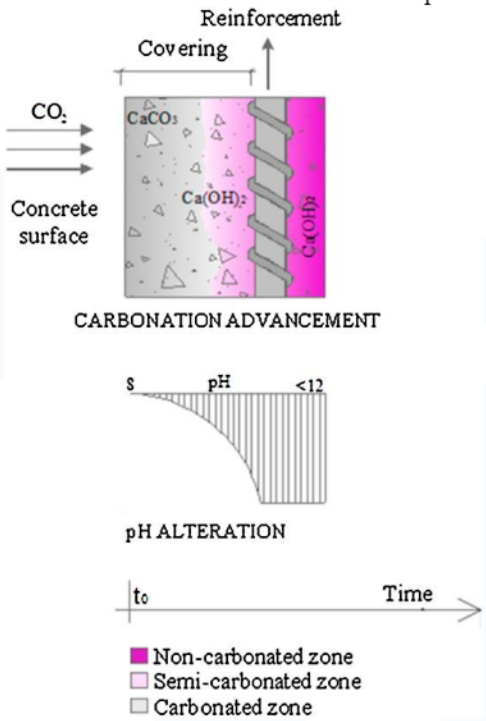

Source: (POSSAN et al., 2017)

Another form of study is through the reproduction of solutions in the laboratory (XU et al., 2019). The use of synthetic solutions for evaluation of chemical processes of cementitious composites is used to facilitate electrochemical analysis, allowing more precise investigations on the influence of chemical compositions, allows a greater control of the variables under study, in addition to reducing the testing time (LIU et al., 2017). Given the above, the articles were classified based on the simulated concrete pore solution (SCP), (Figure 4), electrochemical experiments (Figure 5), spectroscopy (Figure 9) and image analysis (Figure 15).

For the most part, the authors simply adopt a type of SCP composition, not to mention the reason for choosing the chemical composition. Some researchers, however, conducted preliminary study to choose the best SCP composition for the analyses.

As can be seen in Figure 4, there are several ways of producing solution to simulate the environment found in the concrete pores that researchers use to compose the SCP. Although over the years authors have chosen to use a more complex solution, most use saturated Ca(OH)2 solution to simulate the concrete pores (BEN MANSOUR;

DHOUIBI; IDRISSI, 2018; CHEN et al., 2021; TEYMOURI et al., 2022; XU et al., 2019; ZHI et al., 2020).

Figure 4. Types of simulated concrete pore solution used in studies since 2018.

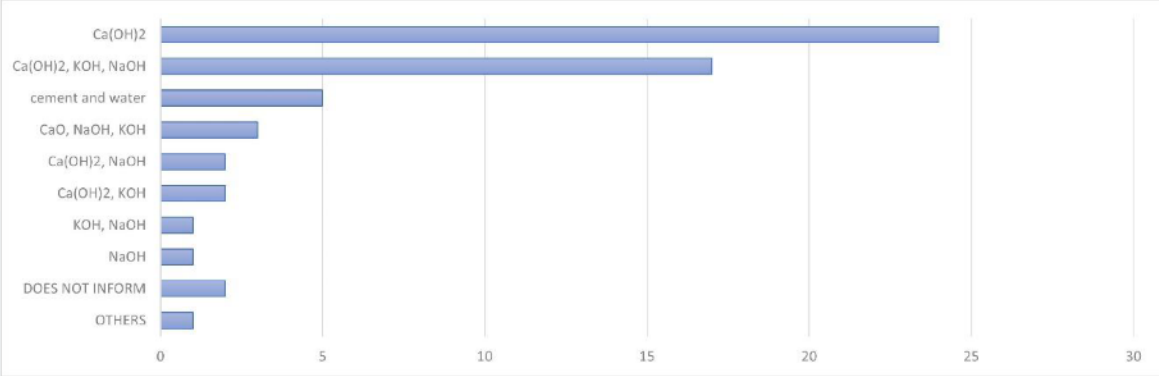

Source: Authors' private collection (May 2023)

Some authors chose to reproduce the alkaline environment of concrete using the mixture of cement and water (GROMBONI et al., 2021; SHI et al., 2020, 2021; XU; TAN; MEI, 2020; YAO et al., 2022). Approaching the reality of concrete production, it was suggested to elaborate a simulated concrete pore solution by mixing all the components of concrete (water, coarse and fine aggregate and cement) with a larger amount of water so that cement hydration was not enough to solidify the mixture(KAPAT; PRADHAN; BHATTACHARJEE, 2006). On the other hand, there were those who chose to extract the powder from cured concrete specimens by mixing it in water to extract the soluble compounds and produce the simulated pore solution (PRADHAN; BHATTACHARJEE, 2007; SHAHEEN; PRADHAN, 2017). It is believed, therefore, that these works are closer to the work reality, because they use the concrete components to produce the SCP. Although aggregates are considered potentially inert in some cases, it is known that there is no guarantee that there is no soluble portion of these materials in water.

In addition, the researchers evaluated the difference between the passive film grown naturally in alkaline solutions and the film grown by anodic polarization. (VELEVA et al., 2002).

ISSN: 1696-8352

Jiang et al (2012) evaluated the influence of the type of salt (KCl, NaCl, CaCl2 and MgCl2) on the threshold value for corrosion initiation of steels in SCP. The solutions used were: 1) saturated solution of Ca (OH)2; 2) cement solution obtained from 20 g of Portland cement dissolved in 2 liters of distilled water. Samples of the steel used in the research were immersed for seven days in each of the solutions, to ensure that they were passivated before being attacked by chlorides. The pH of the solutions was measured after the addition of the salts, being possible to observe that there is no great difference in the behavior of the pH variation with addition of each of the chlorides in solutions 1 and 2. However, as solution 2, due to Portland cement hydration, contains a series of ions (Na+ K+, Ca2+, Mg2+, Al3+ and (SO4)2-), the chlorine ions are physically adsorbed by the CSH (hydrated calcium silicate) and C3A (tri-calcium aluminate) chemically binds the chlorides to produce Friedel's salt (C3A.CaCl2.10H2O), which ensures that the steel has a lower risk of corrosion, as it promotes the removal of a portion of the chlorine ions from the solution. In the saturated solution of Ca(OH)2, the only corrosion inhibitor is the concentration of hydroxyl, which determines the limit of chlorides to initiate corrosion of steel (JIANG et al., 2012). Thus, the authors conclude that the cement solution is more representative of reality.

Although the studies for evaluation of corrosion in reinforced concrete have been carried out through several techniques, the ones that stand out are the electrochemical ones. These techniques, in addition to analysing corrosion as an electrochemical phenomenon and therefore more reliable, have the advantage of being fast and not causing serious damage, such as the destruction of the analyzed specimen at the time of its application; and can be used both in the laboratory and in the field.

Figure 5 illustrates the main electrochemical techniques used for corrosion evaluation of steel immersed in simulated concrete pore solutions. The most used technique is the monitoring of the open potential circuit (OPC), followed by the techniques for obtaining curves and polarization resistance (Rp), which are: cyclic potentiodynamic polarization (CPP), linear polarization resistance (LPR) and scanning linear voltammetry (SLV).

ISSN: 1696-8352

Figure 5. Electrochemical experiments used in the evaluation of simulated concrete pore solutions used in studies since 2018.

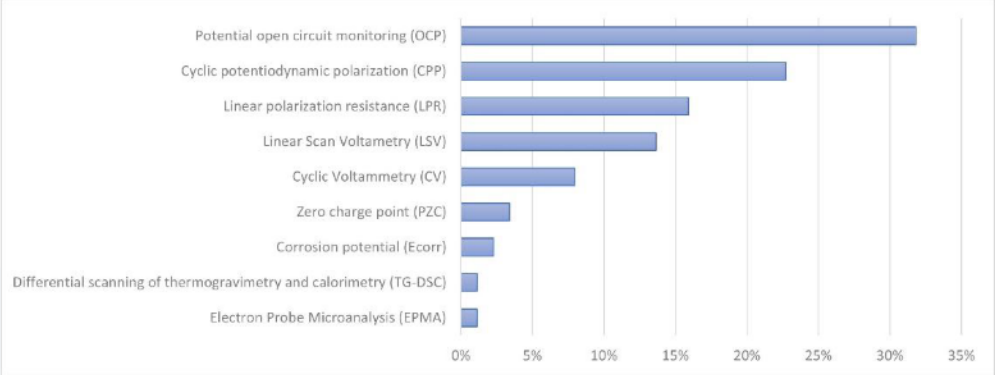

Source: Authors' private collection (May 2023)

Open potential circuit (OPC) monitoring is an electrochemical technique used to initiate most material analyses, especially when it is intended to evaluate the formation of passivating oxide films or corrosive oxides on a metal. It is one of the simplest and most fundamental methods of electrochemistry and the most used in civil engineering to evaluate the corrosion potential by C876-15 (ASTM, 2015). The technique consists of measuring the potential difference between a reference electrode (RE) and the working electrode (WE), immersed in an electrolyte of interest, over time. For this, you can use a simple device, such as a multimeter or a more elaborate one, such as a potentiostat/galvanostat. When a metal is immersed in an electrolyte solution, an electrochemical potential difference (electrical and chemical in nature) occurs between the two phases, the liquid and the solid.

While the electrical double layer (EDL) is formed by organizing ions on the metal surface to stabilize the potential at the metal-solution interface, chemical reactions at the surface cause oscillations in the potential at the metal-solution interface. The formation of the double layer is fast, but the formation of passivating films can have slow growth kinetics (ZIMER, 2009). Thus, with OPC one can track the film growth during potential stabilization.

With the OPC measurement, it is possible to draw a graph similar to the graph in Figure 6 (PENG et al., 2018), which presents the open circuit potential measurements in volts versus a reference electrode (ordered axis) in each time unit (abscissa axis). Before

the complete formation of EDL, the system is not yet in balance. In the case of oxidation of metals in OPC, there is first more oxidation than reduction. Thus, OPC varies constantly until the dynamic equilibrium state is reached. In this state, the chemical reactions are balanced and the OPC ceases to vary, becoming constant. This experiment provides thermodynamic information about the system and serves as an indicator of corrosion or steel passivation (ZIMER, 2009).

Figure 6. Open circuit potential monitoring graph model.

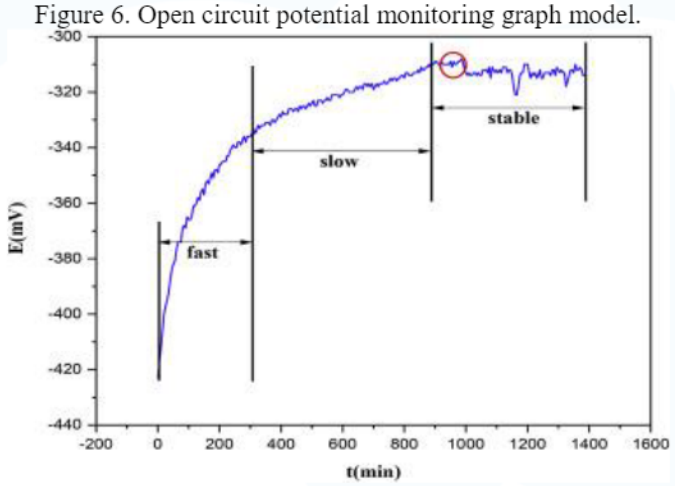

Source: (PENG et al., 2018)

It is worth mentioning again that the level of potential stabilization indicates the moment of high probability that the formation of a passivating film on the surface of the metal has started. In this way, it is possible to find out how long it takes for the formation of a passivation film to be studied.

Most authors perform this measurement based on C876-15 (ASTM, 2015), because they intend to evaluate reinforcement corrosion in aggressive environment (OGUNSANYA; HANSSON, 2019; YANG et al., 2019; ZHAO, Yazhou et al., 2019). Thus, these authors use the reference electrode recommended by the standard, the saturated calomel electrode (SCE). When the researcher's objective is to evaluate the formation of the passivating film, automatic monitoring over a short time interval (maximum one hour) is recommended to observe the change in the electrochemical behavior of the system. Furthermore, SCE should not be used for film formation

ISSN: 1696-8352

measurements because this electrode is not stable in a highly alkaline medium, as is the case with SCP [46]. It is recommended to use an Hg/HgO or Ag/AgCl.

Steel rebars exposed to SCP solution with 3% inhibitor + 3.5% by weight of NaCl contain a significant amount of H+ ions and phosphate ions. H+ and Cl- ions induce corrosion reaction while phosphate ions transform unstable corrosion products into a stable iron phosphate as passive film, respectively. Thus, it is seen that as the exposure periods are increased, the OPC is shifted to a more noble/positive direction. The steel reinforcement, without a passivating layer, has initially deteriorated due to Cl- ions and forms the corrosion products, thus active OPC is observed by 1 h of exposure. However, when the exposure period reaches 24 h to 120 h, these corrosion products deposit on the rebar surface, shifting the OPC to a positive, nobler direction (MANDAL et al., 2020).

The OPC evolution of Q235 carbon steel in SPC with 0.25 mols/L of NaCl and different concentrations of triethanolammonium dodecylbenzene sulfonate (TDS) was evaluated for 8 hours. In the initial 4 h, the OPC of all carbon steel samples immersed in the porous solution presents a declining trend, probably due to the corrosive effect of chloride and carbonation ions; after that, a relatively stable potential value was observed. After 8 h of immersion, the OPC of the sample in the solution without TDS decreased slowly. However, for the solution with TDS, it increases marginally. This can be explained by the adsorption of TDS molecules in carbon steel Q235, which prevent chloride ions from coming into contact with the surface of the steel and repassing the metastable pitting. At the end of immersion, the OPC of the samples in the solution with TDS are much higher than in the solution without TDS and the higher the concentration, the greater the potential (ZHAO, Y et al., 2019).

The great deficiency of this technique is that its values indicate the balance between the anodic and cathodic reaction, without offering quantitative information, that is, it is not possible to obtain results regarding the speed of corrosion of the steel reinforcement. Thus, the corrosion potential of the steel reinforcements in concrete is a quantity that indicates a corrosion situation or passive state of these, approximately.

The Pourbaix diagrams that relate pH and potential present the possibility of predicting the conditions under which corrosion, immunity or possibility of passivation

may occur. These representations are valid for a temperature of 25 °C and under a pressure of 1 atm, taking into account the normal hydrogen electrode (NHE). For a better visualization of corrosion, immunity and passivation conditions, a simplified diagram is shown in Figure 7 (GENTIL, 1996).

Through this diagram it is possible to verify the conditions under which corrosion, immunity or possibility of passivation may occur. The immunity region corresponds to the zone where corrosion is thermodynamically unfavorable, that is, the metal is stable. In the passivation region, metal oxides or hydroxides are stable. In the corrosion region there are combinations of pH and potential that indicate that metal ions or complex ions are the stable phases. The dashed lines "a" and "b" delimit the zone where the water is thermodynamically stable. Below the line "a" hydrogen reduction occurs, while above the line "b" there is the evolution of oxygen (GENTIL, 1996).

Figure 7. Simplified Pourbaix Diagram for the Ferro-Água System at 25 °C

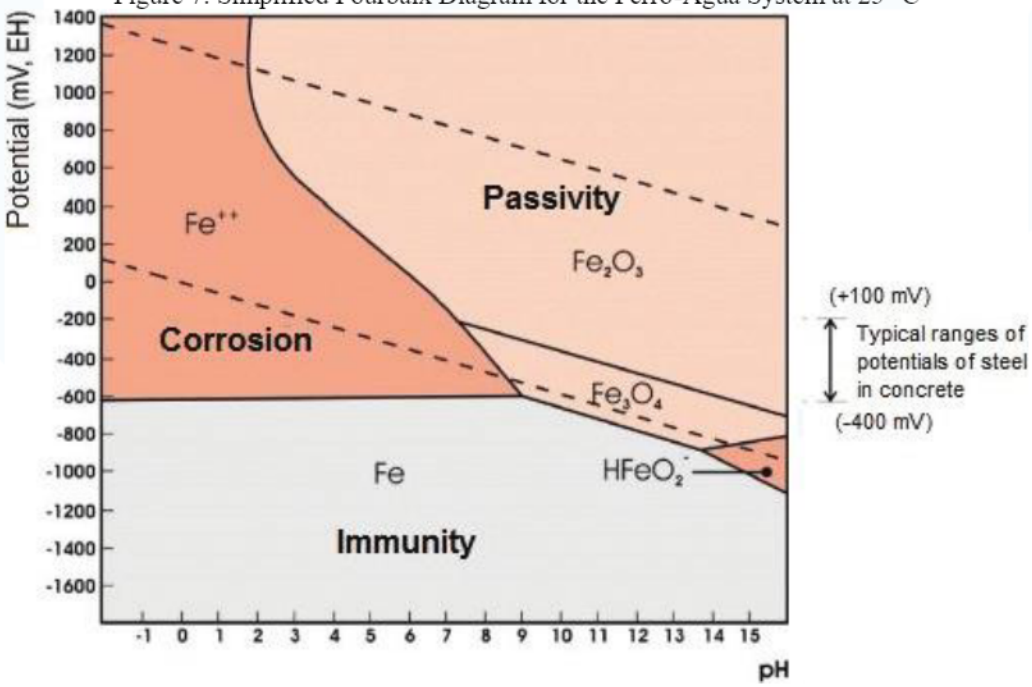

Source: (RIBEIRO et al., 2013)

For the order of magnitude of pH in concrete (between 12.5 and 13.5) and for a usual range of corrosion potential, from +0.1 V to -0.4 V in relation to the standard hydrogen electrode, the electrode reactions verified in iron are passivation. As long as the

pH of the medium is maintained and the passivating film is not destroyed, steel dissolution will not occur and the bars will be protected from corrosion.

The C 876-15 standard presents a correlation between potential intervals and the probability of occurrence of corrosion, taking copper/copper sulfate (Cu/CuSO4, Cu2+) as reference electrode (ASTM, 2015). This correlation, as well as the others, is presented in Table 2.

Table 2. Probability of steel reinforcement corrosion as a function of potential

ELECTRODE TYPE	PROBABILITY OF CORROSION OCCURRING		
	< 10%	10% - 90%	> 90%
STANDARD ELECTRODE OF HYDROGEN (SEH)	> 0,118 V	-0,118 V à -0,032 V	< -0,032 V
CU/CUSO4, CU2+ (ASTM C 876)	> -0,200 V	-0,200 V à -0,350 V	< -0,350 V
HG, HG2CL2, KCL (CALOMELANO)	> -0,124 V	-0,124 V à -0,274 V	< -0,274 V
AG, AGCL/KCL (1M)	> -0,104 V	-0,104 V à -0,254 V	< -0,254 V

Source: ASTM (2015)

According to the theory of mixed potentials, due to polarization phenomena, the corrosion cell tends to achieve a stationary electrochemical state, in which the speed of anodic reactions equals the speed of cathodic reactions, that is, the current densities of both processes are identical (WAGNER; TRAUD, 1938). According to Evans' diagram, shown in Figure 8, the characteristic potential of this state corresponds to the so-called corrosion or mixed potential (Ecorr). It is also observed that this potential is associated with a current density, called corrosion current (icorr).

The most widely used techniques for obtaining the Evans diagram are: the potentiodynamic polarization (CPP), linear polarization resistance (LPR) and scanning linear voltammetry (SLV). These are quantitative tests that allow the instantaneous corrosion rate of a metal to be identified and, by means of measurements, to verify the corrosion rate over a given time (LITTLE; LEE; RAY, 2011). The test procedure is performed by applying a small change in the potential of the steel and checking the change in the existing current and vice-versa.

The technique provides for the continuous scanning of the potential, starting either in the corrosion potential (the one that is established when the material is immersed in the

ISSN: 1696-8352

solution, also called open circuit potential) or in potentials where cathodic reactions predominate (those lower than the corrosion potential), raising the potential at constant scan rate. The scanning speed, the composition of the solution, the immersion time before the potential scan and the test temperature can influence the shape of the polarization curves. The current, in the polarization curves, is shown in absolute values, and is divided by the area of material exposed to the reactions, creating the concept of current density (SEDRIKS, 1986).

Under ideal conditions, a polarization curve (Pc) is the result of an accelerated corrosion experiment in which a metal is polarized in two distinct regions: for potentials more positive than the open potential circuit (OPC) - anodic polarization - and more negative - cathodic polarization. Usually this amplitude is 200 mV to a few volts from the OPC (SRINIVASAN; KANE, 1999). Under certain conditions dissolution can be interrupted by passivation and film formation (CRAMER; B.S. COVINO, JR., 2003; PEREZ, 2004). From the anodic and cathodic polarization curves and the Tafel straight lines, one can analyze the electrochemical system by means of the Evans diagram, as shown in Figure 8 (ZIMER, 2009).

The constant "□" is the charge transfer coefficient, "n" the number of electrons involved in the reaction, R is the universal constant of the gases and T, the temperature. The starting value of the two polarization curves, anodic and cathodic, indicates the corrosion potential of the system (Ecorr).

Figure 8. Representation of the Evans diagram for a metal in solution from the anodic and cathodic polarization curves.

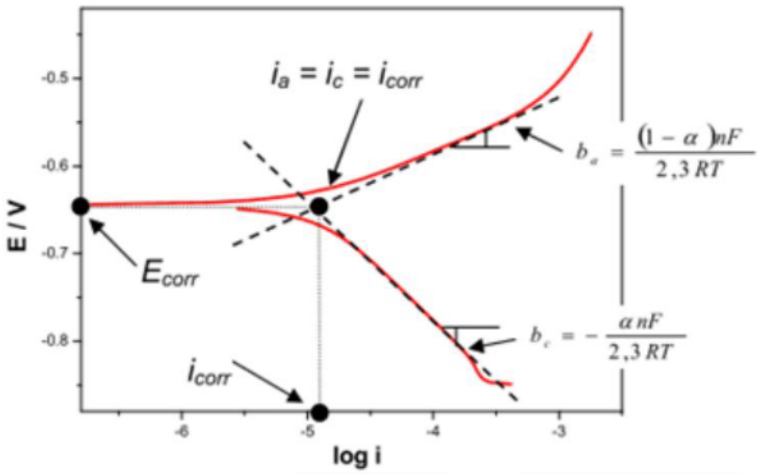

Source: (ZIMER, 2009)

In short, the objective of obtaining the polarization curves is, from the Evans diagram, to obtain direct information about passivation kinetic parameters. The parameters obtained in an electrolyte can be compared to those obtained in another electrolyte when the same electrode is used, knowing that the higher the polarization resistance (Rp), greater is the protection provided by the electrolyte to the electrode. From the Tafel lines can be determined anodic (ba) and cathodic (bc) angular coefficients, which combined, according to Equation 1, will provide the Stern-Gearn coefficient (B).

$$B = \frac{b_a + b_c}{2{,}303 * (b_a + b_c)} \qquad (1)$$

It is worth noting that B varies only between 13 mV and 52 mV for most metal/electrolyte systems analyzed (STERN; WEISERT, 1959), and for concrete steel reinforcement is presented values of B equal to 26 mV for the active state (corrosion) and 52 mV for the passive state (ANDRADE; ALONSO, 1996).

The potential variation ratio (+/- 20 mV or +/- 30 mV), in a given linear stretch, by the voltage variation is called polarization resistance (Rp) (ANDRADE; BUJÁK, 2013; LITTLE; LEE; RAY, 2011). This ratio indicates the resistance to oxidation presented by a material during the application of an external potential. The Rp is inversely

ISSN: 1696-8352

proportional to current density and corrosion rate (ANDRADE; BUJÁK, 2013). From the relation of the coefficient B with the value of the resistance to polarization (Rp) can be found the corrosion current (icorr) related to the said corrosive process, according to Equation 2.

$$i_{corr} = \frac{B}{R_p} \quad (2)$$

As can be seen in Figure 8, the icorr can also be obtained by analyzing the Evans diagram. It is the point where you have the crossing of the tangent lines of cathodic and anodic current. By extrapolating the potential axes, the Ecorr is determined and an indication of the beginning of corrosion is obtained, that is, the potential from which the system will undergo oxidation. It is considered that the steel reinforcement is in corrosion process when icorr > 0,1-0,2 □A/cm2 (ANDRADE; BUJÁK, 2013). From the icorr value one can determine the corrosion velocity (Vcorr) of the system by means of Faraday's Law (GENTIL, 1996), according to Equation 3, where: M is the molar mass of the major constituent of the alloy, in the case of carbon steel it would be the iron; t is the time, in seconds, stipulated for one year; n is the number of electrons involved in the reaction; A is the area, in cm2, of the steel electrode; F is Faraday's constant and d is the density of the alloy, in g/cm3.

$$V_{corr} = \frac{i_{corr} * M * t}{n * A * F * d} \quad (mm/year) \quad (3)$$

The values calculated by Equations 2 and 3 can be compared with Table 3, which relates the current densities with the aggressiveness of the corrosive process (ELSENER et al., 2003).

ISSN: 1696-8352

Table 3. Values of icorr and Vcorr for determination of corrosion aggressiveness

icorr (□A/cm2)	Vcorr (mm/year)	Corrosion level
≤ 0, 1	≤ 0,001	Negligible
0,1 – 0,5	0,001 – 0,005	Low
0,5 – 1,0	0,005 – 0,010	Moderate
> 1, 0	> 0,010	High

Source: ELSENER et al. (2003)

In addition, it is possible to compare the values found in Equation 3 with Table 4 to assign to the system under study, metallic material and corrosive medium, a diagnosis of its corrosion resistance (NACE, 2005).

Table 4. Attribution of corrosion diagnosis by observation of corrosion velocity (Vcorr) of the system

Vcorr calculated		Diagnosis
Uniform corrosion	Pitting corrosion	
Vcorr < 0,025	Vcorr < 0,130	Low Corrosion
0,025 < Vcorr < 0,126	0,130 < Vcorr < 0,200	Moderate corrosion
0,127 < Vcorr < 0,254	0,200 < Vcorr < 0,280	High Corrosion
Vcorr > 0,254	Vcorr > 0,280	Severe Corrosion

Source: NACE (2005)

As a criterion for evaluating the results obtained with the technique, there is a classification based on the icorr found in Table 5 (ALONSO; ANDRADE, 1990).

Table 5. Classification of corrosion degree according to icorr values

icorr (□A/cm2)	Classification
< 0,1 - 0,2	Negligible corrosion
> 0,1 - 0,2	Active corrosion
~ 1,0	Significant, but not severe corrosion
~ 10	Severe corrosion attack

Source: ALONSO; ANDRADE (1990)

The Rp value used in Equation 2 can also be obtained, in practice, by the slope at the point where i=0 in the polarization curve, E versus i, obtained at low scanning speed, on the order of 0.1 mV/s (ASTM, 2014). In addition, it is possible to determine Rp using the electrochemical impedance spectroscopy (EIS) technique, obtaining a response with less experimental error compared to LPR and SLV. EIS is the main spectroscopy technique used for corrosion evaluation of steel immersed in simulated concrete pore solutions, as shown in Figure 9.

Figure 9. Spectroscopies performed on simulated concrete pore solutions used in studies since 2018.

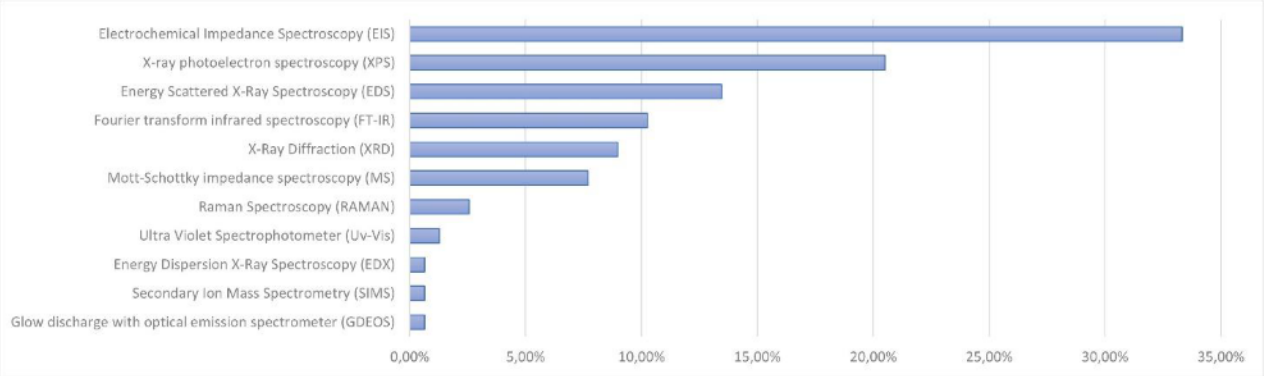

Source: Authors' private collection (May 2023)

Electrochemical impedance spectroscopy (EIS) is a technique used to characterize a wide variety of electrochemical systems and to determine the contribution of individual electrode or electrolyte processes in these systems. It can be used to investigate the dynamics of bound or moving charges in the volume or interface regions of any type of liquid or solid material. The impedance technique assumes that a given electrical circuit, more or less elaborate, can represent the behavior of steel within concrete. (RIBEIRO; SOUZA; ABRANTES, 2015).

Electrochemical impedance spectroscopy (EIS), or AC impedance, is a robust technique where, through the simulation of electrical circuits, with resistors and capacitors, the influence of the components that integrate and are relevant for the study of corrosion in reinforced concrete structures (concrete/ electrolyte, steel/ concrete interface, double electrical layer/ steel) (METHA; MONTEIRO, 2014). EIS has an advantage over LPR, as it suffers less influence and alteration of the results by external interference, besides being able to detect corrosion rates below 10-4 mm/year (SILVERMAN, 2011).

The equivalent electrical models, obtained based on the Impedance Spectroscopy technique, normally generate circuits of type R-C (Resistance - Capacitance). The EIS technique is standardized by ASTM G-106 (COMMITTEE, 2010). Because the analyzed samples do not present an ideal capacitance, a calibration is required for R-CPE models (Resistance - Constant phase element).

ISSN: 1696-8352

In a study on the corrosion inhibition efficiency of carbon steel, in SCP, using compound nitrite with sodium D-gluconate it was possible to verify, through the graphs of Nyquist and Bode, that after adding the corrosion inhibitor, the impedance arc radius in the Nyquist diagram increased greatly and the curve slope in the low frequency region increased, as illustrated in Figure 10 (XU et al., 2021).

Figure 10. Nyquist graph of carbon steel electrode with different levels of corrosion inhibitor

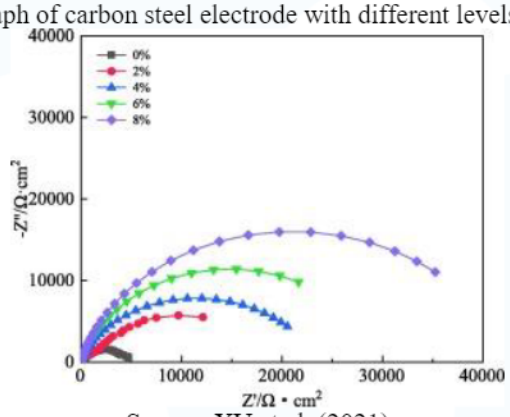

Source: XU et al. (2021)

The efficiency of the protective layer becomes more evident with the increase of the concentration of the nitrite compound with sodium D-gluconate, and works mainly through the cathodic electrochemical process that inhibits the corrosion of steel bars (KORNBLUM; BLACKWOOD; MOOBERRY, 1956; YANG et al., 2012). Figure 11 shows that the low frequency impedance value and the maximum phase angle increased with the corrosion inhibitor (XU et al., 2021). This indicates that the addition of corrosion inhibitor improved the corrosion resistance of carbon steel by promoting the formation of a more stable protective film on the surface, which prevented chloride and oxygen ions from hitting the surface of carbon steel.

ISSN: 1696-8352

Figure 11. Bode graph of carbon steel electrode with different levels of corrosion inhibitor.

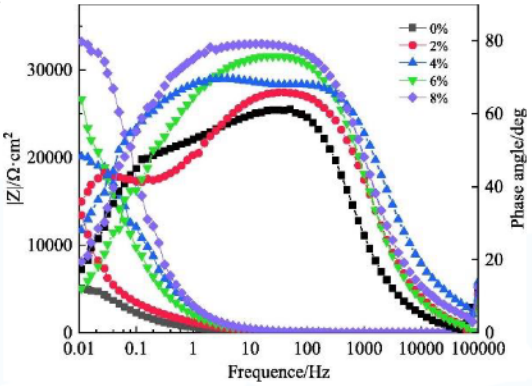

Source: XU et al. (2021)

To quantitatively analyze carbon steel corrosion, the equivalent circuit, illustrated in Figure 12, was used to describe the Nyquist charts (XU et al., 2021). This equivalent circuit was also used by other researchers to model the electrochemical behavior of carbon steel in alkaline médium (ZHAO, Y et al., 2019). In the equivalent circuit, Rs is the resistance of the solution; Rf is the film resistance; Rct is the charge transfer resistance, which reflects the electron transfer difficulty between the anode dissolution and depolarizer reduction; the Cf is the capacitance of the film and the dispersion index a1 constitutes the constant phase angle elemento CPE1; the capacitance of double electrical layer Cdl and the dispersion index a2, constitute the constant phase angle element CPE2.

Figure 12. Equivalent circuit

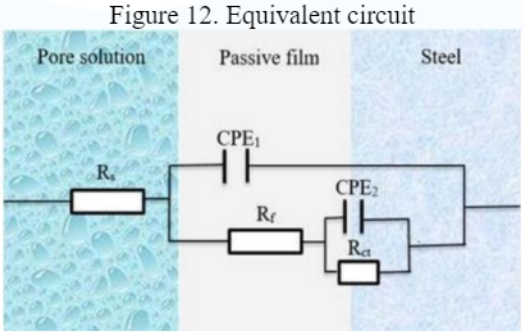

Source: XU et al. (2021)

According to the results found by Xu, et al (2021), in addition to the load transfer resistance Rt, the influence of the protective film on carbon steel can be described by Cdl (FENG et al., 2017; SAHOO; BALASUBRAMANIAM, 2008). The capacitance of the

ISSN: 1696-8352

electric double layer (CPE2) of the solution with corrosion inhibitor was significantly lower than that of the solution without corrosion inhibitor (YANG et al., 2019). According to the Helmholtz model (BOMMERSBACH et al., 2005), the double layer capacitance Cdl can be expressed by Equation 4, where "S" is the surface area of the working electrode, "d" represents the thickness of the double layer, e0 and ε are dielectric vacuum and film constants, respectively.

$$C_{dl} = \frac{\varepsilon_0 * \varepsilon}{d} * S \quad (4)$$

The dielectric constant of water molecules is greater than that of the corrosion inhibitor. When water molecules at the steel/solution interface are replaced by corrosion inhibitors, the capacitance of the solution composed of corrosion inhibitor molecules is significantly lower than that of water molecules, so, Cdl decreases. According to Equation 4, the thickness of the double layer increases with the content of the corrosion inhibitor in the SCP, which indicates that the corrosion inhibitor adsorbed to form a film on the surface of the carbon steel, which blocked the penetration of aggressive ions (XU et al., 2021).

It was also calculated the inhibition efficiency (□) of the corrosion inhibitor, with different concentrations, using Equation 5, where Rct and R'ct efer to the charge transfer resistance of the electrode in SPC without and with corrosion inhibitor, in ohm (□).

$$\eta = \frac{R'_{ct} - R_{ct}}{R'_{ct}} \quad (5)$$

In the study in question, the resistance to charge transfer, Rct and the resistance of Rf film increased after the addition of corrosion inhibitor, implying that the passive film became more stable and resistant. When the inhibitor concentration increased from 2% to 8%, there was an increase in resistance efficiency from 60.73% to 89.96%. The higher inhibitor concentration helped increase the adsorption of the nitrite corrosion inhibitor compound with sodium D-gluconate on the surface of the steel bar and formed

a complete and compact adsorption film to improve the resistance to chloride ions (XU et al., 2021).

In another study the influence of calcium ion in the solution of concrete pores on the passivation of galvanized steel bars was evaluated. They were performed after 264 h of immersion when the potential and polarization resistance were both stationary, in order to define the passive state of the galvanized steel surface (ZHENG et al., 2018). To analyze the EIS results, the surface models and equivalent circuit graphs were established as in figure 13.

According to the results of the linear polarization resistance test and observation of the sample surface in the saturated solution of Ca(OH)2, this was covered by a compact layer of calcium hydroxyzincate (CHZ) with a rough surface exhibiting a high value of resistance to polarization, can be simulated by the model of figure 13(a).The surface of the samples in cement and water solution (ECP), which were covered by porous or loose layers of corrosion products and exhibited lower polarization resistance values, can be simulated by the figure 13(b). The surfaces of the specimens that were covered by a compact layer of Zn(OH)2 and exhibited higher polarization resistance value, can be simulated by 13(c). The samples in which there was little corrosion product observed, exhibited low values of resistance to polarization, therefore, the system could be simulated by the modelo of figure 13(d).

In the equivalent circuit graphics, Rs represents the electrolyte resistance between the working electrode and the reference electrode; Rf is the resistance of the corrosion product layer formed on the surface of the galvanized coating; Rpore the resistance of the alveolar pores on the surface or passive film; Rct the resistance of the alveolar pores on the surface or passive film; Rct represents the charge transfer resistance; Q denotes the constant phase element (CPE) representative of the double electrical layer formed at the steel-concrete interface when its immersion in electrolyte (LI et al., 2016). Qf and Qdl represent the capacitance of the corrosion products layer on the surface of the galvanized steel and the capacitance of the electric double layer respectively (LI et al., 2011; TIAN et al., 2015).

ISSN: 1696-8352

Thus, to work with capacitance values, it is necessary to convert the CPE into a pseudo-capacitance, which can be equated as through an impedance or admittance. . The equation for impedance considering a CPE is presented in Equation 6. Where ZCPE is the impedance of the constant phase element (Ohm.cm2), w is the angular frequency of AC alternating voltage (rad/s), Y0 is the admittance of the CPE (Ohm.cm-2.s-α), and α the exponential term, which represents the ease of diffusion of ions in the passivation film (DIARD; LE GORREC; MONTELLA, 2013).

$$Z_{CPE} = \frac{1}{Y_0 * (j * \omega)^{\alpha}} \quad (6)$$

Figure 13. Surface models of the galvanized steel in the simulated solutions after 264 h of immersion and the equivalent circuits used to adjust the results.

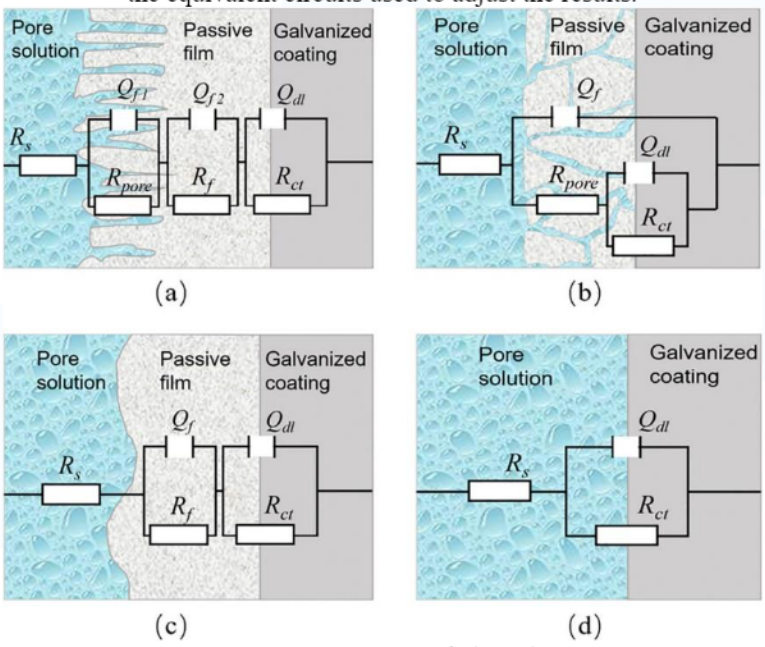

Source: ZHENG et al. (2018)

The parameter "□" is directly related to the microstructure, roughness and irregularity existing on the electrode surface, ranging from 0 to 1, with values closer to 1 indicating an ideal capacitive behavior (KATIYAR; RANDHAWA, 2019), while "□" close to 0.5 indicam that or CPE is becoming a component of Warburg (RETTER et al., 2003). In other words, when "□" is 1, the element is a capacitor, since when the behavior

ISSN: 1696-8352

is governed by a process of mass transfer, "□" approaches 0.5, and intermediate values of "□" relate to the non-homogeneity and surface roughness of the electrode (MACDONALD, 1987).

In addition to the kinetic characteristics of the corrosive process, EIS allows to identify whether corrosion occurs in a generalized or localized way, and it is also possible, through the adaptation of the proposed electrical circuit, to estimate the average thickness of the passivation film (CASCUDO, 1997). As the technique allows separating the elements that compose the electrochemical cell in different electrical components, it is possible to identify the electrical characteristics of the solution and the steel/solution interface [84,85]. The analysis of the results is done through the individual evaluation of each of the parameters of the proposed electric circuit, and also through Nyquist graphs, according to Figure 14, and Bode graphs, where it is possible to analyze the influence of the sample components (CASCUDO, 1997).

Figure 14. Representation of the Nyquist diagram

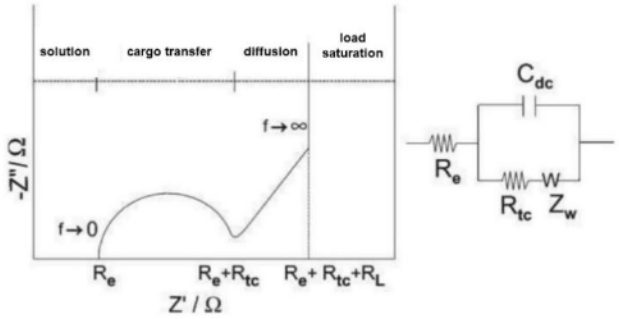

Source: adapted (CASCUDO, 1997)

In parallel impedance measurements some techniques can be employed, such as: scanning electron microscopy (SEM) to determine the morphology; microanalysis by EDS as a technique to determine the local chemical composition; and X-ray diffraction as a technique to determine the phases of corrosion products (FeS2 film, for example) These techniques allow a better understanding of the ex situ corrosion process and can serve as feedback for future assignments of equivalent circuits for impedance measurements. SEM is the main image analysis technique used for corrosion evaluation of steel immersed in simulated concrete pore solutions, as illustrated in Figure 15.

Figure 15. Image analysis performed on simulated concrete pore solutions used in studies since 2018.

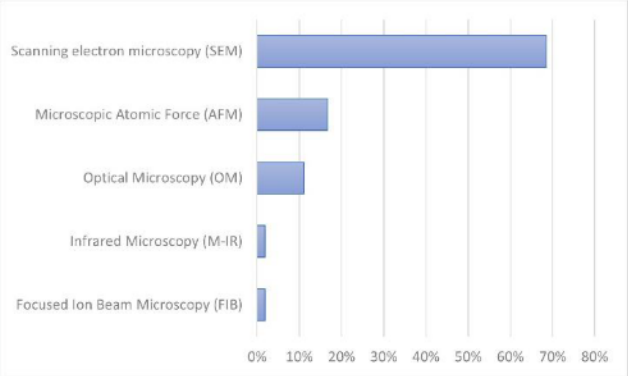

Source: Authors' private collection (May 2023)

The scanning electron microscopy technique (SEM) is an effective tool for the characterization of surface morphology, as it allows the increase of up to 50 thousand times. It consists in scanning the sample with an electron beam, causing the emission of secondary electrons that are used in the formation of the image to be analyzed (CALLISTER; RETHWISCH, 2002).

When the SEM is coupled with equipment capable of performing energy dispersive X-ray spectroscopy (EDS), a point of the image obtained by the microscope is chosen and, through the emission of rays-X in the sample and, with the interpretation of the characteristic return energy of each element, it is possible to say the elements present in the sample. It is also possible to perform a mapping of a SEM image by coloring each element with a specific color, so that it is possible to know where the elements are concentrated in the sample.

SEM was used to investigate and characterize the passive films formed during 5 days of immersion of carbon steel electrodes in reference solution (SCP) and solution with corrosion inhibitor based on sugarcane ash sand (SBAS) (GROMBONI et al., 2021). Figure 16 illustrates the SEM images of the working electrode surfaces.

The passivation products are already visible in Figure 16 (A) and (E), where the defects formed by the polishing process become undetectable as the passivating layer formation process occurs. Rod-shaped precipitates are clearly observed in Figure 16 (B) and (F), which grow at the edge when the amount of precipitate increases with immersion time, leading to a globular structure, starting from the third day, as illustrated in Figure

16 (C) and (G). As seen in the micrographs, the steel surface immersed in the SBAS medium shows a higher total coverage than in the REF medium. This behavior is more evident in the final monitoring period, as per Figure 16 (D), where there is a completely covered surface (GROMBONI et al., 2021).

Figure 16. SEM images of the working electrode surfaces after different numbers of days of immersion

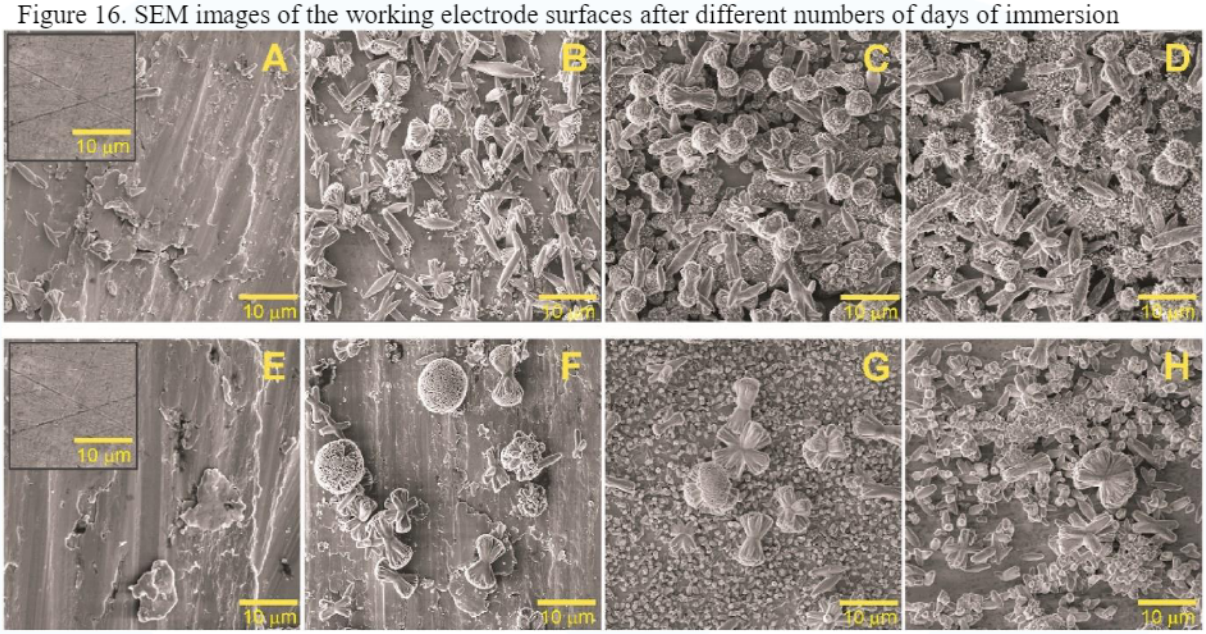

Source: (GROMBONI et al., 2021)

A possible explanation for precipitate formation comes from the local pH variation at the steel/solution interface. It is well known that the formation of passive films (iron oxides and hydroxides) promotes a local pH decrease, causing a pH shift of up to 3 units according to some authors (SILVA et al., 2016). In solutions containing large amounts of calcium hydroxides, as is the case of the solutions investigated here, an important decrease in the solubility of CaCO3 could reasonably explain the precipitation of such compounds in the passivated steel.

SEM was used to characterize the surface morphology of super hydrophobic low carbon steel (SHLCS) and low carbon steel (LCS) in a study on the chloride corrosion resistance of double-layer anti-corrosion coating. The elemental composition of the surface after being immersed in SPC containing 3.5% by weight chloride for 4 days was measured by EDS (QU et al., 2021). Three different modification methods were used to

ISSN: 1696-8352

reduce the surface energy of the rough structure by obtaining a super hydrophobic surface: 1) the LCS surface deposited with Zn/Ag was heated to 100 °C for 1 h (SHLCS-H); 2) the LCS surface deposited with Zn/Ag was soaked in 0.02 M stearic acid ethanol solution for 12 h and then air-dried (SHLCS-STA) and; 3) the LCS surface deposited with Zn/Ag was soaked in an ethanol solution of stearic acid 0,02 M for 12 h and then heated to 100 °C for 1 h, to form the super hydrophobic surface (SHLCS-STA&H).

Figure 17 shows the surface of the LCS after immersion, and spherical rust can be seen in the micrograph, which is a typical feature of goethite (α - FeOOH) (TIAN et al., 2019). At the same time, it is verified in the results of the EDS analysis, in Figure 17(a) that there is chlorine on the surface of the LCS. Furthermore, it can be seen in Figure 17 (b) and (c) that there are other substances adhered to the surface of SHLCS-H and SHLCS-STA from SCP. The EDS analysis in Figure 17 (b) and (c) finds the presence of Cl, K, Ca, Na and other substances. The SEM images and EDS analysis results of SHLCS-H and SHLCS-STA show that the superhydrophobic effects on the surface of the two samples disappear, causing the substances on the SCP to attach to the surface of the samples. However, the SHLCS-STA and SHLCS-H surface still maintain good roughness, as shown in Figure 17 (b) and (c) (QU et al., 2021).

The disappearance of the superhydrophobicity may be due to the loss of low surface energy functional groups on the surface of the structure. Although the superhydrophobic effects of the SHLCS-STA and SHLCS-H surfaces are disappearing, no obvious corrosion traces are observed in the SEM images. This may occur because the rough surface structure and the inner Zn coating may also protect the inner LCS substrate. The surface morphology of SHLCS-STA&H, illustrated in Figure 17 (d), after being immersed for 4 d is not significantly different from that before being immersed. The EDS analysis results also show no chloride and other substances from the pore solution, which indicates that the surface of SHLCS-STA&H is still superhydrophobic (QU et al., 2021).

Figure 17. SEM micrographs and EDS element analysis results of LCS and SHLCS samples after exposure to simulated concrete pore solution containing 3.5% by weight NaCl for 4 days.

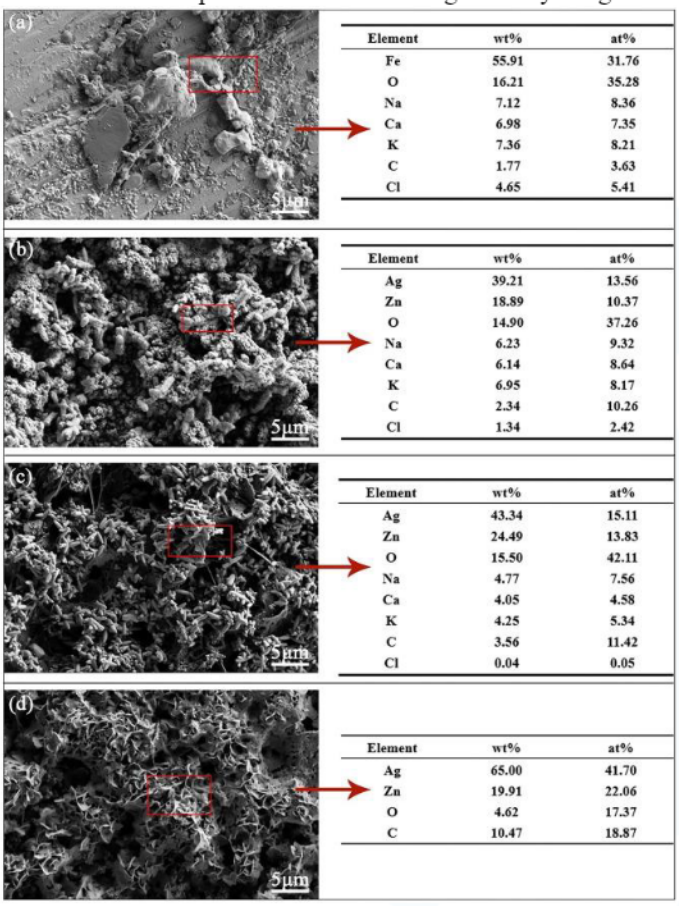

Element	wt%	at%
Fe	55.91	31.76
O	16.21	35.28
Na	7.12	8.36
Ca	6.98	7.35
K	7.36	8.21
C	1.77	3.63
Cl	4.65	5.41

Element	wt%	at%
Ag	39.21	13.56
Zn	18.89	10.37
O	14.90	37.26
Na	6.23	9.32
Ca	6.14	8.64
K	6.95	8.17
C	2.34	10.26
Cl	1.34	2.42

Element	wt%	at%
Ag	43.34	15.11
Zn	24.49	13.83
O	15.50	42.11
Na	4.77	7.56
Ca	4.05	4.58
K	4.25	5.34
C	3.56	11.42
Cl	0.04	0.05

Element	wt%	at%
Ag	65.00	41.70
Zn	19.91	22.06
O	4.62	17.37
C	10.47	18.87

Source: (QU et al., 2021)

In this study, in particular, SHLCS-STA&H showed better corrosion resistance than other samples (SHLCS-STA, SHLCS-H and LCS), with a 97.1% corrosion protection. After immersing the sample in simulated 4 d concrete pore solution, SHLCS-STA&H still maintained the super-hydrophobic property. The double anti-corrosion strategy of the Zn layer and the super-hydrophobic layer significantly improved the anticorrosive efficiency of carbon steel in the simulated solution of concrete pores.

4 CONCLUSION

The systematic review showed that the use of simulated concrete pore solutions (SCP) has gained space in the scientific world, especially with regard to the study of corrosion of steel rebar, because this solution allows simulating, in the environment of an

ISSN: 1696-8352

electrochemical cell, accelerated corrosion, which makes it possible to quickly assess what happens to steel rebar when immersed in concrete as a function of time, in addition to the possibility of simulating attacks such as the maritime environment and carbonation.

However, the use of SCP composed only of saturated calcium hydroxide, even being widely used, is not enough to simulate the content of what is actually present in the pores of concrete, because the only corrosion inhibitor is the concentration of hydroxyl, which determines the limit of chlorides to initiate steel corrosion.

Therefore, the use of an SPC composed by the mixture of cement and water better represents the reality, due to the hydration of the Portland cement contain a series of ions (Na+ , K+ , Ca2, Mg2+, Al2+ and (SO4)2-), the chlorine ions are physically adsorbed by the CSH (hydrated silicate) and C3A (tricalcium aluminate) chemically binds chlorides to produce Friedel salt (C3A.CaCl2.10H2O), which guarantees steel a lower risk of corrosion, as it promotes the removal of a portion of the chlorine ions from the solution.

OCP monitoring is a widely used electrochemical technique to evaluate the formation of passivating oxide films or corrosive oxides on a metal. However, this technique indicates only the balance between the anodic and cathodic reaction, without offering quantitative information, therefore, it is not possible to obtain results regarding the speed of corrosion of the rebar, being, the corrosion potential of the reinforcements in the concrete a quantity that indicates a corrosion situation or passive state of these, in an approximate way.

The techniques used to obtain the Evans diagram, are quantitative tests, which allow to identify the instantaneous corrosion rate of a metal and, through measurements, to verify the corrosion rate in a given time, The objective of obtaining the polarization curve is to have information on kinetic parameters of passivation, such as corrosion potential (Ecorr), using Tafel, polarization resistance (Rp), corrosion current (icorr) and corrosion speed (Vcorr).

The techniques most used to do such analysis are the Linear Polarization Resistance (LPR) and Linear Voltammetry (LSV), but it is also possible to obtain with response, with less experimental error, using electrochemical impedance spectroscopy (EIS).

ISSN: 1696-8352

With the EIS technique, for the steel/concrete system, it is possible to obtain information on various parameters, such as the presence of surface films, concrete characteristics, interfacial corrosion and mass transfer phenomena. However, the interpretation of the results can be a difficult task, and the need for an equivalent circuit, which can change according to steel conditions, makes the technique more acceptable for laboratory studies.

The main advantages of this technique are: 1. Provides information on the kinetics of the process, by the speed of corrosion; 2. Accuracy and reproducibility, suitable for high resistivity environments such as concrete; 3. Provide data on the electrochemical control mechanism, indicating whether the corrosive process occurs by activation, concentration or diffusion; 4. Characterize the steel reinforcement state and corrosion morphology; 5. Be non-destructive and non-disruptive, since signals applied are of small amplitude, so that the corrosion potential is not changed; 6. Allow the monitoring of the evolution of the passive or active state over time.

Given the above, it is evident that for the use of solutions that simulate the pores of concrete the ideal is to use water/cement ratios that allow the filtration and dissolution of ions in solution, so that it is possible to apply electrochemical techniques obtaining a result as close as possible to reality.

ACKNOWLEDGMENTS

The authors would like to thank the Network of Biodiversity and Biotechnology of the Legal Amazon (BIONORTE) and the Coordination of Improvement of Higher Education Personnel (CAPES) for supporting the work.

ISSN: 1696-8352

REFERENCES

ALONSO, C.; ANDRADE, C. Effect of nitrite as a corrosion inhibitor in contaminated and chloride-free carbonated mortar. Materials Journal, [s. l.], v. 87, n. 2, p. 130–137, 1990.

ANDRADE, C.; ALONSO, C. Corrosion rate monitoring in the laboratory and on-site. Construction and building materials, [s. l.], v. 10, n. 5, p. 315–328, 1996.

ANDRADE, C.; BUJÁK, R. Effects of some mineral additions to Portland cement on reinforcement corrosion. Cement and Concrete Research, [s. l.], v. 53, p. 59–67, 2013. Disponível em: http://dx.doi.org/10.1016/j.cemconres.2013.06.004.

ASTM, C. C876 - Standard test method for corrosion potentials of uncoated reinforcing steel in concrete. ASTM International: West Conshohocken, West Conshohocken, PA, USA, 2015.

ASTM, G. G 59-Standard test method for conducting potentiodynamic polarization resistance measurements. [S. l.: s. n.], 2014.

BAKKER, R. F. M. Corrosion of stell in concrete. London: [s. n.], 1988.

BEN MANSOUR, H.; DHOUIBI, L.; IDRISSI, H. Effect of Phosphate-based inhibitor on prestressing tendons corrosion in simulated concrete pore solution contaminated by chloride ions. Construction and Building Materials, [s. l.], v. 171, p. 250–260, 2018. Disponível em: https://doi.org/10.1016/j.conbuildmat.2018.03.118.

BOLINA, F. L.; TUTIKIAN, B. F.; HELENE, P. Patologia de estruturas. [S. l.]: Oficina de Textos, 2019.

BOMMERSBACH, P. et al. Formation and behaviour study of an environment-friendly corrosion inhibitor by electrochemical methods. Electrochimica Acta, [s. l.], v. 51, n. 6, p. 1076–1084, 2005.

CALLISTER, W. D.; RETHWISCH, D. G. Ciência e Engenharia de Materiais: uma introdução. Rio de Janeiro: LTC, 2002. v. 589

CASCUDO, O. O controle da corrosão de Armaduras de Concreto Armado. Goiânia: Editora PINI, 1997.

CHEN, M. et al. Novel Ca-SLS-LDH nanocomposites obtained via lignosulfonate modification for corrosion protection of steel bars in simulated concrete pore solution. Applied Clay Science, [s. l.], v. 211, n. June, p. 106195, 2021. Disponível em: https://doi.org/10.1016/j.clay.2021.106195.

COMMITTEE, G. G106 - Practice for Verification of Algorithm and Equipment for Electrochemical Impedance Measurements. ASTM International, [s. l.], 2010.

CRAMER, S. D.; B.S. COVINO, JR., E. Corrosion: Fundamentals, Testing, and Protection. Journal of Thermal Spray Technology, [s. l.], v. 12, n. 4, p. 459–463, 2003.

ISSN: 1696-8352

DIARD, J. P.; LE GORREC, B.; MONTELLA, C. Handbook of Electrochemical Impedance Spectroscopy-Electrical Circuits containing CPEs. Bio-logic Science Instruments, [s. l.], 2013.

ELSENER, B. et al. Half-cell potential measurements—Potential mapping on reinforced concrete structures. Materials and Structures, New York, v. 36, n. 7, p. 461–471, 2003.

FENG, X. et al. The corrosion inhibition efficiency of aluminum tripolyphosphate on carbon steel in carbonated concrete pore solution. Corrosion Science, [s. l.], v. 124, p. 150–159, 2017.

GENTIL, V. Corrosão. Rio de Janeiro: LTC-Livros Técnicos e Científicos Editora SA, 1996.

GROMBONI, M. F. et al. Impact of agro-industrial waste on steel corrosion susceptibility in media simulating concrete pore solutions. Journal of Cleaner Production, [s. l.], v. 284, p. 124697, 2021. Disponível em: https://doi.org/10.1016/j.jclepro.2020.124697.

GU, G. P.; BEAUDOIN, J. J.; RAMACHANDRAN, V. S. Techniques for corrosion investigation in reinforced concrete. New York: William Andrew Publishing, 2001.

HELENE, P.; ANDRADE, T. Concreto de cimento Portland. São Paulo: IBRACON, 2007.

HOU, B.; LI, X.; CHEN, G. The Roles of Input Matrix and Nodal Dynamics in Network Controllability. IEEE Transactions on Control of Network Systems, [s. l.], v. 5, n. 4, p. 1764–1774, 2018.

JIANG, L. et al. Influence of chloride salt type on threshold level of reinforcement corrosion in simulated concrete pore solutions. Construction and Building Materials, [s. l.], v. 30, p. 516–521, 2012. Disponível em: http://dx.doi.org/10.1016/j.conbuildmat.2011.12.044.

KAPAT, C.; PRADHAN, B.; BHATTACHARJEE, B. Potentiostatic study of reinforcing steel in chloride contaminated concrete powder solution extracts. Corrosion Science, [s. l.], v. 48, n. 7, p. 1757–1769, 2006.

KATIYAR, P. K.; RANDHAWA, N. S. Corrosion behavior of WC-Co tool bits in simulated (concrete , soil , and mine) solutions with and without chloride additions. International Journal of Refractory Metals & Hard Materials, [s. l.], v. 85, n. July, p. 105062, 2019. Disponível em: https://doi.org/10.1016/j.ijrmhm.2019.105062.

KEMPL, J.; ÇOPUROGLU, O. The interaction of pH, pore solution composition and solid phase composition of carbonated blast furnace slag cement paste activated with aqueous sodium monofluorophosphate. 15th Euroseminar on Microscopy Applied to Building Materials, [s. l.], n. June 2015, p. 287–296, 2015.

KOCH, G. Cost of corrosion. In: TRENDS IN OIL AND GAS CORROSION RESEARCH AND TECHNOLOGIES: PRODUCTION AND TRANSMISSION. [S. l.]: Elsevier Ltd, 2017. p. 3–30.

KORNBLUM, N.; BLACKWOOD, R. K.; MOOBERRY, D. D. The Reaction of Aliphatic Nitro Compounds with Nitrite Esters1, 2. Journal of the American Chemical Society, [s. l.], v. 78, n. 7, p. 1501–1504, 1956.

KULAKOWSKI, M. P. Contribuição ao estudo da carbonatação em concretos e argamassas compostos com adição de sílica ativa. 2002. 199 f. - LUME - Repositório Digital, Porto Alegre, 2002.

L.T. MAMMOLITI, L. C.; BROWN, C. M. H.; HOPE, B. B. The influence of surface finish of reinforcing steel and pH of the test solution on the chloride threshold concentration for corrosion initiation in synthetic pore solution. Cement and Concrete Research, [s. l.], v. 26, n. December, p. 545–550, 1996.

LI, J. et al. Effect of heat treatment on corrosion behavior of AZ63 magnesium alloy in 3.5 wt.% sodium chloride solution. Corrosion Science, [s. l.], v. 111, p. 288–301, 2016.

LI, W. et al. Effects of two fungicides on the corrosion resistance of copper in 3 . 5 % NaCl solution under various conditions. Corrosion Science, [s. l.], v. 53, n. 2, p. 735–745, 2011. Disponível em: http://dx.doi.org/10.1016/j.corsci.2010.11.006.

LITTLE, B. J.; LEE, J. S.; RAY, R. I. Diagnosing, measuring and monitoring microbiologically influenced corrosion (MIC) (J. W. e Sons, Org.). Ontario, EUA: REVIE, R. W., 2011.

LIU, J. Z. et al. Corrosion behavior of carbon steel in chloride contaminated simulated concrete pore solution with carboxylate of benzoic acid and dimethylethanolamine. Anti-Corrosion Methods and Materials, [s. l.], v. 64, n. 5, p. 555–562, 2017.

LONGUET, P. La phase liquide du ciment hydraté. Revue des Materiaux de constructions, [s. l.], v. 676, p. 35–41, 1973.

MACDONALD, J. R. Impedence Spectroscopy--Emphasizing Solid Materials and Systems. Wiley-Interscience, John Wiley and Sons, [s. l.], p. 1–346, 1987.

MANDAL, S. et al. Ammonium phosphate as inhibitor to mitigate the corrosion of steel rebar in chloride contaminated concrete pore solution. Molecules, [s. l.], v. 25, n. 17, 2020.

METHA, P. K.; MONTEIRO, P. J. M. Concreto: microestrutura, propriedades e materiais. São Paulo: IBRACON, 2014. v. 2

MOHER, D. et al. Preferred reporting items for systematic review and meta-analysis protocols (PRISMA-P) 2015 statement. Systematic reviews, [s. l.], v. 4, n. 1, p. 1–9, 2015.

NACE. Standard recommended practice: preparation, installation, analysis, and interpretation of corrosion coupons in oilfield operations. [S. l.]: NACE, 2005.

O'CONNOR, A.; SARGEANT, J.; WOOD, H. Systematic reviews. Veterinary Epidemiology, [s. l.], p. 397–420, 2017.

ISSN: 1696-8352

OGUNSANYA, I. G.; HANSSON, C. M. Influence of chloride and sulphate anions on the electronic and electrochemical properties of passive films formed on steel reinforcing bars. Materialia, [s. l.], v. 8, p. 100491, 2019.

ORTOLAN, V. de K. Avaliação da influência do pH e da força iônica da solução dos poros do concreto na resistência à corrosão da armadura. 2015. 128 f. - Unisinos, São Leopoldo, 2015.

PACHECO-TORGAL, F. et al. Biotechnologies and biomimetics for civil engineering. Biotechnologies and Biomimetics for Civil Engineering, [s. l.], p. 1–437, 2015.

PENG, Y. et al. Effect of simulated pore solution on passivation characteristic of P110 steel. Journal of Petroleum Science and Engineering, [s. l.], v. 167, n. March, p. 949–956, 2018. Disponível em: https://doi.org/10.1016/j.petrol.2018.03.009.

PEREZ, N. Electrochemistry and corrosion science. Kluwer Academic publishers, [s. l.], p. 189–246, 2004.

PLUSQUELLEC, G. et al. Determination of the pH and the free alkali metal content in the pore solution of concrete: Review and experimental comparison. Cement and Concrete Research, [s. l.], v. 96, p. 13–26, 2017.

POSSAN, E. et al. CO2 uptake potential due to concrete carbonation: A case study. Case Studies in Construction Materials, [s. l.], v. 6, p. 147–161, 2017. Disponível em: http://dx.doi.org/10.1016/j.cscm.2017.01.007.

POURSAEE, A. Corrosion of steel bars in saturated Ca(OH)2 and concrete pore solution. Concrete Research Letters, [s. l.], v. 1, n. 3, p. 90–97, 2010.

POURSAEE, A.; ANGST, U. M. Principles of corrosion of steel in concrete structures. In: CORROSION OF STEEL IN CONCRETE STRUCTURES. [S. l.]: Elsevier Ltd, 2023. p. 17–34.

PRADHAN, B.; BHATTACHARJEE, B. Corrosion zones of rebar in chloride contaminated concrete through potentiostatic study in concrete powder solution extracts. Corrosion Science, [s. l.], v. 49, n. 10, p. 3935–3952, 2007.

QU, L. et al. Chloride corrosion resistance of double-layer anticorrosive coating in simulated concrete pore solution. Construction and Building Materials, [s. l.], v. 295, p. 123682, 2021. Disponível em: https://doi.org/10.1016/j.conbuildmat.2021.123682.

RANI, B. E. A.; BASU, B. B. J. Green inhibitors for corrosion protection of metals and alloys: An overview. International Journal of Corrosion, [s. l.], v. 2012, n. 6, p. 16–25, 2012.

RETTER, U. et al. On the impedance of potassium nickel (II) hexacyanoferrate (II) composite electrodes * the generalization of the Randles model referring to inhomogeneous electrode materials. Journal of Electroanalytical Chemistry, [s. l.], v. 546, p. 87–96, 2003.

ISSN: 1696-8352

RIBEIRO, D. V. et al. Corrosão em Estruturas de Concreto Armado: Teoria, Controle e Métodos de Análise. São Paulo: Elsevier, 2013. v. 1

RIBEIRO, D. V.; SOUZA, C. A. C.; ABRANTES, J. C. C. Uso da Espectroscopia de Impedância Eletroquímica (EIE) para monitoramento da corrosão em concreto armado. Revista IBRACON de Estruturas e Materiais, [s. l.], v. 8, p. 529–546, 2015.

SAHOO, G.; BALASUBRAMANIAM, R. On the corrosion behaviour of phosphoric irons in simulated concrete pore solution. Corrosion Science, [s. l.], v. 50, n. 1, p. 131–143, 2008.

SCOTT, A.; ALEXANDRE, M. G. Effect of supplementary cementitious materials (binder type) on the pore solution chemistry and the corrosion of steel in alkaline environments. Cement and Concrete Research, [s. l.], v. 89, p. 45–55, 2016.

SEDRIKS, A. J. Effects of Alloy Composition and Microstructure on the Passivity of Stainless Steels. Corrosion, [s. l.], v. 42, n. 7, p. 376–389, 1986.

SHAHEEN, F.; PRADHAN, B. Influence of sulfate ion and associated cation type on steel reinforcement corrosion in concrete powder aqueous solution in the presence of chloride ions. Cement and Concrete Research, [s. l.], v. 91, p. 73–86, 2017.

SHI, J. et al. Improved corrosion resistance of a new 6% Cr steel in simulated concrete pore solution contaminated by chlorides. Corrosion Science, [s. l.], v. 174, 2020.

SHI, J. et al. Role of red mud in natural passivation and chloride-induced depassivation of reinforcing steels in alkaline concrete pore solutions. Corrosion Science, [s. l.], v. 190, n. June, p. 109669, 2021. Disponível em: https://doi.org/10.1016/j.corsci.2021.109669.

SILVA, M. M. et al. Near-surface solution pH measurements during the pitting corrosion of AISI 1020 steel using a ring-shaped sensor. Journal of Electroanalytical Chemistry, [s. l.], v. 780, p. 379–385, 2016.

SILVERMAN, D. C. Practical corrosion prediction using electrochemical techniques. Uhlig's Corrosion Handbook, [s. l.], p. 1129–1166, 2011.

SOUZA, R. H. F. de; TAVARES, M. E. da N.; TEIXEIRA, P. J. B. Avaliação da Capacidade Resistente e da Aderência de Elementos da Marquise do Estádio do Maracanã. Engenharia Estudo e Pesquisa, Rio de Janeiro, v. 13, n. 2, p. 3–9, 2014.

SRINIVASAN, S.; KANE, R. D. Experimental Simulation of Multiphase CO2/H2S Systems. CORROSION 99, [s. l.], 1999.

STERN, M.; WEISERT, E. D. Experimental observations on the relation between polarization resistance and corrosion rate. Proc. Am. Soc. Test. Mater, [s. l.], v. 59, p. 1280, 1959.

TEYMOURI, F. et al. Passive film alteration of reinforcing steel through [MoO42−]/[RCOO−] interfacial co-interaction for enhanced corrosion resistance in chloride contaminated concrete pore solution. [S. l.: s. n.], 2022.

TIAN, Y. et al. Cr-modified low alloy steel reinforcement embedded in mortar for two years: Corrosion result of marine field test. Cement and Concrete Composites, [s. l.], v. 97, p. 190–201, 2019.

TIAN, H. et al. Triazolyl-acylhydrazone derivatives as novel inhibitors for copper corrosion in chloride solutions. Corrosion Science, [s. l.], v. 100, p. 341–352, 2015. Disponível em: http://dx.doi.org/10.1016/j.corsci.2015.08.022.

TRAN, V. T. et al. Magnetic Layer-by-Layer Assembly: From Linear Plasmonic Polymers to Oligomers. ACS Applied Materials and Interfaces, [s. l.], v. 12, n. 14, p. 16584–16591, 2020.

URRA MEDINA, E.; BARRÍA PAILAQUILÉN, R. M. Systematic Reviews and Meta-analysis: Understanding the Best Evidence in Primary Healthcare. Revista latino-americana de enfermagem, [s. l.], v. 18, n. 4, p. 824–831, 2010.

VELEVA, L. et al. Comparative cyclic voltammetry and surface analysis of passive films grown on stainless steel 316 in concrete pore model solutions. Journal of Electroanalytical Chemistry, [s. l.], v. 537, p. 85–93, 2002.

VITÓRIO, J. A. P. Fundamentos da patologia das estruturas nas perícias de engenharia. Instituto Pernambucano de Avaliações e Perícias de Engenharia, [s. l.], p. 58, 2003.

WAGNER, C.; TRAUD, W. Zeitschrift fur Elektrochemie und angewandte physikalische Chemie. Elektrochem, [s. l.], v. 44, p. 391–454, 1938.

XU, P. et al. Corrosion inhibition efficiency of compound nitrite with D-sodium gluconate on carbon steel in simulated concrete pore solution. Construction and Building Materials, [s. l.], v. 288, p. 123101, 2021. Disponível em: https://doi.org/10.1016/j.conbuildmat.2021.123101.

XU, P. et al. Influence of sulfate salt type on passive film of steel in simulated concrete pore solution. Construction and Building Materials, [s. l.], v. 223, p. 352–359, 2019.

XU, J.; TAN, Q.; MEI, Y. Corrosion protection of steel by Mg-Al layered double hydroxides in simulated concrete pore solution: Effect of SO42-. Corrosion Science, [s. l.], v. 163, n. September 2019, 2020.

YANG, R.-J. et al. Effect of sodium d-gluconate-based inhibitor in preventing corrosion of reinforcing steel in simulated concrete pore solutions. Acta Physico-Chimica Sinica, [s. l.], v. 28, n. 8, p. 1923–1928, 2012.

YANG, H. et al. Preparation of corrosion inhibitor loaded zeolites and corrosion resistance of carbon steel in simulated concrete pore solution. Construction and Building Materials, [s. l.], v. 225, p. 90–98, 2019. Disponível em: https://doi.org/10.1016/j.conbuildmat.2019.07.141.

YAO, N. et al. Synergistic effect of red mud and fly ash on passivation and corrosion resistance of 304 stainless steel in alkaline concrete pore solutions. Cement and Concrete Composites, [s. l.], v. 132, 2022.

ISSN: 1696-8352

ZHAI, M. et al. Layered double hydroxides (LDHs) modified cement-based materials: A systematic review. Nanotechnology Reviews, [s. l.], v. 11, n. 1, p. 2857–2874, 2022.

ZHAO, Yazhou et al. Corrosion inhibition efficiency of triethanolammonium dodecylbenzene sulfonate on Q235 carbon steel in simulated concrete pore solution. Corrosion Science, [s. l.], v. 158, n. June, p. 108097, 2019. Disponível em: https://doi.org/10.1016/j.corsci.2019.108097.

ZHAO, Y et al. Corrosion inhibition efficiency of triethanolammonium dodecylbenzene sulfonate on Q235 carbon steel in simulated concrete pore solution. Corrosion Science, [s. l.], v. 158, 2019.

ZHENG, H. et al. Influence of calcium ion in concrete pore solution on the passivation of galvanized steel bars. Cement and Concrete Research, [s. l.], v. 108, n. October 2017, p. 46–58, 2018. Disponível em: https://doi.org/10.1016/j.cemconres.2018.03.001.

ZHI, F. et al. Inhibition effect and mechanism of polyacrylamide for steel corrosion in simulated concrete pore solution. Construction and Building Materials, [s. l.], v. 259, p. 120425, 2020. Disponível em: https://doi.org/10.1016/j.conbuildmat.2020.120425.

ZIMER, A. M. Estudo da corrosão do aço ao carbono em meio de sulfeto. 2009. 241 f. - UFSCar, São Carlos, 2009.

Capítulo III: Evaluation of Cellulose-Derived Biopolymers on Steel Corrosion Susceptibility in Environments Simulating Concrete Pore Solutions - A Statistical Analysis Using CCRD

Evaluation of Cellulose-Derived Biopolymers on Steel Corrosion Susceptibility in Environments Simulating Concrete Pore Solutions - A Statistical Analysis Using CCRD

Abstract

Hydroxypropyl Methylcellulose (HPMC) can be used as a bioactive in concrete, but little is known about its effects on the steel corrosion process. This article reports on the estimation of steel corrosion susceptibility when immersed in simulated concrete pore solutions with HPMC added. The aim is to understand the corrosion process of reinforced concrete structures. An experimental design was employed to determine the optimal concentrations of HPMC as a corrosion inhibitor in a chloride-contaminated environment. For this analysis, the following experiments were conducted in an electrochemical cell: open-circuit potential (OCP) and linear sweep voltammetry (LSV), in addition to pH and conductivity measurements. The experimental design adopted was a central composite rotatable design (CCRD), with the variables being the amount of HPMC and NaCl, and the responses being the corrosion potential (E_{corr}), polarization resistance (R_p), and conductivity. The statistical analysis of the design showed that for E_{corr}, R_p, and conductivity, the variables HPMC and NaCl were significant ($p < 0.10$), with the statistical model showing a correlation of over 90% with the experimental data. The OCP analysis and polarization curves indicate the formation of a passive film on the steel immersed in a solution containing HPMC. The Tafel polarization demonstrates promising anti-corrosive performance of HPMC. The statistical analysis, through the CCRD, confirmed that the medium containing HPMC exhibits better passivating properties, showing that this biopolymer can be used as a corrosion inhibitor for reinforced concrete in civil construction.

Keywords: corrosion inhibitor; hydroxypropyl methylcellulose (HPMC); concrete pore solution; experimental design; CCRD.

1. Introduction

In recent years, there has been a growing demand for natural or biotechnology-based products for use in industrial applications due to environmental concerns, waste disposal issues, and the depletion of non-renewable resources. In 2002, the European Union (EU) launched the biotechnology strategy, and in 2012 the European Commission created the world's first bioeconomy strategy and action plan (COMMISSION, 2012).

The Portland cement concrete (PCC) industry, which uses the most consumed material in the world, relies on chemical additives to improve its physicochemical properties. However, these mixtures are derived from the exploitation of fossil fuels, which is associated with various types of issues (ATLAS; HAZEN, 2011; BELL *et al.*, 2017; COLGAN, 2014; PITTAU *et al.*, 2019).

One of the challenges faced by the reinforced concrete industry is the corrosion of steel reinforcement. This is a natural electrolytic phenomenon with progressive detrimental effects on material integrity, leading to significant economic losses in various industries (HOU; LI; CHEN, 2018; TRAN *et al.*, 2020).

Among the various methods available to reduce the problem of corrosion, the use of corrosion inhibitors is often the most suitable and effective approach to achieve this goal. This involves isolating the metal from corrosive agents through the adsorption of compounds containing inhibiting molecules on the surface, forming a protective barrier (ARUKALAM *et al.*,

2014; CECCHETTO; DELABOUGLISE; PETIT, 2007; KIM *et al.*, 2006; OGUZIE *et al.*, 2011; PRAVEEN *et al.*, 2007).

One option for green inhibitors is biopolymers whose functional groups interact with metal ions and form complexes that act as a barrier separating the aggressive solution from the metal surface. Therefore, corrosion inhibition is achieved through adsorption (KUMPAWAT; GARG; TAK, 2009; UMOREN, 2008).

Cellulose and its derivatives, such as hydroxypropyl methylcellulose (HPMC), are carbohydrate biopolymers found in larger quantities compared to other biopolymers. It is present in plant tissues and constitutes about one-third of the plant. It has pharmaceutical, cosmetic, and food applications, and various derivatives of cellulose have been used as corrosion inhibitors(NWANONENYI *et al.*, 2016; SOLOMON *et al.*, 2010; UMOREN *et al.*, 2018).

In order to better investigate the impact of using HPMC in concrete formulation and identify its practical effects in civil engineering, this article presents an electrochemical approach to study the durability of carbon steel reinforcement in the presence of HPMC compared to an HPMC-free environment.

The focus was to analyze the early stages of passive film formation on carbon steel reinforcement in contact with simulated concrete pore solutions (SCPS) rather than using mortar as the medium, with or without HPMC in their compositions, using electrochemical experiments. The SPSs exhibit much lower resistivity and equivalent results compared to those conducted in concrete matrices (GHODS, P. *et al.*, 2009; LEE *et al.*, 2018; TOUJAS; VÁZQUEZ; VALCARCE, 2017; YONEZAWA; ASHWORTH; PROCTER, 1988).

For the definition of the SPSs composition, statistical process optimization was used, which offers advantages over classical optimization by changing one variable at a time(BOX; HUNTER; HUNTER, 1978), with a smaller number of experiments and the possibility of evaluating the effects of interaction between variables. Such systematic experimental design techniques aim at optimizing products and processes, minimizing costs and operational times. The methodology of central composite rotatable design (CCRD) consists of a group of statistical and mathematical procedures that can be used to study the interrelationships between one or more responses (dependent variables) and numerous factors (independent variables) (NETO; SCARMINIO; BRUNS, 1996).

Therefore, the objective of this work was to optimize the use of HPMC as a corrosion inhibitor in chloride-contaminated environments, evaluating the significant variables for corrosion analysis and optimizing these variables through response surface methodology. This is a simpler and faster methodology that could be applied to investigate the formation of a passive film on steel, thus contributing to the current understanding of the impact of the environment on rebar corrosion susceptibility.

2. Materials and methods

2.1. Preparation of the simulated concrete pore solution (SPS)

The materials used were commercial-grade raw materials, and when necessary, they were of analytical grade. CPII-F32 cement from the Goiás brand, purchased in Palmas/TO city, was used. CPII-F32 cement is composed of carbonate material, the majority of which is calcium carbonate, with a compressive strength class of 32 MPa. In order to control and inhibit possible interference and unforeseen external reactions as much as possible, this type of cement was chosen mainly due to its composition, which does not contain alternative materials such as blast furnace slag and pozzolana, as in other types of cement. , as there is no research on the reactivity of hydroxypropylmethylcellulose (HPMC) with these compounds, it was preferable to eliminate them from the research. Table 1 shows the chemical composition of the cement used in this research.

Table 1. Chemical composition of CPII-F32 cement.

Chemical element	***%***
Total calcium oxide (CaO)	61.2
Total silicon dioxide (SiO_2)	18.87
Aluminum oxide (Al_2O_3)	4.42
Carbonic anhydride (CO_2)	3.85
Magnesium oxide (MgO)	3.23
Iron oxide (Fe_2O_3)	2.97
Sulfuric anhydride (SO_3)	2.75
Insoluble residue	1.26
Potassium oxide (K_2O)	0.86
Others	0.46
Sodium oxide (Na_2O)	0.13

Source: ABCP, 2020

The HPMC used in this work was manufactured by AROMAT Produtos Químicos LTDA. Sodium chloride PA (NaCl) was manufactured by Nox Lab Solutions and has a purity of 99.0%, according to the manufacturer. Mili-Q® water was produced using equipment manufactured by PERMUTION, and the deionized water has the following parameters: pH around 7.0 and conductivity below 2 µS/cm.

Due to the difficulty of faithfully reproducing the solution present in the pores of a reinforced concrete structure through solution synthesis, in this research, we chose to simulate the concrete pore solution using a mixture of cement and Mili-Q® water. To achieve this, a cement-to-water ratio of 0.075 (PACEWSKA *et al.*, 2002). The composition of SPS is basically sodium hydroxide (NaOH), potassium hydroxide (KOH) and saturated calcium hydroxide ($Ca(OH)_2$) (POURSAEE; ANGST, 2023), in addition to the additions of HPMC and NaCl.

The dry material (cement and HPMC) was mixed with Mili-Q® water in an electromagnetic stirrer for 60 minutes. After this period, the solution was vacuum filtered, separating the inert material, so that the supernatants did not interfere with the polarization of the steel. To simulate the corrosive environment, sodium chloride (NaCl) was inserted into the SPS solution.

2.2. Preparation of the working electrode

To produce the working electrodes (WE), a 5 mm CA-50 steel bar was initially filed to remove the side ribs. Soon after, the steel bar went through the polishing process, using water sandpaper. Then the steel bar was cut into 3.0 cm long pieces. To ensure good conductivity, a copper wire was welded to one end of the steel bar, via flux soldering with a silver alloy, as shown in Figure 1. After welding, cleaning was carried out to degrease the electrodes.

Figure 1. Working electrode in the construction process.
Source: author himself

To ensure that only the transverse face of the working electrode (0.18 cm^2) would be in contact with the solution, phosphating was carried out and subsequent polymerization of the working electrode.

Phosphating is a treatment where a metal is converted into an oxide, hydroxide or salt of the metal through electrochemical reactions. It involves the conversion of the metal into an insoluble phosphate of the metal ion. Insoluble phosphate deposits on the metal, modifying its surface properties (RAUSCH, 1990). In this work, the phosphatized layers were obtained by immersing the working electrodes (WE) in a phosphoric acid solution for around 60 minutes.

After phosphating, the working electrodes (WE) were embedded in transparent oepoxy resin supplied by POLIPOX (RL-3028 resin and EL-3041 catalyst) and cured for 48 hours. Finally, the face of the electrode was exposed, using water sandpaper in the granulometric sequence 800, 1500 and 2000. Figure 2 schematically illustrates the finished working electrode (WE).

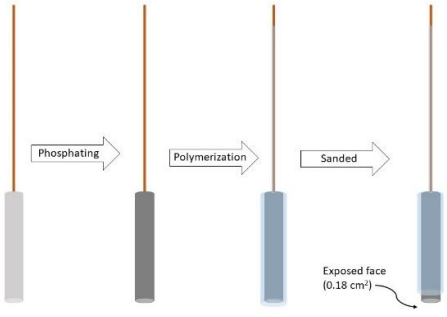

Figure 2. Finished working electrode
Source: author himself

To get closer to the reality of the behavior of steel immersed in concrete, it was necessary to keep the work electrodes immersed in simulated concrete pore solutions (SPS) for 14 days, in order to passivatione the reinforcement, as illustrated in Figure 3.

The conventional carbon steel passivation process in concrete is a spontaneous electrochemical reduction mechanism that occurs on the steel surface through interaction with the alkaline solution in the pores (PEREZ, 2004). This passivation process plays a decisive role in the corrosion model initiation phase of the concrete structure (YEOMANS, 2004).

Figure 3. Working electrode in the passivation process
Source: author himself

2.2. Methods

All electrochemical characterizations were conducted in a conventional three-electrode glass cell at 23°C, using an Vertex potentiostat/galvanostat controlled via IviumSoft software.

Ag/AgCl was used as the reference electrode (RE), and a platinum wire was used as the counter electrode (CE) ,in addition to the working electrode (WE).

The pH and conductivity of the SPSs and the electrochemical analyses were measured on the day of sample preparation and after 14 days of passivation. The pH and conductivity values were measured after a 5-minute stabilization period. The conductivities and pHs of these solutions were determined and are listed in Table 2 as average values obtained from triplicate analyses.

Table 2. Physicochemical Properties of Concrete Pore Solution (SPS)

SPS	NaCl	HPMC	pH		Conductivity (mS/cm)	
	(g/L)	(g/L)	0 dias	14 dias	0 dias	14 dias
REF	-	-	12.86±0.02	13.11±0.03	8.79±2.48	8.38±2.62
H0N3	35.10	-	12.96±0.05	13.01±0.10	42.88±1.68	65.45±3.95
H12N3	35.10	1.20	12.87.6±0.11	12.94.3±0.21	52.45±4.55	60.47±2.43

The pH of all analyzed solutions increased after the electrochemical tests. This phenomenon can be explained by the composition of the solution in question, where SPS has an alkaline pH, with typical values between 12.5 and 13.5 because of the main constituents of the solution which are alkaline. In this pH range, it is viable to use steel reinforcement in conjunction with concrete, considering that with these hydrogenionic potentials the

reinforcement remains in a state of passivation (METHA; MONTEIRO, 2014).

For the analysis of the electrochemical cells, the following techniques were used: open potential circuit monitoring (OCP) and linear swept volvametry (LSV), both using the Vertex potentiostat/galvanostat controlled through the IviumSoft software.

A metal that corrodes in a solution of low electrical resistivity assumes a characteristic potential, known as corrosion potential. This potential is given by the intersection of the anodic polarization curve with the cathodic polarization curve. Corrosion potential is one of the easiest electrochemical parameters to be determined experimentally. As this is a potential assumed by the metal, it is sufficient to obtain a direct measurement of this potential in relation to a reference electrode. This measurement is known as open circuit potential measurement (TICIANELLI, 1998).

OCP monitoring is a typical half-cell potential method, indicating the reaction potential of a metal with an environment. OCP monitoring is widely used to evaluate the corrosion potential of reinforcing steel embedded in concrete relative to a standard reference electrode (e.g., Ag/AgCl electrode). The corrosion risk level of reinforcement in ordinary concrete can be assessed by OCP values in accordance with ASTM C876:2022 (ASTM, 2015).

When the researcher's objective is to evaluate the formation of the passivating film, automatic monitoring is recommended over a short period of time (maximum one hour) to observe the change in the electrochemical behavior of the system (PENG *et al.*, 2018), this was considered for this research.

Linear sweep voltammetry (LSV) is another electrochemical method for characterizing the corrosion state of a metal. A potential range is applied, from lowest to highest, monitoring the response current throughout the sweep. Basically, the application of potential aims to simulate corrosion, but in an accelerated way, to understand the behavior of the metal. To perform the potential sweep, most authors choose to apply a potential between ± 10 mV and ± 20 mV in relation to OCP (BRIZ; BIEZMA; BASTIDAS, 2018; MUNDRA *et al.*, 2017; WANG; ZUO; TANG, 2018).

At potentials below the OCP, the polarization curve (CP) is called the cathodic curve and, for potentials above the OCP, the anodic curve. Polarization curves are also called Evans diagram. In this work, the sweep occurred from -1500 mV to +500 mV, versus OCP, with a speed of 0.167 mV/s.

The polarization curve of a metal represents the global effect of all reactions that occur simultaneously on the electrode, and through it is possible to evaluate the electrochemical behavior of a metal at a potential different from the corrosion potential. It is necessary to use external potential sources, such as a potentiostat, to impose a different potential on an electrode than the corrosion potential. This potential is imposed through a difference between the potential of the electrode and the reference electrode, in media with moderate to high conductivity, thus making it possible to measure the polarization current, in addition to

recording it as a function of the potential (GENTIL, 1996; WOLYNEC, 2003).

To determine the corrosion potential (E_{corr}), extrapolation of Tafel lines was used. Tafel's approach involves plotting the logarithm of the absolute value |i| current density versus potential. The slopes of these linear segments produce transfer coefficients, called Tafel Slopes. Extrapolating these straight lines to the corrosion potential makes it possible to obtain the corrosion current (i_{corr}).

The corrosion current density (j_{cor}) was determined using the method described by McCafferty (MANSFELD, 1976; MCCAFFERTY, 2005), which consists of dividing the net current (i_{corr}) by the exposed area of the working electrode (0.18 cm^2). The polarization resistance (R_p), was determined from the Stern-Geary constant (B) and calculated using the following formula (MANSFELD, 1976).

$$R_p = \frac{B}{j_{cor}} \qquad (1)$$

During the potential sweep the current density goes to zero and then increases to a low anodic value, approximately constant in the passive range. In this range, a thin oxide/hydroxide film, the passivating film, protects the material from high corrosion rates. If the current density decreases when the potential sweep direction has been reversed, the material proves immune to pitting corrosion. However, if on the upward sweep of potential, the current density increases suddenly and remains high on the downward sweep, until finally decreasing to the value of the passive region, the material is shown to undergo a form of pitting corrosion. The pitting potential (E_{pite}) was also determined from the polarization curves. This was the potential at which the current density increased suddenly (WANG, 2016).

Through polarization it is possible to determine the corrosion rate, in mm/year for example, of materials. In this case, corrosion is not necessarily restricted to pitting corrosion, but can reach a level of generalized corrosion. The corrosion rate measurement is, in general, associated with widespread corrosion. From the i_{corr} value, the corrosion rate (V_{corr}) of the system can be determined using Faraday's Law (GENTIL, 1996). The corrosion rate (V_{cor}) is related as follows:

$$V_{corr} = \frac{j_{corr} * M * t}{n * F * d} \qquad (2)$$

where "M" is the molar mass of iron (0.056 kg/mol); "d" is the density of iron (7.847 kg/m^3); "n" is the valency of an Fe+2 ion; "F" is the Faraday's constant (96.485 C/mol); and "t" is the time coefficient (3.15^{*} x $10^{7\cdot}$ s/year). Considering the parameters for iron, Equation 2 reduces to (ANDRADE; ALONSO, 2004):

$$V_{cor} \approx 11.6 * j_{cor} \ \ (mm/year) \qquad (3)$$

where the corrosion current density (j_{cor}) should be in units of (mA/cm^2).

2.3. Experimental Design

The experimental design conducted aims to evaluate the effect of variables for optimizing the composition of the simulated concrete pore solution (SPS) using HPMC and NaCl. This was achieved through a central composite rotational design (CCRD) 2^2 containing 3 central points and 4 axial points. Each parameter was studied at four different levels (-1.41; -1;0; +1 +1.41), generating a matrix of 11 experiments with two factors, using the Protimiza software (2014), as shown in Table 3. in addition to the reference solution containing only cement and water and another solution with the addition of 3.5% by weight of NaCl.

The ranges of variation between the upper and lower limits of each independent variable were established according to the most commonly used data for the analysis of corrosion inhibitors based on biopolymers and the simulation of chloride-contaminated environments (D'OLIVEIRA *et al.*, 2022).

Table 3. List of Central Composite Rotatable Design (CCRD) tests.

Experiment	Coded variables		Real variables	
	X1	X2	HPMC (g/L)	NaCl (g/L)
1	-1.00	-1.00	0.60	17.50
2	1.00	-1.00	1.20	17.50
3	-1.00	1.00	0.60	35.10
4	1.00	1.00	1.20	35.10
5	-1.41	0	0.48	26.30
6	1.41	0	1.32	26.30
7	0	-1.41	0.90	13.85
8	0	1.41	0.90	38.75
9	0	0	0.90	26.30
10	0	0	0.90	26.30
11	0	0	0.90	26.30

2.4. Experiment Validation

In the Central Composite Rotatable Design (CCRD), three central points were used, and two independent variables were considered: the amounts of HPMC and NaCl added to the SPSs. The dependent variables in this design were the electrochemical parameters (OCP, E_{corr} e R_p) and the conductivity.

This experimental design includes an effects table, a Pareto chart, calculated regression coefficients, and statistical analysis using ANOVA. Additionally, its aim was to analyze the effects of HPMC and NaCl on steel rebars and evaluate response surface plots, thus achieving the optimization of HPMC as a corrosion inhibitor for steel in reinforced concrete.

3. Results and discussion

3.1. Open Circuit Potential (OCP) and Sweep Linear Voltammetry (SLV)

Measuring the OCP or half-cell potential is one of the common methods for evaluating the corrosion state of steel rebars in reinforced concrete structures. Due to the simplicity of this method, it is generally used in industrial and laboratory applications. However, it should be

noted that the potential may not accurately reflect the corrosion state because the corrosion process is related to the current transfer or flow of electrons through the anodic dissolution of the metal (M), as in the following reaction:

$$M \rightarrow M^{n+} + ne \qquad (4)$$

According to the ASTM C87.6-22b (ASTM, 2015) standard, which introduces a standard test method for half-cell potentials, this should not be interpreted as an indicator of the corrosion reaction. However, the open circuit potential could be a suitable estimate of the rebar's corrosion state in concrete and could indicate the likelihood of corrosion. According to ASTM C87.6-22b, there are three ranges of OCP for corrosion estimation, and Table 4 shows the correlation between the saturated calomel electrode (SCE) and the Ag/AgCl electrode used in this work.

Table 4. Probability of Reinforcement Corrosion Occurrence as a Function of Potential.

Electrode type	**Likelihood of corrosion occurring**		
	OCP< 10%	**10%<OCP<90%**	**OCP> 90%**
Hg, Hg_2Cl_2. KCl (Calomelano/SCE)	> -126 mV	-126 mV à -27.6 mV	< -276 mV
Ag, AgCl/KCl (1M)	> -106 mV	-106 mV à -256 mV	< -256 mV

Source: Modified (ASTM, 2022)

The variation in OCP values of the steel reinforcement bars in SCPS over a period of 14 days of passivation is shown in Figure 4, where it can be observed that the potentials increased positively during this period, with the exception of the H0N3 solutions (with a concentration of 35.1 g/L of NaCl), which was expected as this solution simulates a highly corrosive environment.

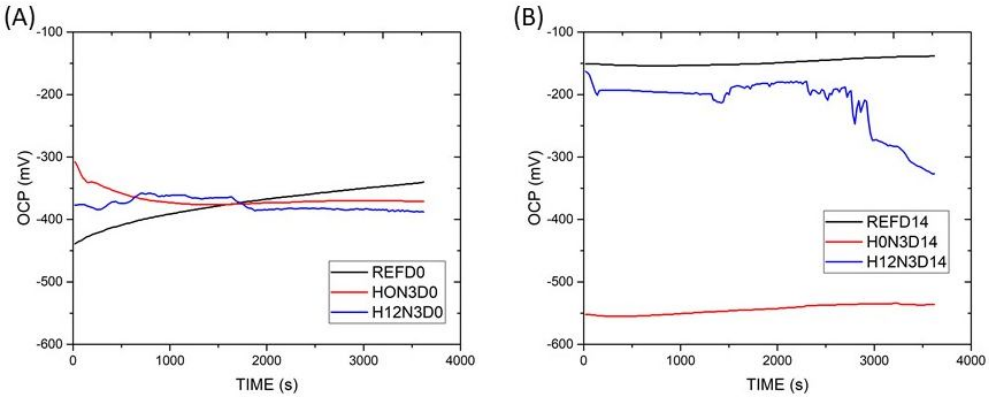

Figure 4. Evolution of open-circuit potential (OCP) values as a function of immersion time, 0 (A) and 14 days (B), for steel samples in simulated reference concrete solution (REFD0 and REFD14); 35.1 g/L of NaCl for simulating a corrosive environment (HON3D0 and HON3D14); and with 35.1 g/L of NaCl and 1.20 g/L of HPMC as a corrosion inhibitor (H12N3D0 and H12N3D14).

During the passivation period, the pH level of the SPS remained above 12 (RÄSÄNEN; PENTTALA, 2004) as shown in Table 2. When the pH is above 12. a passive layer forms on the surface of the steel rebar. This layer is responsible for reducing the corrosion rate and increasing the open-circuit potential.

After the addition of NaCl to the SPS, chloride ions can penetrate through this film and reach the surface of the steel reinforcement, deteriorating the passive layer. Due to the depassivation of the steel bars as a result of chloride attack, the corrosion potential decreases.

It is possible to identify that the use of HPMC, with the aim of inhibiting the corrosive attack, proved to be effective, as even with the presence of NaCl, the sample containing HPMC at a concentration of 1.2 g/L (H12N3) showed an increase in OCP at the end of the 14-day passivation period. However, when using Table 3 to assess the probability of corrosion at 14 days, the REF and H12N3 solutions are in the range between 10% and 90% probability of corrosion occurrence, where uncertainty prevails; whereas the H0N3 sample remained with half-cell potentials below -27.6 mV, suggesting a probability above 90% of corrosion occurrence, indicating that the simulated environment is indeed corrosive.

As suggested by Song and Saraswathy (SONG; SARASWATHY, 2007) half-cell potential measurements alone are not sufficient criteria for corrosion because several factors like limited oxygen diffusion polarization, concrete porosity, and the presence of highly resistive layers can affect the accuracy of potential values. Moreover, the generalization of OCP measurements is debatable since significant variations in corrosion rate can occur within relatively narrow potential ranges (SONG; SARASWATHY, 2007).

Regarding the obtained electrical conductivity values, a significant variation was observed during the measurement period. In some situations, equipment variation was substantial, which affects the accuracy of the results. Few authors have reported electrical conductivity measurements of SCPS. Among the authors who evaluated steel reinforcement corrosion in SCPS made directly with cement, only Shaheen and Pradhan [33] measured the electrical conductivity of this solution. In their study, researchers obtained a value of approximately 5.5 mS/cm, which is roughly half of the values obtained in the present research for the reference solution and much lower when compared to the solutions with the addition of HPMC and NaCl. What is evident from the values obtained in this article is the increase in conductivity with the addition of NaCl. Certainly, this factor influences the corrosion process, as will be explained later, because an increase in electrical conductivity leads to greater ionic movement in the solution, aiding the steel oxidation process.

In order to investigate an initial hypothesis that CPSs containing HPMC exhibited different passivating natures, linear sweep voltammetry (LSV) was conducted at the initial and final measurement periods (0 and 14 days). The resulting comparison between the systems based on these polarization curves was presented in Figure 5. The most important parameters measured from these polarization curves were summarized in Table 5.

Regarding the corrosion potential, E_{corr}, less negative values were obtained for the H12N3D0 solution compared to the reference solution (REFD0), with a difference in E_{corr} f 165 mV between the two electrodes when freshly immersed in the pore solution. After 14 days, the scenario changed slightly, and the E_{corr} values showed a relatively low difference of

approximately 20 mV. The shift of E_{corr} towards less negative values over the 14-day immersion period may indicate that the immersion time in the SPSs improves resistance to the corrosion process, suggesting the formation of a passivating layer. In contrast, for the solution containing only NaCl (H0N3), the result was the opposite, with E_{corr} being the most negative of all samples, and during the 14-day immersion, the potential shifted to even more negative values, indicating a worsening of corrosion resistance.

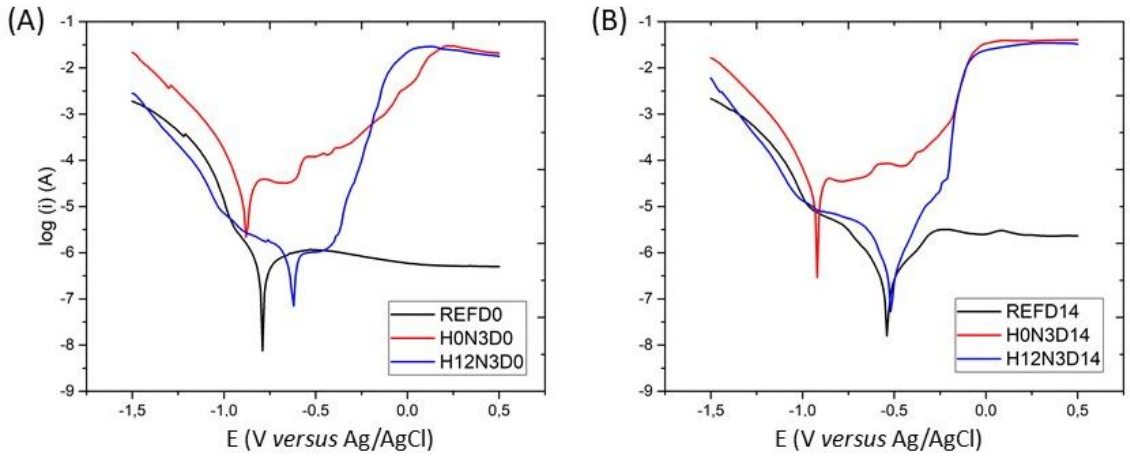

Figure 5. Polarization curves as a function of immersion time, 0 (A) and 14 days (B), of steel samples in simulated concrete solution of reference (REFD0 and REFD14); with only 35.1 g/L of NaCl for simulating the corrosive environment (HON3D0 and HON3D14); and with 35.1 g/L of NaCl and 1.2 g/L of HPMC as a corrosion inhibitor (H12N3D0 and H12N3D14).

Table 5. Tafel data obtained from polarization curves shown in Figure 5.

Solutions	HPMC (g/L)	NaCl (g/L)	E_{corr} (mV vs. Ag/AgCl/NaCl 3M)	J_{cor} ($\mu A/cm^2$)	R_p ($k\Omega/cm^2$)	E_{pite} (mV vs. Ag/AgCl/NaCl 3M)	V_{corr} (mm/year)
REFD0	0	0	-793	0.79	97.40	>+500	0.009
REFD14			-541	0.92	187.80	>+500	0.011
H0N3D0	0	35.1	-883	52.59	2.10	-410	0.610
H0N3D14			-920	20.56	1.90	-200	0.238
H12N3D0	1.2	35.1	-628	1.43	66.10	-380	0.017
H12N3D14			-521	1.11	90.10	-210	0.013

It is worth noting that the values found for OCP during monitoring differ from the values found for E_{corr} using the linear sweep voltammetry (LSV) technique, but the behavior of both measurements is the same.

OCP monitoring is an electrochemical technique widely used to evaluate the formation of passivating oxide films or corrosive oxides on a metal. However, this technique only indicates the balance between the anodic and cathodic reactions, without offering quantitative information, therefore, it is not possible to obtain results regarding the corrosion rate of rebar, with the corrosion potential of reinforcement in concrete being a magnitude which indicates a

situation of corrosion or its passive state, approximately.

The techniques used to obtain the Evans diagram are quantitative tests, which allow identifying the instantaneous corrosion rate of a metal and, through measurements, verifying the corrosion rate in a given time, with the objective of obtaining the polarization curve is to have information on kinetic parameters of passivation, such as corrosion potential (E_{corr}), using Tafel, polarization resistance (R_p), corrosion current (i_{corr}) and corrosion speed (V_{corr}).

It was also observed that the pitting potential (E_{pite}) exhibited the same behavior as E_{corr}. Thus, after 14 days of immersion in the H12N3 solution, Epite shifted by +17.0 mV. These results are consistent with the OCP analysis results shown in Figure 1.

Furthermore, the corrosion current densities (J_{corr}), polarization resistances (R_p), and corrosion rates (V_{corr}) obtained reveal a lower corrosion rate and higher resistivity of the reference solution (REF) and the H12N3 solution compared to the corrosive solution (H0N3), the corrosion rate values being 0.011 mm/year, 0.013 mm/year and 0.238 mm/year and the resistivity of the solutions in question were, respectively, 187.8 kΩ/cm^2, 90.1 kΩ/cm^2 and 1.9 kΩ/cm^2. This reinforcened the hypothesis of passive film formation in the HPMC-containing medium. As R_p is commonly used as a measure of a metal's resistance to corrosion damage, high Rp values are associated with a high corrosion prevention capacity, while low R_p values indicate high corrosive activity (LU; BA, 2010).

3.2. Statistical analysis using CCRD

This experimental design of the CCRD type was chosen to optimize the dosage of HPMC as a corrosion inhibitor for reinforced concrete reinforcement.

The minimum and maximum ranges of the parameters were investigated, and the complete experimental design with its values in both real and coded form is listed in Table 6. Open circuit potential (OCP), corrosion potential (E_{corr}), polarization resistance (R_p), and conductivity were taken as dependent variables or responses (Y_1. Y_2. Y_3 e Y_4). A second-order polynomial equation was fitted to the data using multiple regression analysis for each of the four dependent variables. This resulted in an empirical model that related each of the measured responses to the independent parameters, as per Equations 5, 6, 7, and 8. Only the central point was performed in triplicate, but the experiments were repeated twice. For the 2-factor system, the model equations are as follows:

OCP: $Y_1 = -493.33 + 11.89x_1 + 47.23x_1^2 - 27.55x_2 + 146.23x_2^2\ 191.75x_1x_2$ (5)

E_{corr}: $Y_2 = -829 - 34.75x_1 + 159.36x_1^2 + 6.59x_2 + 106.99x_2^2 + 189.58x_1x_2$ (6)

R_p: $Y_3 = 23.46 + 15.25x_1 + 32.28x_1^2 - 1.25x_2 + 22.67x_2^2 + 5.69x_1x_2$ (7)

Condutividade: $Y_4 = 57.07 - 0.86x_1 - 3.53x_1^2 + 17.89x_2 + 2.84x_2^2 - 1.26x_1x_2$ (8)

where Y_1. Y_2. Y_3 e Y_4 these are the predicted responses., x_1 e x_2 these are linear coefficients; x_1^2. x_2^2 these are quadratic coefficients e x_1x_2 This is the interaction coefficient.

Table 6. CCRD 2^2 experimental design for the optimization of HPMC as a corrosion inhibitor.

Experiment	Independent variables		Dependent variables			
	HPMC (g/L)	NaCl (g/L)	OCP (mV)	E_{corr} (mV)	R_p (kΩ)	Conductivity (mS/cm²)
1	0.60	17.50	-17.0	-384.3	66.21	22.80
2	1.20	17.50	-542	-833.5	98,23	23.42
3	0.60	35.10	-622	-830.0	35.35	67.30
4	1.20	35.10	-227	-520.9	90.14	62.90
5	0.48	26.30	-334	-382.0	81.50	57.70
6	1.32	26.30	-283	-479.5	106.40	55.50
7.	0.90	13.85	-81	-601.2	64.49	37.08
8	0.90	38.75	-140	-469,8	84.95	78.90
9	0.90	26.30	-528	-842.6	27.70	57.10
10	0.90	26.30	-490	-913.6	22.56	57.12
11	0.90	26.30	-462	-730.8	27.06	57.00

According to the results obtained in the experimental design (CCRD), regression coefficients were calculated, and a complete statistical analysis was conducted with ANOVA, Pareto chart, and response surface plots. The results of the linear regression coefficients for OCP, E_{corr}, R_p, and conductivity in the CCRD are presented in Tables 7, 9, 11, and 13, respectively. The ANOVA was presented in Tables 8, 10, 12, and 14, respectively.

3.2.1. Analysis of the open circuit potential (OCP)

Analyzing the results presented in Table 6, we can see that the least negative value of OCP, after the electrode passivation for 14 days, was achieved in experiment 1, with a value of -17.0 mV, for concentrations of 0.60 g/L of HPMC and 17.50 g/L of NaCl. This result indicates that the lower the chloride content, the less corrosive the environment becomes, ensuring the formation of the passivating film with small amounts of HPMC.

The presence of chloride can indeed accelerate the dissolution of the metallic alloy or stabilize the dissolution of favorable regions such as grain boundaries or manganese sulfide (MnS) inclusions (STEWART; WILLIAMS, 1992). Inclusions are referred to as non-metallic material particles with different chemical compositions that are retained within the matrix of various types of steels as a result of their manufacturing process. They are typically already present as impurities in the liquid state of the steel, which makes their removal difficul (ZHANG, 2006).

The results obtained in experiments 9, 10, and 11, which are the central points, did not show significant variability, indicating the good reproducibility of the process.

When comparing the OCP values obtained at the lowest and highest concentrations of HPMC, it is observed that increasing the concentration from 0.60 g/L to 1.20 g/L resulted in an improvement in the OCP values, changing from -622 mV to -227 mV. Regarding the concentrations of NaCl, higher chloride concentrations led to more negative OCP values, and this situation can be modified with the use of corrosion inhibitors.

Table 7 provides the regression coefficients based on the results obtained in the CCRD

experimental design, Table 8 presents a complete statistical analysis with ANOVA, and Figure 6 illustrates the Pareto diagram, all of which pertain to the dependent variable OCP.

Table 7. Linear regression coefficients for the CCRD, related to OCP.

Name	Coefficient	Standard error	Calculated T	P-value
Mean	-493.33	67.43	-7.32	0.0007*
X_1	11.89	41.29	0.29	0.7849
X_1^2	47.23	49.15	0.96	0.3807
X_2	-27.55	41.29	-0.67	0.5341
X_2^2	146.23	49.15	2.98	0.0310*
X_1X_2	191.75	58.39	3.28	0.0219*

* Statistically significant values at 90% confidence level ($p < 0.10$)

Table 8. ANOVA for the CCRD, related to OCP.

Source of variation	Sum of squares	Degrees of freedom	Middle square	F_{calc}	P-value
Regression	275138.5	5	55027.7	4.0	0.07600
Waste	68196.1	5	13639.2		
Lack of adjustment	66001.4	3	22000.5	20.0	0.04788
Pure error	2194.7	2	1097.3		
Total	343334.5	10			

% Explained variation (R^2) = 80.14

The results for the variables x_2^2 e x_1x_2 are statistically significant at a 90% confidence level. Furthermore, they have positive coefficients of 146.23 and 191.75, respectively. It's worth noting that the R^2 value found explains approximately 80% of the experiment, which provides a measure of how much variability in the observed response values can be explained by the experimental factors and their interactions. The closer the R^2 value is to 1, the stronger the model, and the better the predictive capabilities. Therefore, values above 0.8 are considered good for obtaining a valid and useful predictive model.

Figure 6 illustrates which variables and interactions analyzed yielded statistically significant results according to the Pareto chart. It can be observed that only the quadratic variable x_2^2 and the interaction of variables x_1-x_2 were significant, while the others would not influence the process if there was an increase in their concentration from level -1.41 to level +1.41.

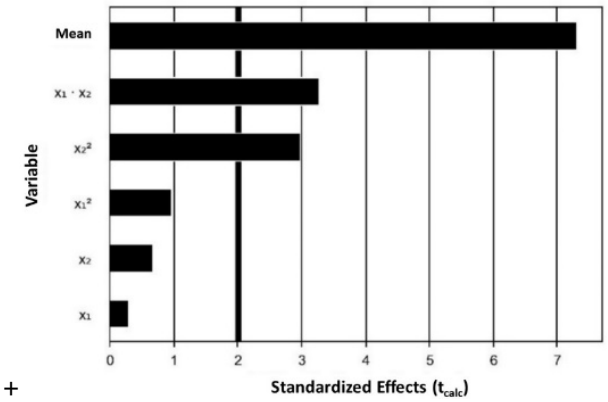

Figure 6. Main effects of significant variables and interactions in the CCRD, related to OCP.
Source: PROTMIZA (2014)

3.2.2. Corrosion potential analysis (E_{corr})

In Table 6, you can observe the E_{corr} values after 14 days of electrode immersion in a solution. In experiment 1, a value of -384.3 mV was achieved for concentrations of 0.60 g/L of HPMC and 17.50 g/L of NaCl. However, in experiments 3 and 4, where the NaCl concentration is at its maximum (35.10 g/L), the increase in HPMC concentration from 0.60 g/L to 1.20 g/L was responsible for shifting the E_{corr} to the right by approximately 309 mV.

This behavior was already expected since the solutions have a pH greater than 12. With these high hydrogenic potentials, the reinforcement remains in a state of passivation (WOLYNEC, 2003), and the OCP is also less negative, indicating a likely passivation zone.

The results obtained in the experiments related to the central points did not show significant variability, indicating good process reproducibility.

Table 9 provides the regression coefficients based on the results obtained in the CCRD experimental design, Table 10 presents a complete statistical analysis with ANOVA, and Figure 7 illustrates the Pareto diagram, all of which pertain to the dependent variable E_{corr}.

Table 9. Linear regression coefficients for the CCRD, related to E_{corr}.

Name	Coefficient	Standard error	Calculated T	P-value
Mean	-829,00	73.16	-11.33	0.0001*
X_1	-34.7.5	44.80	-0.78	0.4731
X_1^2	159.36	53.33	2.99	0.0305*
X_2	6.59	44.80	0.15	0.8888
X_2^2	106.99	53.33	2.01	0.1011*
X_1X_2	189.58	63.36	2.99	0.0304*

* Statistically significant values at 90% confidence ($p<0.10$)

Tabela 10. ANOVA para o CCRD, referente ao E_{corr}.

Source of variation	Sum of squares	Degrees of freedom	Middle square	F_{calc}	P-value
Regression	319517.6	5	63903.5	4.0	0.07791
Waste	80294.1	5	16058.8		
Lack of adjustment	63308.8	3	21102.9	2.5	0.29988
Pure error	16985.4	2	8492.7		
Total	399811.7	10			

% Explained variation (R^2) = 79.92

The linear regression coefficients for the CCRD experimental design concerning the dependent variable, E_{corr}, can be found in Table 9. The results for the variables $x_1^{2\cdot}$ x_2^2 and x_1 x_2 are statistically significant at a 90% confidence level. Additionally, they have positive coefficients of 159.36, 106.99, and 189.58, respectively.

Table 10 provides the ANOVA statistical analysis for the dependent variable, E_{corr}. The R^2 value was approximately 80%, indicating that only 20% of the variation was not explained by the model, which is considered good for obtaining a valid and useful predictive model.

In Figure 7, you can see which variables and interactions analyzed yielded statistically significant results according to the Pareto chart. It can be observed that only variables x_1 and x_2 x_1 and x_2 were not significant, while the others would influence the process if there was an increase in their concentration from level -1.41 to level +1.41.

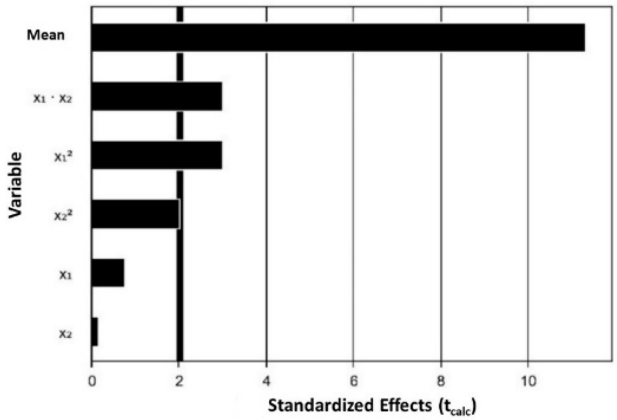

Figura 7. Main effects of significant variables and interactions in the CCRD, related to E_{corr}.
Source: PROTMIZA (2014)

3.2.3. Polarization resistance analysis (R_p)

The Rp values, after 14 days of passivation, are also found in Table 6. It can be observed that, similar to the OCP and E_{corr} values, the polarization resistance (R_p) in experiments 1, 3, and 4 shows a trend where the reduction in corrosion is directly related to the increase in HPMC concentration in the solution. Even in highly corrosive environments, the presence of HPMC serves to alleviate the potential consequences of chloride attacks on the steel rebar. We can see that the highest R_p value was achieved in experiment 6, with a value of 106.4 kΩ, for concentrations of 1.32 g/L of HPMC and 26.30 g/L of NaCl. This result indicates that the higher the HPMC content, the greater the likelihood of it acting as a corrosion inhibitor, ensuring the formation of the passivating film.

If we compare experiments 3 and 4, where the NaCl concentration is 35.10 g/L, we can see that R_p nearly tripled in value, going from 35.35 kΩ to 90.14 kΩ, with just the addition of 0.12 g/L of HPMC.

R_p is used as a parameter to assess a metal's resistance to corrosion damage. Therefore, high Rp values indicate a high corrosion prevention capacity (LU; BA, 2010).

The results obtained in experiments 9, 10, and 11, which are the central points, did not show significant variability, indicating the good reproducibility of the process.

Table 11 provides the regression coefficients based on the results obtained in the CCRD experimental design, Table 12 presents a complete statistical analysis with ANOVA, and Figure 8 illustrates the Pareto diagram, all of which pertain to the dependent variable R_p.

Table 11. Linear regression coefficients for the CCRD, related to R_p.

Name	Coefficient	Standard error	Calculated t	P-value
Mean	23.46	8.98	2.61	0.047.6*
X_1	15.25	5.50	2.77	0.0393*
X_1^2	32.28	6.55	4.93	0.0044*
X_2	-1.25	5.50	-0.23	0.8290
X_2^2	22.67	6.55	3.46	0.0180*
X_1X_2	5.69	7.78	0.73	0.4972

* Statistically significant values at a 90% confidence level (p<0.10)

Tabela 12. ANOVA for the CCRD, related to R_p.

Source of variation	Sum of squares	Degrees of freedom	Middle square	F_{calc}	P-value
Regression	8960.1	5	1792.0	7.4	0.02325
Waste	1210.8	5	242.2		
Lack of adjustment	1189.8	3	396.6	37.8	0.02591
Pure error	21.0	2	10.5		
Total	10170.9	10			

% Explained variation (R^2) = 88.10

The linear regression coefficients for the CCRD experimental design concerning the dependent variable, R_p, can be found in Table 11. The results for the variables x_1. x_1^2 and x_2^2 are statistically significant at the 90% confidence level. Furthermore, they presented positive coefficients of 15, 25, 32, 28 and 22.67, respectively.

Table 12 provides the ANOVA statistical analysis for the dependent variable, R_p. The R^2 value was approximately 88%, indicating that only 12% of the variation was not explained by the model, which is considered good for obtaining a valid and useful predictive model.

In Figure 8, you can see which variables and interactions analyzed yielded statistically significant results according to the Pareto chart. It can be observed that only variables x_2 e x_1x_2 were not significant, while the others would influence the process if there was an increase in their concentration from level -1.41 to level +1.41.

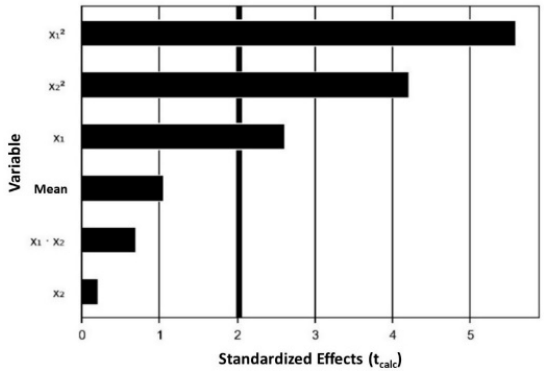

Figure 8. Main effects of significant variables and interactions in the CCRD, related to R_p.
Source: PROTMIZA (2014)

3.2.4. Conductivity analysis

Analyzing the results shown in Table 6, it can be observed that the highest conductivity result was achieved in experiment 8, with 78.90 mS/cm^2, conducted with 0.9 g/L of HPMC and 38.75 g/L of NaCl. On the other hand, the lowest conductivity value was observed in experiment 1, with 22.80 mS/cm^2, where the independent variable concentrations were 0.6 g/L of HPMC and 17.5 g/L of NaCl. When comparing experiment 1 with experiment 3, where the HPMC concentration is kept at 0.6 g/L and the NaCl concentration is doubled to 35.10 g/L, the conductivity triples, reaching 67.30 mS/cm^2. However, the opposite does not occur when maintaining the HPMC concentration at 1.2 g/L and reducing the NaCl concentration by 50%; the impact on conductivity is insignificant.

It is expected that higher conductivity would facilitate corrosion due to the increased mobility of reactive species, allowing the flow of electrons and, therefore, promoting the corrosion of the steel rebar. However, it is not possible to assess the performance of this material based solely on this measurement because many other factors affect the characteristics of the passivating layer, such as the water-to-cement ratio, alkalinity of the pore solution, presence of additives, type of cement, environmental conditions (temperature and relative humidity), and the action of aggressive agents (chloride penetration and carbonation). These factors collectively contribute to the corrosion behavior of the steel reinforcement in concrete (RIBEIRO; LABRINCHA; MORELLI, 2012).

The results obtained in experiments 9, 10, and 11, which are the central points, did not show significant variability, indicating the good reproducibility of the process.

Table 13 provides the regression coefficients based on the results obtained in the CCRD experimental design, Table 14 presents a complete statistical analysis with ANOVA, and Figure 6 illustrates the Pareto chart, all of which pertain to the dependent variable conductivity.

Table 13. Linear regression coefficients for the CCRD, related to conductivity.

Name	Coefficient	Standard error	Calculated T	P-value
Mean	57.07	5.32	10.72	0.0001*
X_1	-0.86	3.26	-0.26	0.8021
X_1^2	-3.53	3.88	-0.91	0.4042
X_2	17.,89	3.26	5.49	0.0027*
X_2^2	-2.84	3.88	-0.73	0.497.2
X_1X_2	-1.26	4.61	-0.27	0.7963

* Statistically significant values at a 90% confidence level (p<0.10)

Table 14. ANOVA for the CCRD, related to conductivity.

Source of variation	Sum of squares	Degrees of freedom	Middle square	F_{calc}	P-value
Regression	2663.3	5	532.7	6.3	0.03271
Waste	425.1	5	85.0		
Lack of adjustment	425.1	3	141.7	34284.0	0.00003
Pure error	0.0	2	0.0		
Total	3088.4	10			

% Explained variation (R^2) = 86.23

Table 13 provides the linear regression coefficients for the CCRD experimental design. The only variable whose results are statistically significant at a 90% confidence level is the variable x_2 (concentration of NaCl in the solution) with a coefficient of 17.89. All other variables, besides not being statistically significant, have negative coefficients.

Table 14 provides a statistical analysis using ANOVA. It's important to note that the R^2 value explains approximately 86% of the experiment, which is a measure of how much variability in the observed response values can be explained by the experimental factors. The closer R^2 is to 1 the stronger the model and the better the predictive capabilities.

In the same table, it is possible to observe that the effect of variable x_1 and the interaction of variables x_1x_2 were very small, as they are smaller than the standard error, and they also had a negative effect. This means that the increase in HPMC concentration and the interaction of HPMC with NaCl did not influence the conductivity value with 90% confidence. This indicates that the NaCl concentration is the only factor responsible for increasing conductivity, which in turn increases ionic mobility, favoring the corrosive process.

In Figure 9, you can see which variables and interactions analyzed yielded statistically significant results according to the Pareto chart. It can be observed that only variable x_2 was significant, while the others would not influence the process if there was an increase in their concentration from level -1.41 to level +1.41.

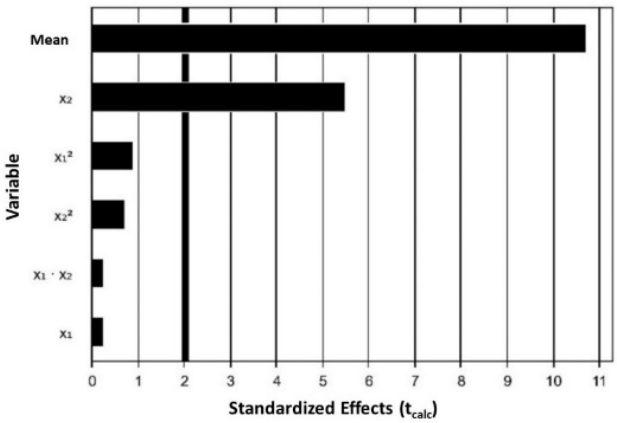

Figure 9. Main effects of significant variables and interactions in the CCRD, related to conductivity.
Source: PROTMIZA (2014)

3.2.5. Response surface analysis for optimization of HPMC use as a corrosion inhibitor

The effect of the two independent variables (HPMC concentration and NaCl concentration) on the use of HPMC as a corrosion inhibitor was analyzed by three-dimensional response surface curves (3D), as illustrated in Figure 10. These curves reflect the relationship between the independent variables, suggesting the corresponding maximum point within the experimental domain. Simultaneously, these surfaces show the influence of various factors on corrosion inhibition analysis. The 3D response surface curves, plotted by a statistically

significant model, serve to understand the interaction of the medium components and the ideal concentration required for each component to assess corrosion inhibition (SONG *et al.*, 2022).

The 3D graphs presented in Figure 10 were based on the concentration function of two variables, where the significance of interactions between the corresponding variables is indicated by an elliptical feature and contour plots. Thus, Figure 10 shows the response surface generated for OCP (A), E_{corr} (B), R_p (C) and conductivity (D), all obtained by the interaction of HPMC with NaCl. The shape of the response surface curves showed moderate interaction between the variables tested, with the exception of the curve in Figure 10(D).

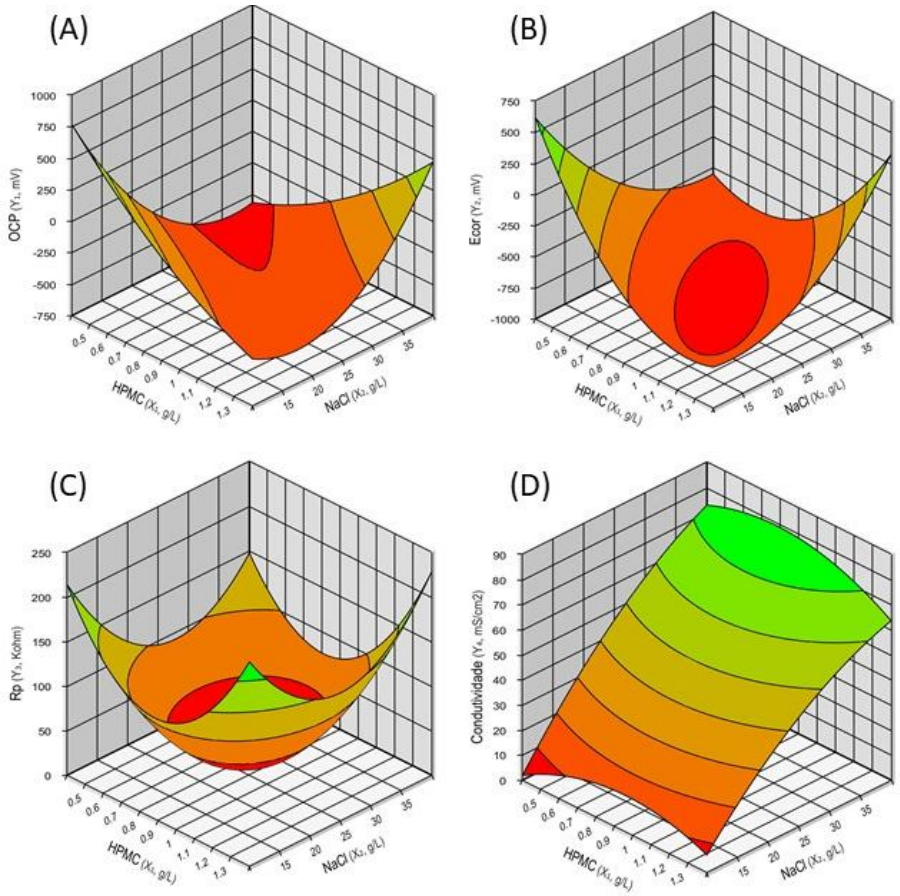

Figure 10. Response surface for the use of HPMC as a corrosion inhibitor for the dependent variables (A) OCP; (B) E_{corr}; (C) R_p; e (D) conductivity.
Source: PROTMIZA (2014)

Figure 10(A) refers to the open circuit potential, where it can be observed that less negative OCP values can be achieved in regions of higher HPMC and NaCl concentration.

Figure 10(B) refers to the corrosion potential, where less negative values suggest a low probability of corrosion. Once again, it can be observed that the region of the graph suggesting this interpretation is where the concentrations of HPMC and NaCl are higher.

In Figure 10(C), high values of polarization resistance (R_p), as this could indicate the formation of a passivating film. It can be seen that this happens when there are high concentrations of HPMC, suggesting that it is responsible for improving passivation formation.

Finally, Figure 10(D) depicts the relationship between conductivity and the simulated concrete pore solution. It's evident that the concentration of HPMC does not influence conductivity, and the only influence is caused by the concentration of NaCl in a directly proportional relationship. This supports the fact that an environment with high chloride ion concentrations is highly corrosive, without showing a direct relationship with the use of HPMC in corrosion inhibition.

4. Conclusions

- According to the OCP and potentiodynamic profiles, a passive film grew rapidly on the surface of steel immersed in a solution containing HPMC, indicating that it can indeed function as a corrosion inhibitor.
- The potentiodynamic studies confirmed that solutions containing 3.5% NaCl, without the corrosion inhibitor (HPMC), H0N3, exhibited high corrosion rates and low polarization resistance values, indicating the presence of flaws or the absence of passivation film formation.
- Once corrosion is initiated, the propagation rate is higher in solutions containing HPMC with concentrations exceeding 50%, likely due to the increase in the conductivity of the pore solution. A concentration of 0.60 g/L of HPMC may result in a physical and electrochemical balance between the closure of micropores and the propagation of suitable pore solution conductivity that controls susceptibility to chloride attack on steel bars. This balance prevents the propagation of higher corrosion currents and creates a propagation condition comparable to the behavior of a reference solution.
- The CCRD experimental design showed that the dependent variables were significant ($p<0.10$), and the statistical model exhibited a correlation of over 90% with the experimental data.
- The ANOVA, along with the Pareto diagram, demonstrated a direct correlation between the increase in HPMC concentration and the improvement of dependent variables (OCP, E_{corr} and R_p), except for an increase in conductivity, which is unrelated to HPMC concentration and instead linked to chloride ion concentration in the solution. However, even with high conductivity, it was evident that HPMC was able to inhibit corrosion, as evidenced by the results of the other dependent variables.

Overall, this study has shown that the addition of HPMC in the concrete mix has potential benefits regarding its passivating properties, meaning that concrete containing HPMC appears to be a less aggressive environment for steel. The reduced susceptibility to steel corrosion in the presence of HPMC is attributed to faster passivation characteristics, as evidenced by monitoring various electrochemical parameters and statistical analysis.

References

ANDRADE, C.; ALONSO, C. Test methods for on-site corrosion rate measurement of steel reinforcement in concrete by means of the polarization resistance method. **Materials and Structures**, [*s. l.*], v. 37, n. 9, p. 623–643, 2004.

ARUKALAM, I. O. *et al.* Experimental and theoretical studies of hydroxyethyl cellulose as inhibitor for acid corrosion inhibition of mild steel and aluminium. **The open corrosion Journal**, [*s. l.*], v. 6, n. 1, 2014.

ASTM. C 876–22b. Standard Test Method for CorrosionPotentials of Uncoated Reinforcing Steel in Concrete. **ASTMInternational**, [*s. l.*], 2022.

ASTM, C. C876 - Standard test method for corrosion potentials of uncoated reinforcing steel in concrete. **ASTM International: West Conshohocken**, West Conshohocken, PA, USA, 2015.

ATLAS, R. M.; HAZEN, T. C. Oil biodegradation and bioremediation: A tale of the two worst spills in U.S. history. **Environmental Science and Technology**, [*s. l.*], v. 45, n. 16, p. 6709–6715, 2011.

BELL, J. *et al.* EU ambition to build the world's leading bioeconomy—Uncertain times demand innovative and sustainable solutions | Elsevier Enhanced Reader. **New Biotechnology**, [*s. l.*], v. 40, n. parte A, p. 25–30, 2017.

BOX, G. E. P.; HUNTER, W. H.; HUNTER, S. **Statistics for experimenters**. [*S. l.*]: John Wiley and sons New York, 1978. v. 664

BRIZ, E.; BIEZMA, M. V.; BASTIDAS, D. M. Stress corrosion cracking of new 2001 lean–duplex stainless steel reinforcements in chloride contained concrete pore solution: An electrochemical study. **Construction and Building Materials**, [*s. l.*], v. 192, p. 1–8, 2018. Disponível em: https://doi.org/10.1016/j.conbuildmat.2018.10.108.

CECCHETTO, L.; DELABOUGLISE, D.; PETIT, J.-P. On the mechanism of the anodic protection of aluminium alloy AA5182 by emeraldine base coatings: Evidences of a galvanic coupling. **Electrochimica acta**, [*s. l.*], v. 52, n. 11, p. 3485–3492, 2007.

COLGAN, J. D. Oil, Domestic Politics, and International Conflict. **Energy Research and Social Science**, [*s. l.*], v. 1, p. 198–205, 2014. Disponível em: http://dx.doi.org/10.1016/j.erss.2014.03.005.

COMMISSION, E. **Innovating for Sustainable Growth: A Bioeconomy for Europe: Communication from the Commission to the European Parliament, the Council and the European Economic and Social Committee and the Committee of the Regions**. [*S. l.*]: Publications Office of the European Union, 2012.

D'OLIVEIRA, M. C. de P. E. *et al.* Estudos recentes sobre compósitos de carboidratos para inibição da corrosão: uma revisão sistemática. **Research, Society and Development**, [*s. l.*], v. 11, n. 9, p. e41811932021, 2022.

GENTIL, V. **Corrosão**. Rio de Janeiro: LTC-Livros Técnicos e Científicos Editora SA, 1996.

GHODS, P. *et al.* The effect of concrete pore solution composition on the quality of passive oxide films on black steel reinforcement. **Cement and Concrete Composites**, [*s. l.*], v. 31, n. 1, p. 2–11, 2009. Disponível em: http://dx.doi.org/10.1016/j.cemconcomp.2008.10.003.

HOU, B.; LI, X.; CHEN, G. The Roles of Input Matrix and Nodal Dynamics in Network Controllability. **IEEE Transactions on Control of Network Systems**, [*s. l.*], v. 5, n. 4, p. 1764–1774, 2018.

KIM, D.-K. *et al.* Electrochemical studies on the alternating current corrosion of mild steel under cathodic protection condition in marine environments. **Electrochimica Acta**, [*s. l.*], v. 51, n. 25, p. 5259–5267, 2006.

KUMPAWAT, V.; GARG, U.; TAK, R. K. Corrosion inhibition of aluminium in acid media by naturally occurring plant Artocarpus heterophyllus and Acacia senegal. **Journal of Indian Council of Chemists**, [*s. l.*], v. 26, n. 1, p. 82–84, 2009.

LEE, H. S. *et al.* Corrosion mitigation of steel rebars in chloride contaminated concrete pore solution using inhibitor: An electrochemical investigation. **Construction and Building Materials**, [*s. l.*], v. 173, p. 443–451, 2018. Disponível em: https://doi.org/10.1016/j.conbuildmat.2018.04.069.

LU, S.; BA, H. J. Corrosion sensor for monitoring the service condition of chloride-contaminated cement mortar. **Sensors**, [*s. l.*], v. 10, n. 4, p. 4145–4158, 2010.

MANSFELD, F. The polarization resistance technique for measuring corrosion currents. *In*: ADVANCES IN CORROSION SCIENCE AND TECHNOLOGY: VOLUME 6. [*S. l.*]: Springer, 1976. p. 163–262.

MCCAFFERTY, E. Validation of corrosion rates measured by the Tafel extrapolation method. **Corrosion science**, [*s. l.*], v. 47, n. 12, p. 3202–3215, 2005.

METHA, P. K.; MONTEIRO, P. J. M. **Concreto: microestrutura, propriedades e materiais**. São Paulo: IBRACON, 2014. v. 2

MUNDRA, S. *et al.* Cement and Concrete Research Chloride-induced corrosion of steel rebars in simulated pore solutions of alkali-activated concretes. **Cement and Concrete Research**, [*s. l.*], v. 100, n. August, p. 385–397, 2017. Disponível em: https://doi.org/10.1016/j.cemconres.2017.08.006.

NETO, B. B.; SCARMINIO, I. S.; BRUNS, R. E. **Planejamento e otimização de experimentos**. [*S. l.*]: Ed. da UNICAMP, 1996.

NWANONENYI, S. *et al.* Inhibitive Performance of Hydroxypropyl Cellulose and Potassium Iodide on the Corrosion of Mild Steel in Sulphuric Acid Environment. **American Chemical Science Journal**, [*s. l.*], v. 16, n. 2, p. 1–12, 2016.

OGUZIE, E. E. *et al.* Understanding corrosion inhibition mechanisms—experimental and theoretical approach. **Rsc Advances**, [*s. l.*], v. 1, n. 5, p. 866–873, 2011.

PACEWSKA, B. *et al.* Modification of the properties of concrete by a new pozzolan - A waste catalyst from the catalytic process in a fluidized bed. **Cement and Concrete Research**, [*s. l.*], v. 32, n. 1, p. 145–152, 2002.

PENG, Y. *et al.* Effect of simulated pore solution on passivation characteristic of P110 steel. **Journal of Petroleum Science and Engineering**, [*s. l.*], v. 167, n. March, p. 949–956, 2018. Disponível em: https://doi.org/10.1016/j.petrol.2018.03.009.

PEREZ, N. Electrochemistry and corrosion science. **Kluwer Academic publishers**, [*s. l.*], p. 189–246, 2004.

PITTAU, F. *et al.* Retrofit as a carbon sink: The carbon storage potentials of the EU housing stock. **Journal of Cleaner Production**, [*s. l.*], v. 214, p. 365–376, 2019. Disponível em: https://doi.org/10.1016/j.jclepro.2018.12.304.

POURSAEE, A.; ANGST, U. M. Principles of corrosion of steel in concrete structures. *In*: CORROSION OF STEEL IN CONCRETE STRUCTURES. [*S. l.*]: Elsevier Ltd, 2023. p. 17–34.

PRAVEEN, B. M. *et al.* Corrosion studies of carbon nanotubes–Zn composite coating. **Surface and Coatings Technology**, [*s. l.*], v. 201, n. 12, p. 5836–5842, 2007.

RÄSÄNEN, V.; PENTTALA, V. The pH measurement of concrete and smoothing mortar using a concrete powder suspension. **Cement and Concrete Research**, [*s. l.*], v. 34, n. 5, p. 813–820, 2004.

RAUSCH, W. **The Phosphating of Metals**. [*S. l.*]: Finishing Publications, 1990. *E-book*. Disponível em: https://books.google.com.br/books?id=8RRUAAAAMAAJ.

RIBEIRO, D. V.; LABRINCHA, J. A.; MORELLI, M. R. Effect of the addition of red mud on the corrosion parameters of reinforced concrete. **Cement and Concrete Research**, [*s. l.*], v. 42, n. 1, p. 124–133, 2012. Disponível em: http://dx.doi.org/10.1016/j.cemconres.2011.09.002.

SOLOMON, M. M. *et al.* Inhibitive and adsorption behaviour of carboxymethyl

cellulose on mild steel corrosion in sulphuric acid solution. **Corrosion Science**, [*s. l.*], v. 52, n. 4, p. 1317–1325, 2010.

SONG, Z. *et al.* Performance of corrosion inhibitor extracted from enzymatic hydrolysate of waste Platanus acerifolia leaves. **Journal of Industrial and Engineering Chemistry**, [*s. l.*], v. 111, p. 464–479, 2022. Disponível em: https://doi.org/10.1016/j.jiec.2022.04.027.

SONG, H.-W.; SARASWATHY, V. Corrosion Monitoring of Reinforced Concrete Structures - A Review. **Int. J. Electrochem. Sci**, [*s. l.*], n. January, p. 1–28, 2007.

STEWART, J.; WILLIAMS, D. E. The initiation of pitting corrosion on austenitic stainless steel: on the role and importance of sulphide inclusions. **Corrosion Science**, [*s. l.*], v. 33, n. 3, 1992.

TICIANELLI, E. A. **Eletroquímica: Princípios e Aplicações Vol. 17**. [*S. l.*]: Edusp, 1998.

TOUJAS, S.; VÁZQUEZ, M.; VALCARCE, M. B. Unexpected effect of citrate ions on the corrosion process of carbon steel in alkaline solutions. **Corrosion Science**, [*s. l.*], v. 128, n. February, p. 94–99, 2017. Disponível em: http://dx.doi.org/10.1016/j.corsci.2017.08.018.

TRAN, V. T. *et al.* Magnetic Layer-by-Layer Assembly: From Linear Plasmonic Polymers to Oligomers. **ACS Applied Materials and Interfaces**, [*s. l.*], v. 12, n. 14, p. 16584–16591, 2020.

UMOREN, S. A. *et al.* Evaluation of chitosan and carboxymethyl cellulose as ecofriendly corrosion inhibitors for steel. **International Journal of Biological Macromolecules**, [*s. l.*], v. 117, p. 1017–1028, 2018.

UMOREN, S. A. Inhibition of aluminium and mild steel corrosion in acidic medium using Gum Arabic. **Cellulose**, [*s. l.*], v. 15, p. 751–761, 2008.

WANG, S. Corrosion resistance and electrocatalytic properties of metallic glasses. **Metallic Glasses-Formation and Properties**, [*s. l.*], v. 395, p. 116–124, 2016.

WANG, Y.; ZUO, Y.; TANG, Y. Inhibition effect and mechanism of sodium oleate on passivation and pitting corrosion of steel in simulated concrete pore solution. **Construction and Building Materials**, [*s. l.*], v. 167, p. 197–204, 2018. Disponível em: https://doi.org/10.1016/j.conbuildmat.2018.01.170.

WOLYNEC, S. **Técnicas Eletroquimicas de corrosão**. 1ªed. São Paulo: [*s. n.*], 2003.

YEOMANS, S. **Galvanized steel reinforcement in concrete**. [*S. l.*]: Elsevier, 2004.

YONEZAWA, T.; ASHWORTH, V.; PROCTER, R. P. M. Pore Solution Composition

and Chloride Effects on the Corrosion of Steel in Concrete. **Corrosion**, [*s. l.*], v. 44, n. 7, p. 489–499, 1988.

ZHANG, L. feng. Inclusion and Bubble in Steel-A Review. **Journal of Iron and Steel Research International**, [*s. l.*], v. 13, n. 3, p. 1–8, 2006.

Capítulo IV: Evaluation of the use of hydroxypropylmethylcellulose (HPMC) as a steel corrosion inhibitor, in media that simulate concrete pore solutions: an electrochemical investigation

Avaliação do uso da hidroxipropilmetilcelulose (HPMC) como inibidor de corrosão do aço, em meios que simulam soluções de poros de concreto: uma investigação eletroquímica

Destaques

- O desempenho da hidroxipropilmetilcelulose (HPMC) como inibidor de corrosão em aço carbono em solução simulada de poros de concreto foram estudados.
- A hidroxipropilmetilcelulose (HPMC) funcionou de forma eficaz como inibidor de corrosão do aço.
- A concentração de HPMC ideal para mitigar a corrosão do aço é mais próxima ao limite superior.
- Foi encontrada eficiência de 98% para a concentração de 1,2 g/l de HPMC em solução contaminada com 71,5 g/L de NaCl.

Resumo

Este artigo trata da caracterização da hidroxipropilmetilcelulose (HPMC) como um inibidor de corrosão ecologicamente correto, formulado para vergalhões de aço de estruturas de concreto. Monitoramento do circuito de potencial aberto (OCP) e medições de espectroscopia de impedância eletroquímica (EIS) e voltametria linear de varredura (LSV) revelam a formação de um filme passivo na interface metal/eletrólito. Este filme bloquei a oxidação dos íons de ferro formando uma barreira na superfície metálica. Os resultados de EIS revelaram um aumento na resistência a transferência de carga das amostras na presença de HPMC, em comparação com o sistema referência. O HPMC teve uma maior eficiência como inibidor de corrosão nas amostras contaminadas com 17,5 g/L de NaCl, de 75% a 98%. Já nas soluções que continham 35,1 g/L de NaCl somente a dosagem máxima de HPMC (1,2 g/L) obteve êxito como inibidor de corrosão, com eficiência de 58%.

Palavras chaves: hidroxipropilmetilcelulose (HPMC); solução de poros de concreto; inibidor de corrosão; circuito de potencial aberto; espectroscopia de impedância eletroquímica; voltametria linear de varredura

1. Introdução

A corrosão das armaduras de aço é uma das principais causas de falhas em estruturas de concreto e tem um efeito prejudicial no uso sustentável dos recursos naturais e na economia (KENNY; KATZ, 2020), induzindo problemas de durabilidade das estruturas o que reduz significativamente a vida útil (BAEK *et al.*, 2012), levando a grave deterioração da capacidade de manutenção e segurança estrutural.

O aço carbono pode passivar nas soluções de poros do concreto Portland, onde o pH está em torno de 13, resultando no aço em um estado passivado de acordo com o diagrama de Pourbaix para o sistema ferro-água a 25°C (BEVERSKOG, 1996). A faixa de pH entre 12 e 14 é gerada por reações de hidratação na solução intersticial dos poros do concreto que produzem hidróxidos como $Ca(OH)_2$, NaOH e KOH (YANG, H. *et al.*, 2019). Dentro desta faixa, o aço se comporta de forma metaestável e tende a oxidar, levando à formação de compostos sólidos na superfície do metal, devido à formação de um filme passivo (GREEN, 2020).

No entanto, a entrada de cloreto pode gradualmente causar acidificação nas proximidades do vergalhão e tornar o filme passivo instável (KHAN; AHMAD; AL-GAHTANI, 2017; MUNDRA *et al.*, 2017). Quando o conteúdo acumulado de cloreto atinge um limite crítico ($C_{crít}$), o filme passivo será destruído e a corrosão iniciará na superfície do vergalhão (ANGST *et al.*, 2009). O valor de $C_{críte}$ é influenciado por um grade número de fatores, incluindo: a química e a alcalinidade da solução dos poros (GHODS, P *et al.*, 2009; KAYYALI; HAQUE, 1995; LI; SAGUES, 2001), ligação de cloreto nos hidratos de cimento (ANGST *et al.*, 2011; GLASS; BUENFELD, 1997; GLASS; REDDY; BUENFELD, 2000), interface aço-concreto (GLASS; BUENFELD, 2000), disponibilidade de oxigênio na interface aço-concreto (GONZALEZ *et al.*, 1993) e condição da superfície e composição química do reforço (LI; SAGUES, 2001). Na literatura científica, o C_{crit} varia principalmente de 0,2% a 0,7% e pode até ir até 8,34% em peso de cimento para concreto externo (ANGST *et al.*, 2009; GLASS; BUENFELD, 1997). Esses valores correspondem a sistemas baseados principalmente em cimento Portland, e foram determinados através de medições eletroquímicas realizadas em estruturas em serviço, soluções simuladas de poros e corpos de prova de laboratório.

Melhorar a resistência à corrosão das armaduras de aço é considerada a forma mais importante de garantir a durabilidade e vida útil das estruturas de concreto armado. Existem muitas medidas para aumentar a resistência à corrosão das barras de aço, como a adição de inibidores de corrosão, aço resistente à corrosão e nano revestimento.(ASIPITA *et al.*, 2014; SALEH, 2020; SULEIMAN *et al.*, 2020) Dentre essas medidas, o inibidor de corrosão é considerado uma das tecnologias mais convenientes e eficazes (HARUNA; SALEH, 2021).

Os inibidores de corrosão tradicionais podem ser divididos em inorgânicos, orgânicos e misturas, dependendo da sua composição química. Desde a década de 1970, os compostos inorgânicos de nitrito têm sido um dos inibidores de corrosão mais eficazes para o aço carbono (LIU *et al.*, 2013). O nitrito pode reagir com Fe^{2+} para formar uma camada protetora de Fe_2O_3, que reduz a taxa de corrosão de barras de aço (GARCÉS *et al.*, 2008; RAMASUBRAMANIAN *et al.*, 2001; VAYSBURD; EMMONS, 2004). No entanto, o uso de inibidores inorgânicos é limitado devido à sua toxicidade e ao aumento da taxa de corrosão quando há presença insuficiente de nitrito (GARCÉS *et al.*, 2008).

Atualmente, as indústrias de construção de infraestruturas civis têm testemunhado

crescentes exigências de proteção ambiental. No campo da inibição de corrosão, pesquisadores e profissionais têm prestado atenção crescente ao desenvolvimento de inibidores de corrosão verdes pois eles são mais eficaz e altamente benigno do ponto de vista ambiental em comparação com inibidores orgânicos e inorgânicos utilizados nas indústrias químicas e petroquímicas (D'OLIVEIRA *et al.*, 2022; HALDHAR *et al.*, 2021). Entre os numerosos compostos orgânicos que foram testados e aplicados industrialmente como inibidores de corrosão, os não tóxicos são agora muito mais estratégicos (ABDULRAHMAN; ISMAIL; HUSSAIN, 2011; BOONSONG; LAOHAKUNJIT; KERDCHOECHUEN, 2012).

A celulose e seus derivados, como a hidroxipropilmetilcelulose (HPMC), são biopolímeros de carboidrato existente em maior quantidade em comparação com outros biopolímeros. Encontra-se nos tecidos da planta e constitui cerca de um terço dela. Tem aplicações farmacêuticas, cosméticas e alimentícias, e vários derivados dela têm sido usados como inibidores de corrosão (NWANONENYI *et al.*, 2016; SOLOMON *et al.*, 2010; UMOREN *et al.*, 2018).

Considerando tudo que foi mencionado, o objetivo deste trabalho foi investigar a eficiência de inibição da corrosão da HPMC em aço carbono em solução simulada de poros de concreto. O desempenho eletroquímico foi investigado em função da variação do teor de inibidor de corrosão em um ambiente contaminado por cloreto (3,5% de NaCl em peso de cimento), utilizando o monitoramento do circuito de potencial aberto (OCP) e espectroscopia de impedância eletroquímica (EIS) para analisar o mecanismo de inibição de corrosão.

2. Materiais e métodos

2.1. Preparação da solução simulada de poros de concreto (SPC)

Os materiais utilizados foram matérias primas de pureza comercial e quando necessário, grau PA. Foi utilizado cimento CPII-F32, da marca Goiás, adquirido na cidade de Palmas/TO. O cimento CPII-F32 é composto por material carbonático que em sua maioria é carbonato de cálcio, com classe de resistência à compressão de 32 MPa. A fim de controlar e inibir ao máximo possíveis interferências e reações externas não previstas, este tipo de cimento foi então escolhido devido, principalmente, a sua composição, que não apresenta materiais alternativos como escória de alto forno e pozolana, como nos outros tipos de cimento, pois como não há pesquisas sobre a reatividade da hidroxipropilmetilcelulose (HPMC) com estes compostos foi preferível eliminá-los da pesquisa. A Tabela 1 mostra a composição química do cimento utilizado nessa pesquisa.

O HPMC utilizado neste trabalho, foi fabricado pela AROMAT Produtos Químicos LTDA. O cloreto de sódio PA (NaCl), foi fabricado pela Nox Lab Solutions, possui um teor de 99,0%, segundo o fabricante. A água Mili-Q® foi produzida utilizando o equipamento, fabricado por PERMUTION, cuja água deionizada tem os seguintes parâmetro: pH em torno de 7.0 e condutividade inferior à 2 µS/cm.

Tabela 1. Composição química do cimento CPII-F32.

Elemento Químico	***%***
Óxido de cálcio total (CaO)	61.2
Dióxido de silício total (SiO_2)	18.87
Óxido de alumínio (Al_2O_3)	4.42
Anidrido carbônico (CO_2)	3.85
Óxido de magnésio (MgO)	3.23
Óxido de ferro (Fe_2O_3)	2.97
Anidrido sulfúrico (SO_3)	2.75
Resíduo insolúvel	1.26
Óxido de potássio (K_2O)	0.86
Outros	0.46
Óxido de sódio (Na_2O)	0.13

Fonte: ABCP (2020)

Por conta da dificuldade em reproduzir fielmente a solução presente nos poros de uma estrutura de concreto armado por meio de síntese de soluções, optou-se, nesta pesquisa, por simular a solução de poros do concreto utilizando a mistura de cimento e água Mili-Q®. Para isso, foi adotado o teor de material cimento/água igual a 0.075 (PACEWSKA *et al.*, 2002). A composição da SPC é, basicamente, hidróxido de sódio (NaOH), hidróxido de potássio (KOH) e hidróxido de cálcio saturado ($Ca(OH)_2$) (POURSAEE; ANGST, 2023), além das adições de HPMC e NaCl.

A mistura do material seco (cimento e HPMC) com a água Mili-Q® foi feito no agitador eletromagnético, por 60 minutos. Após esse período a solução foi filtrada a vácuo, separando o material inerte, para que os sobrenadantes não interferissem na polarização do aço.Para simulação do ambiente corrosivo foi inserido cloreto de sódio (NaCl) na solução SPC.

Foram preparadas 5 soluções com variação na concentração de HPMC e de NaCl, conforme mostra a Tabela 2.

Tabela 2 – Soluções de poro de concreto simuladas

ID	**SPC**	**HPMC**	**NaCl**
		(g/L)	(g/L)
1	H0N3	0	35.1
2	H6N3	0.6	35.1
3	H12N3	1.2	35.1
4	H6N2	0.6	17.5
5	H12N2	1.2	17.5

2.2 Preparação do eletrodo de trabalho

Para a produção dos eletrodos de trabalho (WE), uma barra de aço CA-50 de 5 mm foi inicialmente limada para retirada das nervuras laterais. Logo após, a barra de aço passou pelo processo de polimento, com lixas d'água. Em seguida a barra de aço foi cortada em pedaços de 3 cm de comprimento. Para garantir uma boa condutividade foi soldado um fio de

cobre, em uma das extremidades da barra de aço, via solda de fluxo com liga de prata, conforme ilustra a Figura 1. Após a soldagem foi realizada a limpeza para desengordurar os eletrodos.

Figura 1. Eletrodo de trabalho em processo de construção.

Fonte: próprio autor

Para garantir que somente a face transversal do eletrodo de trabalho (0,18 cm^2) estaria em contato com a solução foi realizada a fosfatização e posterior polimerização do eletrodo de trabalho.

A fosfatização é um tratamento onde ocorre a conversão de um metal em um óxido, hidróxido ou sal do metal por meio de reações eletroquímicas. Trata-se da conversão do metal em um fosfato insolúvel do íon metálico. O fosfato insolúvel se deposita sobre o metal modificando as suas propriedades superficiais (RAUSCH, 1990). Nesse trabalho as camadas fosfatizadas foram obtidas a partir da imersão dos eletrodos de trabalho (WE) em solução de ácido fosfórico por cerca de 60 minutos.

Após a fosfatização, os eletrodos de trabalho (WE) foram embutidos em resina epóxi transparente fornecida pela POLIPOX (resina RL-3028 e catalisador EL-3041) e curados por 48 h. Por fim, foi exposta a face do eletrodo, utilizando lixas d'água na sequência granulométrica 800, 1500 e 2000. A Figura 2 ilustra, esquematicamente, o eletrodo de trabalho (WE) finalizado.

Figura 2. Eletrodo de trabalho finalizado

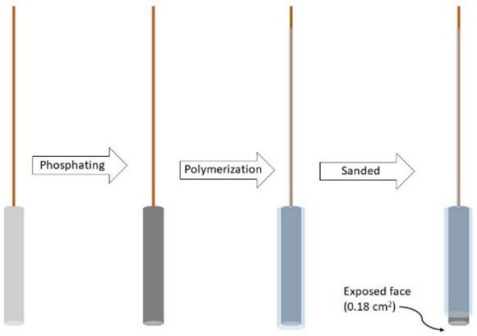

Fonte: próprio autor

Para chegar mais próximo da realidade do comportamento do aço imerso em concreto foi necessário manter os eletrodos de trabalhos imersos nas soluções de poros de concreto simulado (SPS), por 14 dias, com a finalidade de passivar a armadura, conforme ilustra a Figura 3.

O processo de passivação do aço carbono convencional no concreto é um mecanismo de redução eletroquímica espontânea que ocorre na superfície do aço através da interação com a solução alcalina dos poros (PEREZ, 2004). Este processo de passivação desempenha um papel decisivo na durante a fase de iniciação do modelo de corrosão da estrutura de concreto (YEOMANS, 2004).

Figura 3. Eletrodo de trabalho em processo de passivação

Fonte: próprio autor

2.3 Métodos

Todas as caracterizações eletroquímicas foram realizadas em uma célula de vidro convencional de três eletrodos, a 23 °C, utilizando um potenciostato/galvanostato da Vertex controlado por meio do software IviumSoft. Foram utilizados como eletrodo de referência (RE) o Ag/AgCl e como contra eletrodo (CE) o fio de platina, além do eletrodo de trabalho (WE).

O pH e a condutividade das SPCs e as análises eletroquímicas foram aferidos no dia da preparação da amostra e após a passivação de 14 dias. O valor do pH e da condutividade foram medidos após a estabilização de 5 minutos. As condutividades e os pHs dessas soluções foram determinados e estão listados na Tabela 3 como valores médios, obtidos a partir de uma análise em triplicata.

Tabela 3. Propriedades físico-químicas das soluções porosas do concreto (SPC).

SPC	pH		Conductivity (mS/cm)	
	0 dias	14 dias	0 dias	14 dias
H0N3	12.96±0.1	13.01±0.1	42,.88±1.7	65.45±3.9
H6N3	12.88±0.0	12.94±0.0	45.41±2.3	43.65±3.7
H12N3	12.87±0.1	12.94±0.2	52.45±4.6	60.47±2.4
H6N2	12.91±0.0	12.95±0.0	29.64±0.2	23.45±0.6
H12N2	12.76±0,2	12.82±0.2	41.06±2.9	40.24±0.7

O pH de todas as soluções analisadas aumentou após os ensaios eletroquímicos. Esse fenômeno pode ser explicado pela composição da solução em questão, onde a SPC possui

pH alcalino, com valores típicos entre 12.5 e 13.5 por causa dos principais constituintes da solução que são alcalinos. Nesse intervalo de pH, é viável o uso da armadura de aço em conjunto com o concreto, tendo em vista que com estes potenciais hidrogeniônicos a armadura permanece em um estado de passivação (METHA; MONTEIRO, 2014).

Para as análises das céculas eletroquímicas foram utilizadas as técnicas de: monitoramento de circuito de potencial aberto (OCP), espectroscopia de impedância eletroquímca (EIS) e voltametria linear de varredura, todas utilizando o potenciostato/galvanostato da Vertex controlado por meio do software IviumSoft.

Um metal que sofre corrosão numa solução de baixa resistividade elétrica assume um potencial característico, designado como potencial de corrosão. Esse potencial é dado pela intersecção da curva de polarização anódica com a de polarização catódica. O potencial de corrosão é um dos parâmetros eletroquímicos de mais fácil determinação experimental. Como se trata de um potencial assumido pelo metal, é suficiente obter a medida direta desse potencial com relação a um eletrodo de referência. Essa medida é conhecida como medida de potencial de circuito aberto(TICIANELLI, 1998).

O OCP denota o potencial de repouso medido entre o eletrodo de referência (RE) e de trabalho (WE) para definir se o sistema eletroquímico se estabilizou. O potencial do metal é caracterizado pelo equilíbrio das reações anódica e catódica . No ponto OCP, o fluxo líquido de elétrons é zero (YE *et al.*, 2013). O nível de risco de corrosão da armadura em concreto comum pode ser avaliado pelos valores de OCP de acordo com ASTM C876:2022 (ASTM, 2022). A Tabela 4 mostra a correlação do eletrodo de calomelano (SCE) com o de Ag/AgCl, utilizado nesse trabalho.

Tabela 4. Probabilidade de ocorrência de corrosão da armadura em função do potencial.

Electrode type	**Likelihood of Corrosion Occurring**		
	OCP< 10%	**10%<OCP<90%**	**OCP> 90%**
Hg, Hg_2Cl_2, KCl (calomelano/SCE)	> -126 mV	-126 mV à -276 mV	< -276 mV
Ag, AgCl/KCl (1M)	> -106 mV	-106 mV à -256 mV	< -256 mV

Fonte: modificada (ASTM, 2022)

Quando o objetivo do pesquisador é avaliar a formação do filme passivador, é recomendado um monitoramento automático em um intervalo de tempo curto (no máximo uma hora), para observar a mudança de comportamento eletroquímico do sistema (PENG *et al.*, 2018), isso foi considerado para essa pesquisa.

A espectroscopia de impedância eletroquímica (EIS) é uma técnica que trabalha no domínio da frequência. O conceito básico envolvido no EIS é que uma interface eletroquímica pode ser vista como uma combinação de elementos passivos de circuito elétrico, ou seja, resistência, capacitância e indutância. Quando uma tensão alternada é aplicada a estes elementos, a corrente resultante é obtida utilizando a lei de Ohm. De uma forma simples, a impedância pode ser considerada como a resistência de um circuito a uma forma de onda alternada (FERREIRA; MONTEMOR; SIMÕES, 2003).

O EIS fornece informações sobre o mecanismo das reações de corrosão a presença de filmes superficiais, característica de solução, corrosão interfacial e fenômenos de transferência de massa (RIBEIRO; ABRANTES, 2016), além de ser uma técnica não destrutiva e não invasiva porque os sinais aplicados são de pequena amplitude, portanto o potencial de corrosão não é alterado. Porém, a interpretação dos resultados pode ser difícil e a utilização de um circuito equivalente, que pode mudar de acordo com as condições do aço, torna a técnica mais adequada para estudos de laboratório (FERREIRA; MONTEMOR; SIMÕES, 2003).

As medições EIS são geralmente interpretadas utilizando uma correlação entre os dados de impedância e um circuito equivalente representando os processos físicos que ocorrem no sistema sob investigação ou através de representações gráficas. O diagrama de Nyquist é representado por um gráfico de $Z = Z' + j.Z''$ (onde Z' e $j.Z''$ são a parte real e a parte imaginária) medido em diferentes frequências. Outra representação é chamada de diagrama de Bode, que mostra o logaritmo do módulo de impedância ($\log |Z|$) e o deslocamento de fase em função do logaritmo da frequência.

A voltametria linear de varredura (LSV) é outro método eletroquímico para caracterizar o estado de corrosão de um metal. Aplica-se uma faixa de potencial, do menor para o maior, monitorando a corrente de resposta ao longo da varredura. Basicamente, a aplicação de potencial pretende simular a corrosão, mas de forma acelerada, para entender o comportamento do metal. Para realizar a varredura do potencial, a maioria dos autores opta por aplicar um potencial entre ± 10 mV e ± 20 mV em relação ao OCP (BRIZ; BIEZMA; BASTIDAS, 2018; MUNDRA *et al.*, 2017; WANG; ZUO; TANG, 2018). Em potenciais abaixo do OCP, denomina-se a curva de polarização (CP) como curva catódica e, para potenciais acima do OCP, curva anódica. As curvas de polarização são também denominadas como diagrama de Evans.

A curva de polarização de um metal representa o efeito global de todas as reações que ocorrem simultaneamente sobre o eletrodo, e por meio dela pode-se avaliar o comportamento eletroquímico de um metal num potencial diferente do potencial de corrosão. É necessário utilizar fontes externas de potencial, como um potenciostato, para impor a um eletrodo um potencial diferente de corrosão. Este potencial é imposto através de uma diferença entre o potencial do eletrodo e do eletrodo de referência, em meios com condutividade moderada a alta, possibilitando dessa forma, medir a corrente de polarização, além de registrá-la em função do potencial (GENTIL, 1996; WOLYNEC, 2003).

Para determinação do potencial de corrosão (E_{corr}) foi utilizado a extrapolação das retas de Tafel. A abordagem de Tafel envolve traçar o logaritmo do valor absoluto $|i|$ da densidade de corrente versus potencial. As inclinações desses segmentos lineares produzem os coeficientes de transferência, chamados de Tafel Slopes. A extrapolação dessas retas ao potencial de corrosão possibilita a obtenção da corrente de corrosão (i_{corr}).

A densidade da corrente de corrosão (j_{cor}) foi determinada usando o método descrito por McCafferty(MANSFELD, 1976; MCCAFFERTY, 2005), que consiste em dividir a corrente líquida (i_{cor}) pela área exposta do eletrodo de trabalho (0,18 cm^2).

A resistência de polarização (R_p), foi determinada a partir da constante de Stern-Geary (B), sendo calculada pela seguinte fórmula (MANSFELD, 1976).

$$R_p = \frac{B}{j_{cor}} \qquad (1)$$

Durante a varredura de potencial a densidade de corrente vai para zero e depois aumenta para um valor anódico baixo, aproximadamente constante na faixa passiva. Nesta faixa, um filme fino de óxido/hidróxido, o filme passivador, protege o material de altas taxas de corrosão. Se a densidade de corrente diminuir quando a direção de varredura de potencial foi invertida, o material mostra-se imune à corrosão por pite. No entanto, se na varredura ascendente de potencial, a densidade de corrente aumentar repentinamente e permanecer alta na varredura descendente, até finalmente diminuir para o valor da região passiva, o material é mostrado sofrendo uma forma de corrosão por pite. O potencial de pite (E_{pite}) também foi determinado a partir das curvas de polarização. Este foi o potencial onde a densidade de corrente aumentou repentinamente (WANG, 2016).

Através da polarização é possível determinar a taxa de corrosão, em mm/ano por exemplo, dos materiais. Neste caso, a corrosão não necessariamente está restrita à corrosão por pite, podendo alcançar um nível de corrosão generalizada. A medida de taxa de corrosão é, em geral, associada à corrosão generalizada. A partir do valor de i_{corr} pode-se determinar a velocidade de corrosão (V_{corr}) do sistema por meio da Lei de Faraday (GENTIL, 1996).A taxa de corrosão (V_{cor}) está relacionada da seguinte maneira:

$$V_{cor} = \frac{j_{cor} * M * t}{n * F * d} \qquad (2)$$

onde “M” é a massa molar do ferro (0,056 kg/mol); “d” a densidade do ferro (7.847 kg/m^3); “n” a valência de um íon Fe^{+2}; “F” a constante de Faraday (96.485 C/mol) e “t” o coeficiente de tempo ($3{,}15*10^7$ s/ano). Considerando os parâmetros do ferro, a equação 2 reduz para (ANDRADE; ALONSO, 2004):

$$V_{cor} \approx 11{,}6 * j_{cor} \ \ (mm/ano) \qquad (3)$$

onde a densidade da corrente de corrosão (j_{cor}) deve estar em unidades de (mA/cm^2).

Neste trabalho, após a estabilização do OCP por 1 h, iniciou-se a medida de EIS, com amplitude adotada de 10 mV, entre 10 kHz e 10 mHz, com dez pontos por década. Em seguida foi feita a voltametria linear de varredura entre -1500 mV a +500 mV, versus OCP, com velocidade de 0,167 mV/s.

3. Resultados e discussão

3.1. Perfil de evolução potencial de circuito aberto (OCP)

O perfil gráfico do monitoramento OCP das armaduras de aço em SCP ao longo de 14 dias de passivação é apresentada na Figura 4, já na Tabela 5 é possível verificar o valor médio do OCP nos últimos 2000 s de monitoramento. Os potenciais aumentaram positivamente durante o período de passivação, entre 0 e 14 dias, com exceção das soluções H0N3 e H6N3. Na H0N3 ocorreu o que já era esperado visto que essa é uma solução que simula o ambiente altamente corrosivo, sem a presença do possível inibidor de corrosão. Já na H6N3 pode ser a sinalização de que a concentração de 0,6 g/L de HPMC não seja suficiente para inibir a corrosão em um ambiente altamente corrosivo, com 35,1 g/L de NaCl.

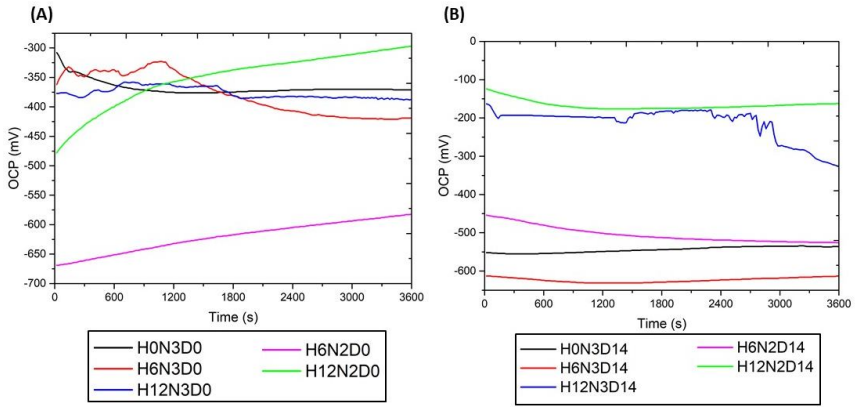

Figura 4. Evolução dos valores de potencial de circuito aberto (OCP) em função do tempo de imersão, 0 (a) e 14 dias (b), de amostras de aço em solução de poros concreto simulada.

Tabela 5. Valores médios de OCP durante os últimos 2000 s de monitoramento.

SPC	OCP (mV)	
	0 dias	14 dias
H0N3	-371.59±1.8	-538.28±3.4
H6N3	-407.02±14.7	-621.58±5.7
H12N3	-382.94±4.3	-227.45±51.8
H6N2	-600.98±11.3	-519.73±4.5
H12N2	-319.25±13.1	-169.78±4.4

De fato, durante o período de passivação o nível do pH da SPC manteve-se acima de 12 (RÄSÄNEN; PENTTALA, 2004), conforme mostrado na Tabela 4. Quando o pH se encontra acima de 12 ocorre a formação de uma camada passiva na superfície do vergalhão de aço. Esta camada é responsável por diminuir a taxa de corrosão e aumentar o potencial do circuito aberto.

Após a inserção de NaCl na SPC, os íons cloretos podem penetrar através dessa cama e atingir a superfície das amaduras de aço, deteriorando a camada passiva. Devido a despassivação das barras de aço como resultado do ataque por cloretos, o potencial de corrosão cai (D'OLIVEIRA *et al.*, 2023).

Porém é possível identificar que o uso do HPMC, com o intuito de inibir o ataque

corrosivo , se mostrou eficaz, visto que mesmo com a presença de NaCl as amostras H12N3, H6N2 e H12N2, tiveram um aumento do OCP ao final dos 14 dias de passivação. No entanto, quando se utiliza a Tabela 4 para avaliar a probabilidade de corrosão, aos 14 dias, as soluções H12N3 e H12N2 encontram-se na faixa entre 10% e 90% de probabilidade de ocorrência de corrosão, onde o que predomina é a incerteza; já as amostras H0N3 e H6N3 se mantiveram com potenciais de meia célula abaixo de -276 mV, o que sugere uma probabilidade acima de 90% de ocorrência de corrosão, evidenciando que o ambiente simulado realmente é corrosivo.

Como sugerido por Song e Saraswathy (SONG; SARASWATHY, 2007), os potenciais das medições de potencial de meia célula não são suficientes como critérios para corrosão, porque uma série de fatores como polarização por difusão limitada de oxigênio, porosidade do concreto e presença de camadas altamente resistivas, podem afetar a precisão dos valores de potenciais. Além disso, a generalização das medições de OCP é discutível, uma vez que grandes variações na taxa de corrosão podem ocorrer dentro de faixas de potencial relativamente estreitas (SONG; SARASWATHY, 2007).

Em relação aos valores obtidos de condutividade elétrica, observou-se que apresentaram grande variação no período de medição. Em algumas situações, a variação no equipamento era grande o que impacta na assertividade do resultado. Poucos autores expuseram medidas de condutividade elétrica de SPC. Dentre os autores que avaliaram a corrosão de armaduras em SPC feitas diretamente com cimento, apenas Shaheen & Pradhan (SHAHEEN; PRADHAN, 2015) mediram a condutividade elétrica dessa solução. No caso, os pesquisadores obtiveram o valor de 5,5 mS/cm, aproximadamente metade dos valores obtidos na presente pesquisa, comparando a solução referência e muito inferior quando comparado as soluções com adição de HPMC e NaCl. O que é evidente nos valores obtidos neste artigo é o aumento da condutividade com a adição de NaCl. Certamente, esse fator influencia no processo corrosivo, pois o aumento da condutividade elétrica acarreta na maior movimentação iônica na solução, auxiliando no processo de oxidação do aço.

A fim de investigar uma hipótese inicial de que as SPCs que contém HPMC apresentaram diferentes naturezas passivantes, foi realizada a Espectroscopia de Impedância Eletroquímica (EIS) nos períodos inicial e final de medição (0 e 14 dias).

3.2. Espectroscopia de impedância eletroquímica (EIS)

A Figura 5 ilustra os gráficos de Nyquist e Bode do aço carbono em diversas SPC. Na Figura 5(a), após 1 h de imersão, os diâmetros dos arcos capacitivos não apresentam diferença significativa, exceto para as soluções contendo a concentração de 0,6 g/L de HPMC, além disso, o raio do arco de impedância sem inibidor de corrosão foi o menor. Com o passar dos 14 dias de passivação, os diâmetros dos arcos capacitivos apresentam tendência de aumento com a concentração de HPMC. A eficiência protetora fica mais evidente com o aumento da concentração do HPMC, e atua principalmente através do processo eletroquímico

catódico que inibe a corrosão do aço (KORNBLUM; BLACKWOOD; MOOBERRY, 1956; YANG *et al.*, 2012). Nas Figuras 5(d) e (f), pode-se verificar que o valor da impedância em baixa frequência e o ângulo máximo de fase aumentaram com o inibidor de corrosão. Isto indica que a adição do HPMC melhorou a resistência a corrosão do aço carbono, promovendo a formação de uma película protetora mais estável na superfície do aço, o que impediu que íons cloreto e oxigênio atingissem a superfície do aço carbono.

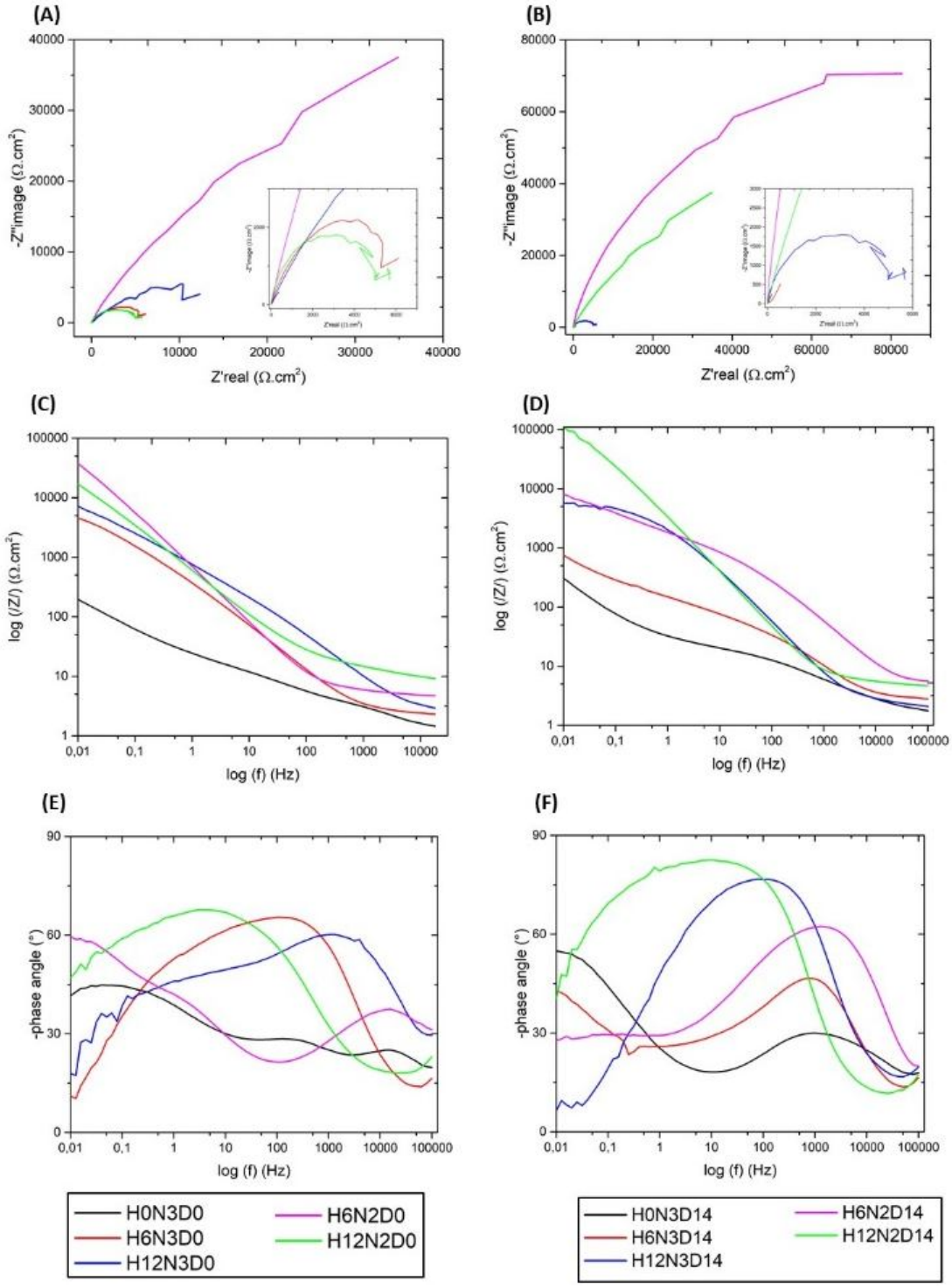

Figura 5. Diagrama EIS de aços imersos na solução SPC. (a) Gráfico de Nyquist em D0, (b) Gráfico de Nyquist em D14, (c) e (e) Gráficos de Bode em D0 e (d) e (f) Gráficos de Bode em D14.

A partir dos resultados da EIS, um circuito elétrico equivalente (CEE) pode ser proposto para modelar a interface eletrólito/amostra. O CEE proposto na Figura 6 é classicamente proposto para revestimento (BEAUNIER *et al.*, 1976). É constituído por elementos que descrevem propriedades do filme inibidor (Q_f e R_f) e outros relativos aos processos de corrosão (R_{ct} e Q_{dl}) na superfície do aço. Ao ajustar diagramas experimentais de impedância, este EEC contribui para estabelecer uma evolução dos parâmetros físicos relacionados ao filme inibidor e aos processos de corrosão ao longo do tempo. Foi obtida uma boa correlação entre os dados experimentais e simulados (o erro dos parâmetros ajustados foi feito pelo qui-quadrado, χ^2, para todos os ajustes entre 1,61E10^{-2} e 8,04E10^{-3}).

O circuito equivalente da Figura 6 também foi utilizado por outros pesquisadores ao modelar o comportamento eletroquímico do aço carbono em meio alcalino (DEUS *et al.*, 2014; JOIRET *et al.*, 2002; SÁNCHEZ *et al.*, 2007; XU *et al.*, 2021; ZHAO, Yazhou *et al.*, 2019).No circuito equivalente, R_s é a resistência da solução; R_f é a resistência do filme; R_{ct} é a resistência da transferência de carga, que reflete a dificuldade de transferência de elétrons entre a dissolução do ânodo e a redução do despolarizador. A capacitância do filme, C_f, e o índice de dispersão, n_1, constitui o elemento de ângulo de fase constante, CPE_1; e a capacitância da dupla camada elétrica, C_{dl}, e o índice de dispersão, n_2, constituem o elemento de ângulo de fase constante, CPE_2. A eficiência de inibição (%η) do inibidor de corrosão com diferentes concentrações foi calculada a partir da fórmula:

$$\eta = \frac{R'_{ct} - R_{ct}}{R'_{ct}} \qquad (2)$$

Onde R_{ct} e R'_{ct} referem-se à resistência à transferência de carga do eletrodo na solução simulada de poros de concreto sem e com inibidor de corrosão, em Ω.

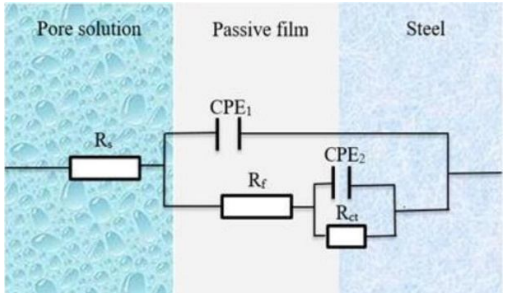

Figura 6. Circuito equivalente.

Tabela 6. Resultados equivalentes de ajuste de circuitos gráficos de Nyquist com diferentes conteúdos de inibidor de corrosão

SPC	R_s	CPE_1	n_1	R_f	CPE_2	n_2	R_{ct}	η%
	Ω.cm²	μF.cm⁻²		Ω.cm²	μF.cm⁻²		Ω.cm²	
H0N3	1,68	393,06	0,70	18,32	20911,11	0,70	2153	-
H6N3	2,52	268,28	0,70	108,94	5650,00	0,70	1113	< 0%
H12N3	1,07	69,83	0,70	2,23	22088,89	0,97	5171	58%
H6N2	3,94	32,33	0,73	1532,52	365,61	0,70	8564	75%
H12N2	5,18	56,44	0,91	76014,00	45,65	0,75	123930	98%

Como mostrado na Tabela 6, a resistência à transferência de carga, R_{ct}, e a resistência do filme, R_f, aumentaram após a adição do inibidor de corrosão, implicando que o filme passivo se tornou mais estável e resistivo. Além da resistência à transferência de carga R_t, a influência da película protetora no aço pode ser descrita por C_{dl} (FENG *et al.*, 2017; SAHOO; BALASUBRAMANIAM, 2008). A capacitância da dupla camada elétrica, CPE_2, da solução com inibidor de corrosão foi significativamente menor que a solução sem inibidor de corrosão (YANG, H. *et al.*, 2019).

Assim, para se trabalhar com valores de capacitância, é necessário a conversão do CPE em uma pseudo-capacitância, a qual pode ser equacionado como por meio de uma impedância ou admitância. O equacionamento para a impedância, considerando um CPE é:

$$Z_{CPE} = \frac{1}{Q.(j.\omega)^n} \qquad (3)$$

Onde Z_{CPE} é a impedância do elemento de fase constante (Ohm.cm^2), ω é a frequência angular da tensão alternada AC (rad/s), Q é a admitância do CPE (Ohm.cm^{-2}.s$^{-\alpha}$), e n o termo exponencial, que representa a facilidade de difusão de íons no filme de passivação (DIARD; LE GORREC; MONTELLA, 2013).

O parâmetro “n” está diretamente relacionado à microestrutura, rugosidade e irregularidade existente na superfície do eletrodo, variando de 0 a 1, sendo que valores mais próximos de 1 indicam um comportamento capacitivo ideal (KATIYAR; RANDHAWA, 2019), enquanto que “n” próximos a 0,5 indicam que o CPE está se tornando um componente de Warburg (RETTER *et al.*, 2003). Em outras palavras, quando “n” é 1, o elemento é um capacitor, já quando o comportamento é governado por um processo de transferência de massa, “n” se aproxima de 0,5, e valores intermediários de “n*”* relacionam-se com as não homogeneidade e a rugosidade da superfície do eletrodo (COX; WONG, 1995; MACDONALD, 1987). No presente estudo, os valores do expoente “n” obtidos pelo ajuste de circuito equivalente dos dados EIS são superiores a 0,7. Esses valores de n confirmam a heterogeneidade e complexidade da superfície do eletrodo (CAI; PARK, 1996; HASHIMOTO; ASAMI; TERAMOTO, 1979).

De acordo com o modelo de Helmholtz (BOMMERSBACH *et al.*, 2005), a capacitância de camada dupla, C_{dl}, pode ser expressa como:

$$C_{dl} = \frac{\varepsilon_0.\varepsilon}{d} S \qquad (4)$$

Onde S é a área superficial do eletrodo de trabalho, d representa a espessura da dupla camada, ε_0 e ε são constantes dielétricas do vácuo e do filme, respectivamente. A constante dielétrica das moléculas de água é maior que a do inibidor de corrosão. Quando as moléculas de água na interface metal/solução são substituídas por inibidor de corrosão, a capacitância da camada de interface composta por moléculas inibidoras de corrosão é significativamente menor que a das moléculas de água, portanto, C_{dl} diminui.

De acordo com a fórmula 4, a espessura da dupla camada aumentou com o teor do inibidor de corrosão no SPC, o que indica que o inibidor de corrosão foi adsorvido formando um filme na superfície do aço carbono, que bloqueou a penetração de íons agressivos. De acordo com a Tabela 6, na solução contaminada com 35.10 g/L de NaCl quando o teor de HPMC é de 1.20 g/L (H3N12) a eficiência do inibidor de corrosão é de 58%. Já nas soluções contaminadas com 17,5 g/L de NaCl quando a concentração de HPMC foi 0.60 g/L (H6N2) para 1.20 g/L (H12N12), houve um aumento na eficiência do inibidor de corrosão de 75% para 98%. Maior concentração de inibidor ajudou a aumentar a adsorção do composto inibidor de corrosão de HPMC na superfície da barra de aço e formou um filme de adsorção completo e compacto para melhorar a resistência aos íons cloreto.

3.3. Voltametria Linear de Varredura (LSV)

A fim de investigar a hipótese de que as SPCs que contém HPMC apresentaram diferentes naturezas passivantes, foi realizada voltametria linear de varredura (LSV). A comparação resultante entre os sistemas baseados nessas curvas de polarização foi apresentada na Figura 7 e os dados da análise na Tabela 7. Uma ampla faixa passiva apareceu nas curvas de polarização nas soluções H12N3, H6N2 e H12N2.

Comparando com as SPCs sem inibidor de corrosão (H0N3), o potencial de pite das curvas de polarização é maior em soluções contendo inibidor de corrosão. O potencial de corrosão (E_{corr}) e o potencial de pite (E_{pite}) de H0N3 (solução sem inibidor de corrosão) foi de -920 mV e -200 mV, respectivamente.

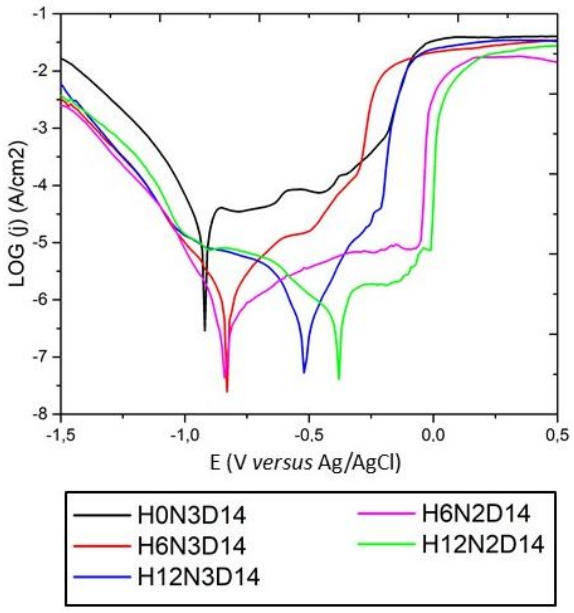

Figura 7. Curva de polarização do aço carbono com diferentes teores de inibidor de corrosão.

À medida que o conteúdo do inibidor de corrosão aumentou, o potencial de pite aumentou gradualmente. O potencial de corrosão apresentou uma mudança significativa em

direção à área do ânodo, e a densidade da corrente de corrosão do ânodo diminuiu significativamente à medida que o conteúdo do inibidor de corrosão aumentou. As soluções H6N2 e H12N2 foram as que apresentaram melhores resultados, potencial de pite: -60 mV e -10 mV, respectivamente.

Tabela 7. Resultados da voltametria linear de varredura (LSV) com diferentes conteúdos de inibidor de corrosão

SOLUTIONS	E_{corr} (mV vs. Ag/AgCl/NaCl 3M)	J_{corr} ($\mu A/cm^2$)	R_p ($k\Omega/cm^2$)	E_{pite} (mV vs. Ag/AgCl/NaCl 3M)	V_{corr} (mm/ano)
H0N3	-920	20.56	1.90	-200	0.238
H6N3	-830	2.71	35,35	-310	0.031
H12N3	-521	1.11	90.10	-210	0.013
H6N2	-834	1.35	98.23	-60	0.016
H12N2	-384	1.28	66.21	-10	0.015

Além disso, as densidades de corrente de corrosão (J_{corr}), resistências de polarização (R_p) e taxas de corrosão (V_{corr}) obtidas revelam uma menor taxa de corrosão e maior resistividade das soluções H6N2, H12N2 e H12N3 em relação a solução corrosiva (H0N3), sendo os valores da resistividade das soluções em questão, respectivamente, 98.23 $k\Omega/cm^2$, 66.21 $k\Omega/cm^2$, 90.10 $k\Omega/cm^2$ e 1.90 $k\Omega/cm^2$. O que reforça a hipótese da formação de um filme passivo no meio contendo HPMC. Como R_p é comumente usados como uma medida de resistência do metal aos danos por corrosão, valores altos de R_p estão associados a uma alta capacidade de prevenção de corrosão, enquanto valores baixos de R_p indicam alta atividade corrosiva (LU; BA, 2010).

4. Conclusões

O efeito inibitório e o mecanismo do inibidor de corrosão da hidroxipropilmetilcelulose (HPMC) sobre o aço carbono em solução simulada de poros de concreto (SPC) foram estudadas e as seguintes conclusões resultaram deste estudo.

1. De acordo com as análises eletroquímicas, um filme passivo cresceu na superfície do aço carbono imerso em SPC contendo HPMC, indicando que pode funcionar como inibidor de corrosão.
2. Foi confirmado que a SPC contaminada com 35,1 g/L de NaCl (H0N3), sem inibidor de corrosão, obteve resultados que evidenciaram falhas ou ausência de formação do filme passivador.
3. Com o aumento do teor de HPMC na SPC, o potencial de pite (E_{pit}) e a resistência a transferência de carga (R_{ct}) aumentaram, enquanto a densidade de corrente (j_{corr}) e a capacitância da dupla camada elétrica (C_{dl}) diminuíram.
4. Este artigo evidencia que a adição de HPMC na formulação do concreto tem benefícios potencias em relação as propriedades passivantes.

Referências

ABDULRAHMAN, A. S.; ISMAIL, M.; HUSSAIN, M. S. Corrosion inhibitors for steel reinforcement in concrete: A review. **Scientific Research and Essays**, [*s. l.*], v. 6, n. 20, p. 4152–4162, 2011.

ANGST, U. M. *et al.* Chloride induced reinforcement corrosion: Electrochemical monitoring of initiation stage and chloride threshold values. **Corrosion Science**, [*s. l.*], v. 53, n. 4, p. 1451–1464, 2011.

ANGST, U. *et al.* Critical chloride content in reinforced concrete—A review. **Cement and concrete research**, [*s. l.*], v. 39, n. 12, p. 1122–1138, 2009.

ASIPITA, S. A. *et al.* Green Bambusa Arundinacea leaves extract as a sustainable corrosion inhibitor in steel reinforced concrete. **Journal of Cleaner Production**, [*s. l.*], v. 67, p. 139–146, 2014.

ASTM. C 876–22b. Standard Test Method for CorrosionPotentials of Uncoated Reinforcing Steel in Concrete. **ASTMInternational**, [*s. l.*], 2022.

BAEK, S. *et al.* Nondestructive corrosion detection in RC through integrated heat induction and IR thermography. **Journal of Nondestructive Evaluation**, [*s. l.*], v. 31, p. 181–190, 2012.

BEAUNIER, L. *et al.* Etude electrochimique, et par microscopie electronique a balayage, du fer recouvert de peinture. **Surface Technology**, [*s. l.*], v. 4, n. 3, p. 237–254, 1976.

BEVERSKOG, B. Revised diagrams for iron at 25–300◦ C Corros. **Sci**, [*s. l.*], v. 38, p. 2121–2135, 1996.

BOMMERSBACH, P. *et al.* Formation and behaviour study of an environment-friendly corrosion inhibitor by electrochemical methods. **Electrochimica Acta**, [*s. l.*], v. 51, n. 6, p. 1076–1084, 2005.

BOONSONG, P.; LAOHAKUNJIT, N.; KERDCHOECHUEN, O. Natural pigments from six species of Thai plants extracted by water for hair dyeing product application. **Journal of cleaner Production**, [*s. l.*], v. 37, p. 93–106, 2012.

BRIZ, E.; BIEZMA, M. V.; BASTIDAS, D. M. Stress corrosion cracking of new 2001 lean–duplex stainless steel reinforcements in chloride contained concrete pore solution: An electrochemical study. **Construction and Building Materials**, [*s. l.*], v. 192, p. 1–8, 2018. Disponível em: https://doi.org/10.1016/j.conbuildmat.2018.10.108.

CAI, M.; PARK, S. Oxidation of zinc in alkaline solutions studied by electrochemical impedance spectroscopy. **Journal of the Electrochemical Society**, [*s. l.*], v. 143, n. 12, p. 3895, 1996.

COX, B.; WONG, Y.-M. Simulating porous oxide films on zirconium alloys. **Journal of nuclear materials**, [*s. l.*], v. 218, n. 3, p. 324–334, 1995.

D'OLIVEIRA, M. C. de P. E. *et al.* Estudos recentes sobre compósitos de carboidratos para inibição da corrosão: uma revisão sistemática. **Research, Society and Development**, [*s. l.*],

v. 11, n. 9, p. e41811932021, 2022.

D'OLIVEIRA, M. C. de P. E. *et al.* **Recent studies on the use of simulated concrete pore solution for corrosion evaluation: a systematic review using prisma**. [*S. l.: s. n.*], 2023.

DEUS, J. M. *et al.* The electrochemical behaviour of steel rebars in concrete: an Electrochemical Impedance Spectroscopy study of the effect of temperature. **Electrochimica Acta**, [*s. l.*], v. 131, p. 106–115, 2014.

DIARD, J. P.; LE GORREC, B.; MONTELLA, C. Handbook of Electrochemical Impedance Spectroscopy-Electrical Circuits containing CPEs. **Bio-logic Science Instruments**, [*s. l.*], 2013.

FENG, X. *et al.* The corrosion inhibition efficiency of aluminum tripolyphosphate on carbon steel in carbonated concrete pore solution. **Corrosion Science**, [*s. l.*], v. 124, p. 150–159, 2017.

FERREIRA, M. G. S.; MONTEMOR, M. F.; SIMÕES, A. M. P. Chloride-induced corrosion on reinforcing steel : from the fundamentals to the monitoring techniques. [*s. l.*], v. 25, p. 491–502, 2003.

GARCÉS, P. *et al.* Effect of nitrite in corrosion of reinforcing steel in neutral and acid solutions simulating the electrolytic environments of micropores of concrete in the propagation period. **Corrosion science**, [*s. l.*], v. 50, n. 2, p. 498–509, 2008.

GENTIL, V. **Corrosão**. Rio de Janeiro: LTC-Livros Técnicos e Científicos Editora SA, 1996.

GHODS, P. *et al.* The effect of concrete pore solution composition on the quality of passive oxide films on black steel reinforcement. **Cement and Concrete Composites**, [*s. l.*], v. 31, n. 1, p. 2–11, 2009.

GLASS, G. K.; BUENFELD, N. R. The inhibitive effects of electrochemical treatment applied to steel in concrete. **Corrosion Science**, [*s. l.*], v. 42, n. 6, p. 923–927, 2000.

GLASS, G. K.; BUENFELD, N. R. The presentation of the chloride threshold level for corrosion of steel in concrete. **Corrosion science**, [*s. l.*], v. 39, n. 5, p. 1001–1013, 1997.

GLASS, G. K.; REDDY, B.; BUENFELD, N. R. The participation of bound chloride in passive film breakdown on steel in concrete. **Corrosion Science**, [*s. l.*], v. 42, n. 11, p. 2013–2021, 2000.

GONZALEZ, J. A. *et al.* Initial steps of corrosion in the steel/Ca (OH) 2+ Cl− system: the role of heterogeneities on the steel surface and oxygen supply. **Cement and Concrete Research**, [*s. l.*], v. 23, n. 1, p. 33–40, 1993.

GREEN, W. K. Steel reinforcement corrosion in concrete–an overview of some fundamentals. **Corrosion Engineering, Science and Technology**, [*s. l.*], v. 55, n. 4, p. 289–302, 2020.

HALDHAR, R. *et al.* Papaver somniferum as an efficient corrosion inhibitor for iron alloy in acidic condition: DFT, MC simulation, LCMS and electrochemical studies. **Journal of Molecular Structure**, [*s. l.*], v. 1242, p. 130822, 2021.

HARUNA, K.; SALEH, T. A. N, N′-Bis-(2-aminoethyl) piperazine functionalized graphene oxide (NAEP-GO) as an effective green corrosion inhibitor for simulated acidizing environment. **Journal of Environmental Chemical Engineering**, [*s. l.*], v. 9, n. 1, p. 104967, 2021.

HASHIMOTO, K.; ASAMI, K.; TERAMOTO, K. An X-ray photo-electron spectroscopic study on the role of molybdenum in increasing the corrosion resistance of ferritic stainless steels in HC1. **Corrosion Science**, [*s. l.*], v. 19, n. 1, p. 3–14, 1979.

JOIRET, S. *et al.* Use of EIS, ring-disk electrode, EQCM and Raman spectroscopy to study the film of oxides formed on iron in 1 M NaOH. **Cement and Concrete Composites**, [*s. l.*], v. 24, n. 1, p. 7–15, 2002.

KATIYAR, P. K.; RANDHAWA, N. S. Corrosion behavior of WC-Co tool bits in simulated (concrete , soil , and mine) solutions with and without chloride additions. **International Journal of Refractory Metals & Hard Materials**, [*s. l.*], v. 85, n. July, p. 105062, 2019. Disponível em: https://doi.org/10.1016/j.ijrmhm.2019.105062.

KAYYALI, O. A.; HAQUE, M. N. The C1−/OH− ratio in chloride-contaminated concrete—A most important criterion. **Magazine of Concrete Research**, [*s. l.*], v. 47, n. 172, p. 235–242, 1995.

KENNY, A.; KATZ, A. Steel-concrete interface influence on chloride threshold for corrosion – Empirical reinforcement to theory. **Construction and Building Materials**, [*s. l.*], v. 244, p. 118376, 2020. Disponível em: https://doi.org/10.1016/j.conbuildmat.2020.118376.

KHAN, M. U.; AHMAD, S.; AL-GAHTANI, H. J. Chloride-induced corrosion of steel in concrete: an overview on chloride diffusion and prediction of corrosion initiation time. **International journal of corrosion**, [*s. l.*], v. 2017, 2017.

KORNBLUM, N.; BLACKWOOD, R. K.; MOOBERRY, D. D. The Reaction of Aliphatic Nitro Compounds with Nitrite Esters1, 2. **Journal of the American Chemical Society**, [*s. l.*], v. 78, n. 7, p. 1501–1504, 1956.

LI, L.; SAGUES, A. A. Chloride corrosion threshold of reinforcing steel in alkaline solutions—open-circuit immersion tests. **Corrosion**, [*s. l.*], v. 57, n. 1, p. 19–28, 2001.

LIU, J. P. *et al.* 1, 3-Bis-dibutylaminopropan-2-ol as inhibitor for reinforcement steel in chloride-contaminated simulated concrete pore solution. **Materials and Corrosion**, [*s. l.*], v. 64, n. 12, p. 1075–1081, 2013.

LU, S.; BA, H. J. Corrosion sensor for monitoring the service condition of chloride-contaminated cement mortar. **Sensors**, [*s. l.*], v. 10, n. 4, p. 4145–4158, 2010.

MACDONALD, J. R. Impedence Spectroscopy--Emphasizing Solid Materials and Systems. **Wiley-Interscience, John Wiley and Sons,** [*s. l.*], p. 1–346, 1987.

MANSFELD, F. The polarization resistance technique for measuring corrosion currents. *In*: ADVANCES IN CORROSION SCIENCE AND TECHNOLOGY: VOLUME 6. [*S. l.*]: Springer, 1976. p. 163–262.

MCCAFFERTY, E. Validation of corrosion rates measured by the Tafel extrapolation method. **Corrosion science**, [*s. l.*], v. 47, n. 12, p. 3202–3215, 2005.

METHA, P. K.; MONTEIRO, P. J. M. **Concreto: microestrutura, propriedades e materiais**. São Paulo: IBRACON, 2014. v. 2

MUNDRA, S. *et al.* Cement and Concrete Research Chloride-induced corrosion of steel rebars in simulated pore solutions of alkali-activated concretes. **Cement and Concrete Research**, [*s. l.*], v. 100, n. August, p. 385–397, 2017. Disponível em: https://doi.org/10.1016/j.cemconres.2017.08.006.

NWANONENYI, S. *et al.* Inhibitive Performance of Hydroxypropyl Cellulose and Potassium Iodide on the Corrosion of Mild Steel in Sulphuric Acid Environment. **American Chemical Science Journal**, [*s. l.*], v. 16, n. 2, p. 1–12, 2016.

PACEWSKA, B. *et al.* Modification of the properties of concrete by a new pozzolan - A waste catalyst from the catalytic process in a fluidized bed. **Cement and Concrete Research**, [*s. l.*], v. 32, n. 1, p. 145–152, 2002.

PENG, Y. *et al.* Effect of simulated pore solution on passivation characteristic of P110 steel. **Journal of Petroleum Science and Engineering**, [*s. l.*], v. 167, n. March, p. 949–956, 2018. Disponível em: https://doi.org/10.1016/j.petrol.2018.03.009.

PEREZ, N. Electrochemistry and corrosion science. **Kluwer Academic publishers**, [*s. l.*], p. 189–246, 2004.

POURSAEE, A.; ANGST, U. M. Principles of corrosion of steel in concrete structures. *In*: CORROSION OF STEEL IN CONCRETE STRUCTURES. [*S. l.*]: Elsevier Ltd, 2023. p. 17–34.

RAMASUBRAMANIAN, M. *et al.* Inhibiting action of calcium nitrite on carbon steel rebars. **Journal of Materials in Civil Engineering**, [*s. l.*], v. 13, n. 1, p. 10–17, 2001.

RÄSÄNEN, V.; PENTTALA, V. The pH measurement of concrete and smoothing mortar using a concrete powder suspension. **Cement and Concrete Research**, [*s. l.*], v. 34, n. 5, p. 813–820, 2004.

RAUSCH, W. **The Phosphating of Metals**. [*S. l.*]: Finishing Publications, 1990. *E-book*. Disponível em: https://books.google.com.br/books?id=8RRUAAAAMAAJ.

RETTER, U. *et al.* On the impedance of potassium nickel (II) hexacyanoferrate (II) composite electrodes * the generalization of the Randles model referring to inhomogeneous electrode materials. **Journal of Electroanalytical Chemistry**, [*s. l.*], v. 546, p. 87–96, 2003.

RIBEIRO, D. V; ABRANTES, J. C. C. Application of electrochemical impedance spectroscopy (EIS) to monitor the corrosion of reinforced concrete: A new approach. **Construction and Building Materials**, [*s. l.*], v. 111, p. 98–104, 2016. Disponível em: https://www.sciencedirect.com/science/article/pii/S0950061816301064.

SAHOO, G.; BALASUBRAMANIAM, R. On the corrosion behaviour of phosphoric irons in simulated concrete pore solution. **Corrosion Science**, [*s. l.*], v. 50, n. 1, p. 131–143, 2008.

SALEH, T. A. Trends in the sample preparation and analysis of nanomaterials as environmental contaminants. **Trends in Environmental Analytical Chemistry**, [*s. l.*], v. 28, p. e00101, 2020.

SÁNCHEZ, M. *et al.* Electrochemical impedance spectroscopy for studying passive layers on steel rebars immersed in alkaline solutions simulating concrete pores. **Electrochimica Acta**, [*s. l.*], v. 52, n. 27 SPEC. ISS., p. 7634–7641, 2007.

SHAHEEN, F.; PRADHAN, B. Effect of chloride and conjoint chloride-sulfate ions on corrosion of reinforcing steel in electrolytic concrete powder solution (ECPS). **Construction and Building Materials**, [*s. l.*], v. 101, p. 99–112, 2015. Disponível em: http://dx.doi.org/10.1016/j.conbuildmat.2015.10.028.

SOLOMON, M. M. *et al.* Inhibitive and adsorption behaviour of carboxymethyl cellulose on mild steel corrosion in sulphuric acid solution. **Corrosion Science**, [*s. l.*], v. 52, n. 4, p. 1317–1325, 2010.

SONG, H.-W.; SARASWATHY, V. Corrosion Monitoring of Reinforced Concrete Structures - A Review. **Int. J. Electrochem. Sci**, [*s. l.*], n. January, p. 1–28, 2007.

SULEIMAN, R. K. *et al.* Effect of metal oxide additives on the structural and barrier properties of a hybrid organosilicon sol-gel coating in 3.5% NaCl medium. **Progress in Organic Coatings**, [*s. l.*], v. 148, 2020. Disponível em: https://www.scopus.com/inward/record.uri?eid=2-s2.0-85086820350&doi=10.1016%2Fj.porgcoat.2020.105825&partnerID=40&md5=c86d6b30e5c038b57e8902177a7d55ee.

TICIANELLI, E. A. **Eletroquímica: Princípios e Aplicações Vol. 17**. [*S. l.*]: Edusp, 1998.

UMOREN, S. A. *et al.* Evaluation of chitosan and carboxymethyl cellulose as ecofriendly corrosion inhibitors for steel. **International Journal of Biological Macromolecules**, [*s. l.*], v. 117, p. 1017–1028, 2018.

VAYSBURD, A. M.; EMMONS, P. H. Corrosion inhibitors and other protective systems in concrete repair: concepts or misconcepts. **Cement and Concrete Composites**, [*s. l.*], v. 26, n. 3, p. 255–263, 2004.

WANG, S. Corrosion resistance and electrocatalytic properties of metallic glasses. **Metallic Glasses-Formation and Properties**, [*s. l.*], v. 395, p. 116–124, 2016.

WANG, Y.; ZUO, Y.; TANG, Y. Inhibition effect and mechanism of sodium oleate on passivation and pitting corrosion of steel in simulated concrete pore solution. **Construction and Building Materials**, [*s. l.*], v. 167, p. 197–204, 2018. Disponível em: https://doi.org/10.1016/j.conbuildmat.2018.01.170.

WOLYNEC, S. **Técnicas Eletroquimicas de corrosão**. 1ªed. São Paulo: [*s. n.*], 2003.

XU, P. *et al.* Corrosion inhibition efficiency of compound nitrite with D-sodium gluconate on carbon steel in simulated concrete pore solution. **Construction and Building Materials**, [*s. l.*], v. 288, p. 123101, 2021. Disponível em:

https://doi.org/10.1016/j.conbuildmat.2021.123101.

YANG, R.-J. *et al.* Effect of sodium d-gluconate-based inhibitor in preventing corrosion of reinforcing steel in simulated concrete pore solutions. **Acta Physico-Chimica Sinica**, [*s. l.*], v. 28, n. 8, p. 1923–1928, 2012.

YANG, H. *et al.* Preparation of corrosion inhibitor loaded zeolites and corrosion resistance of carbon steel in simulated concrete pore solution. **Construction and Building Materials**, [*s. l.*], v. 225, p. 90–98, 2019. Disponível em: https://doi.org/10.1016/j.conbuildmat.2019.07.141.

YE, C.-Q. *et al.* EIS analysis on chloride-induced corrosion behavior of reinforcement steel in simulated carbonated concrete pore solutions. **Journal of Electroanalytical Chemistry**, [*s. l.*], v. 688, p. 275–281, 2013.

YEOMANS, S. **Galvanized steel reinforcement in concrete**. [*S. l.*]: Elsevier, 2004.

ZHAO, Y. *et al.* Corrosion inhibition efficiency of triethanolammonium dodecylbenzene sulfonate on Q235 carbon steel in simulated concrete pore solution. **Corrosion Science**, [*s. l.*], v. 158, n. June, p. 108097, 2019. Disponível em: https://doi.org/10.1016/j.corsci.2019.108097.

3. DISCUSSÃO INTEGRADORA

A revisão sistemática realizado mostrou que o uso de soluções de poro de concreto simulado (SCP) tem ganhado espaço no meio científico, principalmente no que tange ao estudo da corrosão dos vergalhões de aço, pois tal solução permite simular, no ambiente de uma célula eletroquímica, a corrosão acelerada, o que possibilita avaliar, com rapidez, o que acontece com o vergalhão de aço quando imerso no concreto em função do tempo, além da possibilidade de simular ataques como o ambiente marítimo e a carbonatação.

Porém, o uso de SCP composta somente por hidróxido de cálcio saturado, mesmo sendo amplamente utilizada, não é suficiente para simular o conteúdo do que realmente está presente nos poros do concreto, pois o único inibidor de corrosão é a concentração de hidroxila, que determina o limite de cloretos para iniciar a corrosão do aço.

Portanto, o uso de uma SPC composta pela mistura de cimento e água representa melhor a realidade, devido à hidratação do cimento Portland conter uma série de íons (Na^+ , K^+ , Ca^{2+}, Mg^{2+}, Al^{3+} e $(SO_4)^{2-}$), os íons cloro são fisicamente adsorvidos pelo CSH (silicato de cálcio hidratado) e o C_3A (aluminato de tricálcio) liga quimicamente os cloretos para produção do sal de Friedel ($C_3A.CaCl_2.10H_2O$), o que garante ao aço um menor risco à corrosão, pois promove a remoção de uma parcela dos íons cloro da solução.

O monitoramento de OCP é uma técnica eletroquímica muito utilizada para avaliar formação de filmes óxidos passivadores ou óxidos corrosivos sobre um metal. Porém, esta técnica indica somente o balanço entre a reação anódica e a catódica, sem oferecer informações quantitativas, portanto, não é possível obter-se resultados referentes à velocidade de corrosão do vergalhão, sendo, o potencial de corrosão das armaduras no concreto uma grandeza que indica uma situação de corrosão ou estado passivo destas, de forma aproximada.

Já as técnicas utilizadas para obtenção do diagrama de Evans, são ensaios quantitativos, que permitem identificar a taxa de corrosão instantânea de um metal e, por meio de medições, verificar a taxa de corrosão em um determinado tempo, sendo que o objetivo de obter a curva de polarização é ter informações sobre parâmetros cinéticos de passivação, como o potencial de corrosão (E_{corr}), utilizando Tafel, a resistência à polarização (R_p), corrente de corrosão (i_{corr}) e velocidade de corrosão (V_{corr}).

Com a técnica de EIS, para o sistema de aço/concreto, é possível obter informações sobre vários parâmetros, como a presença de filmes de superfície, características do concreto, corrosão interfacial e fenômenos de transferência de massa. Porém, a interpretação dos resultados pode ser uma tarefa difícil, e a necessidade de um circuito equivalente, que pode mudar conforme as condições do aço, torna a técnica mais aceitável para estudos laboratoriais.

Neste trabalho foi avaliado o desempenho da hidroxipropilmetilcelulose (HPMC) como inibidor de corrosão em aço carbono em solução simulada de poros de concreto (SPC), onde

foi verificado que funcionou de forma eficaz como inibidor de corrosão do aço.

Foi utilizado um delineamento experimental para determinar as melhores concentrações de HPMC como inibidor de corrosão em ambiente contaminado por cloretos. O planejamento experimental adotado foi do tipo delineamento composto central rotacional (DCCR), tendo como variáveis a quantidade de HPMC e NaCl, e como respostas o potencial de corrosão (E_{cor}), a resistência a polarização (R_p), e a condutividade. A avaliação estatística do planejamento mostrou que para E_{cor}, R_p e condutividade, as variáveis HPMC e NaCl foram significativas ($p<0,10$), sendo que o modelo estatístico mostrou correlação superior a 90% com os dados experimentais.

Já os resultados da espectroscopia de impedância eletroquímica (EIS) revelaram um aumento na resistência a transferência de carga das amostras na presença de HPMC, em comparação com o sistema referência. O HPMC teve uma maior eficiência como inibidor de corrosão nas amostras contaminadas com 17,5 g/L de NaCl, de 75% a 98%. Já nas soluções que continham 35,1 g/L de NaCl somente a dosagem máxima de HPMC (1,2 g/L) obteve êxito como inibidor de corrosão, com eficiência de 58%.

As análises do OCP e das curvas de polarização indicam a formação de um filme passivo no aço imerso em solução contendo HPMC. A polarização Tafel demonstra desempenho anticorrosivo promissor de HPMC. A análise estatística, por meio do DCCR, confirmou que o meio contendo HPMC apresenta melhores propriedades passivantes, mostrando que esse biopolímero pode ser utilizado como inibidor de corrosão para concreto armado na construção civil.

4. CONCLUSÃO

O efeito inibitório e o mecanismo do inibidor de corrosão da HPMC sobre o aço carbono em SPC foram estudadas e as seguintes conclusões resultaram deste estudo.

1. De acordo com as análises eletroquímicas, um filme passivo cresceu na superfície do aço carbono imerso em SPC contendo HPMC, indicando que pode funcionar como inibidor de corrosão.
2. Os estudos potenciodinâmicos confirmaram que as soluções contendo 3,5% de NaCl, sem o inibidor de corrosão (HPMC), H0N3, obtiveram altas taxas de corrosão, baixos valores de resistência de polarização, evidenciando falhas ou ausência de formação do filme passivador.
3. Uma vez iniciada a corrosão, a taxa de propagação é maior para as soluções que contem HPMC com teores superiores a 50%, provavelmente devido ao aumento da condutividade da solução de poros. Uma concentração de 0,60 g/L de HPMC, pode resultar em um equilíbrio físico e eletroquímico entre o fechamento dos microporos e a propagação de uma condutividade adequada da solução dos poros que controla a suscetibilidade ao ataque de cloreto nas barras de aço. Este equilíbrio evita a propagação de correntes de corrosão mais elevadas e cria uma condição de propagação comparável ao comportamento de uma solução referência.
4. O planejamento experimental DCCR mostrou que as variáveis dependentes foram significativas ($p<0,10$), sendo que o modelo estatístico mostrou correlação superior a 90% com os dados experimentais.
5. A ANOVA, em conjunto com o diagrama de Pareto, mostrou a correlação direta entre o aumento da concentração de HPMC com a melhora dos índices das variáveis dependentes (OCP, E_{cor} e R_p), com exceção do aumento da condutividade, que não tem relação com a concentração do HPMC e sim com a concentração de íons cloreto na solução. No entanto, mesmo com a alta condutividade foi possível verificar que o HPMC conseguiu inibir a corrosão, isso fica evidenciado analisando os resultados das outras variáveis dependentes.
6. Com o aumento do teor de HPMC na SPC, o potencial de pite (E_{pit}) e a resistência a transferência de carga (R_{ct}) aumentaram, enquanto a densidade de corrente (j_{corr}) e a capacitância da dupla camada elétrica (C_{dl}) diminuíram.

No geral, este estudo mostrou que a adição de HPMC na formulação do concreto tem benefícios potenciais em relação às suas propriedades passivantes, ou seja, o concreto contendo HPMC parece ser um meio menos agressivo para o aço. A menor suscetibilidade à corrosão do aço no meio com HPMC é aqui atribuída às características de passivação mais rápidas, com base no monitoramento de diferentes parâmetros eletroquímicos e na análise estatística.

REFERÊNCIAS

AHER, P. D. *et al.* Critical review on biopolymer composites used in concrete. **Materials Today: Proceedings**, [*s. l.*], 2023. Disponível em: https://www.sciencedirect.com/science/article/pii/S2214785323040828.

ALHOZAIMY, A.; HUSSAIN, R. R.; AL-NEGHEIMISH, A. Significance of oxygen concentration on the quality of passive film formation for steel reinforced concrete structures during the initial curing of concrete. **Cement and Concrete Composites**, [*s. l.*], v. 65, p. 171–176, 2016. Disponível em: https://www.sciencedirect.com/science/article/pii/S0958946515300494.

ALVAREZ, L. X. *et al.* Organic compounds as corrosion inhibitors for reinforced concrete: a review. **Corrosion Reviews**, [*s. l.*], v. 41, n. 6, p. 617–634, 2023.

ARUKALAM, I. O. *et al.* Experimental and theoretical studies of hydroxyethyl cellulose as inhibitor for acid corrosion inhibition of mild steel and aluminium. **The open corrosion Journal**, [*s. l.*], v. 6, n. 1, 2014.

BOUBITSAS, D.; TANG, L. The influence of reinforcement steel surface condition on initiation of chloride induced corrosion. **Materials and Structures**, [*s. l.*], v. 48, p. 2641–2658, 2015.

ELSENER, B.; ANGST, U. Corrosion inhibitors for steel in concrete–an update. **La Metallurgia Italiana**, [*s. l.*], v. 7, p. 59–62, 2017.

KUMPAWAT, V.; GARG, U.; TAK, R. K. Corrosion inhibition of aluminium in acid media by naturally occurring plant Artocarpus heterophyllus and Acacia senegal. **Journal of Indian Council of Chemists**, [*s. l.*], v. 26, n. 1, p. 82–84, 2009.

LIN, B.; ZUO, Y. Inhibition of Q235 carbon steel by calcium lignosulfonate and sodium molybdate in carbonated concrete pore solution. **Molecules**, [*s. l.*], v. 24, n. 3, 2019.

LIU, C. *et al.* Coconut coir dust extract as a novel green corrosion inhibitor for carbon steel in the chloride-contaminated concrete pore solution. **Journal of Building Engineering**, [*s. l.*], v. 82, p. 108194, 2024. Disponível em: https://www.sciencedirect.com/science/article/pii/S2352710223023744.

LIU, C.; SRIDHAR, N. The effects of chloride, nitrate, and nitrite on the localized corrosion of carbon steel in simulated concrete pore solutions. **Corrosion**, [*s. l.*], v. 77, n. 3, p. 350–367, 2021.

NAHALI, H.; DHOUIBI, L.; IDRISSI, H. Effect of Na3PO4 addition in mortar on steel reinforcement corrosion behavior in 3% NaCl solution. **Construction and Building Materials**, [*s. l.*], v. 78, p. 92–101, 2015.

NWANONENYI, S. *et al.* Inhibitive Performance of Hydroxypropyl Cellulose and Potassium Iodide on the Corrosion of Mild Steel in Sulphuric Acid Environment. **American Chemical Science Journal**, [*s. l.*], v. 16, n. 2, p. 1–12, 2016.

OGUZIE, E. E. *et al.* Understanding corrosion inhibition mechanisms—experimental and

theoretical approach. **Rsc Advances**, [*s. l.*], v. 1, n. 5, p. 866–873, 2011.

OKAFOR, P. C.; EBENSO, E. E.; EKPE, U. J. Azadirachta indica extracts as corrosion inhibitor for mild steel in acid medium. **Int. J. Electrochem. Sci**, [*s. l.*], v. 5, n. 7, p. 978–993, 2010.

PINA, F. **Resistência à carbonatação de argamassas de reparação para estruturas em betão armado: Estudo das argamassas cimentícias modificadas com polímeros**. [*S. l.*]: Dissertação de Mestrado em Engenharia Civil, Instituto Superior Técnico, Lisboa, 2009.

RANI, B. E. A.; BASU, B. B. J. Green inhibitors for corrosion protection of metals and alloys: An overview. **International Journal of Corrosion**, [*s. l.*], v. 2012, n. 6, p. 16–25, 2012.

SHI, J. J.; SUN, W. Effects of phosphate on the chloride-induced corrosion behavior of reinforcing steel in mortars. **Cement and Concrete Composites**, [*s. l.*], v. 45, p. 166–175, 2014.

SINGH, J. K.; SINGH, D. D. N. The nature of rusts and corrosion characteristics of low alloy and plain carbon steels in three kinds of concrete pore solution with salinity and different pH. **Corrosion Science**, [*s. l.*], v. 56, p. 129–142, 2012. Disponível em: https://www.sciencedirect.com/science/article/pii/S0010938X11006160.

SOLOMON, M. M. *et al.* Inhibitive and adsorption behaviour of carboxymethyl cellulose on mild steel corrosion in sulphuric acid solution. **Corrosion Science**, [*s. l.*], v. 52, n. 4, p. 1317–1325, 2010.

UMOREN, S. A. *et al.* Evaluation of chitosan and carboxymethyl cellulose as ecofriendly corrosion inhibitors for steel. **International Journal of Biological Macromolecules**, [*s. l.*], v. 117, p. 1017–1028, 2018.

UMOREN, S. A. Inhibition of aluminium and mild steel corrosion in acidic medium using Gum Arabic. **Cellulose**, [*s. l.*], v. 15, p. 751–761, 2008.

WU, M.; SHI, J. Beneficial and detrimental impacts of molybdate on corrosion resistance of steels in alkaline concrete pore solution with high chloride contamination. **Corrosion Science**, [*s. l.*], v. 183, n. November 2020, 2021.

YAO, N. *et al.* Synergistic effect of red mud and fly ash on passivation and corrosion resistance of 304 stainless steel in alkaline concrete pore solutions. **Cement and Concrete Composites**, [*s. l.*], v. 132, n. April, p. 104637, 2022. Disponível em: https://doi.org/10.1016/j.cemconcomp.2022.104637.

ANEXO I:Comprovação da submissão do artigo referente ao Capítulo III

Construction and Building Materials

Avaliação de biopolímeros derivados de celulose na suscetibilidade à corrosão do aço em ambientes que simulam soluções de poros de concreto - uma análise estatística usando CCRD

--Manuscript Draft--

Manuscript Number:	
Article Type:	Research Paper
Keywords:	corrosion inhibitor; hydroxypropyl methylcellulose (HPMC); concrete pore solution; experimental design; CCRD
Corresponding Author:	MARIA DE PAULA ESTEVAM DOLIVEIRA, Msc. Federal University of Tocantins Palmas, TO BRAZIL
First Author:	MARIA DE PAULA ESTEVAM DOLIVEIRA, Msc.
Order of Authors:	MARIA DE PAULA ESTEVAM DOLIVEIRA, Msc.
	SALMO MOREIRA SIDEL, Dr.
	EMERSON GUARDA, DR.
	PATRICIA MARTINS GUARDA, Dr.
Abstract:	Hydroxypropyl Methylcellulose (HPMC) can be used as a bioactive in concrete, but little is known about its effects on the steel corrosion process. This article reports on the estimation of steel corrosion susceptibility when immersed in simulated concrete pore solutions with HPMC added. The aim is to understand the corrosion process of reinforced concrete structures. An experimental design was employed to determine the optimal concentrations of HPMC as a corrosion inhibitor in a chloride-contaminated environment. For this analysis, the following experiments were conducted in an electrochemical cell: open-circuit potential (OCP) and linear sweep voltammetry (LSV), in addition to pH and conductivity measurements. The experimental design adopted was a central composite rotatable design (CCRD), with the variables being the amount of HPMC and NaCl, and the responses being the corrosion potential (Ecorr), polarization resistance (Rp), and conductivity. The statistical analysis of the design showed that for Ecorr, Rp, and conductivity, the variables HPMC and NaCl were significant ($p < 0.10$), with the statistical model showing a correlation of over 90% with the experimental data. The OCP analysis and polarization curves indicate the formation of a passive film on the steel immersed in a solution containing HPMC. The Tafel polarization demonstrates promising anti-corrosive performance of HPMC. The statistical analysis, through the CCRD, confirmed that the medium containing HPMC exhibits better passivating properties, showing that this biopolymer can be used as a corrosion inhibitor for reinforced concrete in civil construction.
Suggested Reviewers:	Elisandra Scarpin Federal University of Tocantins elisandrascapin2015@gmail.com
	Elton Carvalho de Lima Federal University of Tocantins eltonlima@uft.edu.br
	Daniel Araujo Gonçalves, doctor daniel.araujogoncalves@gmail.com
	Michael Jones da Silva, doctor michael.silva@unesp.br
	Cicero Rafael Cena da silva cicero.cena@ufms.br

Federal University of Tocantins, Palmas, March 22, 2024.

Dear Editor,

We would like to submit our work entitled “Evaluation of Cellulose-Derived Biopolymers on Steel Corrosion Susceptibility in Environments Simulating Concrete Pore Solutions - A Statistical Analysis Using CCRD” by D'Oliveira, et al. for your diary: **Construction and Building Materials**.

Corrosion of reinforcement in reinforced concrete structures is one of the main factors that reduce their useful life due to the interaction of concrete with the environment, especially when the water/cement ratio, type of cement, curing and coverage are inadequate to the required environmental conditions. . . The use of simulated concrete pore solutions is a viable alternative for studying the behavior of the steel/concrete interface, mainly due to the possibility of reproducibility within the laboratory.

The objective of this work was to optimize the use of HPMC as a corrosion inhibitor in environments contaminated by chlorides, evaluating the significant variables for corrosion analysis and optimizing these variables through the response surface. This is a simpler and faster methodology, which could be applied to investigate the formation of a passive film on steel, thus contributing to the current understanding of the impact of the environment on the propensity of rebar to the corrosion process.

Our study showed that the addition of HPMC in the concrete formulation has potential benefits in relation to its passivating properties, that is, concrete containing HPMC appears to be a less aggressive medium for steel. The lower susceptibility to corrosion of steel in the HPMC medium is here attributed to the faster passivation characteristics, based on monitoring of different electrochemical parameters and statistical analysis.

The publication of the study in the journal **Construction and Building Materials** would be of great importance, becoming a reference work in the area, as the journal focuses on publishing innovative research and application articles that describe laboratory investigations, publishing high-quality articles. quality in the areas that this study will impact. We, the undersigned, declare that this manuscript is original, has not been published before, and is not under consideration for publication elsewhere.

We wish to confirm that there are no known conflicts of interest associated with this publication and that there was no significant financial support for this work that could have influenced its outcome.

We confirm that we have given due consideration to the protection of the intellectual property associated with this work and that there are no impediments to publication, including the timing of publication, with respect to intellectual property. In doing so, we confirm that we follow our institutions' regulations regarding intellectual property.

We confirm that the manuscript has been read and approved by all named authors and that there are no other persons who meet the criteria for authorship but are not listed. We further confirm that the order of authors listed in the manuscript was approved by all of us.

We understand that the Corresponding Author is the only contact for the Editorial process (including the Editorial Manager and direct office communications). He is responsible for communicating with other authors about progress, review submissions, and final approval of proofs.

The name of each author and its appropriate category.
Conception and design of the study: **Maria Carolina de Paula Estevam D'Oliveira [a], Emerson Adriano Guarda [a],**
Data acquisition: **Maria Carolina de Paula Estevam D'Oliveira [a]**
Data analysis and interpretation: **Maria Carolina de Paula Estevam D'Oliveira [a], Emerson Adriano Guarda [a]**
Manuscript preparation: **Maria Carolina de Paula Estevam D'Oliveira [a]**
Critical review: **Emerson Adriano Guarda [a], Patrícia Martins Guard [a], Salmo Moreira Sidel [a]**

Sincerely,

MSc . Maria Carolina de Paula Estevam D'Oliveira
to UFT - LAPEQ

Evaluation of Cellulose-Derived Biopolymers on Steel Corrosion Susceptibility in Environments Simulating Concrete Pore Solutions - A Statistical Analysis Using CCRD

Abstract

Hydroxypropyl Methylcellulose (HPMC) can be used as a bioactive in concrete, but little is known about its effects on the steel corrosion process. This article reports on the estimation of steel corrosion susceptibility when immersed in simulated concrete pore solutions with HPMC added. The aim is to understand the corrosion process of reinforced concrete structures. An experimental design was employed to determine the optimal concentrations of HPMC as a corrosion inhibitor in a chloride-contaminated environment. For this analysis, the following experiments were conducted in an electrochemical cell: open-circuit potential (OCP) and linear sweep voltammetry (LSV), in addition to pH and conductivity measurements. The experimental design adopted was a central composite rotatable design (CCRD), with the variables being the amount of HPMC and NaCl, and the responses being the corrosion potential (E_{corr}), polarization resistance (R_p), and conductivity. The statistical analysis of the design showed that for E_{corr}, R_p, and conductivity, the variables HPMC and NaCl were significant ($p < 0.10$), with the statistical model showing a correlation of over 90% with the experimental data. The OCP analysis and polarization curves indicate the formation of a passive film on the steel immersed in a solution containing HPMC. The Tafel polarization demonstrates promising anti-corrosive performance of HPMC. The statistical analysis, through the CCRD, confirmed that the medium containing HPMC exhibits better passivating properties, showing that this biopolymer can be used as a corrosion inhibitor for reinforced concrete in civil construction.

Keywords: corrosion inhibitor; hydroxypropyl methylcellulose (HPMC); concrete pore solution; experimental design; CCRD.

1. Introduction

In recent years, there has been a growing demand for natural or biotechnology-based products for use in industrial applications due to environmental concerns, waste disposal issues, and the depletion of non-renewable resources. In 2002, the European Union (EU) launched the biotechnology strategy, and in 2012 the European Commission created the world's first bioeconomy strategy and action plan [1].

The Portland cement concrete (PCC) industry, which uses the most consumed material in the world, relies on chemical additives to improve its physicochemical properties. However, these mixtures are derived from the exploitation of fossil fuels, which is associated with various types of issues [2–5].

One of the challenges faced by the reinforced concrete industry is the corrosion of steel reinforcement. This is a natural electrolytic phenomenon with progressive detrimental effects on material integrity, leading to significant economic losses in various industries [6,7].

Among the various methods available to reduce the problem of corrosion, the use of corrosion inhibitors is often the most suitable and effective approach to achieve this goal. This involves isolating the metal from corrosive agents through the adsorption of compounds containing inhibiting molecules on the surface, forming a protective barrier [8–12].

One option for green inhibitors is biopolymers whose functional groups interact with metal ions and form complexes that act as a barrier separating the aggressive solution from the metal surface. Therefore, corrosion inhibition is achieved through adsorption [13,14].

Cellulose and its derivatives, such as hydroxypropyl methylcellulose (HPMC), are carbohydrate biopolymers found in larger quantities compared to other biopolymers. It is present in plant tissues and constitutes about one-third of the plant. It has pharmaceutical, cosmetic, and food applications, and various derivatives of cellulose have been used as corrosion inhibitors[15–17].

In order to better investigate the impact of using HPMC in concrete formulation and identify its practical effects in civil engineering, this article presents an electrochemical approach to study the durability of carbon steel reinforcement in the presence of HPMC compared to an HPMC-free environment.

The focus was to analyze the early stages of passive film formation on carbon steel reinforcement in contact with simulated concrete pore solutions (SCPS) rather than using mortar as the medium, with or without HPMC in their compositions, using electrochemical experiments. The SPSs exhibit much lower resistivity and equivalent results compared to those conducted in concrete matrices [18–21].

For the definition of the SPSs composition, statistical process optimization was used, which offers advantages over classical optimization by changing one variable at a time[22], with a smaller number of experiments and the possibility of evaluating the effects of interaction between variables. Such systematic experimental design techniques aim at optimizing products and processes, minimizing costs and operational times. The methodology of central composite rotatable design (CCRD) consists of a group of statistical and mathematical procedures that can be used to study the interrelationships between one or more responses (dependent variables) and numerous factors (independent variables) [23].

Therefore, the objective of this work was to optimize the use of HPMC as a corrosion inhibitor in chloride-contaminated environments, evaluating the significant variables for corrosion analysis and optimizing these variables through response surface methodology. This is a simpler and faster methodology that could be applied

to investigate the formation of a passive film on steel, thus contributing to the current understanding of the impact of the environment on rebar corrosion susceptibility.

2. Materials and methods

2.1. Preparation of the simulated concrete pore solution (SPS)

The materials used were commercial-grade raw materials, and when necessary, they were of analytical grade. CPII-F32 cement from the Goiás brand, purchased in Palmas/TO city, was used. CPII-F32 cement is composed of carbonate material, the majority of which is calcium carbonate, with a compressive strength class of 32 MPa. In order to control and inhibit possible interference and unforeseen external reactions as much as possible, this type of cement was chosen mainly due to its composition, which does not contain alternative materials such as blast furnace slag and pozzolana, as in other types of cement. , as there is no research on the reactivity of hydroxypropylmethylcellulose (HPMC) with these compounds, it was preferable to eliminate them from the research. Table 1 shows the chemical composition of the cement used in this research.

Table 1. Chemical composition of CPII-F32 cement.

Chemical element	***%***
Total calcium oxide (CaO)	61,2
Total silicon dioxide (SiO_2)	18,87
Aluminum oxide (Al_2O_3)	4,42
Carbonic anhydride (CO_2)	3,85
Magnesium oxide (MgO)	3,23
Iron oxide (Fe_2O_3)	2,97
Sulfuric anhydride (SO_3)	2,75
Insoluble residue	1,26
Potassium oxide (K_2O)	0,86
Others	0,46
Sodium oxide (Na_2O)	0,13

Source: ABCP, 2020

The HPMC used in this work was manufactured by AROMAT Produtos Químicos LTDA. Sodium chloride PA (NaCl) was manufactured by Nox Lab Solutions and has a purity of 99.0%, according to the manufacturer. Mili-Q® water was produced using equipment manufactured by PERMUTION, and the deionized water has the following parameters: pH around 7.0 and conductivity below 2 μS/cm.

Due to the difficulty of faithfully reproducing the solution present in the pores of a reinforced concrete structure through solution synthesis, in this research, we chose to simulate the concrete pore solution using a mixture of cement and Mili-Q® water. To achieve this, a cement-to-water ratio of 0.075 [24]. The composition of SPS is basically sodium hydroxide (NaOH), potassium hydroxide (KOH) and saturated calcium hydroxide ($Ca(OH)_2$) [25], in addition to the additions of HPMC and NaCl.

The dry material (cement and HPMC) was mixed with Mili-Q® water in an electromagnetic stirrer for 60 minutes. After this period, the solution was vacuum filtered, separating the inert material, so that the supernatants did not interfere with the polarization of the steel. To simulate the corrosive environment, sodium chloride (NaCl) was inserted into the SPS solution.

2.2. Preparation of the working electrode

To produce the working electrodes (WE), a 5 mm CA-50 steel bar was initially filed to remove the side ribs. Soon after, the steel bar went through the polishing process, using water sandpaper. Then the steel bar was cut into 3.0 cm long pieces. To ensure good conductivity, a copper wire was welded to one end of the steel bar, via flux soldering with a silver alloy, as shown in Figure 1. After welding, cleaning was carried out to degrease the electrodes.

Figure 1. Working electrode in the construction process.
Source: author himself

To ensure that only the transverse face of the working electrode (0.18 cm^2) would be in contact with the solution, phosphating was carried out and subsequent polymerization of the working electrode.

Phosphating is a treatment where a metal is converted into an oxide, hydroxide or salt of the metal through electrochemical reactions. It involves the conversion of the metal into an insoluble phosphate of the metal ion. Insoluble phosphate deposits on the metal, modifying its surface properties [26]. In this work, the phosphatized layers were obtained by immersing the working electrodes (WE) in a phosphoric acid solution for around 60 minutes.

After phosphating, the working electrodes (WE) were embedded in transparent oepoxy resin supplied by POLIPOX (RL-3028 resin and EL-3041 catalyst) and cured for 48 hours. Finally, the face of the electrode was exposed, using water sandpaper in the granulometric sequence 800, 1500 and 2000. Figure 2 schematically illustrates the finished working electrode (WE).

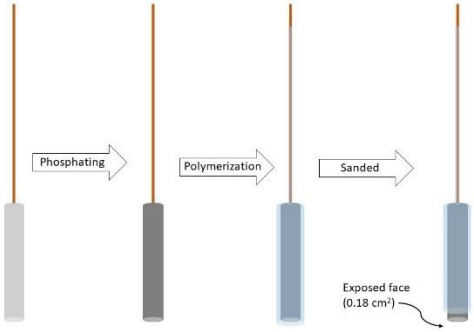

Figure 2. Finished working electrode

Source: author himself

To get closer to the reality of the behavior of steel immersed in concrete, it was necessary to keep the work electrodes immersed in simulated concrete pore solutions (SPS) for 14 days, in order to passivate the reinforcement, as illustrated in Figure 3.

The conventional carbon steel passivation process in concrete is a spontaneous electrochemical reduction mechanism that occurs on the steel surface through interaction with the alkaline solution in the pores [27]. This passivation process plays a decisive role in the corrosion model initiation phase of the concrete structure [28].

Figure 3. Working electrode in the passivation process

Source: author himself

2.2. Methods

All electrochemical characterizations were conducted in a conventional three-electrode glass cell at 23°C, using an Vertex potentiostat/galvanostat controlled via IviumSoft software.

Ag/AgCl was used as the reference electrode (RE), and a platinum wire was used as the counter electrode (CE) ,in addition to the working electrode (WE).

The pH and conductivity of the SPSs and the electrochemical analyses were measured on the day of sample preparation and after 14 days of passivation. The pH and conductivity values were measured after a 5-minute stabilization period. The conductivities and pHs of these solutions were determined and are listed in Table 2 as average values obtained from triplicate analyses.

Table 2. Physicochemical Properties of Concrete Pore Solution (SPS)

SPS	NaCl	HPMC	pH		Conductivity (ms/cm)	
	(g/L)	(g/L)	0 dias	14 dias	0 dias	14 dias
REF	-	-	12.86±0.02	13.11±0.03	8.79±2.48	8.38±2.62
H0N3	35.1	-	12.96±0.05	13.01±0.10	42.88±1.68	65.45±3.95
H12N3	-	1.20	12.87.6±0.11	12.94.3±0.21	52.45±4.55	60.47±2.43

The pH of all analyzed solutions increased after the electrochemical tests. This phenomenon can be explained by the composition of the solution in question, where SPS has an alkaline pH, with typical values between 12.5 and 13.5 because of the main constituents of the solution which are alkaline. In this pH range, it is viable to use steel reinforcement in conjunction with concrete, considering that with these hydrogenionic potentials the reinforcement remains in a state of passivation [29].

For the analysis of the electrochemical cells, the following techniques were used: open potential circuit monitoring (OCP) and linear swept volvametry (LSV), both using the Vertex potentiostat/galvanostat controlled through the IviumSoft software.

A metal that corrodes in a solution of low electrical resistivity assumes a characteristic potential, known as corrosion potential. This potential is given by the intersection of the anodic polarization curve with the cathodic polarization curve. Corrosion potential is one of the easiest electrochemical parameters to be determined experimentally. As this is a potential assumed by the metal, it is sufficient to obtain a direct measurement of this potential in relation to a reference electrode. This measurement is known as open circuit potential measurement [30].

OCP monitoring is a typical half-cell potential method, indicating the reaction potential of a metal with an environment. OCP monitoring is widely used to evaluate the corrosion potential of reinforcing steel embedded in concrete relative to a standard reference electrode (e.g., Ag/AgCl electrode). The corrosion risk level of reinforcement in ordinary concrete can be assessed by OCP values in accordance with ASTM C876:2022 [31].

When the researcher's objective is to evaluate the formation of the passivating film, automatic monitoring is recommended over a short period of time (maximum one hour) to observe the change in the electrochemical behavior of the system [32], this was considered for this research.

Linear sweep voltammetry (LSV) is another electrochemical method for characterizing the corrosion state of a metal. A potential range is applied, from lowest to highest, monitoring the response current throughout the sweep. Basically, the application of potential aims to simulate corrosion, but in an accelerated way, to understand the

behavior of the metal. To perform the potential sweep, most authors choose to apply a potential between ± 10 mV and ± 20 mV in relation to OCP [33–35].

At potentials below the OCP, the polarization curve (CP) is called the cathodic curve and, for potentials above the OCP, the anodic curve. Polarization curves are also called Evans diagram. In this work, the sweep occurred from -1500 mV to +500 mV, versus OCP, with a speed of 0.167 mV/s.

The polarization curve of a metal represents the global effect of all reactions that occur simultaneously on the electrode, and through it is possible to evaluate the electrochemical behavior of a metal at a potential different from the corrosion potential. It is necessary to use external potential sources, such as a potentiostat, to impose a different potential on an electrode than the corrosion potential. This potential is imposed through a difference between the potential of the electrode and the reference electrode, in media with moderate to high conductivity, thus making it possible to measure the polarization current, in addition to recording it as a function of the potential [36,37].

To determine the corrosion potential (E_{corr}), extrapolation of Tafel lines was used. Tafel's approach involves plotting the logarithm of the absolute value |i| current density versus potential. The slopes of these linear segments produce transfer coefficients, called Tafel Slopes. Extrapolating these straight lines to the corrosion potential makes it possible to obtain the corrosion current (i_{corr}).

The corrosion current density (j_{cor}) was determined using the method described by McCafferty [38,39], which consists of dividing the net current (i_{corr}) by the exposed area of the working electrode (0.18 cm^2). The polarization resistance (R_p), was determined from the Stern-Geary constant (B) and calculated using the following formula [38].

$$R_p = \frac{B}{j_{cor}} \qquad (1)$$

During the potential sweep the current density goes to zero and then increases to a low anodic value, approximately constant in the passive range. In this range, a thin oxide/hydroxide film, the passivating film, protects the material from high corrosion rates. If the current density decreases when the potential sweep direction has been reversed, the material proves immune to pitting corrosion. However, if on the upward sweep of potential, the current density increases suddenly and remains high on the downward sweep, until finally decreasing to the value of the passive region, the material is shown to undergo a form of pitting corrosion. The pitting potential (E_{pite}) was also determined from the polarization curves. This was the potential at which the current density increased suddenly [40].

Through polarization it is possible to determine the corrosion rate, in mm/year for example, of materials. In this case, corrosion is not necessarily restricted to pitting corrosion, but can reach a level of generalized corrosion. The corrosion rate measurement is, in general, associated with widespread corrosion. From the i_{corr} value, the corrosion rate (V_{corr}) of the system can be determined using Faraday's Law [36]. The corrosion rate (V_{cor}) is related as follows:

$$V_{corr} = \frac{j_{cor} * M * t}{n * F * d} \qquad (2)$$

where "M" is the molar mass of iron (0.056 kg/mol); "d" is the density of iron (7.847 kg/m³); "n" is the valency of an Fe+2 ion; "F" is the Faraday's constant (96.485 C/mol); and "t" is the time coefficient (3.15^{*} x $10^{7\cdot}$ s/year). Considering the parameters for iron, Equation 2 reduces to [41]:

$$V_{cor} \approx 11.6 * j_{cor} \ \ (mm/year) \qquad (3)$$

where the corrosion current density (j_{cor}) should be in units of (mA/cm²).

2.3. Experimental Design

The experimental design conducted aims to evaluate the effect of variables for optimizing the composition of the simulated concrete pore solution (SPS) using HPMC and NaCl. This was achieved through a central composite rotational design (CCRD) 2^2 containing 3 central points and 4 axial points. Each parameter was studied at four different levels (-1.41; -1;0; +1 +1.41), generating a matrix of 11 experiments with two factors, using the Protimiza software (2014), as shown in Table 3. in addition to the reference solution containing only cement and water and another solution with the addition of 3.5% by weight of NaCl.

The ranges of variation between the upper and lower limits of each independent variable were established according to the most commonly used data for the analysis of corrosion inhibitors based on biopolymers and the simulation of chloride-contaminated environments [42].

Table 3. List of Central Composite Rotatable Design (CCRD) tests.

Experiment	Coded variables		Real variables	
	X1	X2	HPMC (g/L)	NaCl (g/L)
1	-1	-1	0,6	17,5
2	1	-1	1,2	17,5
3	-1	1	0,6	35,1
4	1	1	1,2	35,1
5	-1,41	0	0,48	26,3
6	1,41	0	1,32	26,3
7	0	-1,41	0,9	13,85

8	0	1,41	0,9	38,75
9	0	0	0,9	26,3
10	0	0	0,9	26,3
11	0	0	0,9	26,3

2.4. Experiment Validation

In the Central Composite Rotatable Design (CCRD), three central points were used, and two independent variables were considered: the amounts of HPMC and NaCl added to the SPSs. The dependent variables in this design were the electrochemical parameters (OCP, E_{corr} e R_p) and the conductivity.

This experimental design includes an effects table, a Pareto chart, calculated regression coefficients, and statistical analysis using ANOVA. Additionally, its aim was to analyze the effects of HPMC and NaCl on steel rebars and evaluate response surface plots, thus achieving the optimization of HPMC as a corrosion inhibitor for steel in reinforced concrete.

3. Results and discussion

3.1. Open Circuit Potential (OCP) and Sweep Linear Voltammetry (SLV)

Measuring the OCP or half-cell potential is one of the common methods for evaluating the corrosion state of steel rebars in reinforced concrete structures. Due to the simplicity of this method, it is generally used in industrial and laboratory applications. However, it should be noted that the potential may not accurately reflect the corrosion state because the corrosion process is related to the current transfer or flow of electrons through the anodic dissolution of the metal (M), as in the following reaction:

$$M \rightarrow M^{n+} + ne \qquad (4)$$

According to the ASTM C87.6-22b [31] standard, which introduces a standard test method for half-cell potentials, this should not be interpreted as an indicator of the corrosion reaction. However, the open circuit potential could be a suitable estimate of the rebar's corrosion state in concrete and could indicate the likelihood of corrosion. According to ASTM C87.6-22b, there are three ranges of OCP for corrosion estimation, and Table 4 shows the correlation between the saturated calomel electrode (SCE) and the Ag/AgCl electrode used in this work.

Table 4. Probability of Reinforcement Corrosion Occurrence as a Function of Potential.

Electrode type	**Likelihood of corrosion occurring**		
	OCP< 10%	**10%<OCP<90%**	**OCP> 90%**
Hg, Hg_2Cl_2. KCl (Calomelano/SCE)	> -126 mV	-126 mV à -27.6 mV	< -27.6 mV

Ag, AgCl/KCl (1M)	> -106 mV	-106 mV à -256 mV	< -256 mV

Source: Modified [43]

The variation in OCP values of the steel reinforcement bars in SCPS over a period of 14 days of passivation is shown in Figure 4, where it can be observed that the potentials increased positively during this period, with the exception of the H0N3 solutions (with a concentration of 35.1 g/L of NaCl), which was expected as this solution simulates a highly corrosive environment.

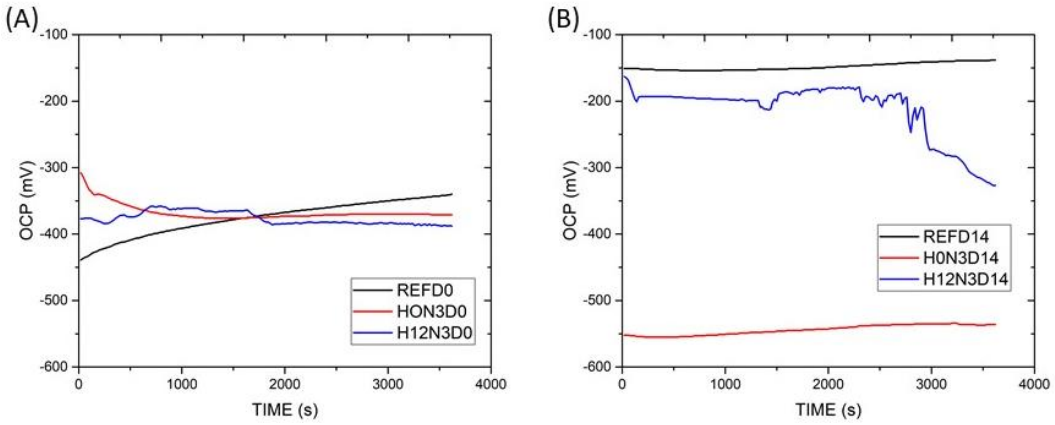

Figure 4. Evolution of open-circuit potential (OCP) values as a function of immersion time, 0 (A) and 14 days (B), for steel samples in simulated reference concrete solution (REFD0 and REFD14); 35.1 g/L of NaCl for simulating a corrosive environment (HON3D0 and HON3D14); and with 35.1 g/L of NaCl and 1.20 g/L of HPMC as a corrosion inhibitor (H12N3D0 and H12N3D14).

During the passivation period, the pH level of the SPS remained above 12 [44] as shown in Table 2. When the pH is above 12. a passive layer forms on the surface of the steel rebar. This layer is responsible for reducing the corrosion rate and increasing the open-circuit potential.

After the addition of NaCl to the SPS, chloride ions can penetrate through this film and reach the surface of the steel reinforcement, deteriorating the passive layer. Due to the depassivation of the steel bars as a result of chloride attack, the corrosion potential decreases.

It is possible to identify that the use of HPMC, with the aim of inhibiting the corrosive attack, proved to be effective, as even with the presence of NaCl, the sample containing HPMC at a concentration of 1.2 g/L (H12N3) showed an increase in OCP at the end of the 14-day passivation period. However, when using Table 3 to assess the probability of corrosion at 14 days, the REF and H12N3 solutions are in the range between 10% and 90% probability of corrosion occurrence, where uncertainty prevails; whereas the H0N3 sample remained with half-cell potentials below -27.6 mV, suggesting a probability above 90% of corrosion occurrence, indicating that the simulated environment is indeed corrosive.

As suggested by Song and Saraswathy [45] half-cell potential measurements alone are not sufficient criteria for corrosion because several factors like limited oxygen diffusion polarization, concrete porosity, and the presence of highly resistive layers can affect the accuracy of potential values. Moreover, the generalization of OCP measurements is debatable since significant variations in corrosion rate can occur within relatively narrow potential ranges [45].

Regarding the obtained electrical conductivity values, a significant variation was observed during the measurement period. In some situations, equipment variation was substantial, which affects the accuracy of the results. Few authors have reported electrical conductivity measurements of SCPS. Among the authors who evaluated steel reinforcement corrosion in SCPS made directly with cement, only Shaheen and Pradhan [33] measured the electrical conductivity of this solution. In their study, researchers obtained a value of approximately 5.5 mS/cm, which is roughly half of the values obtained in the present research for the reference solution and much lower when compared to the solutions with the addition of HPMC and NaCl. What is evident from the values obtained in this article is the increase in conductivity with the addition of NaCl. Certainly, this factor influences the corrosion process, as will be explained later, because an increase in electrical conductivity leads to greater ionic movement in the solution, aiding the steel oxidation process.

In order to investigate an initial hypothesis that CPSs containing HPMC exhibited different passivating natures, linear sweep voltammetry (LSV) was conducted at the initial and final measurement periods (0 and 14 days). The resulting comparison between the systems based on these polarization curves was presented in Figure 5. The most important parameters measured from these polarization curves were summarized in Table 5.

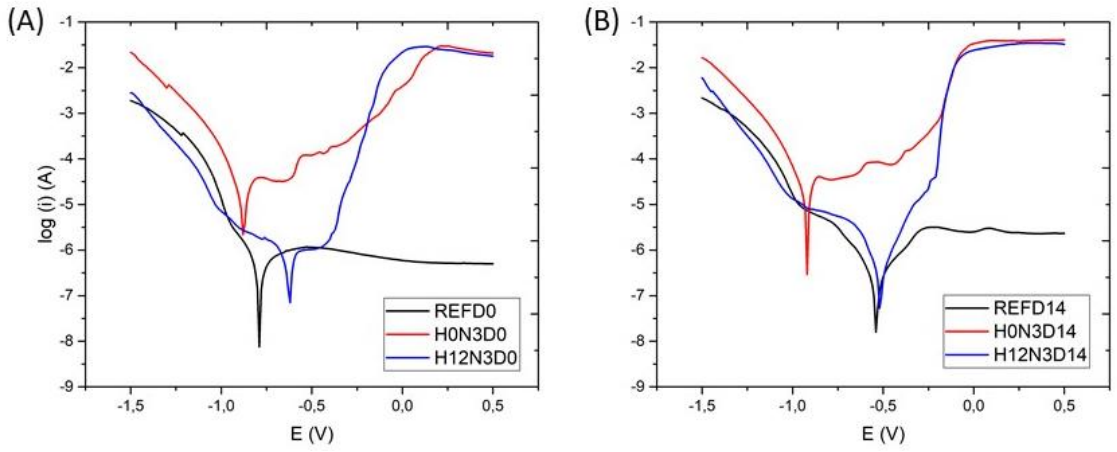

Figure 5. Polarization curves as a function of immersion time, 0 (A) and 14 days (B), of steel samples in simulated concrete solution of reference (REFD0 and REFD14); with only 35.1 g/L of

NaCl for simulating the corrosive environment (HON3D0 and HON3D14); and with 35.1 g/L of NaCl and 1.2 g/L of HPMC as a corrosion inhibitor (H12N3D0 and H12N3D14).

Table 5. Tafel data obtained from polarization curves shown in Figure 5.

Solutions	HPMC (g/L)	NaCl (g/L)	E_{corr} (mV vs. Ag/AgCl/NaCl 3M)	J_{cor} ($\mu A/cm^2$)	R_p ($K\Omega/cm^2$)	E_{pite} (mV vs. Ag/AgCl/NaCl 3M)	V_{corr} (mm/year)
REFD0	0	0	-7.93	0.7.9	97.4	>+500	0.009
REFD14			-541	0.92	187.8	>+500	0.011
H0N3D0	0	35.1	-883	52.59	2.1	-410	0.610
H0N3D14			-920	20.56	1.9	-200	0.238
H12N3D0	1.2	35.1	-628	1.43	66.1	-380	0.017
H12N3D14			-521	1.11	90.1	-210	0.013

Regarding the corrosion potential, E_{corr}, less negative values were obtained for the H12N3D0 solution compared to the reference solution (REFD0), with a difference in E_{corr} f 165 mV between the two electrodes when freshly immersed in the pore solution. After 14 days, the scenario changed slightly, and the E_{corr} values showed a relatively low difference of approximately 20 mV. The shift of E_{corr} towards less negative values over the 14-day immersion period may indicate that the immersion time in the SPSs improves resistance to the corrosion process, suggesting the formation of a passivating layer. In contrast, for the solution containing only NaCl (H0N3), the result was the opposite, with E_{cor} being the most negative of all samples, and during the 14-day immersion, the potential shifted to even more negative values, indicating a worsening of corrosion resistance.

It is worth noting that the values found for OCP during monitoring differ from the values found for E_{corr} using the linear sweep voltammetry (LSV) technique, but the behavior of both measurements is the same.

OCP monitoring is an electrochemical technique widely used to evaluate the formation of passivating oxide films or corrosive oxides on a metal. However, this technique only indicates the balance between the anodic and cathodic reactions, without offering quantitative information, therefore, it is not possible to obtain results regarding the corrosion rate of rebar, with the corrosion potential of reinforcement in concrete being a magnitude which indicates a situation of corrosion or its passive state, approximately.

The techniques used to obtain the Evans diagram are quantitative tests, which allow identifying the instantaneous corrosion rate of a metal and, through measurements, verifying the corrosion rate in a given time, with the objective of obtaining the polarization curve is to have information on kinetic parameters of passivation, such as corrosion

potential (E_{corr}), using Tafel, polarization resistance (R_p), corrosion current (i_{corr}) and corrosion speed (V_{corr}).

It was also observed that the pitting potential (E_{pite}) exhibited the same behavior as E_{corr}. Thus, after 14 days of immersion in the H12N3 solution, Epite shifted by +17.0 mV. These results are consistent with the OCP analysis results shown in Figure 1.

Furthermore, the corrosion current densities (J_{corr}), polarization resistances (R_p), and corrosion rates (V_{corr}) obtained reveal a lower corrosion rate and higher resistivity of the reference solution (REF) and the H12N3 solution compared to the corrosive solution (H0N3), the corrosion rate values being 0.011 mm/year, 0.013 mm/year and 0.238 mm/year and the resistivity of the solutions in question were, respectively, 187.8 kΩ/cm^2, 90.1 kΩ/cm^2 and 1.9 kΩ/cm^2. This reinforcened the hypothesis of passive film formation in the HPMC-containing medium. As R_p is commonly used as a measure of a metal's resistance to corrosion damage, high Rp values are associated with a high corrosion prevention capacity, while low R_p values indicate high corrosive activity [46].

3.2. Statistical analysis using CCRD

This experimental design of the CCRD type was chosen to optimize the dosage of HPMC as a corrosion inhibitor for reinforced concrete reinforcement.

The minimum and maximum ranges of the parameters were investigated, and the complete experimental design with its values in both real and coded form is listed in Table 6. Open circuit potential (OCP), corrosion potential (E_{corr}), polarization resistance (R_p), and conductivity were taken as dependent variables or responses (Y_1. Y_2. Y_3 e Y_4). A second-order polynomial equation was fitted to the data using multiple regression analysis for each of the four dependent variables. This resulted in an empirical model that related each of the measured responses to the independent parameters, as per Equations 5, 6, 7, and 8. Only the central point was performed in triplicate, but the experiments were repeated twice. For the 2-factor system, the model equations are as follows:

OCP: $Y_1 = -493.33 + 11.89x_1 + 47.23x_1^2 - 27.55x_2 + 146.23x_2^2\ 191.75x_1x_2$ (5)

E_{corr}: $Y_2 = -829 - 34.75x_1 + 159.36x_1^2 + 6.59x_2 + 106.99x_2^2 + 189.58x_1x_2$ (6)

R_p: $Y_3 = 23.46 + 15.25x_1 + 32.28x_1^2 - 1.25x_2 + 22.67x_2^2 + 5.69x_1x_2$ (7)

Condutividade: $Y_4 = 57.07 - 0.86x_1 - 3.53x_1^2 + 17.89x_2 + 2.84x_2^2 - 1.26x_1x_2$ (8)

where Y_1. Y_2. Y_3 e Y_4 these are the predicted responses., x_1 e x_2 these are linear coefficients; x_1^2. x_2^2 these are quadratic coefficients e x_1x_2 This is the interaction coefficient.

Table 6. CCRD 2^2 experimental design for the optimization of HPMC as a corrosion inhibitor.

Experiment	Independent variables		Dependent variables			
	HPMC (g/L)	NaCl (g/L)	OCP (mV)	E_{corr} (mV)	R_p (KΩ)	Conductivity (mS/cm²)
1	0.60	17.50	-17.0	-384.3	66.21	22.8
2	1.20	17.50	-542	-833.5	98,23	23.42
3	0.60	35.10	-622	-830	35.35	67.3
4	1.20	35.10	-227.	-520.9	90.14	62.9
5	0.48	26.30	-334	-382	81.5	57.7
6	1.32	26.30	-283	-47.9,5	106.4	55.5
7.	0.90	13.85	-81	-601.2	64.49	37.08
8	0.90	38.75	-140	-469,8	84.95	78.9
9	0.90	26.30	-528	-842.6	20.7.7.	57.,1
10	0.90	26.30	-490	-913.6	22.56	57.12
11	0.90	26.30	-462	-730.8	27.06	57

According to the results obtained in the experimental design (CCRD), regression coefficients were calculated, and a complete statistical analysis was conducted with ANOVA, Pareto chart, and response surface plots. The results of the linear regression coefficients for OCP, E_{corr}, R_p, and conductivity in the CCRD are presented in Tables 7, 9, 11, and 13, respectively. The ANOVA was presented in Tables 8, 10, 12, and 14, respectively.

3.2.1. Analysis of the open circuit potential (OCP)

Analyzing the results presented in Table 6, we can see that the least negative value of OCP, after the electrode passivation for 14 days, was achieved in experiment 1, with a value of -17.0 mV, for concentrations of 0.60 g/L of HPMC and 17.50 g/L of NaCl. This result indicates that the lower the chloride content, the less corrosive the environment becomes, ensuring the formation of the passivating film with small amounts of HPMC.

The presence of chloride can indeed accelerate the dissolution of the metallic alloy or stabilize the dissolution of favorable regions such as grain boundaries or manganese sulfide (MnS) inclusions [47]. Inclusions are referred to as non-metallic material particles with different chemical compositions that are retained within the matrix of various types of steels as a result of their manufacturing process. They are typically already present as impurities in the liquid state of the steel, which makes their removal difficul [48].

The results obtained in experiments 9, 10, and 11, which are the central points, did not show significant variability, indicating the good reproducibility of the process.

When comparing the OCP values obtained at the lowest and highest concentrations of HPMC, it is observed that increasing the concentration from 0.60 g/L to 1.20 g/L resulted in an improvement in the OCP values, changing from -622 mV to -227 mV. Regarding the concentrations of NaCl, higher chloride concentrations led to more negative OCP values, and this situation can be modified with the use of corrosion inhibitors.

Table 7 provides the regression coefficients based on the results obtained in the CCRD experimental design, Table 8 presents a complete statistical analysis with ANOVA, and Figure 6 illustrates the Pareto diagram, all of which pertain to the dependent variable OCP.

Table 7. Linear regression coefficients for the CCRD, related to OCP.

Name	Coefficient	Standard error	Calculated T	P-value
Mean	-493.33	67.43	-7.32	0.0007*
X_1	11.89	41.29	0.29	0.7849
X_1^2	47.,23	49,15	0.96	0.3807
X_2	-27.55	41.29	-0.67	0.5341
X_2^2	146.23	49,15	2.98	0.0310*
X_1X_2	191.7.5	58.39	3.28	0.0219*

* Statistically significant values at 90% confidence level ($p < 0.10$)

Table 8. ANOVA for the CCRD, related to OCP.

Source of variation	Sum of squares	Degrees of freedom	Middle square	F_{calc}	P-value
Regression	275138.5	5	55027.7	4.0	0.07600
Waste	68196.1	5	13639.2		
Lack of adjustment	66001.4	3	22000.5	20.0	0.04788
Pure error	2194.7	2	1097.3		
Total	343334.5	10			

% Explained variation (R^2) = 80.14

The results for the variables x_2^2 e x_1x_2 are statistically significant at a 90% confidence level. Furthermore, they have positive coefficients of 146.23 and 191.75, respectively. It's worth noting that the R^2 value found explains approximately 80% of the experiment, which provides a measure of how much variability in the observed response values can be explained by the experimental factors and their interactions. The closer the R^2 value is to 1.00, the stronger the model, and the better the predictive capabilities. Therefore, values above 0.8 are considered good for obtaining a valid and useful predictive model.

Figure 6 illustrates which variables and interactions analyzed yielded statistically significant results according to the Pareto chart. It can be observed that only the quadratic variable x_2^2 and the interaction of variables x_1-x_2 were significant, while the others would not influence the process if there was an increase in their concentration from level -1.41 to level +1.41.

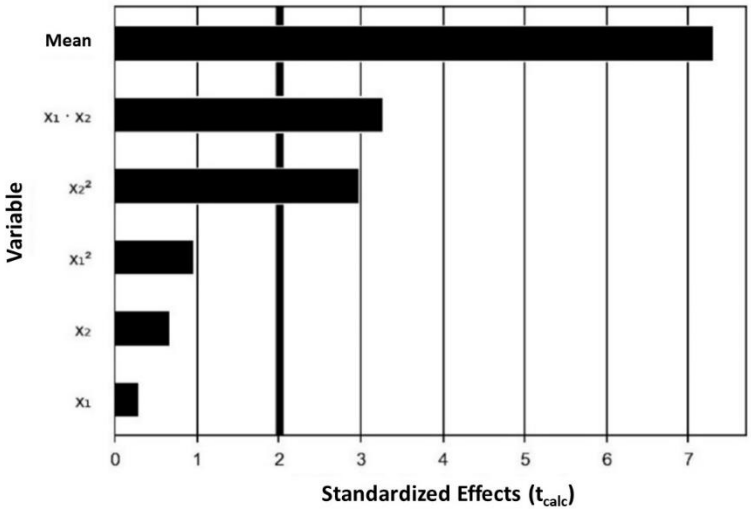

Figure 6. Main effects of significant variables and interactions in the CCRD, related to OCP.
Source: PROTMIZA (2014)

3.2.2. Corrosion potential analysis (E_{corr})

In Table 6, you can observe the E_{corr} values after 14 days of electrode immersion in a solution. In experiment 1, a value of -384.3 mV was achieved for concentrations of 0.60 g/L of HPMC and 17.50 g/L of NaCl. However, in experiments 3 and 4, where the NaCl concentration is at its maximum (35.10 g/L), the increase in HPMC concentration from 0.60 g/L to 1.20 g/L was responsible for shifting the E_{corr} to the right by approximately 309 mV.

This behavior was already expected since the solutions have a pH greater than 12. With these high hydrogenic potentials, the reinforcement remains in a state of passivation [37], and the OCP is also less negative, indicating a likely passivation zone.

The results obtained in the experiments related to the central points did not show significant variability, indicating good process reproducibility.

Table 9 provides the regression coefficients based on the results obtained in the CCRD experimental design, Table 10 presents a complete statistical analysis with ANOVA, and Figure 7 illustrates the Pareto diagram, all of which pertain to the dependent variable E_{corr}.

Table 9. Linear regression coefficients for the CCRD, related to E_{corr}.

Name	Coefficient	Standard error	Calculated T	P-value
Mean	-829,00	73.16	-11.33	0.0001*
X_1	-34.7.5	44.80	-0.78	0.4731

X_1^2	159.36	53.33	2.99	0.0305*
X_2	6.59	44.80	0.15	0.8888
X_2^2	106.99	53.33	2.01	0.1011*
X_1X_2	189.58	63.36	2.99	0.0304*

* Statistically significant values at 90% confidence ($p<0.10$)

Tabela 10. ANOVA para o CCRD, referente ao E_{corr}.

Source of variation	Sum of squares	Degrees of freedom	Middle square	F_{calc}	P-value
Regression	319517.6	5	63903.5	4.0	0.07791
Waste	80294.1	5	16058.8		
Lack of adjustment	63308.8	3	21102.9	2.5	0.29988
Pure error	16985.4	2	8492.7		
Total	399811.7	10			

% Explained variation (R^2) = 79.92

The linear regression coefficients for the CCRD experimental design concerning the dependent variable, E_{corr}, can be found in Table 9. The results for the variables x_1^2, x_2^2 and $x_1 x_2$ are statistically significant at a 90% confidence level. Additionally, they have positive coefficients of 159.36, 106.99, and 189.58, respectively.

Table 10 provides the ANOVA statistical analysis for the dependent variable, E_{corr}. The R^2 value was approximately 80%, indicating that only 20% of the variation was not explained by the model, which is considered good for obtaining a valid and useful predictive model.

In Figure 7, you can see which variables and interactions analyzed yielded statistically significant results according to the Pareto chart. It can be observed that only variables x_1 and x_2 x_1 and x_2 were not significant, while the others would influence the process if there was an increase in their concentration from level -1.41 to level +1.41.

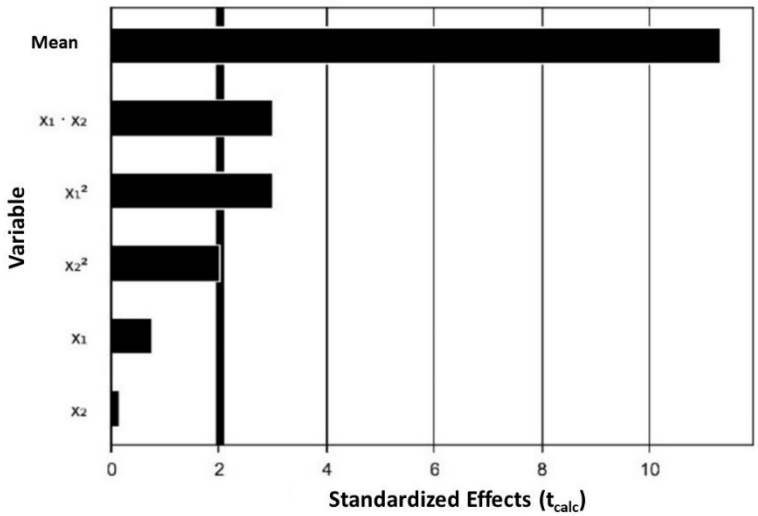

Figura 7. Main effects of significant variables and interactions in the CCRD, related to E_{corr}.
Source: PROTMIZA (2014)

3.2.3. Polarization resistance analysis (R_p)

The Rp values, after 14 days of passivation, are also found in Table 6. It can be observed that, similar to the OCP and E_{corr} values, the polarization resistance (R_p) in experiments 1, 3, and 4 shows a trend where the reduction in corrosion is directly related to the increase in HPMC concentration in the solution. Even in highly corrosive environments, the presence of HPMC serves to alleviate the potential consequences of chloride attacks on the steel rebar. We can see that the highest R_p value was achieved in experiment 6, with a value of 106.4 kΩ, for concentrations of 1.32 g/L of HPMC and 26.30 g/L of NaCl. This result indicates that the higher the HPMC content, the greater the likelihood of it acting as a corrosion inhibitor, ensuring the formation of the passivating film.

If we compare experiments 3 and 4, where the NaCl concentration is 35.10 g/L, we can see that R_p nearly tripled in value, going from 35.35 kΩ to 90.14 kΩ, with just the addition of 0.12 g/L of HPMC.

R_p is used as a parameter to assess a metal's resistance to corrosion damage. Therefore, high Rp values indicate a high corrosion prevention capacity [46].

The results obtained in experiments 9, 10, and 11, which are the central points, did not show significant variability, indicating the good reproducibility of the process.

Table 11 provides the regression coefficients based on the results obtained in the CCRD experimental design, Table 12 presents a complete statistical analysis with ANOVA, and Figure 8 illustrates the Pareto diagram, all of which pertain to the dependent variable R_p.

Table 11. Linear regression coefficients for the CCRD, related to R_p.

Name	Coefficient	Standard error	Calculated t	P-value
Mean	23.46	8.98	2.61	0.047.6*
X_1	15.25	5.50	2.77	0.0393*
X_1^2	32.28	6.55	4.93	0.0044*
X_2	-1.25	5.50	-0.23	0.8290
X_2^2	22.67	6.55	3.46	0.0180*
X_1X_2	5.69	7.78	0.73	0.4972

* Statistically significant values at a 90% confidence level (p<0.10)

Tabela 12. ANOVA for the CCRD, related to R_p.

Source of variation	Sum of squares	Degrees of freedom	Middle square	F_{calc}	P-value
Regression	8960.1	5	1792.0	7.4	0.02325
Waste	1210.8	5	242.2		
Lack of adjustment	1189.8	3	396.6	37.8	0.02591
Pure error	21.0	2	10.5		
Total	10170.9	10			

% Explained variation (R^2) = 88.10

The linear regression coefficients for the CCRD experimental design concerning the dependent variable, R_p, can be found in Table 11. The results for the variables x_1. x_1^2 and x_2^2 são estatisticamente significativos ao nível de confiança de 90%. Além disso apresentaram coeficientes positivo 15, 25, 32, 28 and 22, 67, respectivamente.

Table 12 provides the ANOVA statistical analysis for the dependent variable, R_p. The R^2 value was approximately 88%, indicating that only 12% of the variation was not explained by the model, which is considered good for obtaining a valid and useful predictive model.

In Figure 8, you can see which variables and interactions analyzed yielded statistically significant results according to the Pareto chart. It can be observed that only variables x_2 e x_1x_2 were not significant, while the others would influence the process if there was an increase in their concentration from level -1.41 to level +1.41.

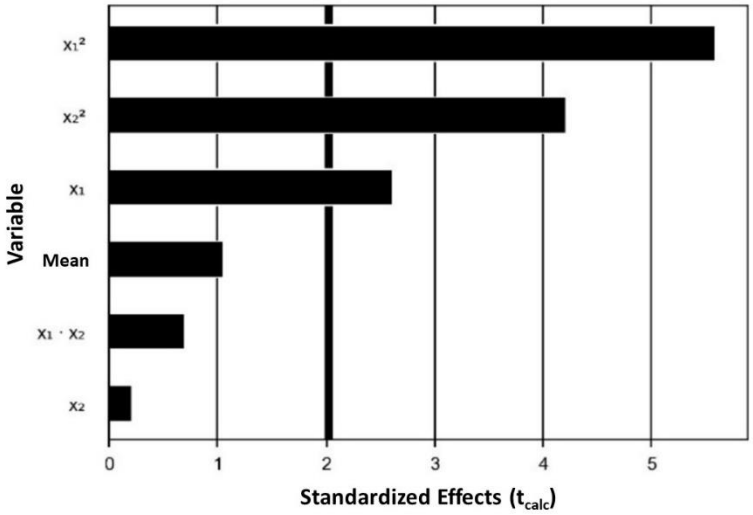

Figure 8. Main effects of significant variables and interactions in the CCRD, related to R_p.
Source: PROTMIZA (2014)

3.2.4. Conductivity analysis

Analyzing the results shown in Table 6, it can be observed that the highest conductivity result was achieved in experiment 8, with 78.90 mS/cm^2, conducted with 0.9 g/L of HPMC and 38.75 g/L of NaCl. On the other hand, the lowest conductivity value was observed in experiment 1, with 22.80 mS/cm^2, where the independent variable concentrations were 0.6 g/L of HPMC and 17.5 g/L of NaCl. When comparing experiment 1 with experiment 3, where the HPMC concentration is kept at 0.6 g/L and the NaCl concentration is doubled to 35.10 g/L, the conductivity triples, reaching 67.30 mS/cm^2. However, the opposite does not occur when maintaining the HPMC concentration at 1.2 g/L and reducing the NaCl concentration by 50%; the impact on conductivity is insignificant.

It is expected that higher conductivity would facilitate corrosion due to the increased mobility of reactive species, allowing the flow of electrons and, therefore, promoting the corrosion of the steel rebar. However, it is not possible to assess the performance of this material based solely on this measurement because many other factors affect the characteristics of the passivating layer, such as the water-to-cement ratio, alkalinity of the pore solution, presence of additives, type of cement, environmental conditions (temperature and relative humidity), and the action of aggressive agents (chloride penetration and carbonation). These factors collectively contribute to the corrosion behavior of the steel reinforcement in concrete [49].

The results obtained in experiments 9, 10, and 11, which are the central points, did not show significant variability, indicating the good reproducibility of the process.

Table 13 provides the regression coefficients based on the results obtained in the CCRD experimental design, Table 14 presents a complete statistical analysis with ANOVA, and Figure 6 illustrates the Pareto chart, all of which pertain to the dependent variable conductivity.

Table 13. Linear regression coefficients for the CCRD, related to conductivity.

Name	Coefficient	Standard error	Calculated T	P-value
Mean	57.,07.	5.32	10.7.2	0.0001*
X_1	-0.86	3.26	-0.26	0.8021
X_1^2	-3.53	3.88	-0.91	0.4042
X_2	17.,89	3.26	5.49	0.0027.*
X_2^2	-2.84	3.88	-0.7.3	0.497.2
X_1X_2	-1.26	4.61	-0.27.	0.7.963

* Statistically significant values at a 90% confidence level ($p<0.10$)

Table 14. ANOVA for the CCRD, related to conductivity.

Source of variation	Sum of squares	Degrees of freedom	Middle square	F_{calc}	P-value
Regression	2663.3	5	532.7	6.3	0.03271
Waste	425.1	5	85.0		
Lack of adjustment	425.1	3	141.7	34284.0	0.00003
Pure error	0.0	2	0.0		
Total	3088.4	10			

% Explained variation (R^2) = 86.23

Table 13 provides the linear regression coefficients for the CCRD experimental design. The only variable whose results are statistically significant at a 90% confidence level is the variable x_2 (concentration of NaCl in the solution) with a coefficient of 17.89. All other variables, besides not being statistically significant, have negative coefficients.

Table 14 provides a statistical analysis using ANOVA. It's important to note that the R^2 value explains approximately 86% of the experiment, which is a measure of how much variability in the observed response values can be explained by the experimental factors. The closer R^2 is to 1.00 the stronger the model and the better the predictive capabilities.

In the same table, it is possible to observe that the effect of variable x_1 and the interaction of variables x_1x_2 were very small, as they are smaller than the standard error, and they also had a negative effect. This means that the increase in HPMC concentration and the interaction of HPMC with NaCl did not influence the conductivity value with 90% confidence. This indicates that the NaCl concentration is the only factor responsible for increasing conductivity, which in turn increases ionic mobility, favoring the corrosive process.

In Figure 9, you can see which variables and interactions analyzed yielded statistically significant results according to the Pareto chart. It can be observed that only variable x_2 was significant, while the others would not influence the process if there was an increase in their concentration from level -1.41 to level +1.41.

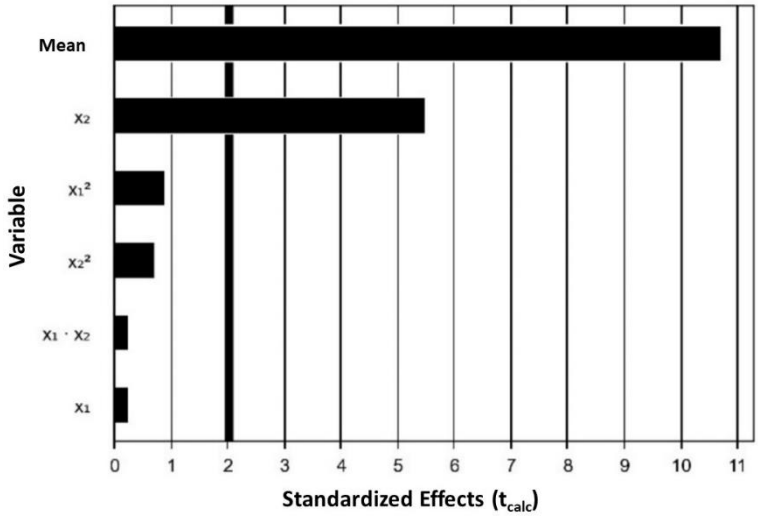

Figure 9. Main effects of significant variables and interactions in the CCRD, related to conductivity.
Source: PROTMIZA (2014)

3.2.5. Response surface analysis for optimization of HPMC use as a corrosion inhibitor

The effect of the two independent variables (HPMC concentration and NaCl concentration) on the use of HPMC as a corrosion inhibitor was analyzed by three-dimensional response surface curves (3D), as illustrated in Figure 10. These curves reflect the relationship between the independent variables, suggesting the corresponding maximum point within the experimental domain. Simultaneously, these surfaces show

the influence of various factors on corrosion inhibition analysis. The 3D response surface curves, plotted by a statistically significant model, serve to understand the interaction of the medium components and the ideal concentration required for each component to assess corrosion inhibition [50].

The 3D graphs presented in Figure 10 were based on the concentration function of two variables, where the significance of interactions between the corresponding variables is indicated by an elliptical feature and contour plots. Thus, Figure 10 shows the response surface generated for OCP (A), E_{corr} (B), R_p (C) and conductivity (D), all obtained by the interaction of HPMC with NaCl. The shape of the response surface curves showed moderate interaction between the variables tested, with the exception of the curve in Figure 10(D).

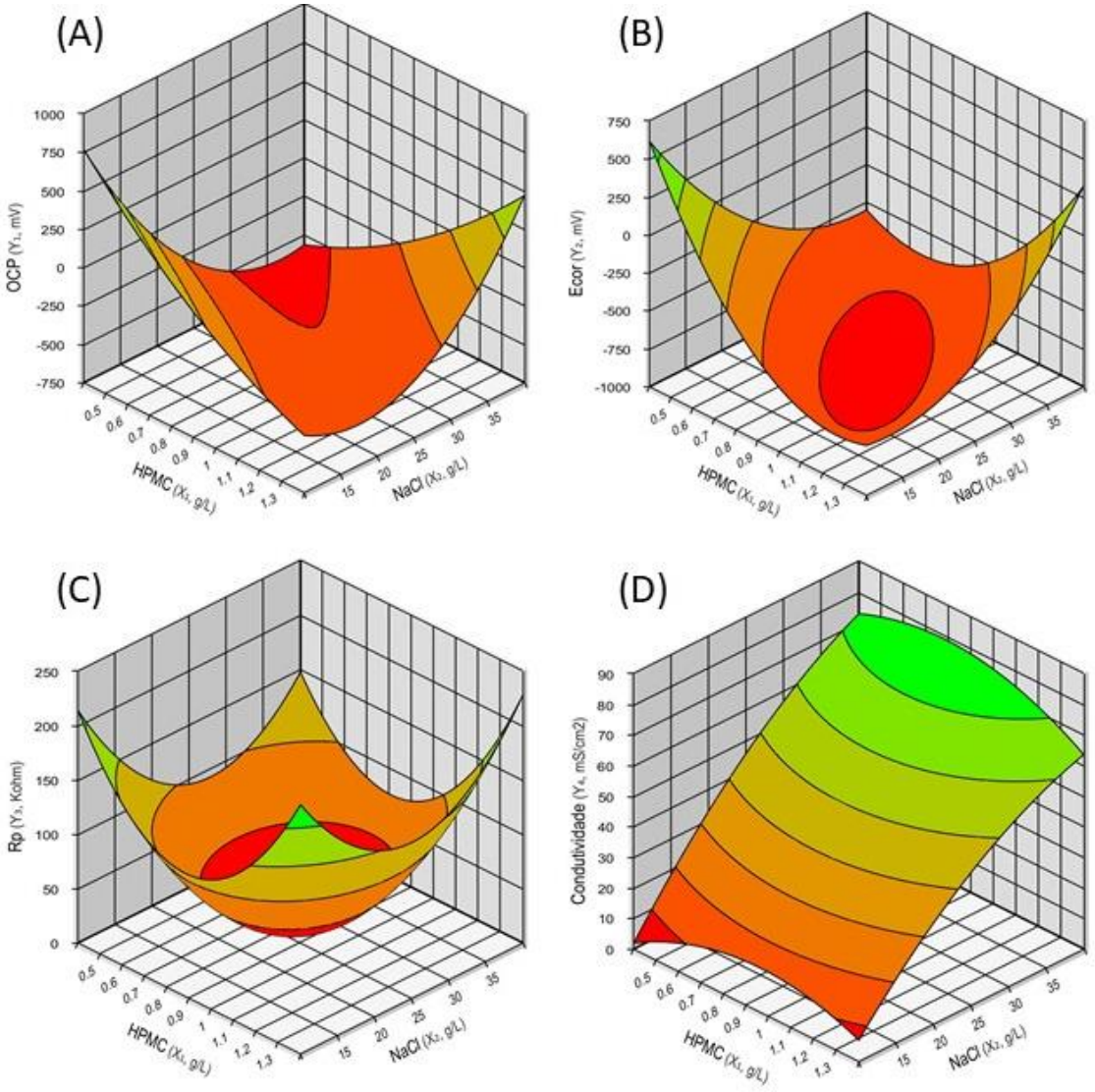

Figure 10. Response surface for the use of HPMC as a corrosion inhibitor for the dependent variables (A) OCP; (B) E_{corr}; (C) R_p; e (D) conductivity.
Source: PROTMIZA (2014)

Figure 10(A) refers to the open circuit potential, where it can be observed that less negative OCP values can be achieved in regions of higher HPMC and NaCl concentration.

Figure 10(B) refers to the corrosion potential, where less negative values suggest a low probability of corrosion. Once again, it can be observed that the region of the graph suggesting this interpretation is where the concentrations of HPMC and NaCl are higher.

In Figure 10(C), high values of polarization resistance (R_p), as this could indicate the formation of a passivating film. It can be seen that this happens when there are high concentrations of HPMC, suggesting that it is responsible for improving passivation formation.

Finally, Figure 10(D) depicts the relationship between conductivity and the simulated concrete pore solution. It's evident that the concentration of HPMC does not influence conductivity, and the only influence is caused by the concentration of NaCl in a directly proportional relationship. This supports the fact that an environment with high chloride ion concentrations is highly corrosive, without showing a direct relationship with the use of HPMC in corrosion inhibition.

4. Conclusions

- According to the OCP and potentiodynamic profiles, a passive film grew rapidly on the surface of steel immersed in a solution containing HPMC, indicating that it can indeed function as a corrosion inhibitor.
- The potentiodynamic studies confirmed that solutions containing 3.5% NaCl, without the corrosion inhibitor (HPMC), H0N3, exhibited high corrosion rates and low polarization resistance values, indicating the presence of flaws or the absence of passivation film formation.
- Once corrosion is initiated, the propagation rate is higher in solutions containing HPMC with concentrations exceeding 50%, likely due to the increase in the conductivity of the pore solution. A concentration of 0.60 g/L of HPMC may result in a physical and electrochemical balance between the closure of micropores and the propagation of suitable pore solution conductivity that controls susceptibility to chloride attack on steel bars. This balance prevents the propagation of higher corrosion currents and creates a propagation condition comparable to the behavior of a reference solution.

- The CCRD experimental design showed that the dependent variables were significant ($p<0.10$), and the statistical model exhibited a correlation of over 90% with the experimental data.
- The ANOVA, along with the Pareto diagram, demonstrated a direct correlation between the increase in HPMC concentration and the improvement of dependent variables (OCP, E_{corr} and R_p), except for an increase in conductivity, which is unrelated to HPMC concentration and instead linked to chloride ion concentration in the solution. However, even with high conductivity, it was evident that HPMC was able to inhibit corrosion, as evidenced by the results of the other dependent variables.

Overall, this study has shown that the addition of HPMC in the concrete mix has potential benefits regarding its passivating properties, meaning that concrete containing HPMC appears to be a less aggressive environment for steel. The reduced susceptibility to steel corrosion in the presence of HPMC is attributed to faster passivation characteristics, as evidenced by monitoring various electrochemical parameters and statistical analysis.

References

[1] E. Commission, Innovating for Sustainable Growth: A Bioeconomy for Europe: Communication from the Commission to the European Parliament, the Council and the European Economic and Social Committee and the Committee of the Regions, Publications Office of the European Union, 2012.

[2] J. Bell, L. Paula, T. Dodd, S. Németh, C. Nanou, V. Mega, P. Campos, EU ambition to build the world's leading bioeconomy—Uncertain times demand innovative and sustainable solutions | Elsevier Enhanced Reader, N. Biotechnol. 40 (2017) 25–30. https://doi.org/https://doi.org/10.1016/j.nbt.2017.06.010.

[3] F. Pittau, G. Lumia, N. Heeren, G. Iannaccone, G. Habert, Retrofit as a carbon sink: The carbon storage potentials of the EU housing stock, J. Clean. Prod. 214 (2019) 365–376. https://doi.org/10.1016/j.jclepro.2018.12.304.

[4] J.D. Colgan, Oil, Domestic Politics, and International Conflict, Energy Res. Soc. Sci. 1 (2014) 198–205. https://doi.org/10.1016/j.erss.2014.03.005.

[5] R.M. Atlas, T.C. Hazen, Oil biodegradation and bioremediation: A tale of the two worst spills in U.S. history, Environ. Sci. Technol. 45 (2011) 6709–6715. https://doi.org/10.1021/es2013227.

[6] B. Hou, X. Li, G. Chen, The Roles of Input Matrix and Nodal Dynamics in Network Controllability, IEEE Trans. Control Netw. Syst. 5 (2018) 1764–1774. https://doi.org/10.1109/TCNS.2017.2760848.

[7] V.T. Tran, D.K. Lee, J. Kim, K.J. Jeong, C.S. Kim, J. Lee, Magnetic Layer-by-Layer Assembly: From Linear Plasmonic Polymers to Oligomers, ACS Appl. Mater. Interfaces. 12 (2020) 16584–16591. https://doi.org/10.1021/acsami.9b22684.

[8] I.O. Arukalam, I.C. Madufor, O. Ogbobe, E. Oguzie, Experimental and theoretical studies of hydroxyethyl cellulose as inhibitor for acid corrosion inhibition of mild steel and aluminium, Open Corros. J. 6 (2014). https://doi.org/10.2174/1876503301406010001.

[9] E.E. Oguzie, Y. Li, S.G. Wang, F. Wang, Understanding corrosion inhibition mechanisms—experimental and theoretical approach, Rsc Adv. 1 (2011) 866–873.

[10] L. Cecchetto, D. Delabouglise, J.-P. Petit, On the mechanism of the anodic protection of aluminium alloy AA5182 by emeraldine base coatings: Evidences of a galvanic coupling, Electrochim. Acta. 52 (2007) 3485–3492. https://doi.org/doi.org/10.1016/j.electacta.2006.10.009.

[11] D.-K. Kim, S. Muralidharan, T.-H. Ha, J.-H. Bae, Y.-C. Ha, H.-G. Lee, J.D. Scantlebury, Electrochemical studies on the alternating current corrosion of mild steel under cathodic protection condition in marine environments, Electrochim. Acta. 51 (2006) 5259–5267.

[12] B.M. Praveen, T. V Venkatesha, Y.A. Naik, K. Prashantha, Corrosion studies of carbon nanotubes–Zn composite coating, Surf. Coatings Technol. 201 (2007) 5836–5842.

[13] V. Kumpawat, U. Garg, R.K. Tak, Corrosion inhibition of aluminium in acid media by naturally occurring plant Artocarpus heterophyllus and Acacia senegal, J. Indian Counc. Chem. 26 (2009) 82–84.

[14] S.A. Umoren, Inhibition of aluminium and mild steel corrosion in acidic medium using Gum Arabic, Cellulose. 15 (2008) 751–761.

[15] S. Nwanonenyi, O. Ogbobe, I. Madufor, E. Oguzie, Inhibitive Performance

of Hydroxypropyl Cellulose and Potassium Iodide on the Corrosion of Mild Steel in Sulphuric Acid Environment, Am. Chem. Sci. J. 16 (2016) 1–12. https://doi.org/10.9734/acsj/2016/28250.

[16] M.M. Solomon, S.A. Umoren, I.I. Udosoro, A.P. Udoh, Inhibitive and adsorption behaviour of carboxymethyl cellulose on mild steel corrosion in sulphuric acid solution, Corros. Sci. 52 (2010) 1317–1325. https://doi.org/10.1016/j.corsci.2009.11.041.

[17] S.A. Umoren, A.A. AlAhmary, Z.M. Gasem, M.M. Solomon, Evaluation of chitosan and carboxymethyl cellulose as ecofriendly corrosion inhibitors for steel, Int. J. Biol. Macromol. 117 (2018) 1017–1028. https://doi.org/10.1016/j.ijbiomac.2018.06.014.

[18] P. Ghods, O.B. Isgor, G. McRae, T. Miller, The effect of concrete pore solution composition on the quality of passive oxide films on black steel reinforcement, Cem. Concr. Compos. 31 (2009) 2–11. https://doi.org/10.1016/j.cemconcomp.2008.10.003.

[19] H.S. Lee, H.M. Yang, J.K. Singh, S.K. Prasad, B. Yoo, Corrosion mitigation of steel rebars in chloride contaminated concrete pore solution using inhibitor: An electrochemical investigation, Constr. Build. Mater. 173 (2018) 443–451. https://doi.org/10.1016/j.conbuildmat.2018.04.069.

[20] S. Toujas, M. Vázquez, M.B. Valcarce, Unexpected effect of citrate ions on the corrosion process of carbon steel in alkaline solutions, Corros. Sci. 128 (2017) 94–99. https://doi.org/10.1016/j.corsci.2017.08.018.

[21] T. Yonezawa, V. Ashworth, R.P.M. Procter, Pore Solution Composition and Chloride Effects on the Corrosion of Steel in Concrete., Corrosion. 44 (1988) 489–499. https://doi.org/10.5006/1.3583967.

[22] G.E.P. Box, W.H. Hunter, S. Hunter, Statistics for experimenters, John Wiley and sons New York, 1978.

[23] B.B. Neto, I.S. Scarminio, R.E. Bruns, Planejamento e otimização de experimentos, Ed. da UNICAMP, 1996.

[24] B. Pacewska, M. Bukowska, I. Wilińska, M. Swat, Modification of the properties of concrete by a new pozzolan - A waste catalyst from the catalytic process in a fluidized bed, Cem. Concr. Res. 32 (2002) 145–152. https://doi.org/10.1016/S0008-8846(01)00646-9.

[25] A. POURSAEE, U.M. ANGST, Principles of corrosion of steel in concrete

structures, in: Corros. Steel Concr. Struct., Elsevier Ltd, 2023: pp. 17–34. https://doi.org/10.1016/B978-0-12-821840-2.00004-3.

[26] W. Rausch, The Phosphating of Metals, Finishing Publications, 1990. https://books.google.com.br/books?id=8RRUAAAAMAAJ.

[27] N. Perez, Electrochemistry and corrosion science, Kluwer Acad. Publ. (2004) 189–246. https://doi.org/10.1007/1-4020-7860-9_7.

[28] S. Yeomans, Galvanized steel reinforcement in concrete, Elsevier, 2004.

[29] P.K. Metha, P.J.M. Monteiro, Concreto: microestrutura, propriedades e materiais, IBRACON, São Paulo, 2014.

[30] E.A. Ticianelli, Eletroquímica: Princípios e Aplicações Vol. 17, Edusp, 1998.

[31] C. ASTM, C876 - Standard test method for corrosion potentials of uncoated reinforcing steel in concrete, ASTM Int. West Conshohocken. (2015).

[32] Y. Peng, L. Liu, S. Wang, Y. Lin, Y. Sun, R. Xia, Effect of simulated pore solution on passivation characteristic of P110 steel, J. Pet. Sci. Eng. 167 (2018) 949–956. https://doi.org/10.1016/j.petrol.2018.03.009.

[33] Y. Wang, Y. Zuo, Y. Tang, Inhibition effect and mechanism of sodium oleate on passivation and pitting corrosion of steel in simulated concrete pore solution, Constr. Build. Mater. 167 (2018) 197–204. https://doi.org/10.1016/j.conbuildmat.2018.01.170.

[34] S. Mundra, M. Criado, S.A. Bernal, J.L. Provis, Cement and Concrete Research Chloride-induced corrosion of steel rebars in simulated pore solutions of alkali-activated concretes, Cem. Concr. Res. 100 (2017) 385–397. https://doi.org/10.1016/j.cemconres.2017.08.006.

[35] E. Briz, M. V. Biezma, D.M. Bastidas, Stress corrosion cracking of new 2001 lean–duplex stainless steel reinforcements in chloride contained concrete pore solution: An electrochemical study, Constr. Build. Mater. 192 (2018) 1–8. https://doi.org/10.1016/j.conbuildmat.2018.10.108.

[36] V. GENTIL, Corrosão, LTC-Livros Técnicos e Científicos Editora SA, Rio de Janeiro, 1996.

[37] S. Wolynec, Técnicas Eletroquimicas de corrosão, 1ª, São Paulo, 2003.

[38] F. Mansfeld, The polarization resistance technique for measuring corrosion currents, in: Adv. Corros. Sci. Technol. Vol. 6, Springer, 1976:

pp. 163–262.

[39] E. McCafferty, Validation of corrosion rates measured by the Tafel extrapolation method, Corros. Sci. 47 (2005) 3202–3215.

[40] S. Wang, Corrosion resistance and electrocatalytic properties of metallic glasses, Met. Glas. Prop. 395 (2016) 116–124.

[41] C. Andrade, C. Alonso, Test methods for on-site corrosion rate measurement of steel reinforcement in concrete by means of the polarization resistance method, Mater. Struct. 37 (2004) 623–643.

[42] M.C. de P.E. D'Oliveira, E.A. Guarda, P.M. Guarda, S.M. Sidel, Estudos recentes sobre compósitos de carboidratos para inibição da corrosão: uma revisão sistemática, Res. Soc. Dev. 11 (2022) e41811932021. https://doi.org/10.33448/rsd-v11i9.32021.

[43] ASTM, C 876–22b. Standard Test Method for CorrosionPotentials of Uncoated Reinforcing Steel in Concrete, ASTMInternational. (2022).

[44] V. Räsänen, V. Penttala, The pH measurement of concrete and smoothing mortar using a concrete powder suspension, Cem. Concr. Res. 34 (2004) 813–820. https://doi.org/10.1016/j.cemconres.2003.09.017.

[45] H.-W. Song, V. Saraswathy, Corrosion Monitoring of Reinforced Concrete Structures - A Review, Int. J. Electrochem. Sci. (2007) 1–28.

[46] S. Lu, H.J. Ba, Corrosion sensor for monitoring the service condition of chloride-contaminated cement mortar, Sensors. 10 (2010) 4145–4158. https://doi.org/10.3390/s100404145.

[47] J. Stewart, D.E. Williams, The initiation of pitting corrosion on austenitic stainless steel: on the role and importance of sulphide inclusions, Corros. Sci. 33 (1992). https://doi.org/10.1016/0010-938X(92)90074-D.

[48] L. feng ZHANG, Inclusion and Bubble in Steel-A Review, J. Iron Steel Res. Int. 13 (2006) 1–8. https://doi.org/10.1016/S1006-706X(06)60051-4.

[49] D. V. Ribeiro, J.A. Labrincha, M.R. Morelli, Effect of the addition of red mud on the corrosion parameters of reinforced concrete, Cem. Concr. Res. 42 (2012) 124–133. https://doi.org/10.1016/j.cemconres.2011.09.002.

[50] Z. Song, H. Cai, Q. Liu, L. Jiang, H. Chu, Performance of corrosion inhibitor extracted from enzymatic hydrolysate of waste Platanus

acerifolia leaves, J. Ind. Eng. Chem. 111 (2022) 464–479.
https://doi.org/10.1016/j.jiec.2022.04.027.

Highlights

* Hydroxypropyl Methylcellulose (HPMC) can be used as an additive in concrete formulation.
* Using HPMC as a corrosion inhibitor in concrete is a greener strategy.
* A positive change in the Open Circuit Potential (OCP) value is obtained for samples in solutions containing HPMC.
* Concrete pore solutions containing HPMC show improvements in their corrosion resistance.
* Favorable growth of a passive film on steel was observed in HPMC-containing solutions.
* Statistical analysis showed a high level of significance, exceeding 90%.
* In the ANOVA, all R^2 values evaluated were above 0.8.

Declaration of interests

☒The authors declare that they have no known competing financial interests or personal relationships that could have appeared to influence the work reported in this paper.

☐The authors declare the following financial interests/personal relationships which may be considered as potential competing interests: